Experiments with Interacting Bose and Fermi Gases

by

Claudiu Andrei Stan

Submitted to the Department of Physics
in partial fulfillment of the requirements for the degree of

Doctor of Philosophy

at the

MASSACHUSETTS INSTITUTE OF TECHNOLOGY

July 2005

Author .....
Department of Physics
July 10, 2005

Certified by .....
Wolfgang Ketterle
John D. MacArthur Professor of Physics
Thesis Supervisor

Accepted by .....
Thomas J. Greytak
Professor of Physics, Associate Department Head for Education

Experiments with Interacting Bose and Fermi Gases

by

Claudiu Andrei Stan

Submitted to the Department of Physics
on July 10, 2005, in partial fulfillment of the
requirements for the degree of
Doctor of Philosophy

Abstract

In the past few years, the study of trapped fermionic atoms evolved from the first cooling experiments which produced quantum degenerate samples to becoming one of the most exciting branches of current atomic physics research. This thesis covers experiments done throughout this period, which can be grouped in three sets of studies.

First, degenerate ^{6}Li Fermi gases have been produced by sympathethic cooling with bosonic ^{23}Na. For this, an existing ^{23}Na Bose-Einstein condensation apparatus was upgraded to an experiment capable of producing degenerate ^{6}Li Fermi gases and ^{6}Li–^{23}Na degenerate Fermi-Bose mixtures.

The cooling methods have been developed in two different stages, resulting in the production of degenerate ^{6}Li Fermi gases with temperatures below 0.05 T_F and up to 7×10^7 atoms, and of degenerate ^{6}Li–^{23}Na mixtures with a few million atoms in each of the components.

Second, the properties of ^{6}Li–^{23}Na mixtures at different magnetic fields have been investigated, resulting in the discovery of three interspecies ^{6}Li–^{23}Na Feshbach resonances, which opens up the possibility to study strongly interacting Bose-Fermi mixtures in this system. This investigations also led to the observation of other Feshbach resonances in ^{6}Li and ^{23}Na.

Third, the properties of strongly interacting ^{6}Li spin mixtures in the strong interacting regime near a Feshbach resonance have been investigated. Weakly bound $^6Li_2$ molecules have been produced and Bose condensed on the repulsive side of the Feshbach resonance. Pure molecular condensates with up to 3×10^6 molecules have been produced.

The properties of the interacting Fermi gas were investigated on the attractive side of the resonance using rapid field ramps to the other side of the resonance. Fermion pairing, and condensation of these pairs was observed near the resonance, offering evidence for superfluid behavior in a strongly interacting Fermi gas.

Thesis Supervisor: Wolfgang Ketterle
Title: John D. MacArthur Professor of Physics

To all from whom I have learned

Acknowledgments

The years I have spent at MIT were the ones in which, so far, I have learnt the most and slept the least. One of the things I treasure most about this period, and benefited me most, was the opportunity to work, interact with, and learn from the people I have found here. Which was unexpected for the lone problem solver I used to like to be.

First I have to thank Wolfgang Ketterle for offering me to work in his lab, for his guidance, and for providing a work environment in which what counts most is the quality of the work, and in which the administrative chores which usually other graduate students are largely extinct. I was amazed by his work ethics and by the range of his expertise, from the nuts and bolts of the experiment to how to conduct high-impact research. At a time in which he had two other working experiments, he was also able to put a lot of time into the development of the lithium experiment and of the two unexperienced graduate students, Zoran and me, who started it. Wolfgang is the first real leader I have encountered, and he was my main role model during my first years here.

Dave Pritchard is the first atomic physicist I have met upon coming here, and had a decisive role in my path throughout the grad school, initially bringing me to the atomic physics research by keeping me in his labs during my first term, and then by advising me to join Wolfgang's group at a time at which I was not considering this very seriously. He later played much more than his required role as an academic advisor. Our interactions during these years were rather brief, but he always gave me excellent advice when this was needed. Each term, Dave made the fifteen minutes of the registration feel almost like an exam, and triggered useful personal reflections on where I was and where I was going in my endeavors at MIT.

It is a rare thing that all the graduate students, undergrads and postdocs I have worked with shared not only a great passion for their work, but also the capacity to work hard and the to learn quickly the skills needed to bring difficult tasks to fruition. The lithium experiment started with Zoran Hadzibabic and me, and except for our

Eastern European origin and upbringing, the most obvious thing we shared than was that none of us knew anything about building an atomic physics experiment. Our mode of collaboration initially puzzled many people, since our work schedules were almost orthogonal and it was not unusual not to meet in the lab during a day of work. But this worked quite well, mostly because the general skills we brought with us were complementary, and the tasks we have chosen largely non-overlapping. On top of doing his share of experiment-building and excellent research, I thank Zoran for contributing with a broad scientific curiosity and a cheerful attitude which I could not have supplied myself then, and without which the lithium experiment could not have been what it is now.

Martin Zwierlein joined us early during the experiment building phase, and starting with his first evening in Cambridge when we all went for a beer at the Middle East, it was clear that he is one of the most enthusiastic persons I've ever meet, this applying to everything from building a laser lock and figuring the exact mathematical formula for the error signal, to playing soccer after a full night run, biking across Martha's Vineyard, or singing at parties. Martin finished his months as an exchange student leaving behind solid hardware and many fond memories, and luckily he returned soon as a graduate student. His ever strong determination to make things work was not deterred even when others, including myself, were not sure whether we were going in the right direction. Martin's contribution to the lab's best achievements to date was essential, and a big share of my most fruitful nights in the lab were shared with him during the fall and winter of 2003.

Deep Gupta always impressed me with his imperturbable calmness. Deep's patient and yet stubborn way of, as he would put it, 'wrestling the machine' puzzled me initially. But as soon as I had to do it myself it was obvious that it was one of the best ways to make things working in our lab, and it was one of the most useful things I have learnt. Kai Dieckmann had done his fair share of experiment building during his years as a postdoc, and he is one of the people who got the research started. His stubbornness in suggesting me to add thermocouples to the new magnetic trap paid off through the existence of a better safety interlock setup.

As Martin, Christian Schunck joined us for a shorter period first as a diploma student, and his qualities soon pointed him as the best choice for the next graduate student in our group. The weeks in which we have built, 'due to a small error' as Christian, who is one of the nicest persons I know, would put it, not one but two magnetic traps, were filled with fun despite working round the clock to get the experiment running again. Christian was also a great officemate, always ready to chat about wines, or to explain to me the musical structure of my favorite songs.

Yet another excellent diploma student and officemate, Sebastian Raupach was with us through the rather crazy academic year of 2003/2004, working as hard as everyone else, bringing some much-needed cheerfulness to the group, and still finding time able to throw a 'Bad Taste' party which I will always remember. Andrew 'Jamie' Kerman joined us during the same period as a postdoc, and impressed me with his professional attitude, his range of scientific and technical skills, and by making solid contributions almost from the first day. With Peter Zarth, one of the latest members of the lithium group, I've shared the office, and even though we didn't have the opportunity to work together, I've been peeking over his shoulders and was impressed by his electronics building skills.

Ever since I have started to work with the BEC2 lab towards building a new lithium experiment, their big office in 26-259 was always an oasis to which I went for much-needed breaks from job searching and thesis writing. Even better, working with them was great source of satisfaction throughout my hectic last year.

Jit Kee Chin was a wonderful friend and teammate throughout this period. Her commitment to the new lithium project is exemplary, and I have been impressed by her ability and willingness to learn the more arcane details of our vacuum systems while maintaining a healthy critical attitude towards the solutions I have found myself. Sharing the frustrations and joys of experiment building and of getting the first lithium MOT was a fulfilling experience. I am grateful to Jit Kee for more things that could fit here, but I will still mention hosting a great party after my defense, and trying to develop in me a taste for healthier food.

An anti-establishment thinker, Dan Miller was the fiercest critic of my technical

solutions whenever he felt that they only resulted in enhanced aesthetic. While I sometimes wished I could explain to Dan their hidden practicality, I have to admit I cannot find either any fundamental faults of his non-aesthetic-focused style. Dan's somewhat unpredictable bursts of energy did save otherwise hopeless experimental runs in the lab, and surprised me even more outside it, enough to accept some of his challenges, as the legs-taped-together jumping races in the hallway of building 26.

Widagdo Setiawan gained a solid position as the long-term UROP of group, partly by bringing a bit of the undergraduate MIT culture in the lab, partly by mass producing AOM drivers with front panels which sport some of the most powerful LEDs than money can buy, and partly by withstanding the mocking generated by the aforementioned LEDs. Well, what counts in the end is that the insides to these drivers have quietly evolved towards better reliability. I am particularly glad that Widagdo was receptive to my equipment suggestions and starts to develop a passion for good-looking, reliable hardware. I wish him a lot of luck with his endeavors in the lab and outside it.

I hope that my interactions with Yingmei Liu and Kaiwen Xu have been as useful and entertaining to them as they were to me. I have always enjoyed the playful intellectual sparrings with Kaiwen, which ranged from predicting the outcome of rather impossible physical events to the subtle logic of embassy employees (or lack of), and were sometimes a serious annoyance to the other people in the office. Yingmei showed me that is is possible to combine a postdoc's maturity with an undergraduate enthusiasm towards the lab events, and even towards my stories about random subjects as the military uses of lithium-6.

To the members of Wolfgang's other two experiments, BEC3 and Rubidium, I am indebted for bits of help, information or equipment that were always readily available, and even more indebted for sharing some of the best times I had outside the lab during these years.

Michele Saba was always ready to give a thoughtful advice when needed, or to review a paper on a very short notice, and I have benefited a lot from his help lately. I will remember Jamil Abo-Shaeer not only for throwing a few outstanding parties

and constantly taking care that our self-esteem doesn't become unreasonable, but also for giving me the first haircut in ten years. With Gretchen Campbell, Yong-Il Shin and Takashi Mukayiama I had a great time during a conference in Spain, both at the conference site and on the streets of Barcelona. Andre Schirotzek's preference for noisy music matches mine, and during his days as a diploma student in the BEC3 experiment we had fun trying to start and play synchronously a particular Sepultura song, in rather loud volume, using lab computers from both experiments. I also have to mention Tom Pasquini for being one of the few people in our labs which whom I share a rather unusual preference for lab cleanliness.

One of the things I don't expect to encounter again soon was the amazingly efficient infrastructure of MIT and the excellent professionals which keep it going. The late Carol Costa, who was the CUA secretary throughout most of my stay here, made everyone's life, including myself, much easier, and was always ready to slip the right piece of advice. Ellenor Emery Barish took Carol's place only recently, but I've already benefited many times from her timely help. Of the people in the RLE headquarters, Maxine Samuels went through hundreds of my requisitions quick and without mistakes, and to my embarrassment she took care of them the same day even when I was turning requisitions in Fridays after 4 pm. Peter Morley and Andrew Gallant from MIT's Central Machine Shop took care of making some of the more unusual pieces of equipment and were always ready to give me expert design advice or lend me sophisticated measurement devices.

MIT's excellence in education applies at all levels. I had the luck of attending the classes of two exceptional teachers, Susan Silbey (sociology and anthropology) and Jay Scheib (theater arts), during their first term here, and feed from their enthusiasm in discovering that MIT is a place where the high standards of hard work and creativity apply not only to science and engineering. Susan had awakened my curiosity towards social sciences, and in a more general sense towards the non-exact aspects of this world. On the practical side, the basic English writing rules learned while taking her class later turned out to be very useful for scientific paper writing. Jay shared his insider's knowledge of performing arts, and inspired me to try theater acting and

experience the fun and thrill of being on the stage. I'm grateful to Susan and Jay for making these extra-curricular explorations an important part of my learning and growing while at MIT.

My closest Romanian friends at MIT, Mihai Ibanescu, Iuliana Radu, Alex Salcianu, and Tudor Leu formed the right group of people from and with whom to acquire and exchange knowledge about the unfamiliar new world we arrived to a few years ago. Although having different paths during these years, we have influenced each other, grew up together, and looking back I'm amazed by how much we have all changed.

Last, I would like to thank my family for its understanding support. Through their entrepreneurship, work ethics, and moral values, my parents were the most influential models I had during my years in school, thus, unknowingly to me then, putting me on the path I am now.

Contents

List of Figures

List of Tables

Chapter 1

Introduction

1.1 Trapped ultracold atomic gases

The physical system which is the object of our experiments is an ultracold gas, typically at microkelvin temperatures. This immediately raises three questions: how are they produced, why those gases do not form a condensed phase, and what is the physical container in which we keep them.

The reason for which a solid or liquid phase is not (immediately) formed is that for typical ultracold gas densities of 10^{12}-10^{13} cm^{-3}, roughly one millionth of the density of air, ultracold gases are metastable towards liquefaction or solidification. A typical sample of ultracold atoms can have a lifetime of a few minutes. At the same time, the thermal equilibration of the metastable gas occurs relatively fast, typically in less than one second, which is essential for cooling them. The timescales for metastable and full thermal equilibration define the range of densities for which ultracold gases can be produced.

The coldest temperatures which can be achieved by cryogenic techniques are currently in the millikelvin range, which means that ultracold gases cannot be kept in a standard container as they will thermalize fast with the container walls. The solution is to keep them in atom traps inside an environment evacuated to very low pressures, typically below 10^{-8} Torr.

Making a levitating atom trap is not a straightforward task. The problem is that

atoms are electrically neutral and respond to external fields only through higher-order charge moments. If a particle with an elementary unit of charge has an potential energy equal to the thermal energy at room temperature for an electric potential of only 25 mV, a magnetic field of 500 T (so far achieved only by destructive methods) is needed for a particle with a magnetic moment equal to the Bohr magneton. For atoms electrical fields cannot be used for trapping; even for manipulation of room temperature atoms, impractical electric fields are needed.

Of course, atom traps are possible if the thermal energy is much lower. Initial energy reduction is achieved by laser cooling. The basic idea is to slow down a moving atom by using a counter-propagating resonant laser beam [**?**]. Every time the atom absorbs a photon, its momentum will be reduced by an amount equal to the photon momentum. For a typical alkali atom at room the relative momentum change is small, typically 10^{-4} to 10^{-5}. What makes laser cooling practical is the high maximum rate at which resonant photons are scattered, 10^7-10^8 s^{-1}, and clever applications of this mechanism. For reviews of the field of laser cooling and its development, a good source are the addresses of Steven Chu [33], Claude Cohen-Tannoudji [34], and William Phillips [105] on the occasion of their award of the 1997 Nobel Prize in Physics.

Laser cooling made possible the development of a robust radiation pressure trap, the magneto-optical trap, or MOT [106] which provides at the same time relatively deep atom confinement, and cooling. A MOT can capture atoms with speeds up to tens of meters per second (corresponding to temperatures around one Kelvin), and cool them to sub-millikelvin temperatures.

A MOT can catch only atoms with velocities corresponding to a thermal energy in the Kelvin range. At room temperature, only a small fraction of the atoms will have such small kinetic energies. Our atom source is an effusive atomic oven with a temperature around 700 ^{o}K. To obtain a flux of slow atoms, they are velocity-selected in the transversal direction by aperturing a narrow atomic beam. In principle, velocity selection is possible along the beam as well by using a mechanical velocity selector, but the flux of low velocity atoms, given by the Maxwell-Boltzmann distribution,

would be too low. In our experiment we use a Zeeman slower [104] to increase the slow atom flux. Slowing is achieved by passing the atoms through a variable magnetic field solenoid coil as a red-detuned resonant laser beam is sent counterpropagating relative to the atoms. Since the Doppler broadening is much larger than the linewidth of the optical transition, the variable magnetic field is used to maintain the atoms resonant with the laser beam throughout their deceleration.

Laser cooling becomes inefficient below typical MOT temperatures, so we use a third stage of cooling to lower the gas temperature from the millikelvin to the microkelvin range. For alkali atoms which have relatively large magnetic moments, on the order of the Bohr magneton, magnetic traps with trap depths deep enough to hold laser-cooled atoms can be built [90].

In a conservative atom trap, as for example the magnetic trap, a new cooling method can be used. Evaporative cooling was initially proposed as a method to achieve Bose-Einstein condensates of spin-polarized atomic hydrogen [57]. Evaporative cooling involves the selective removal of the atoms with highest energy from the trap. Removal is achieved by altering the depth of the trapping potential, which was initially done by changing the magnetic field configuration [86]. To be efficient, evaporative cooling must truncate the high energy particles in small increments, and the truncation rate must be slow enough that the trapped gas can thermally equilibrate between the truncation steps.

The evaporation method we use was originally inspired by early rf spectroscopy of trapped atoms [85], and it involves applying a rf field close to resonant hyperfine frequencies. Since the potential energy of the atoms changes as they move within the trap, it is possible to make only the hottest atoms briefly resonant with the applied field at the extreme ranges of their movement. The rf field then induces transitions to different hyperfine states which are not trapped, resulting in the removal of the hot atoms from the trap.

Evaporative cooling brings the temperature of our trapped gases to the microkelvin range, and is the last basic cooling step. To summarize our entire procedure, we start with a gas at close to 1000 K and we cool it to approximately 1 μK in three distinct

steps, each reducing the temperature by approximately three orders of magnitude: Zeeman slowing, MOT cooling, and evaporative cooling in an optical trap.

Giving an detailed description of these basic cooling methods is not within the scope of this thesis. For a more detailed coverage, Refs. [63], [87], and [100] are good sources. Theses from previous members of our group are another useful references for the cooling methods and experimental apparatuses we actually use.

1.2 Quantum statistical mechanics: bosons, fermions, and the Bose-Einstein condensation

A particle's properties are fully specified by its quantum state, which includes both its internal degrees of freedom, and its external ones. The internal degrees of freedom of an atom can be described by a small set of quantum numbers. Even at room temperature, the typical separation between electronic levels is much larger than thermal energy, so all of our atoms are in the ground electronic manifold. Within this manifold, the rate of spontaneous transition between hyperfine and Zeeman sublevels is extremely low, so it is possible to trap atoms in a single ground state sublevel even if this is not the absolute ground state.

For a given internal state, the position of the external energy levels is defined by the external potential. In magnetic and optical dipole traps, the external potential is well approximated by the one of a 3D harmonic oscillator, and the energy levels are given by

$$\epsilon_{n_x,n_y,n_z} = \frac{1}{2}\hbar[\omega_x(n_x + \frac{1}{2}) + \omega_y(n_y + \frac{1}{2}) + \omega_z(n_z + \frac{1}{2})]$$

so the state of a particle in a single internal state is fully specified by the three quantum numbers n_x, n_y, n_z.

At high temperatures the equilibrium state of a many-particle system can be described statistically by the average occupation number of each energy level, given

by the Maxwell-Boltzmann distribution [74]:

$$f_{MB}(\epsilon) = \exp[(\mu - \epsilon)/T]$$

where μ is the chemical potential of the system in contact with a reservoir at temperature T.

At temperatures for which the average occupation number of the lowest energy states becomes comparable to unity, the quantum statistics of identical particles beacomes manifest and the classical Maxwell-Boltzmann distribution is no longer a good approximation.

For a system of identical particles occupying a set of quantum levels, it is impossible to distinguish between two configurations which are different by particle exchanges, for example particle A in state |1> and particle B in state |2> from particle B in state |1> and particle A in state |2>[1]. Taking this into account, the total wavefunction of a system of particles is described by a linear combination of all possible product states of single particle wavefunctions.

The total wavefunction must be either symmetric or antisymmetric with respect to identical particles exchanges. Particles which have a symmetric wavefunction are called bosons, and the ones with anti-symmetric wavefunction are called fermions. Bosons have integer total spin, and fermions half-integer total spin. This separation has profound implication for the quantum statistics. In particular, the average occupancy is given by [74]:

$$f_{BE}(\epsilon) = \frac{1}{\exp[(\epsilon - \mu)/T] - 1}$$

$$f_{FD}(\epsilon) = \frac{1}{\exp[(\epsilon - \mu)/T] + 1}$$

for Bose-Einstein and Fermi-Dirac distributions.

[1]I've been confused for quite a while by this textbook way of describing particle indistinguishability, because in this statement you can distinguish the particles. It is probably more accurate to state that you cannot distinguish particle A in state |1> and particle A in state |2> from particle A in state |1> and particle A in state |2>, although it might be equally confusing.

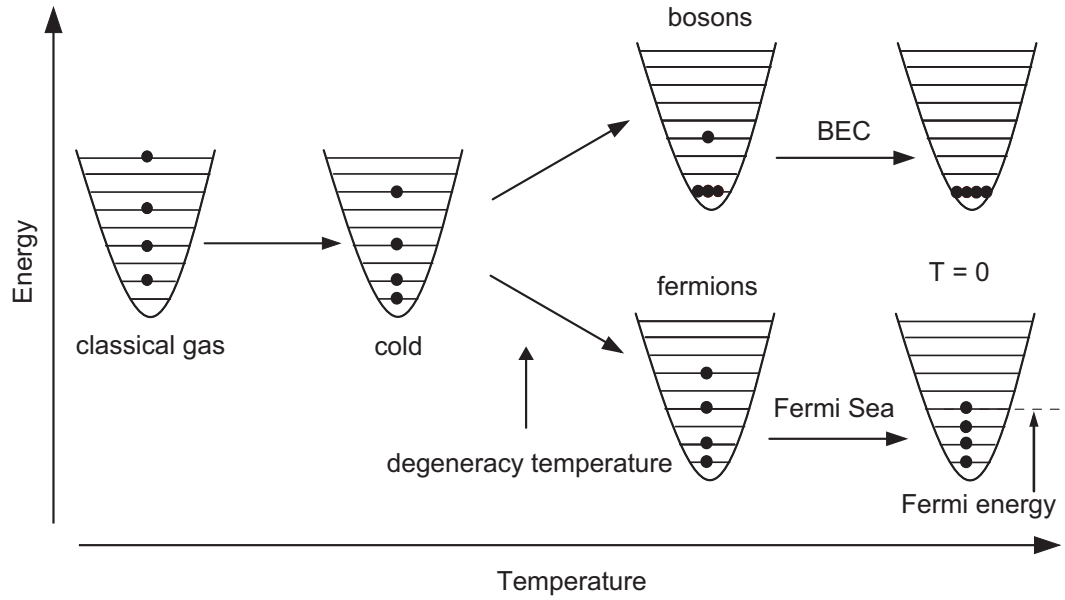

Figure 1-1: Trapped ultracold atoms. The atoms occupy a discrete set of quantum states corresponding to different energies. At high temperatures, a classical Maxwell-Boltzmann distribution describes accurately the average state occupation, which for the lowest energy levels increases with decreasing temperature. At lower temperatures quantum statistics becomes manifest. Bosons accumulate in large numbers in the ground state, even at finite temperatures. Fermions tend to a zero-temperature state in which each energy level is occupied by a single particle, up to a maximum energy called Fermi energy.

At very low temperatures (Figure 1-1), as at most on fermion can occupy a quantum level, fermions occupy one by one levels with increasing energy up to a an energy called Fermi energy. In contrast, bosons all accumulate in the ground state, and the ground state occupation can be macroscopic even at finite temperatures, a phenomenon called Bose-Einstein condensation.

In the case of trapped bosons, a more practical criteria for the onset of condensation is given by the phase-space density

$$\rho = n\lambda_{DB}^3$$

where n is the peak atomic density, and $\lambda_{DB} = h/\sqrt{2\pi m k_B T}$ is the thermal deBroglie wavelength. The condensation occurs when the phase-space density approaches unity,

or more precisely when $\rho = 2.612$. In a physical picture, this corresponds to the situation in which the deBroglie wavepackets of individual atoms start to overlap in real space. Thus, the progress towards Bose-Einstein condensation in trapped atoms is more accurately described as an effort to achieve higher phase space densities, and not only lower temperatures.

The achievement of Bose-Einstein condensation in trapped ultracold gases was a long-standing goal of laser cooling and spin-polarized hydrogen cooling, and was achieved in 1995 in gases of alkali vapors [18, 39] by using the cooling techniques described in the previous section. To a large extent, this provided the apparatus and the experimental methods we are using to study degenerate Fermi gases today. For reviews of the field of Bose-Einstein condensation and its development, a good source are the addresses of Eric Cornell and Carl Wieman [35], and Wolfgang Ketterle [70] on the occasion of their award of the 2001 Nobel Prize in Physics.

1.3 Ultracold collisions

The description of collisions between ultracold atoms is greatly simplified by their low energies, and the scattering process depends on only one parameter, which is usually chosen to be the scattering length a.

Scattering can be described quantum mechanically by specifying the center-of-mass wavefunction for the colliding particles. This wavefunction defines a scattering state which, neglecting normalization factors, can be written as [38, 100]:

$$\psi = e^{ikr} + \psi_{sc}(\mathbf{r})$$

which is the sum of an incoming plane wave e^{ikr} and a scattered wave $\psi_{sc}(\mathbf{r})$. For a spherically symmetric scattering potential, the scattering wave is an outgoing spherical wave, $\psi_{sc}(\mathbf{r}) = f(k,\theta)\exp(ikr)/r$, where $f(k,\theta)$ is the scattering amplitude.

The scattering state can be expanded in terms of Legendre polinomials, leading to a partial wave expansion. The partial waves with $l > 0$ describe effective unidimen-

sional scattering potentials which have a centrifugal barrier. In the case of ultracold atoms, this barrier is high compared to the kinetic energy of the colliding atoms, and the contribution of higher partial waves can be neglected. Thus, the collisions can only take place only in the s-wave channel.

The effect of the s-wave interaction is to introduce a phase shift $\delta(k)$ in the scattered wave. For very low energies, it scales linearly with the wavevector amplitude, and the proportionality constant,

$$a = -\lim_{k\to 0}(\delta(k)/k)$$

called the scattering length, is the only parameter which characterizes low-energy collisions.

A positive value of a corresponds to a repulsive effective interaction, and a negative value to an attractive one. The elastic collisional cross section is related to the scattering length by a simple formula. For distinguishable particles, such as atoms in different internal states, the cross-section is given by

$$\sigma = 4\pi a^2$$

For identical bosons, the scattering length is enhanced to

$$\sigma = 8\pi a^2$$

and it vanishes for identical fermions. The result for fermions shows that a gas of identical fermions is non-interacting at low temperatures, and as one practical consequence it makes the evaporative cooling of identical fermions impracticable because of the long thermalization times.

The s-wave scattering also leads to a mean-field change in the energy of a particle moving through a gas of scatterers with density n given by:

$$\frac{4\pi\hbar^2 an}{m}$$

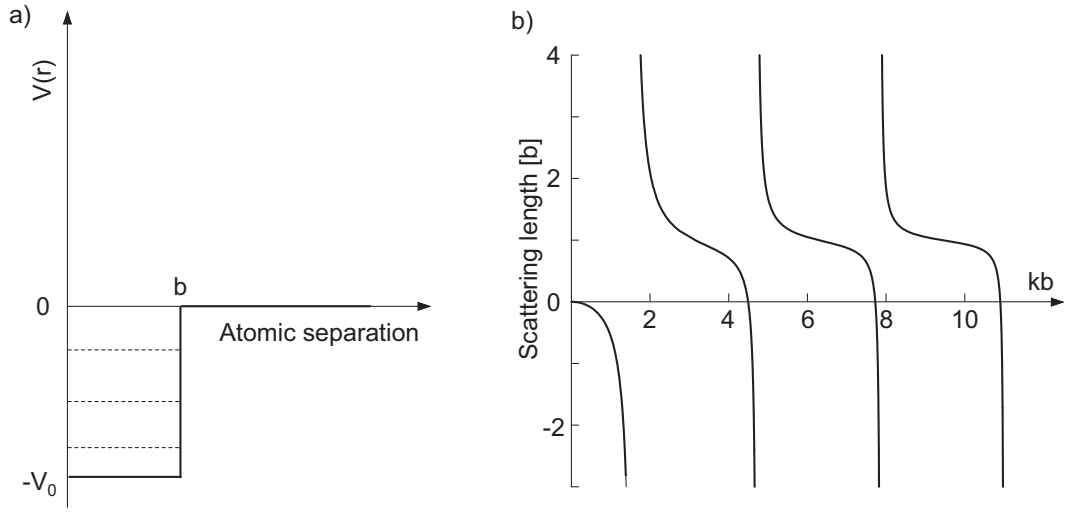

Figure 1-2: Scattering resonances for a box potential. In a) the potential is plotted as a function of interparticle separation. In b) the scattering length is shown in units of the potential range b, and as a function of the parameter kb where $k = \sqrt{2\mu V_0}/\hbar$. The scattering length diverges for potential parameters which correspond to the appearance of bound states as the potential is changed.

where m is the mass of the particle.

1.3.1 Scattering resonances

The value of the scattering potential can have very large values if the conditions for a scattering resonance are met. To illustrate this phenomenon, we can use a simple unidimensional model [38]. For an attractive square potential with a depth $-V_0$ and length b, the solution of the Schrödinger equation outside the range of the potential b has the form $\psi(r) = C(r - a)$, from which we can identify a as the scattering length. Defining a 'wavevector' k by $k = \sqrt{2\mu V_0}/\hbar$, where μ is the reduced mass, a is given by

$$a = b - \frac{\tan(kb)}{k}$$

and is plotted in Figure 1-2.

The scattering length diverges for values of V_0 and k for which $kb = (2n + 1)\pi/2$. This corresponds to the appearance of a new bound state as the potential parameters are varied. This is an example of a potential scattering resonance in which only the

external degrees of freedom of the scatterers are involved; the coupling between the spin degrees of freedom of the free particles and of the bound state is ignored. Nevertheless, this illustrates the more general connection between scattering resonances and the appearance of bound states.

A different type of scattering resonance is more important for the studies of ultracold gases. These are the zero-energy Feshbach resonances (Figure 1-3). Unlike the simple single-channel model presented above, they occur when the energy of the incoming atoms equals the energy of a bound state. This bound state has different quantum numbers than the scattering state, but can be coupled to it by interactions which are non-diagonal in the hyperfine states, as the exchange interaction or the much weaker magnetic dipole interaction.

If for a given Feshbach resonance the energy of the incoming atoms and that of the bound state have different field dependence, it is possible to tune the scattering length by changing the value of the magnetic field:

$$a(B) = a_{bg}(1 + \frac{\Delta B}{B - B_0})$$

where a_{bg} is the background scattering length and B_0 is the resonance field. The resonance width ΔB is proportional to the free-bound coupling matrix element squared.

Since the Feshbach resonances happen when a coupling between free and bound states occurs, they can be used to produce bound states from free atoms. Nevertheless, the initial interest in them was driven by the possibility of tuning the sign and strength of atom-atom interactions by simply changing the magnetic field, which allows a degree of control not available in solid-state systems.

In the case of bosonic atoms, Feshbach resonances have found only limited applicability as a tool to alter the interaction strength. Soon after their first observation in ultracold bosonic gases [36, 64], it was found that they are also associated with very fast atom losses [123].

Fortunately, Feshbach resonances have proven much more forgiving in the case of fermionic atoms, and they have made possible the research covered in Chapters 5 and

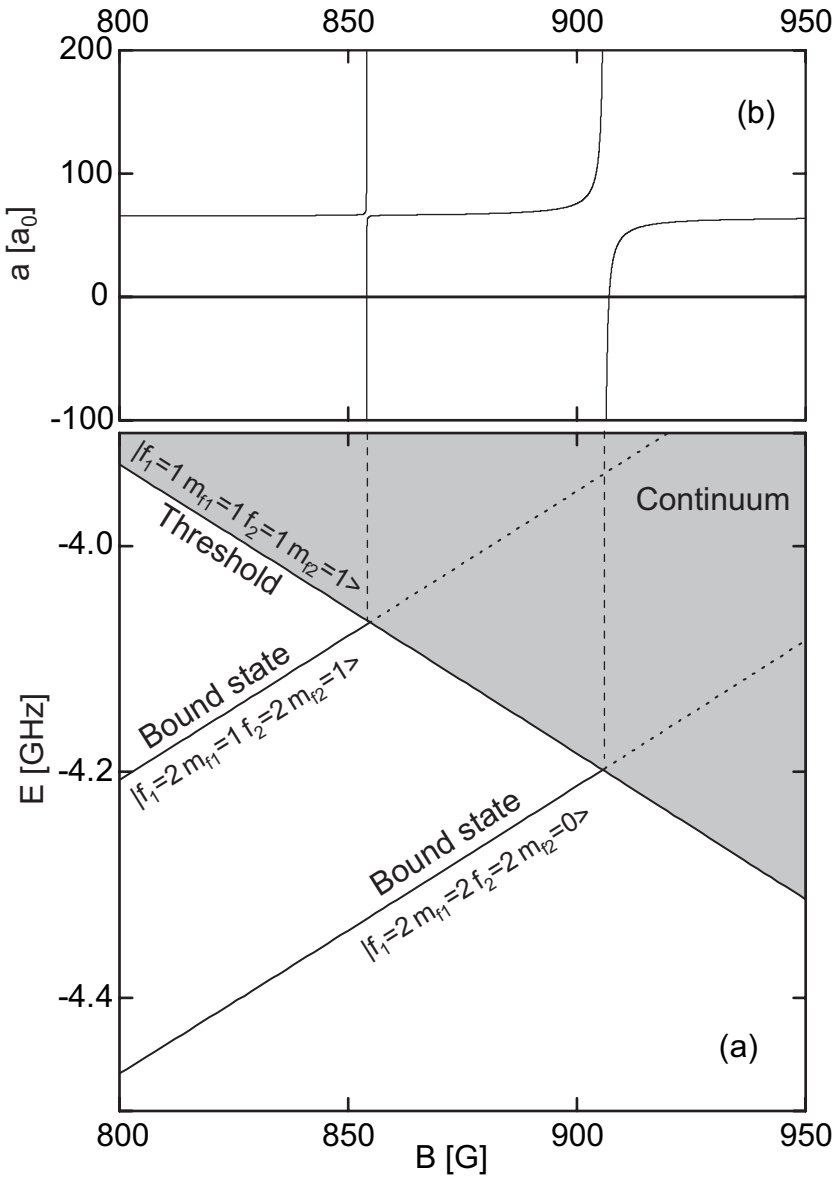

Figure 1-3: Feshbach resonances between sodium atoms, from [132]. a) Magnetic field dependent threshold energy and two field dependent bound states for a pair of ^{23}Na atoms with $m_F = +2$. The grey area above the zero kinetic energy of the incoming atoms (the threshold) is accessible to the open channel states. The rising bound states have the approximate spin structures $|f_1 = 2, m_{f1} = 1, f_2 = 2, m_{f2} = 1 >$ and $|f_1 = 2, m_{f1} = 2, f_2 = 2, m_{f2} = 0 >$. b) The zero-energy scattering length for collisions between $|F = 1, m_f = 1 >$ sodium atoms.

6 of this thesis.

1.3.2 s-wave Feshbach resonances in ^{6}Li

Even before the first experiments which succeeded in cooling fermionic lithium to quantum degeneracy [129, 118], the predicted collisional properties of ^{6}Li raised interest in the ultracold atom community. Of course, this applies to the collisional properties of ^{6}Li spin mixtures, since a single quantum state fermionic gas is non-interacting.

First, it was calculated from data obtained by two-photon photoassociative spectroscopy [17] that the triplet scattering length is unusually large, $a_t = (-2160 \pm 250) a_0$, where a_0 is the Bohr radius. This results in a large attractive interaction which could by itself be enough to observe Cooper pairing in in an interacting Fermi gas.

Further calculations of the value of the s-wave scattering length revealed that for different pairs of hyperfine states the interstate scattering length a_{ij} is much lower at small magnetic fields, but increases sharply towards the triplet scattering length value in a field range between 100 and 1000 G [62]. In addition, Feshbach resonances were predicted at magnetic fields of 800 G and 1.98×10^5 G in collisions between atoms in the $|1>$ and $|2>$ high field hyperfine states ($F, m_F = |1/2, 1/2>$ and $F, m_F = |1/2, -1/2>$, respectively, at low field).

Using these prediction, we have been able to observe the first resonance in 2002 [7], and another resonance at lower fields, which was not predicted. This allowed more precise calculations of the scattering length. The variation of a_{12} is shown in Figure 1-4.

Since the resonance positions could not be predicted with high accuracy initially, the measurement of the resonance positions was performed repeatedly with increasing precision by different groups. Currently, the best experimental data located the first resonance at 543.28 ± 0.08 G by atom loss measurements [9], and the second one at 837 ± 5 G by rf spectroscopy [23]. The field at which the scattering length crosses zero was measured at 528 ± 4 G by studies of evaporation rate in an optical trap [98].

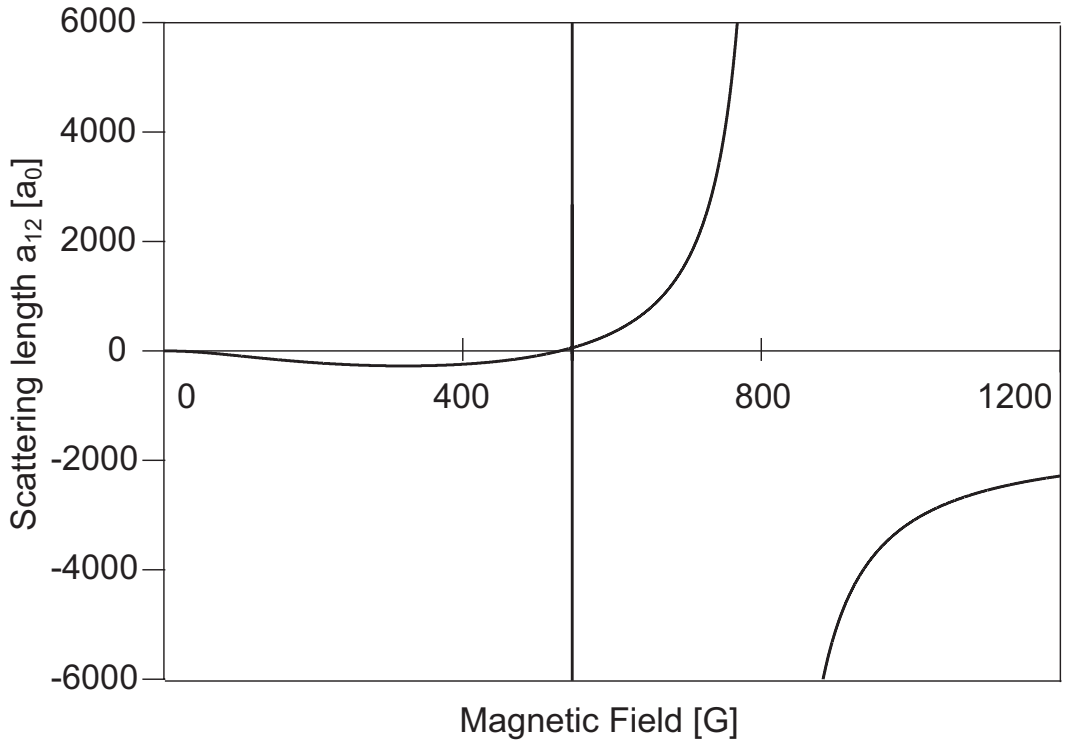

Figure 1-4: s-wave Feshbach resonances between lithium atoms in the |1> and |2> high field hyperfine states ($F, m_F = |1/2, 1/2 >$ and $F, m_F = |1/2, -1/2 >$, respectively, at low field), as recently calculated by the group of B. J. Verhaar at Eindhoven. The s-wave scattering length a_{12}, is shown as a function of magnetic field. Two Feshbach resonances occur, a narrow one at 543 G (not resolved in this graph) and a wide one at 837 G. Another important field is 528 G, where the scattering length crosses zero.

1.4 The BEC-BCS crossover

In comparison with the Bose-Einstein condensation, the zero-temperature behaviour of a Fermi gas made from identical particles is relatively unexciting: no phase transition occurs, and the system approaches slowly its zero-temperature limit.

The situation is changed in the case of mixtures of fermions which are interacting. At low temperature a superfluid phase transition can occur. This behavior was previously observed in liquid Helium-3, where a superfluid phase develops, and in the case of superconductors. In general, the transition occurs at very low temperatures relative to the Fermi energy of the system; for metallic superconductors this ratio is only 10^{-4}.

For superconductors, the existence of the phase transition is explained by the Bardeen-Cooper-Schrieffer (BCS) theory [21]. In the presence of an attractive interaction, the electron gas can lower its energy by pairwise correlating the momentum of electrons; this pairs are the Cooper pairs. These pairs have zero net momentum, and the onset of superconductivity can be understood as the formation of Cooper pairs and their simultaneous Bose-Einstein condensation.

The early proposals for observing a superfluid transition in an atomic fermionic gas [124, 61] calculated the transition temperature according to the BCS model. This temperature is given by [61]

$$T_c = \frac{E_F}{k_B} \exp(-\frac{\pi}{2k_F|a|})$$

where k_F is the Fermi wavevector and $|a|$ the scattering length. The exponential dependence on the interaction strength normally leads to a vanishingly small value for T_c, but near a Feshbach resonance the $k_F|a|$ product can, in the first approximation, reach near unity values.

BCS theory is not applicable to the the strong interaction regime, defined by near unity values of $k_F|a|$. The theoretical treatment of the regime in which the transition temperature approaches the Fermi temperature was initiated an attempt to explain the properties of thin-film superconductors [45] and later to explain the properties of high-T_c superconductors [81, 95]. As the coupling strength is increased from zero to very high values, two limiting situations occur. At weak coupling, BCS theory is valid and superfluidity occurs through the formation of Cooper pairs. At very strong coupling, bound pairs (molecules) form initially, and only at a much lower temperatures these bosonic pairs condense giving rise to superfluid behavior. The transition between these two regimes is smooth, and in the crossover region pair formation and pair condensation occur at distinct, but comparable temperatures.

The application of these models to ultracold atoms led to proposals for observing the phase transition in the BEC-BCS crossover [60, 128, 75, 91, 99]. High relative transition temperatures have been predicted, sometimes as high as 0.5 T_F, and more

usually around 0.2 T_F. These temperatures were definitely within our reach, and this thesis covers our progress towards observing the resonance superfluidity in an ultracold fermionic lithium gas.

1.5 Outline of this thesis

This thesis covers most of the research I was involved in as a member of the 'Lithium experiment' since the start of this project in January 2000.

The first chapter is an introduction to this research, and briefly reviews the basic techniques and concepts we use in our work. This knowledge was accumulated during years of research in and outside our lab, and forms the foundation from which we started the exploration of the physics of ultracold fermions.

Chapter 2 describes those parts of the development of the experimental apparatus in which I was involved, both during the initial set-up stage and throughout the following years. In addition to this chapter, Appendix H lists many of the suppliers we have used to build and upgrade the apparatus.

Chapters 3 through 6 cover research done using our ultracold ^{23}Na - ^{6}Li apparatus. The original reporting of these results was done in published papers which can be found in the Appendices. The chapters covering this work are an introduction and at the same time a complement to the published papers. The comprehensive experimental details and parameters can be found in the appended papers.

The first of these chapters covers our efforts to cool fermionic ^{6}Li to quantum degeneracy, and to produce a degenerate ^{23}Na - ^{6}Li Fermi-Bose mixture, including recent cooling techniques not covered in the first papers.

Chapter 4 covers the first observation of Feshbach resonance between different atomic species, which in our case are fermionic ^{6}Li and bosonic ^{23}Na. Extending the data analysis presented in the published paper a full list of predicted resonances was generated and can be found in Appendix G.

Chapters 5 and 6 cover the production of weakly bound $^{6}Li_2$ molecules, and the exploration of the BEC-BCS crossover in a strongly interacting fermionic gas, through

the observation of Bose-Einstein condensation of molecules, and through the observation of fermion pairing and the condensation of these pairs.

Part of the collaborative research done as a member of the 'Lithium lab' is not covered here, and can be found in the following papers:

K. Dieckmann, C. A. Stan, S. Gupta, Z. Hadzibabic, C. Schunck, and W. Ketterle, 'Decay of ultracold fermionic lithium gas near a Feshbach resonance', Phys. Rev. Lett. 89, 203201 (2002).

S. Gupta, Z. Hadzibabic, M. W. Zwierlein, C. A. Stan, K. Dieckmann, C. H. Schunck, E. G. M. van Kempen, B. J. Verhaar, and W. Ketterle, 'Radio-Frequency Spectroscopy of Ultracold Fermions', Science 300, 1723 (2003).

C. H. Schunck, M. W. Zwierlein, C. A. Stan, S. M. F. Raupach, W. Ketterle, A. Simoni, E. Tiesinga, C. J. Williams, and P. S. Julienne , 'Feshbach resonances in fermionic ^{6}Li ', Phys. Rev. A 71, 045601 (2005).

M. W. Zwierlein, C. H. Schunck, C. A. Stan, S. M. F. Raupach, and W. Ketterle , 'Formation Dynamics of a Fermion Pair Condensate', Phys. Rev. Lett. 94, 180401 (2005).

Chapter 2

Apparatus for cooling ^{6}Li and ^{23}Na

This chapter describes the apparatus used for the production of degenerate lithium and sodium gases. This apparatus has a long history of cooling alkali gases to degeneracy, and it was constantly upgraded for more complex experiments. The most significant modification was the upgrade from a ^{23}Na BEC apparatus to a degenerate Bose-Fermi, ^{6}Li-^{23}Na apparatus.

Starting with the conversion to a two-species machine, the major upgrades not already described in other theses [11, 13, 14]are covered in detail. Detailed descriptions of the ^{23}Na BEC apparatus can be found in previous theses from our group [67, 122].

2.1 Overview of the experimental setup

This is a brief overview of the experimental setup. This division of the setup into different parts is not the only one possible. The one presented here is partly inspired by the division of experiment building into technically similar tasks.

2.1.1 Isolation from the environment and the atom sources: the vacuum chamber

Except for the trapped atoms, all the experiment is at room temperature or above. Taking into account that cold atom experiments hold the record for the lowest tem-

peratures ever achieved, the thermal isolation between atoms and the experiment is remarkable.

The isolation is achieved by levitating the atoms in a trap placed inside an ultra-high vacuum (UHV) chamber. Atoms can be coupled to the environment in three ways: by thermal radiation, by fluctuations of the potential of the atom trap, and by collisions with the background gas existing in the experimental region. The first two couplings are or can be made negligible [43]. In our apparatus the collisions with the background gas are the limiting factor for the lifetime of a ultracold atom sample, and can be reduced by reducing the pressure in the experiment chamber.

Any collision between a trapped atom and a fast background gas molecule results, with a high probability, in removing the atom from the trap. The lifetime of the trapped atoms is then defined by the collision rate with background atoms R_{bg}, estimated by $R_{bg} = n_{bg}\sigma_{bg}v_{bg}/4$ where n_{bg} is the density of the background gas molecules, v_{bg} the average thermal speed of these molecules, and σ_{bg} the collision cross-section. Assuming a pressure of 10^{-11} Torr, room temperature, and a typical cross section of 10 Å^2, this gives a rate of 0.04min^{-1}, which suggests that at 10^{-11} Torr the background losses are negligible.

However, the collision cross sections of alkali are very large compared to those of usual gases. Sodium's cross sections with molecular hydrogen, argon, and sodium at room temperature are 158Å^2, 401Å^2, and 1100Å^2 respectively [114, 28]. Lithium's cross sections are less than a factor of two smaller. This brings the estimated loss rate per atom to 2-4min^{-1} and agrees with our experimental knowledge that it is impossible to cool to degeneracy (which takes around one minute) at pressures higher than a few 10^{-11} Torr.

Our experiment takes place in a multiple section steel vacuum chamber. The main section consists of a 18-way cross to which the atom source and the pumps are attached, in which the pressure is normally smaller than 10^{-11} Torr. Viewports are used to bring laser beams to the atom trap region. A detailed description of the main section can be found in [67].

The atoms used in our experiment have to be produced in the vacuum chamber,

making the atom source a part of the vacuum setup. The design of our atom source, a two-species sodium-lithium oven, is covered in the next section. As the pressure near the atom source is limited to 10^{-8} Torr, a differential pumping setup is used in joining the source with the main section of our vacuum chamber. The differential pumping was upgraded from the setup described in [67], and is covered in the next section.

2.1.2 Photons for laser cooling and imaging: the laser systems

The light used for laser cooling and trapping must satisfy a few basic requirements: it should be monochromatic and narrowband relative to the linewidth of the resonant optical transition of the trapped atoms, the light frequency must be stable within the atomic linewidth, and the intensity of the beams should be on the order of the saturation intensity of the trapped atoms.

For alkali, this requirements mean that the light used should have a linewidth of less than 1 MHz, and an absolute frequency stability better than 1 MHz. The total power needed ranges from tens to hundreds of milliwats.

Our laser systems are composed of a stable narrowband laser which is locked to an atomic resonance transition for frequency stability. The output of the laser is divided into different cooling and trapping beams. The frequency of these beams is shifted in precise amounts by acousto-optical modulators and remains referenced to the source frequency. Electro-optical modulators are used to generate additional frequency components in the same beam.

For sodium, the laser source is a Coherent 899-21 dye laser pumped by a 10W, 532nm, Millenia Xs 110 laser produced by Spectra-Physics. Details of the optical setup for sodium can be found in [122].

Lithium light is generated by grating-stabilized diode laser, DL100 produced by Toptica. The power output of this laser, 15 mW, is too low for laser cooling, and independent frequencies are amplified by seeding high-power single-mode diode lasers.

The optical setup for lithium is described in the Ph.D thesis of Zoran Hadzibabic [11] and research stage rapport of Marin Zwierlein [13].

2.1.3 Generation of magnetic fields for cooling and trapping

Magnetic fields, along with laser beams, are the basic tools used for laser cooling. The usefulness of the magnetic fields comes from the fact that that alkali atoms have relatively large magnetic moments due to their unpaired electron. Also, unlike bar magnets, atoms will not 'turn' towards the field source during experimentally relevant timescales; in a classical sense, the orientation of the dipole relative to the magnetic field remains constant.

To the first approximation, atomic energy scales linearly with the modulus of the magnetic field, which makes the design of static potential traps easy to understand: generate a field configuration with a spatial extremum in the field modulus and the atoms will be trapped (or expelled, depending on the orientation of the moment) there. In addition, different electronic levels have different magnetic moments, which leads to the original Zeeman effect: the wavelength of atomic transitions varies with the magnetic field. This effect is used in magneto-optical trapping and in the Zeeman slowing.

A given spatial configuration of the field can be achieved with either electric currents or permanent magnets. Permanent magnets cannot be switched off and they found limited applicability in laser cooling, which is a succession of a few different cooling stages which require different field configurations. Coils with high permeability cores, a common solution for basic lab magnets, have the disadvantage of core hysteresis, which makes the switch-off slow and incomplete.

Creating a given field configuration with currents is achieved in most of the cases by adding loops of wire connected in series, forming coils or solenoids. For our experiments, the design of the coils often reduces to the problem of filling a limited volume of space with loops of wire in the most efficient way.

The fields which have to be produced, up to 0.1 T, might seem small compared to the few Tesla easily achievable in a standard lab electromagnet. However, we cannot

take advantage of iron cores which enhance the field thousands of times, and the design of our coils is quite demanding. We operate our coils at current densities at which the ohmic heating rate of the copper approaches 100^oC *per second*. Of course, we do not let the temperature raise indefinitely, but we actively cool the coils. It is the cooling capacity which ultimately limits the fields we can achieve.

Given the target field parameters and the physical space in which a coil can be placed (condition especially important for the magnetic trap)one can choose to wind many turns using thin wire or a few turns using thick wire, or equivalently, one can use small or large currents to achieve the target fields. Our choice of large currents and low voltages has its roots in early atom cooling experiments at MIT which used in-vacuum coils. Such coils must have a simple design (few loops of thick wire) for compatibility with high vacuum. The high current know-how which was accumulated since then made it practical to keep using the high current design. Compared to a high-voltage design, switching and connecting are more difficult, but it is safer and allows faster switch-off times.

Our experiment was the first in which a cloverleaf magnetic trap [88] was used. This first trap served us faithfully for six years, until it was heated to destruction in just a few seconds as a result of a combined failure of the cooling setup and of the safety interlock. Our new trap, although built on the same principles as the original one [122], was optimized for steady-state production of dc magnetic fields up to 1000 G. The construction materials, the cooling system, and the safety interlock were all significantly upgraded over the first generation trap, and the description of this technological tour-de-force can be found in Christian Schunck's diploma thesis [14]. With careful temperature monitoring, uniform dc fields up to 2000 G should be achievable, but the dc power supplies needed are not yet commercially available.

Small magnetic fields needed for Earth field compensation are generated by uncooled coils made from heater wire, and wrapped around the main vacuum chamber in pairs aligned with the three orthogonal axes of the machine.

2.1.4 Optical trapping

First experiments on degenerate atomic gases, in both bosons and fermions, used a magnetic trap for the last stage of cooling. Magnetic trapping works only for hyperfine states which have an increasing energy with the increasing field, and the inhomogenous magnetic fields experienced by the trapped atoms can only be varied over a limited range. Optical dipole traps can trap any spin state in arbitrary homogenous magnetic fields, but the price to be paid is a reduced trap depth compared to magnetic traps. Nevertheless, optical traps have become an essential tool in ultracold atom research.

Optical trapping can be intuitively understood by assuming that atoms are loose neutral charge distributions which can be deformed by an applied electric field. In a static uniform field the atom will develop a dipole moment aligned with the field. If the field has gradient, the atom will experience a force towards the region of higher field intensity. This is a quite general response of a polarizable object: it also explains why light neutral objects as dust particles are captured by electrostatically charged bodies.

A light field is a time-varying electrical field. The induced dipole moment of the atom will, in general, be out of phase with the driving field. Let's assume that the atom has a single resonant frequency, which is a good approximation for alkali atoms. If driven well below the resonant frequency, the dipole will be able to adjust to changes in the field and will be always aligned to the field, thus experiencing a force towards the high intensity regions. Well above the resonant frequency, the momentary induced dipole will be in opposite phase to the field, and thus antialigned to the field. The atom will be repelled by the high intensity regions. In our lab practice, red-detuned beams are used to create attractive potentials for trapping, and blue-detuned beams to create repulsive potentials for optical manipulations of the trapped atoms.

Optical traps for ultracold atoms are realized by focusing a laser beam which has a frequency below the optical resonance of the trapped atom. The focal region has the highest intensity and atoms are trapped there. We trap both sodium and lithium

using a 20W, 1064 nm Nd-YAG laser focused to a few tens of microns.

Switching of the trap on or off faster than one microsecond is achieved by controlling the power of the rf source which drives an AOM inserted in the beam path. rf power modulation is also used to control laser intensity, and thus trap depth, over four orders of magnitude.

2.1.5 Hyperfine state manipulation: the rf setup

Transfer between different hyperfine ground states can be done by driving direct transitions between states, or by optical pumping involving temporary transfer to an excited state. The direct transfer is slower than the optical pumping, but increases the kinetic energy of the atoms by a negligible amount compared to the energy scales in an ultracold gas. It is the preferred method for state manipulation in ultracold gases when speed is not critical.

Evaporation in the magnetic trap is done by selective transfer of the highest energy trapped atoms to magnetically untrapped states. Direct transfer between different hyperfine states in lithium is required by our cooling procedure. These tranfers are done by either using rf radiation at the transition frequency, or by performing an adiabatic Landau-Zener sweep across the transition frequency.

The rf fields are generated by a setup in which rf signal from a frequency synthesizer is amplified to a few watts power amplifier, and sent to an antenna placed near the atom sample. Up to 500 MHz we use a rectangular multi-loop antenna placed inside our vacuum chamber, and from 1 to 2 GHz an external circular single-loop antenna. The available frequencies ranges, 1-500 MHz and 1-2 GHz, are defined by the operation ranges of the two power amplifiers we use. However, these ranges cover all frequencies needed in our experiment.

Frequency sweeping for evaporation is done in steps by updating synthesizer frequency and amplitude every 50 ms. The sweep is remotely controlled via a GPIB interface, which allows programming nonlinear sweep rates.

Hyperfine transfer is usually done with Landau-Zener sweeps which give more stable results compared to a single frequency pulse. Landau-Zener sweeps require

continuous frequency change. Fast, continuous linear sweeps with upper frequencies up to 80 MHz can be executed by synthesizers which use direct digital synthesis (DDS) technology. Above 80 MHz a continuous sweep is achieved by mixing the sweep from a DDS synthesizer with a high single frequency signal. Another sweep method we used for magnetic field dependent transitions was to keep the RF frequency constant and sweep the magnetic field instead.

2.1.6 Data taking: the imaging setup

Most of the data in our experiments is provided by pictures of the atom clouds. The atoms are illuminated with resonant light, and imaged on the surface of a sensitive CCD camera. As atoms absorb the resonant light, the image taken by the camera will contain the shadow of the atom cloud. In principle, images of the atoms in the trap could be taken, giving information about the density distribution in the trap, but the resolution of the imaging system is not high enough for detailed pictures. The usual approach is to release the atoms from the trap and image them after a variable time of flight, from which the total atom number and the atom momentum distribution in the trap can be extracted.

We have two imaging setups, one along the vertical axis of the machine and the other along the horizontal axis (parallel with the long axis of the magnetic trap). For each setup three lenses with focal lengths in the order of hundreds of millimeters bring the imaged point approximately one meter away from the atom traps, where space for our relatively large camera is available. Magnifications between 0.5X and 10X can be set by changing the focal length of the imaging lenses. Most of the time we operate at a magnification of 2X for both vertical and horizontal imaging. For 2X imaging we achieve an optical resolution of approximately 10 μm, comparable to the 13 μm pixel size of the camera chip.

Lithium and sodium are imaged separately by illuminating the trapped sample with the proper resonant light. In the case of mixtures using light resonant with one given species will image only that species as the light is not absorbed by the other species. Imaging both species in the same experimental sequence is possible by either

taking a lithium and then a sodium image in rapid sequence, or by setting the imaging such that sodium and lithium clouds are imaged in different positions on the camera chip, case in which both resonant light beams can be turned on simultaneously and the resulting image will contain shadows from both species.

2.1.7 Control of the experiment

The remotely controllable parameters of our experiment are either digital (whether a given laser beam is on or off, for example) or analog (the value of the current given by a power supply), and a set of these values defines the state of the apparatus. In total, we can control 64 digital values and 16 analog values. An experimental sequence is then defined by the time variation of the apparatus state (or the 'word' in lab jargon).

A computer program used to generate the experimental sequence as a series of consecutive apparatus states, each state being maintained for a given time. The experimenter inputs the sequence of states and their duration. This sequence divided into a sequence of equal and much shorter experimental states which loaded into the memory of the computer. Two digital, and two analog digital output PC cards use the memory data to generate synchronously TTL and 0-10 V analog signals which we use to control the apparatus state.

The simplest experiments, as for example the production of a BEC, need less then 10 states which are the basic laser cooling stages: MOT loading, capture in the magnetic trap, evaporative cooling, and an imaging sequence. Some of the experiments described in this thesis needed up to 50 successive experimental states.

2.2 Upgrade of the vacuum chamber for two-species experiments

A lithium-sodium experiment built on the structure of a sodium experiment needs, in addition to the built-in atomic sodium source, an additional atomic lithium source. Adding a second lithium source is the straightforward solution, but rather than in-

creasing the complexity of the experiment, we have chosen to develop a single dual atomic source. This approach allowed for a simplified Zeeman cooling scheme, and saved time by limiting the extent of modifications to our existing vacuum chamber. Also, since it was not clear initially that the goal of cooling fermions can be achieved, easily reversible modifications to our running BEC experiment were the best choice. The new dual source was designed to be fully interchangeable with the existing sodium oven.

Another reason for which the dual source was appealing to us is linked to the history of the original ^{23}Na BEC machine which was to be upgraded to a two-species experiment. It has been under vacuum since 1996, and there were concerns that the assembly of the vacuum chamber was not perfect. Despite reliable performance since 1996, it was hard to predict whether the chamber could achieve ultra-high vacuum after being vented. The main concern was (and still is) that repeated baking at too high temperatures in the past will prevent us from re-baking the chamber.

To keep the upgrade to a two-species experiments simple, not loosing the vacuum in the main chamber was considered crucial. We know now, from the experience of BEC II lab, that after a very clean venting with ultrapure argon it is possible to achieve UHV without baking. However, given the knowledge about vacuum technology within our group at that time, the 'vacuum fear' was legitimate.

As stated in the previous section of this thesis, the only place for the atom source(s) is inside the vacuum chamber. Apparently, this means that a adding a new species to an experiment cannot be done without breaking vacuum. However, in the old BEC experiment the main chamber and the atomic oven were isolated by a gate valve so that sodium changes can be performed without losing the vacuum in the main chamber.

The gate valve is placed before the Zeeman slower. This means that the only way for the lithium atoms into the machine is to come along with sodium through the Zeeman slower which was designed for sodium. In addition, if we wanted to load a reasonably-sized lithium MOT from an atomic beam, we also had to increase the flux of slow lithium atoms. Fortunately, calculations show that a Zeeman slower designed

for sodium will work for lithium, the price to be paid being a smaller relative velocity capture range (see discussion in [1]).

Summing all these considerations, the design requirements for the new atom source were that it should produce overlapping atomic beams of sodium and lithium, sodium beam being (at least) as intense as the existing sodium beam, and ideally the sodium/lithium fluxes should be independently tunable. Also, the fast atom beams should be both slowed by the existing Zeeman slower.

The vacuum upgrade parts and concepts were built and verified separately from the BEC machine. We have built an auxiliary atomic beam experiment, which contained an effusive lithium oven with the same design as the sodium ovens used in our BEC experiments, a third generation spin-flip Zeeman slower designed for sodium [30], and a magneto-optical trap for lithium.

The auxiliary setup allowed us to test the concept of two-species Zeeman slowing, and also to accumulate a lot of useful knowledge about the properties of lithium. The Zeeman slower designed for sodium worked well for lithium. However the construction of the lithium oven was more challenging. While the simple design imported from the sodium ovens used in the BEC machines was good, the standard materials we used caused failures in the new operating regimes.

The lithium oven had to be operated at 400-450 °C. At this temperature, the external band heaters corroded and sometimes failed, and the copper gaskets bonded to the knife edge flanges. A bonded flange is extremely difficult to disassemble; if enough force is applied (by this meaning hammering it) it will yield, but the flanges cannot be reused.

We have tried nickel gaskets to avoid bonding. As long as they are not wetted by liquid lithium, bonding is avoided. If exposed to liquid lithium, the nickel gaskets absorb lithium forming a brittle, soft, and adhering-to-steel alloy. Both times I have disassembled flanges in which nickel gaskets were exposed to liquid lithium the gasket was torn in two parts, with each part solidly stuck to one of the flanges. In addition, lithium diffuses to some extent through the nickel and green deposits (probably lithium salts) are found outside the flanges.

Even if the lithium wetting is avoided, nickel gaskets did not seal reliably because the gaskets are too hard and the knife edges could not cut deep enough into them for a good seal. The use of flanges made from type 316 stainless steel in combination with nickel gaskets eventually solved the sealing problem. Having figured most of the lithium handling tricks, we were ready to build a two-species sodium-lithium atom source.

2.2.1 The ^{6}Li-^{23}Na atomic oven

The simplest vacuum upgrade strategy required the development of a two-species source. When we have started the upgrade, we could not find any reference about a two-species atom source. A two-species thallium-sodium oven was under development at Berkeley, but we were able to learn about it [113] only after completing our own design.

Facing the task of inventing a two-species source, the best approach was to keep it as simple as possible. The source was going to be a two-species oven based as much as possible on our own sodium oven design, which will have a single nozzle from which both sodium and lithium will effuse forming a two-species atomic beam.

The main design challenge was the big difference in the vapor pressures of sodium and lithium at the same temperature, which meant that a single-chamber oven in which both lithium and sodium would be heated will not perform well enough as a lithium source. The solution for the difference in vapor pressures was a multiple chamber oven design, shown in Fig. 2-1.

What took most of the build time – almost one year – was learning how to deal with lithium. It took only one Saturday morning to design the chambers and the nozzles, and this design worked from the first attempt. Ovens are relatively simple devices and their properties can easily be calculated analytically. This design operated with excellent performances, and it was duplicated in the BEC2 apparatus as part of their upgrade to lithium-sodium operation.

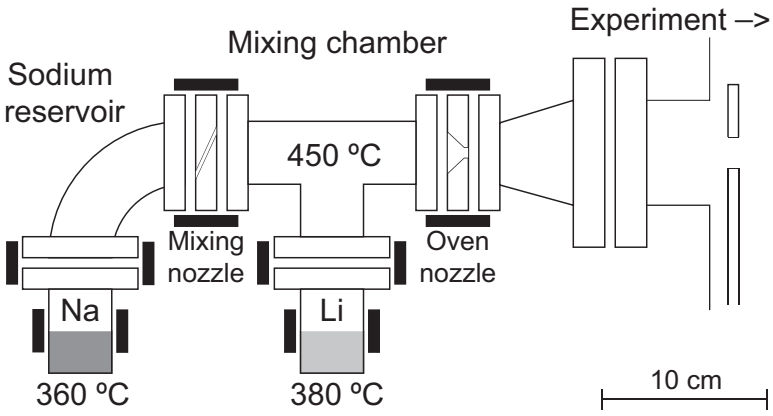

Figure 2-1: Exploded cross section view, to scale, of the ^{23}Na-^{6}Li source. The oven is built from 2.75 inch ConFlat fittings, made from 316 SS. Alkali receptacles are capped half nipples, and the nozzles are machined from double-sided blanks. The 2 mm diameter mixing nozzle is angled to achieve a length of 32 mm, and the thin oven nozzle has a diameter of 4 mm. A copper plate with a 7.5 mm hole, shown at the right edge of the figure, acts as a collimation aperture. Black rectangles represent the six resistive band heaters used for temperature adjustment. The shown temperatures of the alkali receptacles and of the mixing chamber are typical for double species operation.

Design and construction of the multiple species oven

A detailed description of the oven, and the design criteria for a more general multiple species source are found in the following publication:

C. A. Stan and W. Ketterle, 'Multiple species atom source for laser-cooling experiments', Rev. Sci. Instrum. ***76****, 063113 (2005).*

(Included in Appendix A) Ref.[1]

For those interested in effusive ovens design, two old, but still useful design references can be found in Norman Ramsey's book [107] and in a review of thermal atomic sources[115].

Main oven nozzle construction

The construction of the main oven nozzle (Fig. 2-2) has features not covered in the paper referenced above. It is adjustable relative to the long axis of the machine. It is

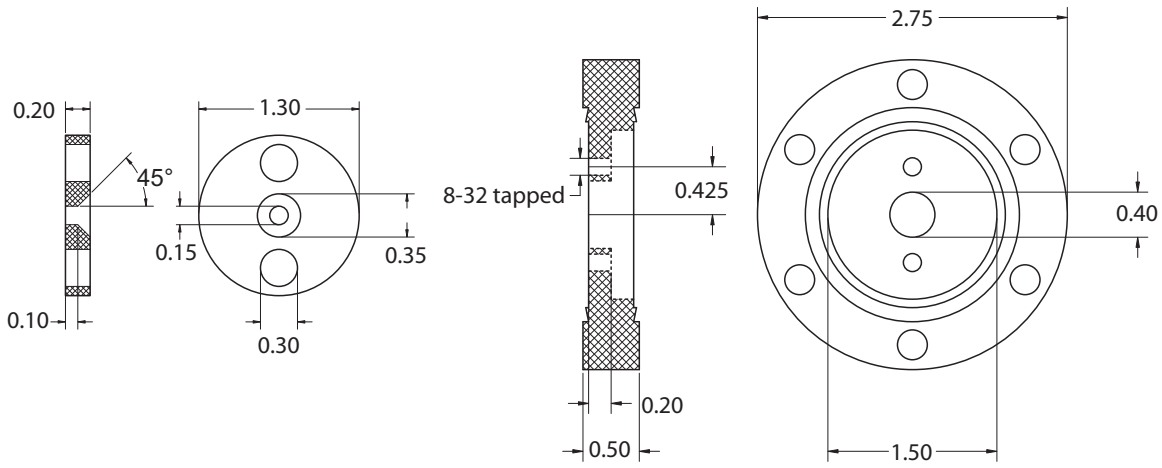

Figure 2-2: Main oven nozzle. Dimensions in inches. On the right side, the fixed part is machined from a double-sided, 2.75" CF blank. On the left side, the mobile part, is machined from 304 SS stock; the hole in the center is the oven nozzle and its position can be adjusted relative to the center of the two-sided flange. The two parts are kept together with wide head 8-32 machine screws made from 304 SS.

a necessary caution, because the oven is attached to an older chamber which cannot be easily realigned. The figure shown specifies the design of the nozzle used in the BEC1 experiment. The nozzle used in the BEC2 experiment is identical with the exception of the nozzle diameter, 0.2" instead of 0.15". This modification was done to compensate for an additional misalignment of the BEC2 apparatus.

Thermal management considerations

In my own view, most of the 'voodoo' associated with the design and operation of atomic ovens comes from bad thermal management. Proper thermal management is essential for proper operation of the double oven, and of any effusive oven. By this I mean knowing what is the target temperature for any spot in the oven, achieving that temperature reasonably fast, and with good stability. This goal can be achieved without using a large number of heaters and temperature controllers.

The number of heaters can be minimized by the proper use of insulation: the more insulation is used, the better the temperature uniformity. However, over-insulating the oven is also bad, because cooling power is necessary to lower the thermal time

constant of the oven, which leads to faster equilibration and better temperature control. In principle, an effusive oven can be operated by a single heater placed near the nozzle, but extra heaters provide more flexible control.

Band heaters should be placed around flanges and alkali receptacles; tape heaters, hard to install reproducibly, should be avoided. Tape heaters are ideal for vacuum baking though, where the goal is to heat a large proportion of the internal surface of the chamber fast, and flanges (which have a small internal surface) can lag behind. For ovens though, heating should be applied to the parts which have the highest thermal inertia, and to points where precise temperature control is desired, as the alkali receptacles.

The power of band heaters should match their thermal load; at normal operating temperature, a heater should operate at one third to one half of its full power. A smooth thermal gradient should be achieved, with the nozzle the hottest point and the alkali metal the coldest part. For alkali, 30-40 °C difference between the hottest and coldest spots is enough to prevent clogging if the gradient is smooth; the higher the difference, the better.

Using faulty gaskets and fittings

Unfortunately, the quality of 'standard' nickel gaskets varies between different manufacturers and even from different batches. Older nickel gaskets were manufactured by punching them from a nickel plate. Their surface is rugged, and they cannot be used for multiple sealing because gasket's surface features imprint on the knife edges. Newer gaskets are machined to achieve surface uniformity. However, machining sometimes hardens the gasket surface to the point at which a reliable seal cannot be achieved. The best nickel gaskets we have used (a particular batch from MDC) can seal even against standard 304 SS fittings, while the best 316 SS fittings (made by A&N) work even with punched nickel gaskets.

While building the oven for the BEC2 apparatus, we have experienced repeated sealing failures because we tried to use lower quality fittings with relatively hard gaskets. The quality of the fittings is ultimately defined by their sealing properties,

but in this case the difference between the good and the bad fittings was visible in the quality of the machining.

For a first seal (at least), leaks can be fixed by heating the flange to high temperatures. We have done it at 500 °C for one hour. Most likely this works because the nickel alloy used, Nickel 200, has a sharp change in mechanical properties between 300 and 400 °C, its elongation under constant stress increasing by almost 50%. It is therefore possible that heating to only 400 °C will be enough.

We have recently ordered a new set of nickel gaskets from Vacs SEV Co. We have not tested them yet, but we hope these are the best gaskets we can get, for two reasons. First, according to the manufacturer machining and annealing are very well controlled. Second, Nickel 201 instead of Nickel 200 is used. With a lower carbon content than 200, 201 is softer and rated to higher temperature: 677 °C instead of 315 °C.

2.2.2 Two-stage differential pumping

Combining high intensity atomic beams with UHV in our apparatuses requires the use of a differential pumping setup. A collimated atomic beam is compatible with UHV because as long as there are no collisions in the beam, all atoms will travel to the same spot, where they can be captured before randomly re-scattering, which would lead to a pressure raise. For lithium and sodium the sticking coefficient to a stainless steel surface at room temperature is close to unity and special beam catchers are not needed.

In our case, introducing the atomic beam in the main chamber is complicated by the fact that the beam is generated in a section of the machine in which the pressure cannot be easily lowered below 10^{-8} Torr. In addition to the atomic beam, background gas will diffuse into the main chamber compromising the vacuum.

Reduction of the background gas diffusion while maintaining the beam flux is achieved by connecting the main and the oven chamber with a long narrow tube. In a molecular picture, what the tube does is to geometrically favor the passage of atoms in the beam, which would pass through the tube without collisions. Background gas

have to bounce randomly inside the tube many times before they can enter the main chamber, and with high probability bouncing results in returning to the high pressure chamber.

The differential pumping factor, given by the ratio of the pressures in the oven and the main chamber, is calculated from pumping speeds and conductances. As an example, we can consider the simple case of two vacuum chambers connected by a differential pumping tube. In first chamber the pressure is P_1. In the second chamber the base pressure is negligible, and the pumping speed is S_2. The conductance of the tube is C. For a typical differential pumping application we can assume that the pressure in the second chamber is much smaller and that the conductance C is small.

The gas leak into the second chamber given by P_1C. This leak is the dominant gas load in the second chamber, so the pressure there is $P_2 = P_1C/S_2$. The ratio of pressures, of the differential pumping factor, is given by $P_1/P_2 = S_2/C$ and in in principle can be made very large.

However, in our apparatuses the main chamber pumping speed is on the order of 1000 L/s, and the differential pumping tube conductance cannot be lowered below a few tenths L/s without obstructing the atomic beam. This means that to achieve below 10^{-11} Torr in the main chamber, the pressure in the oven chamber should be at most 10^{-8} Torr. Such an oven pressure was difficult to achieve, and the BEC1 apparatus needed to boost its differential pumping rate by increasing the pumping speed in the main chamber. This was done by cooling with liquid nitrogen surfaces inside the main chamber, adding one more procedure to an already complicated experiment. Also, achieving an oven pressure low enough required baking after each sodium loading, and the oven chamber had to be cleaned twice a year, which stopped the experiments up to one week for each cleaning.

The new two-species oven was expected to create a bigger gas load because its higher operating temperatures, making the original differential pumping problematic. To solve this problem we have rebuilt the whole oven section from scratch, adding an additional differential pumping stage.

The new setup is shown in Fig. 2-3. The fundamental modification is the addition

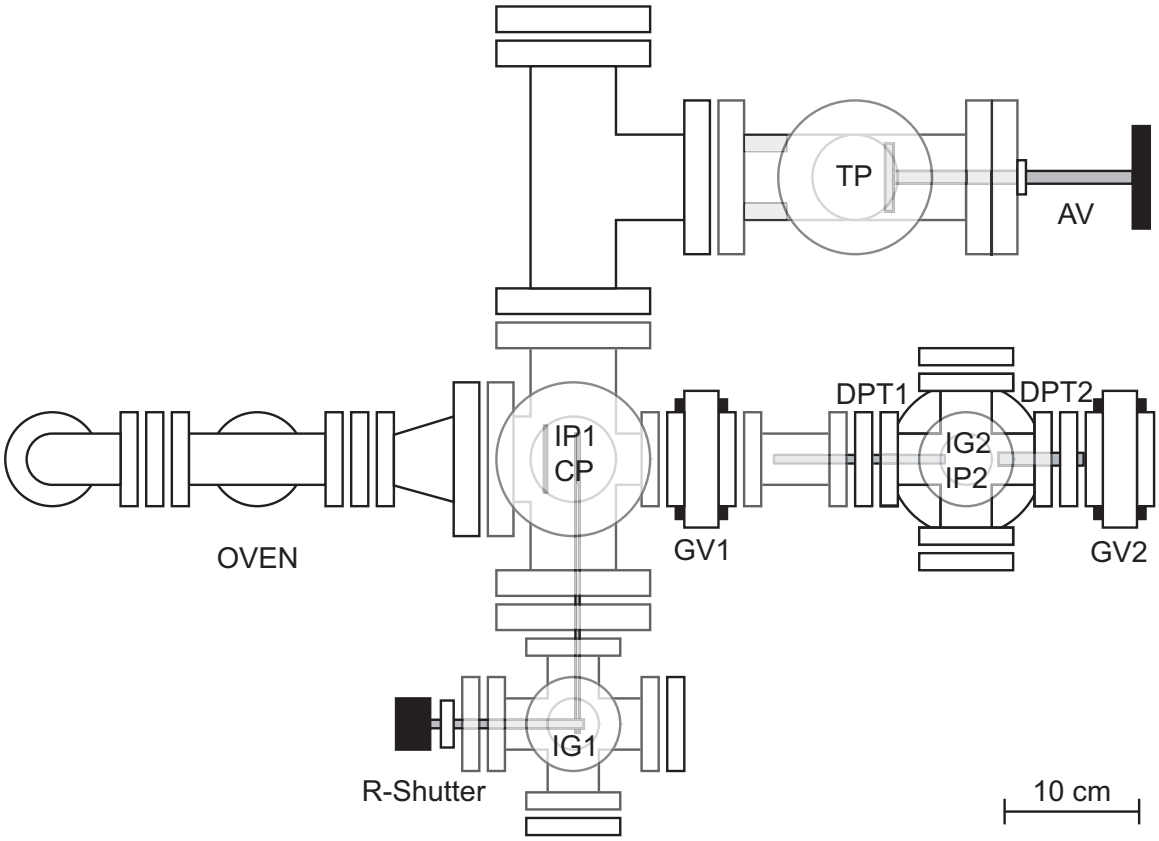

Figure 2-3: Exploded top view, to scale, of the upgraded vacuum setup. Only the components in the main horizontal plane are explicitly shown. The main parts installed above and below this plane are the ion pumps (IP1 on top, IP2 on bottom), turbopump (TP, top), ion gauges (IG1 and IG2, top) and the collimating plate (CP, bottom). Also indicated in the figure are the positions of the: oven, rotary feedthrough shutter (R-Shutter), intermediate gate valve (GV1), main gate valve (GV2), differential pumping tubes (DPT1 and DPT2) and manual angle valve (AV). The main gate valve is connects the setup to the main vacuum chamber.

of an intermediate vacuum chamber, which is a simple 2.75" CF six-way cross to which an 55 L/s ion pump, an ion gauge and the two differential pumping tubes are attached. The setup installed in BEC2 is identical with the exception of the shutter setup and the use of a 4.5" CF four-way cross instead of the 2.75" six-way cross to which the rotary feedthrough is attached.

The differential pumping tubes are shown in Fig. 2-4. The first one is similar in size and conductance to the old DPT, and creates a pressure ratio between the oven and the intermediate chamber approximately 500. The second DPT created a pressure

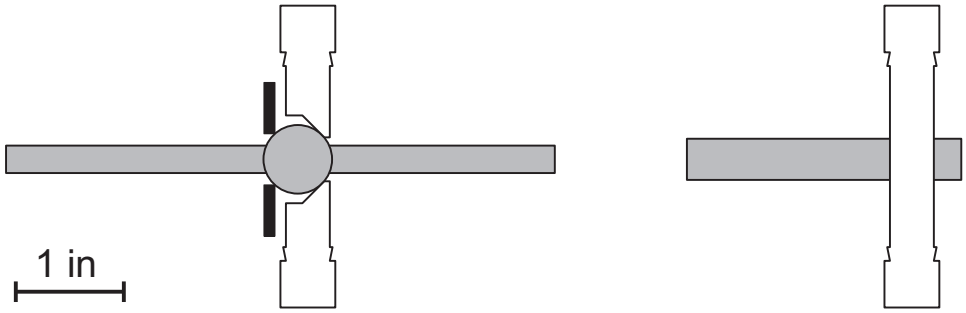

Figure 2-4: The differential pumping tubes. The image is to scale, including the relative position of the tubes. On the left side, the first DPT is made from a 5" long, 0.25" OD stainless steel vacuum tubing. It is passing through a steel ball to which it is welded. The first DPT can freely rotate against the circular hole in the flange, thus adjusting the pointing of the atomic beam. It is locked by squeezing the ball between the flange and a counterplate (shown in black in the figure). The second DPT is a 2.5" long, 0.375" OD vacuum tubing centered and welded orthogonally to another 2.75" CF flange.

ratio between the intermediate chamber and the main chamber of approximately 100. The maximum pressure ratio between oven and the main chamber, $5 \cdot 10^4$, is achieved when the pressure in the oven is high. At lower pressures the gas load originating from the oven diminishes and becomes comparable to the background load in the intermediate and main chambers and the pressure ratio drops (but the vacuum level in the main chamber still improves).

The two-stage differential pumping setup allows for quite high oven pressures. In BEC2, healthy sodium BEC's have been produced at an oven pressure of $7 \cdot 10^{-7}$ Torr. Such oven pressures are actually hard to achieve because even after a sodium change the pressure drops fast below 10^{-7} Torr; in the case of BEC2 we 'took advantage' of the fact that the system was freshly installed and not properly pumped down. In BEC1 we don't know the highest pressure at which experiment runs reliably, but it should be above 10^{-7} Torr.

In addition to the new differential pumping setup, the design on the oven chamber was improved for faster pumpdown after sodium changes. This was achieved by keeping the setup as simple as possible and by installing the pumps close to the custom six-way cross to which the oven is attached, to avoid losing pumping speed.

The ion pump is mounted on the top of the custom six-way cross. Previously, the fear of alkali poisoning of the pump led to a design in which the ion pump was connected to the cross via an elbow and a chevron baffle which both reduced the pumping speed. Only a baffle is used now to shield the 60 L/s pump from alkali atoms, and we had no problems with alkali poisoning in three years of operation with an already old ion pump. The 70 L/s turbopump is connected to (and isolated from) the chamber by a 4.5" CF right-angle valve which has high conductance. These upgrades and a better loading procedure (see next sections) result in achieving pressures good enough for running the experiment within hours of a sodium change, and without baking.

The total length of the vacuum apparatus exceeds the length of the optical table on which the experiment is set up. As a result, the oven section 'hangs' outside the optical table and needs a stable support. In BEC1 and BEC2 this was achieved with stainless steel profiles (Dexion and UniStrut, respectively), which were both hard to adjust and prone to sagging over extended periods of time. The new ovens and differential pumping setups are supported by cross-linked, T-slot aluminum profiles (80/20 Inc.). The setup avoids eccentric weights which would torque the chamber. The heavy ion pumps are mounted directly under or above the axis of the apparatus, improving its mechanical stability. We have discovered that even under the whole weight of the setup the structure in BEC1 did not sag or deform in three years of operation.

2.2.3 Million-cycle beam shutter and the 'cold' plate

The atomic beam has to be turned off during cooling, because the flux of hot atoms is high enough to cause significant trap losses. Also, exposing the trapped atoms for a short time to the hot atomic beam is probably the most reproducible way of reducing the number of ultracold atoms in the trap. We know empirically that our apparatus can be tuned to produce large degenerate clouds, however it is hard to reduce the number of degenerate atoms by adjusting MOT loading or the cooling parameters.

Switching the atomic beam on or off is done by mechanical shuttering. The shutter has to be reliable, reasonably fast (50-100 ms), and easy to adjust and service. The

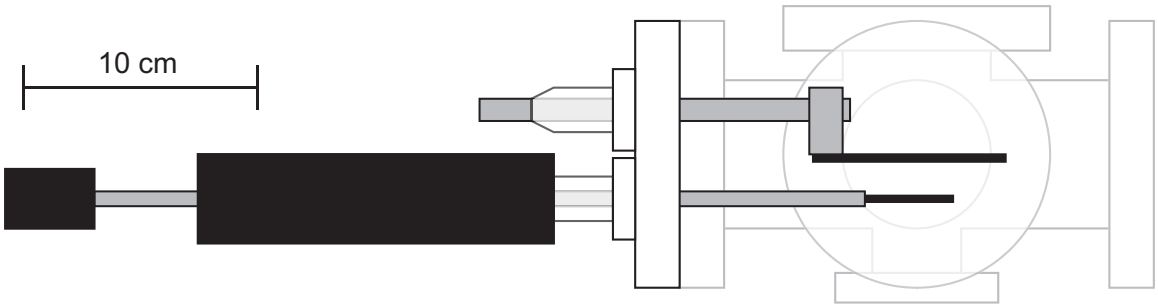

Figure 2-5: New shutter and cold plate assembly, rotated 90°. Atomic beam direction is from top to bottom. A custom 4.5" CF reducer flange has two diametrally opposed 1.33" ports. The distance between port centers is 1.5". For the cold plate the 0.375" copper rod of a commercial high-current feedthrough is attached via a joining piece to a 1/8" thick collimating plate (shown in black). The shutter consists of a pneumatically actuated linear motion actuator. A stainless steel flag (shown in black) attached to the end of the actuator's rod shutters the atomic beam.

shutter used with the old sodium oven was actuated by a solenoid placed in the oven chamber, and servicing required breaking the vacuum in the oven chamber.

When the oven in BEC1 apparatus was changed, this design was abandoned in favor of one based on a rotary feedthrough (Fig. 2-3). Although adjustable without opening the chamber, a proper balance between shutter speed and shutter backlash has to be achieved by trial and error. Initially it took a few weeks of operation to get the proper setting, and we had occasional problems caused by the sticking of the shutter rod to alkali-coated surfaces inside the custom six-way cross.

The installation of a two-species oven in the BEC2 apparatus provided the opportunity for designing a better beam shutter (Fig. 2-5). To move in vacuum, across 1-2 cm, a beam block weighing not more than a few grams, the best actuators available are linear motion feedthroughs. Coupled with a pneumatic actuator, they provide low backlash and constant force across the movement range. Also, a linear feedthrough design is simpler to attach to the vacuum chamber than a rotary one.

However, the reliability of these actuators was of serious concern: vacuum manufacturers were only guaranteeing it to 10^4 cycles, and one such actuator used in our experiment in the early 90's had a catastrophic failure leading to the venting the vacuum chamber after only a few months of operation.

The inspiration (and courage) to design such a shutter came from learning that Veeco offers such a shutter, guaranteed for one million cycles, for molecular beam epitaxy systems. Nevertheless, this commercial shutter is expensive and difficult to integrate into our design.

The 'trick' we use to vastly improve the actuator bellows' reliability is to use it only in the center, and across one-third to one-fourth, of its rated operating travel. Since we typically need half inch of travel to shutter the beam, we use pneumatically actuated, 2" linear motion feedthroughs. Restriction of the range of movement and some damping are done by stacking a few reinforced rubber washers[1] around the external shaft of the actuator. On one side they are easily stacked after removing the external stop knob; on the other side they have to be cut radially and slid through the slit in the actuator body because in the MDC feedthroughs the pneumatic actuator shaft is welded to the vacuum bellows. The total cost of the components used in this shutter is less than one-fifth of price of the Veeco shutter.

The linear shutter design was bench-tested for endurance[2] by repeatedly turning it on and off at a rate of one cycle per second. After almost two weeks of continuous operation, one million cycles were completed without damaging the bellows, which corresponds to around 20 years of running the experiment. However, the sealing o-rings of the pneumatic actuator were not lubricated during the test and started to leak after 400000 cycles. For the shutter installed in the experiment lubrication is provided by an oil mister in the compressed air line.

One of the advantages of using a linear feedthrough is the possibility to mount it on the same 4.5" CF flange as the collimating plate, as seen in Fig. 2-5. As it will be detailed in the oven maintenance section, this simplifies considerably the periodic cleaning of the oven chamber.

In the past, the collimating plate had to be TEC or liquid nitrogen cooled to achieve good pressures in the oven chamber. We have discovered that because of the better pumping speed in the new setup, cooling the collimating plate (historically

[1] McMaster-Carr, part number 90131A103

[2] It was highly unusual to do such a thorough testing, but it was granted by the fact the shutter had to 'live' for 100 manufacturer specified lifetimes.

called the 'cold' plate) is unnecessary. In the new shutter and collimating plate design we are still providing for external cooling if this is ever going to be needed, however the plate support is simplified. The plate is attached via an eccentric piece to an 1.33" CF current feedthrough. The feedthrough's 3/8" copper rod offers enough thermal conductivity to maintain a temperature difference of only a few degrees between the plate and the external part of the rod. Eccentric mounting allows for a bigger amount of alkali to be collected by the plate before cleaning is needed.

2.2.4 Lithium vs. glass: avoiding deposition on the slower window

An universal annoyance associated with the use of a Zeeman slower is the deposition of the atoms from the beam on the window through the laser slowing light is introduced into the machine. For sodium this problem is solved by heating the slower window to 80-90 °C, which makes the evaporation rate of the sodium layer on the window faster than the deposition rate.

Since our first experiments on the beam line we have tried to use the same method in the case of lithium, assuming that only the temperature will be different. A deposition formed on the slower window as expected, but upon heating to around 200 °C it was not completely cleared. Heating the window to about 300 °C made things worse: the opacity of the deposition increased, and the viewports developed vacuum leaks. Correlating this to instances of window etching when our lithium absorption cell was heated without a buffer gas inside, we arrived at the conclusion that lithium, once deposited onto glass, diffuses into the glass and chemically reacts with it, leading to permanent damage to the viewports.

Window damage occurred within one month of operation of the lithium beam setup. However, this setup did not have an atomic shutter and we estimated that for the BEC apparatus which has a lower beam duty cycle we can still run experiments for one year or more before having to worry about the slower window. Also, mild heating of the slower window was expected to reduce the deposition rate. We have

chosen the temperature to be 100 °C, which based on experimental observations we assumed it was below the threshold at which chemical reaction with the glass occurs.

Although a visible deposition formed on the slower window within months of using the BEC apparatus, we have continued to use it for three years and still have good enough MOT loading rates. From the loading rates and the visual inspection of the slower window we concluded that the transmission loss through the deposited layer was still small.

After around three years of operation, the two-species oven was removed to clean the oven chamber of deposited sodium. This allowed us to measure directly the transmission of the slower window. We have been more than a bit surprised to discover that the transmission through the deposited layer was only 20%. Such a transmission is unacceptably low, and we almost took the decision to break the main chamber vacuum for the first time in nine years and exchange the slower window.

However, as a last attempt we have tried to heat the slower window to high temperatures. This time, we calculated what temperature would be needed to desorb the layer in one day, if we ignore chemical reactions. The total thickness layer was calculated from the lithium beam flux and the estimated time spent with the atomic beam on, and evaporation rate can be calculated from the vapor pressure curves.

These back-of-the-envelope calculations resulted in a required heating temperature of 240 °C. Although the estimate of the evaporation rate was a factor of ten too optimistic, we have been able to improve the transmission of the layer to more than 50%, and thus avoid changing the slower window.

Being able to clean, even partially, the deposition, contradicts the previous observations in the beam line and lithium cell. The lithium we use was stored under oil and then chemically cleaned; vacuum cleanliness, on the other hand, could be only achieved by vacuum distillation. My best assumption is that the first time it is heated lithium releases oils and solvents and it is these substances which damage the window most. In a BEC apparatus this dirt is probably removed during the first oven bake.

To avoid lithium deposition, we are heating now the slower window to 200 °C. It is possible to heat the slower windows up to 260 °C and still maintain good vacuum

in the main chamber, although some outgassing occurs during the first heating. The only concern is the thermal insulation of the slower window.

The window has to be heated uniformly, which around 200 °C becomes a challenge as glass is thermally insulating and air currents have significant cooling power. A second viewport is externally stacked against the window, creating an insulating air cushion. To avoid a fast temperature drop during a power failure which could damage the window, thick insulation is used around the heater and the flanges.

2.2.5 Lithium preparation, beam alignment, sodium changes, and machine cleaning

Lithium preparation

Natural lithium has contains 7.5% Lithium-6 and 92.5% Lithium-7. Atomic ovens are not, to the first approximation, isotopically selective, so using natural lithium results in only 7.5% of the atoms in the beam being the isotope Lithium-6. As the resonant light frequencies are well separated, we do not have to worry about concurrent Lithium-7 laser cooling when Lithium-6 cooling light is used. Nevertheless, we use 95% isotopically enriched Lithium-6, which increases the atom source efficiency.

Enriched isotopes are usually very expensive, but Lithium-6 was produced and stocked in large quantities in US during the fifties and sixties because it is one of the strategic nuclear materials, used for rapid production of tritium in thermonuclear devices. Small quantities of enriched Lithium-6 are readily available at a price of 20-30$ per gram.

The only packaging available from commercial suppliers is in metal chunks stored under mineral oil, which are typically surface oxidized. For our experiments we need to remove the oil as much as possible, or else the oil will contaminate the vacuum chamber. However, since the lithium is a reactive metal a safe cleaning procedure is needed.

In our first lithium cleaning procedure, the chunks were first dipped in cyclohexane to remove the oil, and then the oxide layer was removed by scraping it with a knife.

It was a tedious procedure because it had to be done in a glove box.

We are now having the Lithium-6 cleaned and repackaged in sealed glass ampoules by a laboratory[3]. We have used their chemical cleaning procedure ourselves once and we have found it superior to the our first cleaning method.

The new procedure can be performed in a ventilated hood. The oil is removed using acetone, and some additional oxidation can occur. The oxide layer is chemically cleaned next by dipping in a methanol-dry ice solution. If lithium is kept in the solution for too long, it will all react with methanol and be lost. As soon the lithium surface becomes shiny and yellow, the metal is transferred to a CF nipple which is then filled with clean argon. A white powdery layer formed on the metal we cleaned since we did not work in an inert atmoshpere. However, the lithium repackaged by the laboratory has a metallic appearance and is probably cleaner.

After cleaning the lithium is not fully vacuum compatible. Baking is necessary to outgas foreign substances, which takes around one day at 400 °C. Attack of viewport glass surfaces by the outgassed substances can occur but is preventable by keeping a few millitorrs of clean argon in the chamber during baking.

Beam alignment

Alignment of the atomic beam during the installation of the new ovens was complicated by the requirement that main chamber vacuum had to be preserved. Without this requirement, it is possible to look or send a laser beam through the machine during assembly.

The two points which define the direction of the atomic beam are the center of the slower window and the center of the MOT trapping volume. The direct line of sight between these two points is obstructed by the main gate valve during the assembly of the oven section. Therefore the alignment is done to two orthogonal planes. The vertical plane of the beam is defined by two plumb lines, one suspended in front of the slower window, the other right above the MOT trapping region. The horizontal plane is defined by two rigid bars aligned parallel and at the same height as the two

[3]Materials Process Center, Ames Laboratory, Ames, IA

reference points.

The alignment of the first differential pumping tube and of the oven nozzle to the two planes can be done by eye. The accuracy of the alignment by eye is very good; telescopes or collimated laser beams are not necessary. It was necessary, both for BEC1 and BEC2, to change the position of the oven end of the slower tube. Although connected to the main chamber and under vacuum, this end can be safely and easily moved by 1-2 cm in any direction.

The alignment was checked before loading the alkali by exchanging the oven with a 2.75" CF viewport. Gate valves were opened and an unobstructed line view through the machine from the oven to the slower window was observed. The viewport exchange can be also used to verify slower window transmission and for alignment of the slower beams.

Sodium changes

With the new setup the sodium changes became easier and faster. The use of a cup allows loading more sodium than before. Instead of using a few 5 g sodium ampoules, a single 25 g or 50 g ampoule is used, which extends the time between sodium changes to three or six months.

Because some of the sodium dissolves into the lithium in the mixing chamber, depletion of sodium is not evident as soon as the sodium reservoir is depleted. It takes about half a day of sodium operation until the sodium MOT becomes much smaller than usual and the florescence of the atomic beam near the oven drops considerably, which signals that a sodium change is needed. The drop in fluorescence and MOT size can be caused by bad laser performance and it takes some experience to diagnose sodium depletion. An useful parameter for diagnose is the elapsed time since the last sodium change which is measured by a timer linked to the sodium cup heater. The sodium consumption rate is around 0.02 g/hr and can vary by at most 10-20%. With a 25 g load, sodium is not going to be depleted after only 500 hours of oven operation[4]!

[4]This is valid for BEC1's oven operating at 360°C; the consumption rate in BEC2 has yet to be

A sodium change starts with switching off all oven heaters a few hours before the oven is opened. After removing the insulation around the sodium cup and elbow, the cup flange is opened, the glass residue is thrown away, a new ampoule is broken and placed in the cup, and the cup is resealed. The insulation is refitted and the new sodium is baked by turning on the oven for a few hours. Pressures low enough for running the experiment are achieved in a few hours without baking the whole oven chamber.

For a fast pumpdown after sodium changes, it is essential that proper venting is used, and that the time between opening the oven and resealing is kept as short as possible. Grade 5.0 argon gas is used for venting. If possible, the venting line and the turbopump are kept filled with clean argon at atmospheric pressure between sodium changes. The venting line is flushed with fresh argon for 15 minutes before opening the oven. Opening and resealing the oven can be somewhat difficult because the nickel gaskets require a higher sealing torque, but with proper preparation the change time can be kept below 20 minutes.

Besides venting, two design factors of the two-species oven allow fast sodium changes. First, the narrow mixing nozzle reduces the probability of atmospheric gases diffusion when it is flushed with argon. Second, the high oven operating temperature provide by default a very fast baking of the sodium ampoule and of the sodium oven chamber.

Machine cleaning

In two or three years of operation more than a hundred grams of sodium evaporated from the oven will deposit in most part inside the oven chamber, eventually blocking the atomic beam. When this happens the sodium has to be cleaned from the chamber. In the past, this required complete disassembly of the oven setup and cleaning each part independently, a difficult and hazardous procedure.

A much simpler cleaning procedure was recently performed in the BEC1 apparatus. The sodium deposition pattern is shown in Fig. 2-6. It occurs mainly on the

determined and might be different because the main nozzle diameter is not the same.

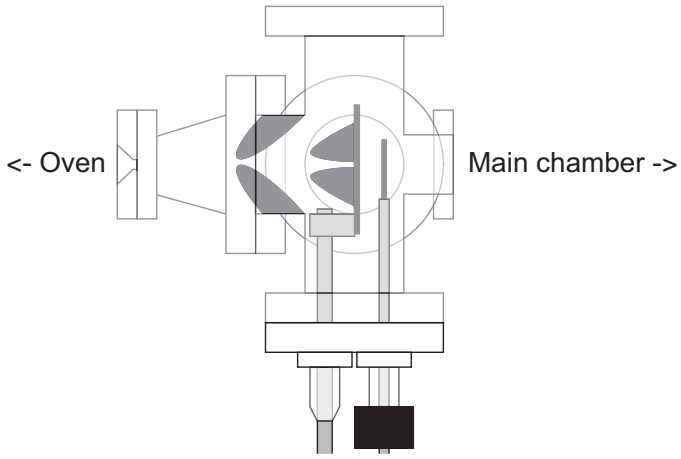

Figure 2-6: Sodium deposition pattern after 3 years of operation. Deposition occurs mainly on the cold plate and in the oven arm of the custom six-way cross. A channel forms in both lumps but becomes narrow enough to obstruct the atom beam. If the thin metal shutter flag is used, the deposition on the flag is negligible. Both lumps can be removed without full disassembly of the oven section.

collimating plate and inside one arm of the six-way cross.

To clean the plate, the most efficient procedure is to simply exchange the full shutter/plate setup with a clean one. Since the two will experiments have the same shutter/plate, a third setup should be ready for quick exchange.

The lump in the six-way cross is best removed by opening the 4.5" flange of the oven's conical reducer. The oven is then placed in an argon-filled bag to avoid degradation of the alkali in the oven. The lump should be removed by using a screwdriver or a knife. Residue on the walls can be scraped off, however extremely cautious cleaning is not necessary. Cleaning with solvents should be avoided as it will introduce vapor in the chamber. Next, the oven is reattached to the setup.

It should be possible to simultaneously clean the plate and the lump in a relatively short time so that baking of the oven chamber is not needed. During our first cleaning we were not aware of the existence of the lump, and the machine was opened twice, once for the plate and once for the lump.

Another place where sodium deposition occurs is the shutter flag. In BEC1, this deposition was always negligible, which is not well understood. My assumption is that this occurs because of shutter flag heating due to the slowing beam. At first

sight, this seems unlikely, but stainless steel, despite its shiny appearance, absorbs approximately half of the incident light at visible wavelengths *regardless of the surface quality*. Taking into account the power of the slowing beam and the small mass of the flag, this results in a local heating above the sodium melting temperature within seconds.

In BEC2, the flag is masked by the actuator's rod and this protecting mechanism will not work. Nevertheless, this suggests a flag cleaning procedure which does not involve opening the vacuum chamber. Focusing a few tens of milliwatts of sodium light at the flag should heat it locally fast enough that the sodium deposition will be melted or evaporated in a reasonable amount of time.

2.3 Lithium saturated absorption cell

Atomic absorption cells must provide a atomic density enough for at least a few percent absorption of a resonant laser beam. For all alkali except lithium, commercial cells are available. They are made of a glass tube ended with optical quality windows. A small amount of metal is placed in the chamber and the cell is then evacuated. To achieve the desired absorption, they are heated above room temperature.

Lithium are more difficult to build because they have to be heated to 350-400 °C, temperature at which reaction of lithium with the glass can make the cell permanently opaque. Also, a glass cell heated to these temperature will have a limited lifetime; in commercial glass sodium cells heated above 200 °C outgassing compromises the vacuum in a few months.

We have tried first to build a lithium cell based on the 'six-shooter' design in [82]. Although we have been able to see fluorescence for the first time by using it, this cell required constant care to avoid lithium deposition, and had a high failure rate of the cartridge heaters when operated around 400 °C. All-metal cells with sapphire windows were an alternative, but we did not attempt to build them as they required heating the whole cell at 350-400 °C.

In the end, we have designed our own cell (Figure 2-7), inspired by our experience

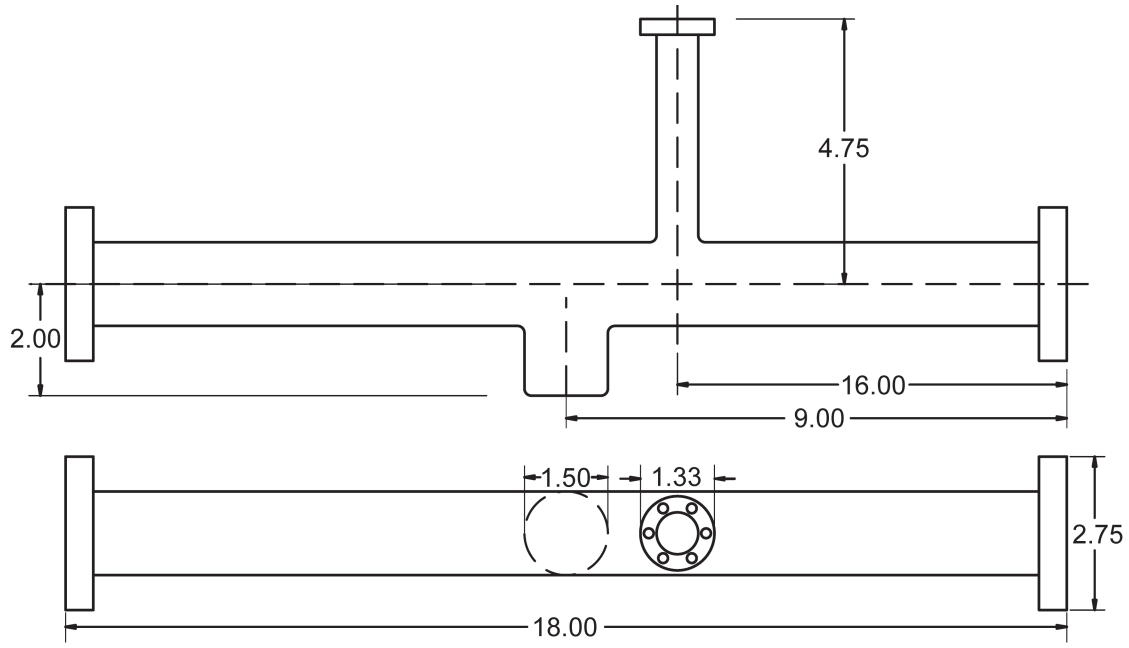

Figure 2-7: Side and top views, to scale, of the main part of the lithium saturated absorption cell. Dimensions in inches. Two standard 2.75" CF viewports are mounted to the sides, and an all-metal valve with 1.33" CF ports is attached to the top. Lithium is placed in the lower appendix. The lower appendix is heated externally by a band heater to approximately 350 °C. The cell is filled with 10 mTorr of high purity argon.

with lithium ovens. Instead of aiming at creating a uniform vapor pressure in the cell, only the lithium reservoir of the cell is heated. The lithium is evaporated from the reservoir and deposits on the cell walls. While this design consumes the lithium, the cell can be operated for a long time before all the lithium is depleted.

The cell is filled with a small amount of argon buffer gas. The buffer gas serves three purposes. First, it prevents lithium deposition on the windows which are not heated. Second, it reduces the lithium evaporation rate, enhancing the life of the cell. Third, above the reservoir the lithium atoms diffuse slowly in the buffer gas instead of flying in a straight path, which enhances the fluorescence signal. The buffer gas pressure is chosen as high as possible, but low enough that the pressure broadening of the Doppler-free signal just becomes noticeable. Buffer gas pressure is tuned by allowing a small argon leak through a metering valve while the cell is pumped with a turbopump. Pressures up to a few hundred mTorr can be set without overloading

the turbopump.

After loading fresh lithium in the reservoir, the cell is first baked at approximately 200 °C for one day, while maintaining a pressure of 100 mTorr of argon. Then, the cell is allowed to cool and the pressure is tuned while the broadening of the Doppler-free signal is monitored. After achieving the optimum pressure the all-metal valve is sealed and the cell can be disconnected from the vacuum pumps. We have found that a pressure of 10 mTorr is optimal[5].

The temperature of the reservoir is set to the lowest value at which the laser locking can be reliably done, 350 °C, for efficient use of the lithium. We first loaded the cell with a few grams of lithium and the cell worked for one year before the lithium was depleted. With a 10g load, the cell still works after two years.

2.4 The rf setup for evaporative cooling and hyperfine state manipulation

In the days of the sodium BEC experiment, the only daily interaction of the trapped atoms with rf was during evaporation. The transition used is $|1,-1> \rightarrow |1,0>$ at low magnetic field. The frequency varies from 30 MHz to 1-2 MHz. The setup consisted of a GPIB-controlled synthesizer, a 2W amplifier, and an antenna placed in the vacuum chamber.

Adding lithium to the experiment needed new frequencies. First, the sodium evaporation must be done to a different state to insure that lithium is not evaporated as well. Initially, the $|1,-1> \rightarrow |2,-1>$ transfer was used to evaporate sodium F=1 atoms. We are now evaporating $|F,m_F>=|2,2>$ atoms using the $|2,2> \rightarrow |1,1>$ transition. Both transitions are typically driven within 100 MHz of the sodium hyperfine frequency, 1.772 Ghz.

The hyperfine state of lithium has to be changed a few times during a typical experiment. The $|3/2,3/2> \rightarrow |1/2,1/2>$ transfer requires a 228 MHz oscillating field, and $|1> \rightarrow |2>$, $|2> \rightarrow |3>$ transitions at high field require around 80 MHz.

[5]The 100 mTorr value given in [13] is erroneous, as we have recently verified.

Except for the 80 MHz, the new frequencies for lithium and sodium needed new setups as the hardware in the original setup did not have the power nor the necessary bandwidth.

Besides frequency accuracy (which can be easily achieved if the frequency source is a synthesizer), the main requirement of an rf setup for generating oscillating fields is that the fields can induce stimulated transitions fast enough. In our experiments, 'fast enough' translates into the qualitatively requirements for evaporative cooling and for state transfers.

Rf-induced evaporation can be understood in the dressed atom picture formalism [68]. In this approach, one considers the total energy of the atom plus the field of N rf photons, which leads to an energy level diagram in which the Zeeman pattern is shifted upwards by $N\hbar\omega$, with ω the rf frequency. At magnetic fields at which the rf frequency is in resonance curves with $\Delta N = 1$ cross, and coupling between states transforms this crossing into an avoided crossing.

In the magnetic trap, the higher the atom energy, the higher the magnetic fields experienced at the extreme range of movement, which means that the rf frequency can be tuned such that only the highest energy atoms reach the level crossing. For efficient evaporation, these crossings have to be passed adiabatically so that any hot atom reaching the crossing can follow its curve to an untrapped. A Landau-Zener probability calculation using typical trap parameters and atom temperatures results in a required rf field amplitude of 10–100 mG.

For state transfers of ultracold atoms, the desired transfer time is on the order of 1 ms, which is typically faster than atomic losses, or the experiments we perform, so the transfer can be done without supplemental losses and not interfere with the rest of the experiment. Equivalently, this requires a Rabi oscillation frequency of $\omega_R \sim 2\pi \cdot 1$ kHz.

The amplitude of the oscillating field can be deduced from the Rabi frequency formula:

$$\omega_R = \frac{|\overrightarrow{\mu} \cdot \overrightarrow{B_{rf}}|}{\hbar}$$

where $\overrightarrow{\mu}$ is the magnetic dipole moment of the transition we want to drive, and $\overrightarrow{B_{rf}}$ is the amplitude of the oscillating field.

For transitions within the same Zeeman sublevel, driven at low field, the numerator in the formula above is equal with $g_F \mu_B B_{rf}$. From this, one concludes that the desired Rabi frequency requires on the order of 1 mG field amplitude - easily achievable centimeters away from a single-loop, centimeter-size antenna driven directly by a synthesizer. However, at high field, lithium states $|1>$,$|2>$, and $|3>$ have the same electronic magnetic spin state, and transitions between these states will have matrix elements on the order of the nuclear magneton as well. Taking this into account, the RF setup should produce oscillating fields with a maximum amplitude of 0.1-1 G; with this amplitude efficient evaporation, and the preparation of any hyperfine state are possible.

Even knowing the desired amplitude of the oscillating field, the RF setup design is complicated by the change of the antenna impedance and of the amplifier power delivered to the antenna as the frequency is varied. Also, the surrounding stainless steel vacuum chamber makes the calculation of the rf fields at the trap site very difficult. As a result I do not advise an analytical approach towards building the setup, unless one has previous expertise with the generation of rf radiation. However, the trial and error procedure can be made easier by measurements.

We have used small pickup loops to estimate the efficiency of a setup. A 1-cm diameter loop can be connected directly to an rf power meter and allows bench comparison of different antennas. The signal from the loop can be amplified for higher sensitivity.

Although we have not tried it, I believe a network analyzer could be used to diagnose and improve our setups. The analyzer's main advantage is the possibility of measuring the rf phase and power delivered to the antenna, information which can be used to make the circuit resonant.

Because of the difficulty of calculating analytically the rf setup parameters, the guidelines given below are empirical ones, learned from assembling such systems for a few different frequency ranges and two experiments, BEC1 and BEC2. They worked,

and with some unavoidable tweaking will be probably appropriate for other ultracold atom experiments.

2.4.1 Antenna design

For low-frequency applications (up to 500 MHz), we use in BEC1[6] the old rf antenna, made of two square 12 by 2.5 cm loops in Helmholtz configuration. The in-vacuum loops, separated by 2.5 cm, are centered around the center of the trap. Its total length (and the distance to the trapped atoms) are smaller than the wavelength, so the antenna operates in a quasistatic mode: the field at the atoms is the one generated by the instantaneous oscillating current in the rf antenna. In dc operation, the antenna creates a field of approximately 300 mG/A. The loop is connected to two vacuum BNC feedthroughs. We use the first one to connect the amplifier, and the second to terminate the circuit with a 5 W rated 50Ω terminator. The same port can be used to measure the power arriving at the terminator if a 50Ω attenuator and a power meter are connected instead.

The inner antenna is driven by an amplifier/multiplexer unit (see next subsection) built around a 20 W amplifier module. At 80 Mhz, up to 15 W of rf can be dissipated in the terminator; at 228 Mhz, only 7 W, probably because of the increased impedance of the coil. The absorbed power data, measured as described, is probably the best source for estimating the amplitude of the oscillating magnetic field when the coil geometry is precisely known. This setup will be duplicated to upgrade the one in use in BEC2.

For high frequency transitions (1-2 GHz in BEC1, 0.8-4 GHz in BEC2, given by the bandwidth of the synthesizers and amplifiers used in each experiment), the inner antenna is no longer appropriate. Its total length equals a few vacuum wavelengths of the rf radiation and its performance will be strongly dependent on frequency. Since we did not want to open the main vacuum chamber, the only option is to use an external antenna.

After a few attempts with different designs, the simplest design performed best.

[6]The similar design of the low-frequency antenna used in BEC2 can be found in [78].

The basic rule is to use a single loop of wire with a total length approximately equal to the vacuum wavelength of the radiated rf. In principle, a multiple wavelength-circumference loop should increase the field linearly with the number of turns, but we always found their performance to be inferior to the single loop.

Regarding construction, the simplest one again performed best: the loop is made from the inner conductor of the coaxial line which transmits the rf from the amplifier. The inner conductor is stripped to the desired length, bent into shape, and its tip soldered to the outer conductor.

In BEC1, we use an approximately 5 cm diameter round loop, built from RG-8/U coaxial conductor. RG-8/U cable was used because it has lower losses than the standard RG-58 cable. At 2 GHz, the rf power transmitted through a few meters of RG-58 drops by more than a factor of 2. The loop is placed as close as possible to the atoms, on top of the recessed top vacuum viewport of the main chamber. The distance between atoms and antenna is 8 cm. Compared to the inner antenna, it has a much weaker DC field, 7 mG/A, but as at higher frequencies the magnetic moment with which atoms respond to the external fields is the Bohr magneton [107], the fields needed are smaller.

In BEC2, 1.77 GHz evaporation was achieved using a 2.5 by 5 cm rectangular loop. The loop was made from RG-58 cable and was wrapped in teflon tape to prevent glass cell scratching and electrical contact with the magnetic trap coils. Custom high quality cables manufactured by Midwest Microwave will be used in the final high-frequency setup to reduce signal loss.

2.4.2 Using high power rf amplifiers

Commercial benchtop rf amplifiers with a few watts output are expensive. We are building our rf amplifier boxes in house, by adding the functionality we need to commercial amplifier modules: ac line operation, rf switching capability, and multiplexing multiple inputs.

Choosing amplifier modules

With the antennas we use, we have observed that amplifiers with a maximum output between 5 and 20 W are needed for 'saturating' the rf driven transitions. By 'saturation' I mean a practical criteria: for more power the gain in evaporation efficiency is negligible. For smaller power outputs, the smaller Rabi frequency makes itself felt, for example by limiting the shortest evaporative cooling time possible.

Compared to other modular rf electronics we routinely use, these high-power amplifiers are relatively expensive ($ 1-3 K, depending on power and frequency range), generally need a matched load at all times, and dissipate considerable heat. Class A amplifiers, for example, acquire their excellent operating charcteristics by consuming a constant total power regardless of the input. Part of this power is dissipated thermally, and the amplifier actually runs cooler when it delivers maximum output power.

One important (and not obvious) consideration in choosing the amplifier module is the protection options it has. It should have thermal protection (switching the amplifier off if the case temperature exceeds a certain value), input overload protection, and good load mismatch survival (operating for a while at full input, and with the output shorted or open). I have seen a few non-protected amplifier modules made by MiniCircuits failing suddenly after months or years of operation, but so far this didn't happen to any of the protected amplifiers.

The quality of the amplifier design can be judged in part by the size of the module (smaller is better) and by the power consumed for a given maximum output power(again, smaller is better).

For low frequency, we use 2-525 MHz, 20 W amplifiers produced by Delta RF Technology. For high frequency we use in BEC1 a 1-2 Ghz, 10 W amplifier made by OPHIR RF, and in BEC2 a 0.8-4.2 Ghz, 8 W amplifier manufactured by EmPower RF Systems.

Assembling an 'amplifier box'

The main concern with high power amplifiers is the proper dissipation of heat. Heatsinks are a must, and often they must be installed by us as manufacturers typically sell only the bare amplifier modules. As ready-made heatsinks of the right size are not always available, we cut them from anodized heatsink stock[7].

Even with a relatively large heatsink, forced air cooling is typically needed. The dissipated heat can slowly increase the internal temperature in a standard size 19" rack enclosure, leading to long warmup times and reducing the lifetime of electronic components.

A typical air cooling setup can be seen in Fig. 2-8. Air at room temperature is admitted through apertures which direct the air flow around heat dissipating devices: the amplifiers and the power supplies. Three or four low-voltage, low noise DC fans are used for redundancy, and circulate the air from inside to the outside of the enclosure (this 'pull' configuration makes the cooling more efficient).

The same thermal management enhances the frequency and power stability of AOM drivers and allows building multiple channels into the same enclosure. A picture of such a 4-channel driver is also shown in Fig. 2-8.

During most of the lithium experiments, multiple rf frequencies are used during a single experimental run. Having a dedicated antenna/amplifier/synthesizer setup for each frequency is impractical. The optimal hardware use and experimental flexibility is achieved by using the same antenna and amplifier, and by changing the frequency of the input signal. Some of the signals are frequency sweeps for Landau-Zener transfers and require a dedicated synthesizer only for this task, therefore we built inside the amplifier enclosure a switching setup capable of choosing between multiple rf inputs.

A 4-to-1 switch controlled by two independent TTL signals is easiest built by using two rows of standard rf switches. The first row has two switches and therefore 4 rf inputs and 2 rf outputs. These outputs are directly connected to the inputs of the second row switch. The first TTL signal controls the switches in the first row, the

[7]We have bought type 66199 and 62705 extrusions in bulk from R-Theta: http://www.r-theta.com/, Mississauga, ON, Canada.

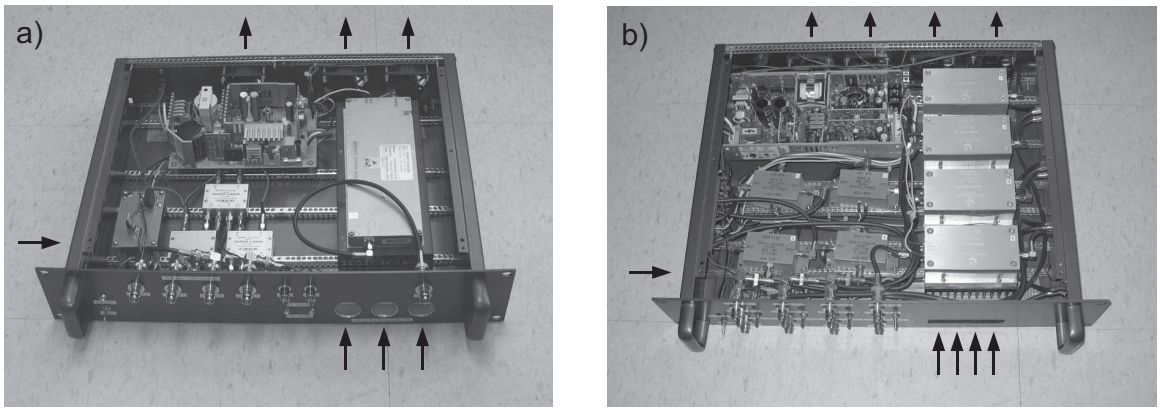

Figure 2-8: Air cooling for a high power rf amplifier. The 8W, 0.8-4.2 GHz amplifier in a) is mounted on a $4 \times 11 \times 1.25$" heatsink, with the fins facing down, in the right half of the box. Arrows indicate the the direction of the airflow. Air enters through three front, and one lateral vent holes, and is expelled by three fans in the back. Also visible inthe lower left side is the 4 to 1 switch assembly made from three rf switches. In picture b), the same cooling method is used for a 4-channel AOM driver. The four amplifiers are mounted on a single large heatsink in the right side of the box, and a large front venting slit is used.

second TTL the second row switch. For any given combination of TTL signals there is one (and only one) input connected to the 4-to-1 output. By adding more switch rows, it is possible to control 2^N channels with N logic signals. For our experiments 4 inputs are sufficient.

The high-frequency amplifier used in BEC1 has an incorporated frequency doubler because the GPIB-controlled synthesizer we use for sodium evaporation has a maximum output frequency of 1.28 GHz. It is the only amplifier box we use that does not have multiple input capability, nevertheless multiple frequency operation is trivial because the synthesizer is remotely controllable.

2.5 Optical traps for fermions using high-power 1064nm lasers

Optical traps are a standard part of our experimental setup, because the lithium hyperfine states used for experiments with interacting fermions, $|1>$ and $|2>$, are

not magnetically trappable. Compared to the optical trapping of sodium BECs, the trapping of fermionic lithium proved more demanding technically.

The cause of additional difficulty arises from the higher trap depth needed to trap fermions. In the case of BECs, the trap depth needs to be bigger than the chemical potential, which for typical experimental parameters is a few hundred nanokelvins. For fermions, the trap depth must be bigger than the Fermi energy, typically a few tens of microkelvins. As the depth of the optical traps scales linearly with the total power used[8], it can be seen that the typical power needed to trap degenerate lithium is one hundred times higher than in the case of sodium BEC's. This agrees well with our first attempts to trap lithum: if 10 mW of IR light was enough to trap a sodium BEC, at least 1 W was needed to efficiently catch lithium from the magnetic trap.

Even more power is needed for efficient evaporative cooling in the ODT. A ratio of trap depth to the temperature of approximately 10 is typically needed [96]. As at the beginning of the evaporation the temperature of lithium is approximately equal to the Fermi temperature, this brings the trap depth requirement to nearly 1 mK, and the IR power needed to approximately 10 W.

Our ODT setup, shown in Fig. 2-9, evolved from a setup appropriate for trapping sodium, going through a few iterations as the requirements for a good lithium ODT became more demanding for new experiments.

The first setup, used for the observation of Feshbach resonances in lithium-6, was typical for a sodium ODT. A 5 W, 1064 nm diode-pumped Nd:YAG laser[9] is used as a source. The beam was passed through a 40 MHz AOM for fast switching and power control, and then coupled into a single-mode fiber which selects the TEM_{00} mode. After the fiber the beam passes through a mechanical shutter and a series of 3 telescopes which expand the it to 1-3 cm diameter. The expanded beam is introduced into the horizontal MOT beam path by a dichroic mirror placed inside the last MOT telescope. The beam is then focused by the last MOT lens.

Transversal alignment of the ODT is achieved by changing the beam pointing. For

[8]Practical numerical formulas for the ODT parameters can be found in [69] for sodium and [12] for lithium.

[9]Spectra-Physics model BL-106C, Mountain View, CA.

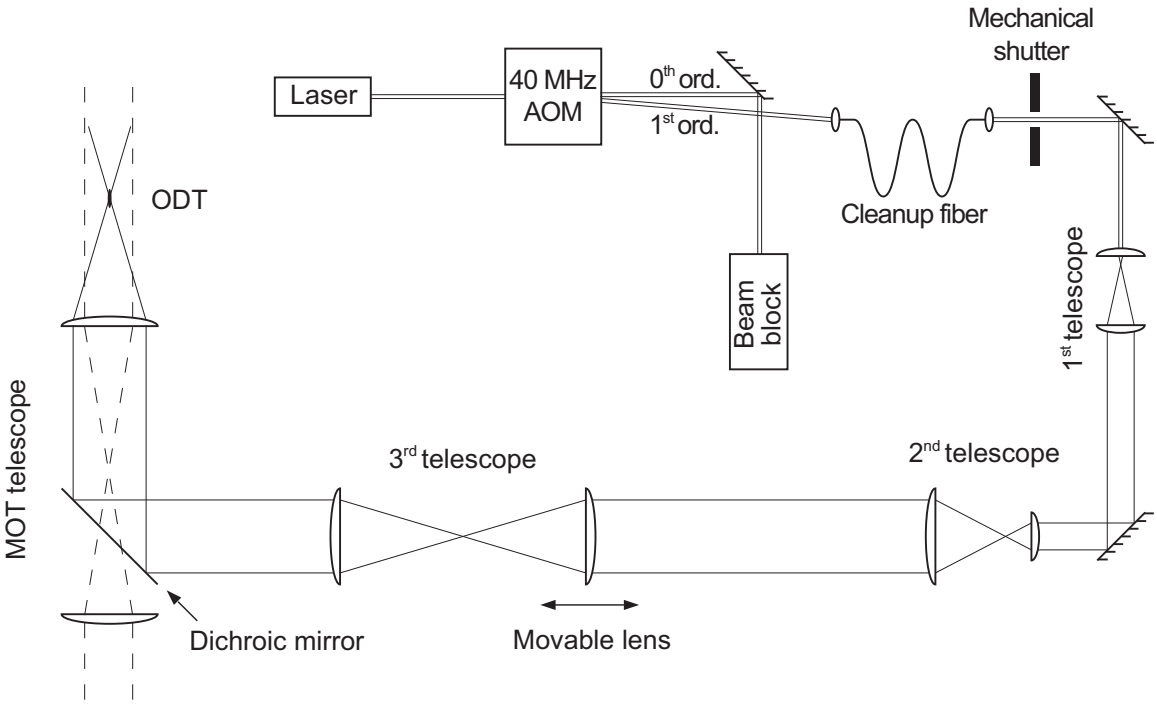

Figure 2-9: Schematic drawing of the ODT setup. The path of the ODT light is shown in thin solid line. The horizontal MOT beam is shown with a thin dashed line.

longitudinal alignment, the last telescope is built such that its focal point is imaged 1:1 onto the ODT focus. The first lens of this telescope is mounted on a longitudinal translation stage, and by moving it the longitudinal position of the focal point can be adjusted. The ODT waist is adjusted by changing the size of the expanded beam introduced into the MOT path.

The main limitation of this first setup was the maximum available power. Of the 5 W of the laser source, only up to 1-2 W can be coupled into the single mode fiber; at higher powers the fiber coupling efficiency varies in time due to the heating and thermal expansion of the fiber input port, and the fiber is easily damaged if the alignment is not perfect. Trapping the lower hyperfine states of lithium at high magnetic fields was also made more difficult by the longitudinal magnetic anti-trapping potential created by the bias coils of our old magnetic trap.

Improvement of the longitudinal trapping was achieved in part by the new magnetic trap which can create a flatter bias magnetic field, and in part by using a more

powerful source, a 20 W, 1064 nm Yb fiber laser[10]. To take advantage of the available power, the single-mode fiber was abandoned, sacrificing somewhat the beam quality. Up to 7 W were now available at the ODT position. With this setup we were able to achieve near 100% ODT loading efficiency from the magnetic trap, and to evaporatively cool lithium and lithium molecules.

This second generation setup was marginal for producing molecular lithium BECs, for two reasons. First, the ODT power could be lowered reproducibly only by a factor of approximately 100 using our power control setup. At low powers, the discreet steps of our computer generated analog signal prevented us from smoothly tuning the final trap depth. Second, the complicated optical setup easily introduced astigmatism in the beam. The trap had an asymmetric longitudinal trapping potential and even multiple longitudinal trapping maxima.

The third generation setup was made by increasing the dynamical range of the power control and by improving the beam quality and stability. The dynamical range limitation originates in the rf setup of the AOM driver. For power control an analog rf attenuator is inserted between the signal generated by an VCO and the amplifier, and controlled by one of the computer analog channels. For high attenuations (resulting in low rf powers to the AOM and low power in the beam) the attenuator becomes too sensitive to small changes in the control signal. We have solved this problem by inserting a second attenuator independently controlled by a second analog channel, which improved the dynamical range to approximately 10000.

To improve beam quality, we have used higher quality optics and more stable mounts. In the first part of the setup (AOM and the first telescope), where the beam is millimeter-sized, the hardware quality is most important. There we use 10-5 surface quality lenses with high energy coatings, and high energy mirrors, mounted on 2" high, 1.5" diameter steel rods. The stiffness of the whole setup was enhanced wherever it was possible. These efforts paid off not only in the ODT profile quality, but also in long- and short-term stability. The lifetime of molecular BECs improved from 200 ms to 10 s. Also, the new setup is stable from run to run. Previously, it was

[10]IPG Photonics model PYL-20-LP, Oxford, MA.

an event to switch on the apparatus and to discover that the ODT was still aligned.

The latest improvement, which brings the ODT quality close to the one of the magnetic trap in terms of smoothness and symmetry, was driven by the study of the rotational properties of the interacting lithium mixture in the BEC-BCS crossover. A new type of single-mode fiber designed for high powers was installed to clean up the beam profile without sacrificing power and trap depth. This setup seems to mark the end of a four-year quest in our lab for the 'perfect' single-focus ODT.

Chapter 3

Cooling ^{6}Li-^{23}Na mixtures to quantum degeneracy

The first goal of our experiment was the production of degenerate ^{6}Li Fermi gases and of ^{6}Li-^{23}Na quantum degenerate Fermi-Bose mixtures. This goal was achieved in two steps. The atom number and temperatures we have initially aimed to (and also achieved) were similar to the parameters of other degenerate fermion experiments. These first cooling experiments are reported in

Z. Hadzibabic, C. A. Stan, K. Dieckmann, S. Gupta, M. W. Zwierlein, A. Görlitz, and W. Ketterle , 'Two-Species Mixture of Quantum Degenerate Bose and Fermi Gases', Phys. Rev. Lett. 88, 160401 (2002)

(Included in Appendix B) Ref.[2]

However, soon after we had the degenerate Fermi-Bose system at our hands it became obvious that for many of the experiments we could think of, better parameters were needed. A second experimental effort was directed at improving the atom number of the degenerate ^{6}Li Fermi seas, and concluded with excellent results. The improved experimental cooling procedure is reported in

Z. Hadzibabic, S. Gupta, C. A. Stan, C. H. Schunck, M. W. Zwierlein, K. Dieckmann, and W. Ketterle , 'Fiftyfold Improvement in the Number of Quantum Degenerate Fermionic Atoms', Phys. Rev. Lett. 91, 160401 (2003)
(Included in Appendix C) Ref.[3]

The success of cooling in the magnetic trap, which is described in the attached papers, is strongly dependent on the choice of spin states for lithium and sodium and the list of 'good' spin mixtures is short. However, the use of optical traps allowed us to produce new degenerate lithium, and lithium-sodium spin mixtures. These new lithium-sodium mixtures allowed us to observe interspecies Feshbach resonances, and evaporation of lithium spin mixtures in the optical trap was essential for the experiments described in the Chapters 5 and 6.

3.1 Sympathethic cooling: our strategy and the first results

The cooling of dilute gases of fermionic atoms to quantum degeneracy was achieved a few years after the observation of Bose-Einstein condensation in dilute gases of bosonic atoms. The reason is the statistics of fermions at very low temperatures. In a sample of degenerate fermions the thermalization rate drops very fast with temperature due to the Pauli suppression of the only thermalization process possible in trapped ultracold gases, the s-wave collisions.

A thermalization rate which is fast relative to the three-body decay is essential to achieve a degenerate gas via evaporative cooling, because at the typical densities and temperatures required the gas is unstable towards the formation of a solid phase. It can be argued that the same Pauli suppression which slows thermalization would slow three-body loss as well, however losses due to the presence of background gas typically limit the duration of ultracold atom experiments to approximately one minute. Significant advances in commercial vacuum technology will be needed before successful evaporative cooling of single quantum state fermion gases can be attempted, and even so the long duty cycle of the experiment might prove impractical.

The solution for cooling fermions is the use of distinguishable particles. This opens the door for new loss processes and increases the complexity of the experiment, but it is the price to pay for producing degenerate fermion gases. A few strategies are possible. One is to use a small amount of different particles (not used for further experiments) to maintain thermalization rates while evaporating the useful component, and was not used so far for cooling fermions. The two strategies which have been used are either to start with a double mixture with equal numbers and evaporate both, or to start with a imbalanced mixture in which the more numerous component is cooled by evaporation while the useful, but less numerous initially, component is sympathethically cooled.

Having at our hands sodium BEC apparatuses which produced the largest alkali condensates to date, our approach was to use a large bosonic sodium cloud to cool sympathethically a relatively small lithium atomic cloud. Using this approach, the best one can hope in degenerate lithium atom numbers is comparable to the number of degenerate bosons, because the heat capacity of lithium (proportional with atom number for non-degenerate samples) must be at most comparable to the sodium heat capacity. Since the lithium is not consumed during evaporation, this allowed us to bypass the requirement for a large amount of precooled lithium atoms, which can be only achieved in a state-of-the-art MOT. A standard lithium MOT with 10^7–10^8 atoms is sufficient, target which can be achieved with a standard optical setup and a low-power laser system.

The experimental setup, described in the previous chapter, was thought as a low-cost modification of an existing sodium BEC apparatus, and one year and a half after starting the fermionic lithium project all the experimental bits were in place and we had a double species sodium-lithium MOT. But to actually cool lithium, a cooling process had to be developed.

At low temperatures, the losses due to spin-exchange collisions are high and usually make evaporative cooling inefficient. They have to be avoided by a proper choice of the spin states, and for single species experiments the usual solution is to use from a given hyperfine F manifold the states with maximum quantum m_F number,

because spin conservation prevents spin exchange collisions. For a mixture with different species, suppression will occur if one uses same-sign maximal m_F states for both components. This gives a few choices for 'good' spin mixtures, which are further selected by requirements for trapping (in the case of magnetic traps, magnetically trappable states must be used), and by the specifics of the experiment.

Initially, the only choice we had for a 'good' mixture was with sodium in the $|F, m_F >= |1, -1 >$ and lithium in the $|F, m_F >= |1/2, -1/2 >$ hyperfine states. In the case of lithium, a strong quadratic Zeeman effect makes the $|1/2, -1/2 >$ untrappable above 27 G, limiting the trap depth in a magnetic trap to an equivalent temperature of 330 μK. Therefore, before lithium can be efficiently trapped in this state, lithium has to be precooled in a different spin state after catching in the magnetic trap. Such a two-stage cooling method was initially used in ^{6}Li-^{7}Li sympathethic cooling experiments [118], and we have adapted it for ^{6}Li-^{23}Na cooling by performing the initial stage of evaporation in a mixture of lithium in the upper hyperfine states which are magnetically trappable, with sodium in the lower $|1, -1 >$ hyperfine state.

The results of these first sympathethic cooling experiments are shown in Fig. 3-1. The data shown is for the last stage of cooling, when lithium in the $|1/2, -1/2 >$ state is sympathethically cooled by sodium in the $|1, -1 >$ state. The number of lithium atoms, typically 2×10^5, remains approximately constant during cooling, as the losses in the this lithium-sodium spin mixture are small.

As it can be seen in the figure, the lithium temperature follows the sodium temperature only to the point at which the lithium cloud has approximately the Fermi temperature. Slower thermalization was ruled out by keeping both lithium and sodium for a few seconds at fixed trap depth, which did not bring the lithium temperature closer to the sodium temperature. The lack of perfect themalization could be due to an unfavorable rate of elastic to inelastic collisions in the sodium-lithium mixture, or just technical, however it was not subject to further studies as a better cooling procedure was later developed.

These first sympathethic cooling experiments resulted in a cold fermion gas with parameters comparable to other ultracold fermion experiments at that time. How-

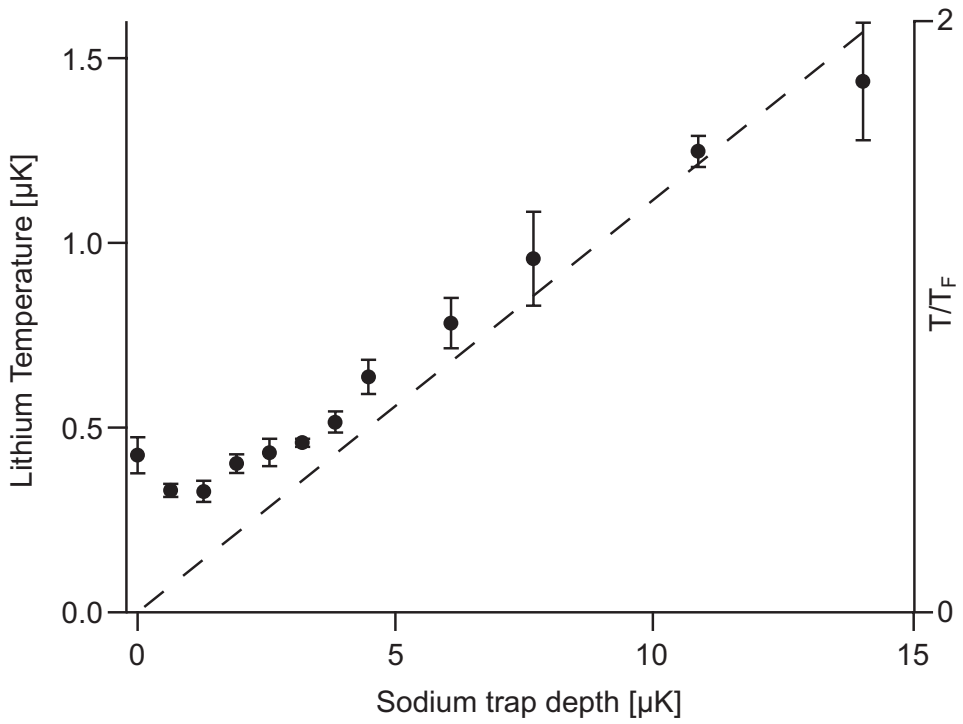

Figure 3-1: Sympathethic cooling results for a mixture of sodium and lithium in the lower hyperfine states. The black circles represent the temperature of lithium as a function of the trap depth for sodium. Lithium temperature was by fitting absorbtion images with semiclssical Thomas-Fermi distributions. The dotted line represents the expected temperature of the sodium, assuming that evaporative cooling practically stops at a ratio of sodium temperature to sodium trap depth of approximately 10. On the right axis the degeneracy is indicated. T/T_F does not scale in a perfect linear fashion with T for this data set, as the atom number varies up to a factor of 2 among different lithium data points.

ever, it soon became obvious that a wide range of standard techniques used in BEC research, as velocimetry at long expansion times or Bragg spectroscopy, could not be used with similar signal-to-noise ratios in fermionic clouds 10 to 100 times smaller than a typical sodium BEC.

The significant improvement achieved by using a sodium-lithium mixture in upper hyperfine states is covered in the next section. However, I do not think that all things being equal, a mixture of sodium and lithium in the lower hyperfine states at microkelvin temperatures is inferior to an upper hyperfine states mixture for sympathethic cooling. The shortcomings of our first cooling procedure most likely originate

in the complicated procedure for evaporation in the magnetic trap. It was not obvious, and therefore not attempted, to optically pump the lithium atoms from the MOT in the $|3/2, 1/2>$ upper hyperfine state which seems to have lowest losses in a mixture with $|1, -1>$ sodium atoms. Also, we were not able at that point to have a highly efficient rf-driven hyperfine transfer between the upper and the lower states. Our skills at transferring atoms using rf and microwave fields have increased since then and I believe if we would try the same procedure today better results can be achieved.

3.2 Sympathethic cooling in the upper hyperfine states

There are two sodium-lithium mixtures in which spin exchange is suppressed, and which are magnetically trappable: $|1, -1>$ sodium with $|1/2, -1/2>$ lithium, and $|2, 2>$ sodium with $|3/2, 3/2>$ lithium. Our first cooling procedure produced the first one. Since the second mixture has a higher energy, it was reasonable to assume that it would be worse than the lower state mixture for sympathethic cooling. However, since the upper states are magnetically trappable at all fields, it was hoped that a simpler (and thus less lossy) cooling procedure was going to lead to better results.

Upper hyperfine state cooling was not initially an option in the magnetic trap, since sodium could not be efficiently cooled and then condensed in the $|2, 2>$ state before. The first upper hyperfine state sodium condensates have been achieved by rf transfer of a $|1, -1>$ sodium condensate in an optical trap [50]. From this work, which investigated the properties of $|2, -2>$ and $|2, 0>$ condensates in an optical trap, and from subsequent work on optically trapped, rf-produced $|2, 2>$ condensates in a magnetic trap [79], two important facts were revealed.

First, the lifetime of $|2, 2>$ and $|2, -2>$ stretched state condensates was a few seconds. Although smaller than the lifetime of a $|1, -1>$ condensates, this lifetime indicated that direct evaporative cooling to BEC in the $|2, 2>$ stretched state should

be possible. The second important observation was the very small lifetime of condensates in the $|2,0>$ non-stretched state, which revealed that the losses and cross section for spin exchange in the upper hyperfine manifold of sodium are very high.

For direct condensation in the upper state, a significant fraction of the MOT atoms have to be loaded into the magnetic trap. Here significant means comparable to the loading efficiency of $|1,-1>$ atoms. Since most of the atoms in our dark MOT are in the lower manifold distributed equally among the sublevels, and out of the three states only one is trappable, approximately one third of the MOT atoms are loaded, and they are all in the same state.

To load $|2,2>$ atoms, the MOT atoms are optically pumped from the F=1 to the F=2 manifold (hyperfine pumping) using F=1→F'=1 resonant light, and within the upper manifold towards the stretched state (Zeeman pumping) using F=2→F'=2 resonant light. Both pumping beams are σ^+–polarized. Although we can control independently the duration and sequence of hyperfine and Zeeman pumping, simultaneous pumping also works well.

The light frequencies for optical pumping were chosen empirically by using different pairs of F→F' transitions for the best results. Although for hyperfine pumping the F=1→F'=2 transition has a better Clebsch-Gordon coefficient, we achieved best results with F=1→F'=1 pumping in both BEC1 and BEC2 F=2 cooling experiments.

After optical pumping the sodium cloud is loaded in the magnetic trap, and is composed of a mixture of $|2,2>$, $|2,1>$, and $|2,0>$ magnetically trappable hyperfine states. Removal of atoms in the $|2,1>$ and $|2,0>$ states is essential as they have a short lifetime due to spin-exchange collisions and produce losses of the $|2,2>$ component as well. This is done by separating the state energies with a 80 G magnetic field and selective RF-induced spin flip to untrapped states of the $|2,1>$ and $|2,0>$ states.

At the highest densities achieved during evaporative cooling, the few second lifetime of the pure $|2,2>$ cloud was too short to obtain a large condensate. Therefore, the cloud density is reduced during evaporation by decompressing the magnetic trap. The decompression point is chosen by stopping the evaporation at various trap depth

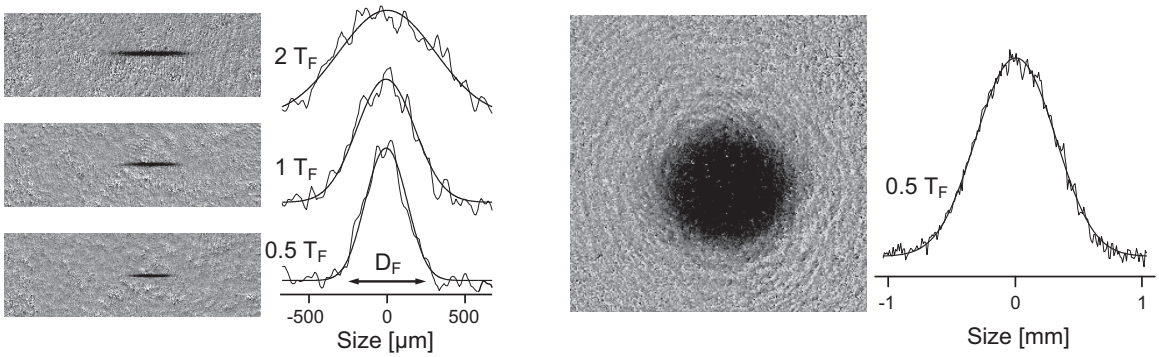

Figure 3-2: Absorption images and corresponding Thomas-Fermi fits of ultracold lithium clouds obtained by two cooling methods. On the left side, three images, in trap, of lithium in the $|1/2, -1/2>$ hyperfine state sympathethically cooled by $|1, -1>$ sodium atoms, at different temperatures. On the right side, a typical lithium image after 8 ms TOF in the case of cooling $|3/2, 3/2>$ lithium atoms with $|2, 2>$ sodium atoms. The size of the images ($\sim$3mm) and the normalization are similar for all images, thus the area of the clouds is indicative of the gain in atom number, from 1-2$\times 10^5$ to 3-7$\times 10^7$. With the first method, the lowest temperatures were around 0.5 T/T_F, while temperatures as low as 0.05 T/T_F have been achieved with the second method.

and observing the losses in the sodium cloud. The trap is decompressed upon reaching the trap depth at which losses start to occur, which corresponds to a temperature of approximately 10 μK. The evaporation is then resumed and F=2 BECs with up to 2$\times 10^7$ atoms are obtained.

Knowing how to cool large numbers of $|2, 2>$ sodium atoms, sympathethic cooling of $|3/2, 3/2>$ lithium atoms was straightforward. Zeeman and hyperfine state optical pumping are done after the lithium MOT in the same fashion as for the sodium, however the lower densities of the lithium cloud allow near full transfer of the MOT atoms to the $|3/2, 3/2>$ state. Throughout the sodium evaporation the lithium atom number remains constant, so most of the lithium caught in the magnetic trap is cooled to degeneracy.

A visual example of the improvement in atom numbers by using the upper hyperfine state method and of the resulting signal to noise can be seen in Fig. 3-2. If before imaging could only be done in trap or at very short time of flights, the increased atom

number allows crisp absorption imaging for millimeter-sized clouds expanded during time-of-flight. As the lithium atom number is similar to the one of the largest alkali BECs, the experimental methods developed for condensates can be applied to our degenerate Fermi gas while achieving the same signal-to-noise levels.

3.3 Production of sodium-lithium degenerate mixtures in other spin states

The degenerate sodium-lithium mixture in the upper hyperfine states, or the just the lithium Fermi gas are the starting sample for our experiments. However, most of the mixture experiments done afterwards, or the one we think of doing, need a sodium-lithium mixture in other hyperfine states. This section covers the production of Bose-Fermi mixtures; the evaporative cooling of lithium-only spin mixtures, which completes the list of cooling methods used in our experiment, can be found in Chapter 5.

The spin state of a single component degenerate cloud can be manipulated relatively easily using rf Landau-Zener sweeps. Using multiple rf fields, the spin state of different components can be in principle changed sequentially or simultaneously to transfer the mixture components to the desired states. We have observed significant losses during our first attempts to do multiple Landau-Zener sweeps. Also, another problem associated with the production of spin mixtures from a degenerate $|2,2>_{\mathrm{Na}}$-$|3/2,3/2>_{\mathrm{Li}}$ mixture by rf transfer is the shot-to-shot stability of atom numbers and sodium/lithium number ratios. We have overcame these problems to create a ground state $|1,1>_{\mathrm{Na}}$-$|1/2,1/2>_{\mathrm{Li}}$ mixture. The procedure used there should be applicable to other mixtures as well.

3.3.1 Production of ground state sodium-lithium mixtures

A degenerate ground state mixture was produced for the observation of interspecies ^{6}Li-^{23}Na resonances [4]. Since the ground states are not magnetically trappable,

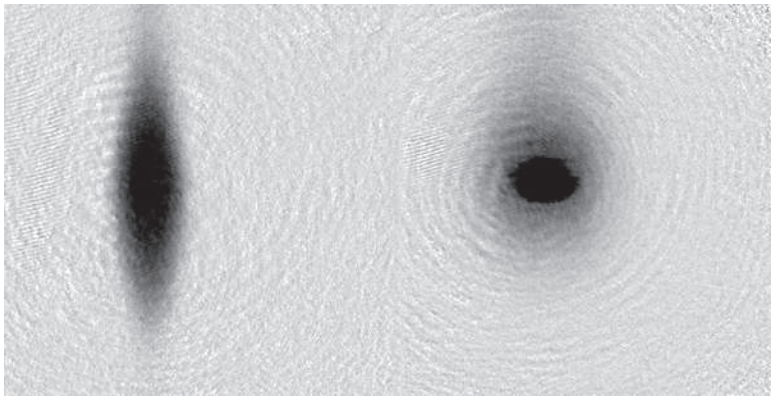

Figure 3-3: Same shot image of a degenerate ground state sodium-lithium mixture in the optical trap. On the left side, lithium is imaged after 3 ms TOF; on the right side, sodium after 13 ms TOF. The mixture contains 3.4×10^6 sodium atoms and 2.8×10^6 lithium atoms.

the mixture was produced, cooled and confined into an optical trap from a hotter $|2,2>_{\mathrm{Na}}$-$|3/2,3/2>_{\mathrm{Li}}$ mixture.

To achieve largest numbers, a sensible approach is to produce first an ultracold lithium-sodium mixture by the best method available, sympathethic cooling in the upper hyperfine states in the magnetic trap. However, directly catching a $|2,2>_{\mathrm{Na}}$-$|3/2,3/2>_{\mathrm{Li}}$ double degenerate mixture in the optical trap has two disadvantages. First, the atom numbers are relatively small, and second, the ratio of sodium to lithium atoms fluctuates and is difficult to control.

These problems have been solved by loading the upper hyperfine state mixture into the ODT before reaching degeneracy. The evaporation was stopped at a sodium trap depth of approximately 20 μK, and the mixture was loaded into a deep optical trap (1064 nm, 9W, 25 μm beam waist) and further cooled evaporatively by ramping down the ODT beam power. ODT evaporation was stopped at a trap depth equal to 2-3 times lithium's Fermi temperature, and to approximately 10 times the sodium's condensation temperature. A typical absorption image is shown in Fig. 3-3: degenerate mixtures with 3 million atoms in each species are produced by this method.

For hyperfine transfer with almost 100% efficiency, simultaneous Landau-Zener sweeps work best. Rather than doing the sweep at constant magnetic field by ramping

the rf frequency, we have found that the transfer can be done faster if the rf frequency is held constant and the magnetic field is ramped. While for our second-lived mixture shorter sweeps only improved the atom number, fast sweeps might be essential if production of a short-lived mixture is desired.

3.3.2 Long-lived spin mixtures: what we have investigated and what might work

For further studies of degenerate sodium-lithium mixtures, the question arises of what spin mixtures are likely to have long enough lifetimes to perform experiments. What is long enough depends on the experiment, but by this I will understand here a lifetime on the order of one second or more, which is enough for most ultracold atom experiments.

Given the current experimental setup, the best approach for making a specified mixture is to prepare it in an optical trap from a precooled upper hyperfine state mixture as described in the previous section; even for the $|1,-1>_{\mathrm{Na}}$-$|1/2,-1/2>_{\mathrm{Li}}$ mixture, it gives better results than the first magnetic trap cooling procedure we have used.

If a mixture has a lifetime on the order of seconds a necessary requirement is that all components have such a lifetime. Ultracold, single-state lithium clouds are long-lived because collisions are suppressed by the Pauli principle. In the case of sodium, all lower hyperfine states have a few seconds lifetime in an optical trap [121], although spin-exchange collisions in a $|1,0>$ cloud will generate a measurable amount of $|1,1>$ and $|1,-1>$ atoms within one second. For the upper hyperfine states, only the stretched states, $|2,-2>$ [50] and $|2,2>$ [79] are stable. Five sodium hyperfine states and all lithium hyperfine states can be in principle used as mixture ingredients.

Mixtures of lithium and sodium in stretched states with the same m_F sign are stable against spin-exchange and should be long-lived. We have investigated so far the properties of $|1,-1>_{\mathrm{Na}}$-$|1/2,-1/2>_{\mathrm{Li}}$, $|1,1>_{\mathrm{Na}}$-$|1/2,1/2>_{\mathrm{Li}}$, and $|2,2>_{\mathrm{Na}}$-$|3/2,3/2>_{\mathrm{Li}}$ mixtures and found all of them to have lifetimes of at least 10 s at

typical magnetic trap densities. It is reasonable to assume that the other five possible mixtures are also long-lived.

For mixtures in which spin exchange is not suppressed, $|1,-1>_{\mathrm{Na}}$-$|3/2,1/2>_{\mathrm{Li}}$ has a loss rate slow enough to be used for sympathethic cooling. Also, in a $|1,-1>_{\mathrm{Na}}$-$|3/2,3/2>_{\mathrm{Li}}$ mixture with a dominant sodium fraction, lithium is depleted, but this process takes a few seconds. These results are somewhat surprising given that the spin exchange rate is expected to be high, however it indicates that even in the presence of spin exchange sodium-lithium mixtures might have a lifetime of a second or more, making them suitable for experiments if not for direct cooling.

Chapter 4

Interacting Bose-Fermi mixtures: the observation of ^{6}Li-^{23}Na interspecies Feshbach resonances

In addition to the sympathethic cooling experiments, the other major part of our studies of Bose-Fermi mixtures is the observation of ^{6}Li-^{23}Na interspecies Feshbach resonances. These results are reported in

C. A. Stan, M.W. Zwierlein, C. H. Schunck, S.M. F. Raupach, and W. Ketterle , 'Observation of Feshbach Resonances between Two Different Atomic Species', Phys. Rev. Lett. 93, 143001 (2004)

(Included in Appendix D) Ref.[4]

The existence of Bose-Fermi resonances at fields which are experimentally accessible makes possible a list of exciting future experiments. Feshbach resonances allow the tuning of interspecies interaction strength, which might lead to the observation of boson-mediated Cooper pairing [54, 25], supersolid order [29], and phase separation [92]. If these resonances can be used for efficient production of ultracold heteronuclear molecules, such molecules can be used for quantum computation [40], for studies of correlated many-body systems [51, 20], and for higher sensitivity electron dipole moment searches [76].

4.1 The observation of lithium-sodium resonances

Near a Feshbach resonance the rate of three-body losses is dramatically enhanced. Losses are easier to measure than the elastic scattering length, and in ultracold gases, as a function of the magnetic field, there is no other strong resonant loss except for a Feshbach resonance. Therefore, the most practical means for observing a resonance is to search for magnetic field resonant losses.

This approach was used before in our lab for the first observations of Feshbach resonances in ^{23}Na [64] and in ^{6}Li [7]. The main difference between these experiments and the observation of ^{6}Li-^{23}Na interspecies resonances is that no theoretical predictions were available in the latter case, so the search was performed across the whole range of magnetic fields available experimentally.

In principle, one can search for Feshbach resonances in a lithium-sodium mixture in which lithium and sodium can be in any of the possible ground hyperfine states, which gives us a list of 6×8=48 possible mixtures. However, for both the observation the future use of these resonances it is important that the Fermi-Bose mixture has a long lifetime, and the most stable mixture is the one made from lithium and sodium in their absolute ground states, $|1/2,1/2\rangle_{\mathrm{Li}}$ and $|1,1\rangle_{\mathrm{Na}}$ ($|1\rangle_{\mathrm{Li}}$ and $|1\rangle_{\mathrm{Na}}$ at high field).

We have chosen to search for resonances in the ground state mixture. The ground hyperfine states are not magnetically trappable, and even if they were, our cloverleaf magnetic trap cannot provide enough stiffness at high fields. The mixture has to be trapped in an optical trap, and then uniform, dc magnetic fields of up to 1040 G can be applied.

For the observation of lithium-lithium resonances, combining the optical trapping with a high magnetic field was difficult because of the anti-trapping potential generated by the bias coils of the old magnetic trap. Fortunately, as the new magnetic trap was specifically designed to generate stable uniform magnetic fields for ^{6}Li experiments, optical trapping of the mixture could be easily accomplished. Making a mixture of lithium and sodium in their ground states with stable shot-to-shot numbers

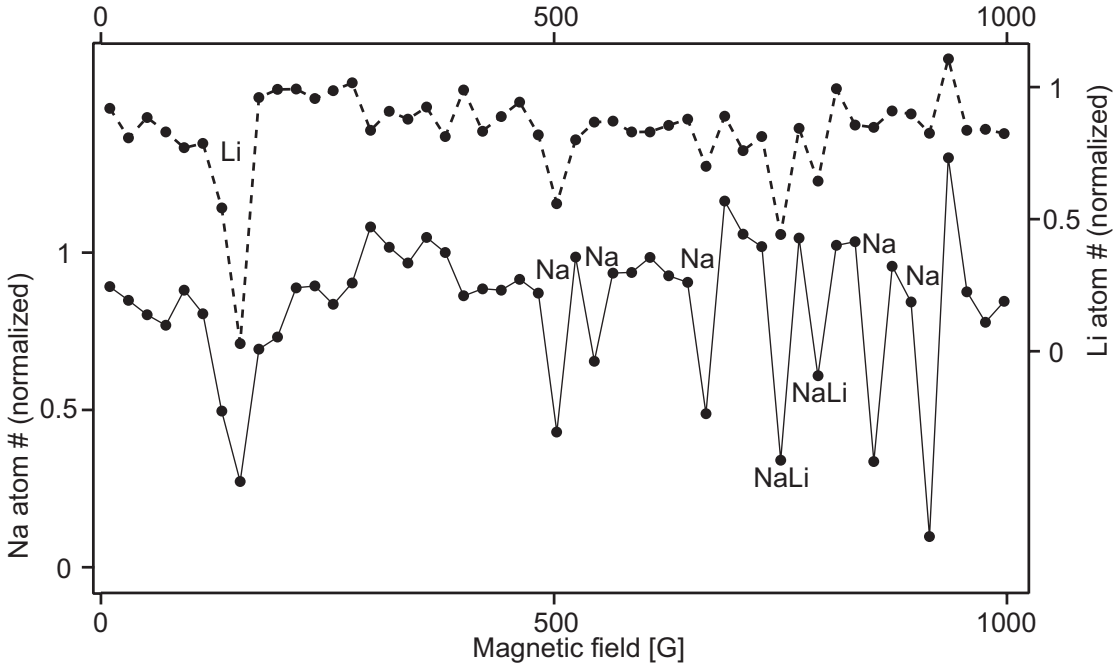

Figure 4-1: Coarse scan for Feshbach resonances in a $|1/2,1/2\rangle_{\mathrm{Li}} - |1,1\rangle_{\mathrm{Na}}$ mixture. Labels in the figure indicate whether the loss occurs because of a lithium only, sodium only, or lithium-sodium resonance. Some of the loss features are composed of multiple resonances, as revealed by a finer scan.

was less straightforward, and the procedure is described in Chapter 3.

The initial search for resonances was performed by dividing the available magnetic field range of 1040 G into 20 G intervals, and sweeping the field across individual ranges at a speed of approximately 20 G/s. The sodium and lithium atom numbers were plotted as a function of magnetic field and normalized to the average atom number, as seen in Figure 4-1.

Before this work, we know only of the existence of two sodium resonances at 855 and 910 G, and we have been pleased to see many new loss features. However, some of these turned out to be lithium-only or sodium-only resonances. The assignment of resonance types was done by measuring losses in a pure sample of lithium or sodium, as well as in the mixture. Seeing a loss in both mixture components, as it is the case for some of the resonances in Figure 4-1, is not sufficient proof for an interspecies resonance, as the energy released in a three-body inelastic collision in one species can be transferred to atoms of the other species. Of the new resonances observed, the ones

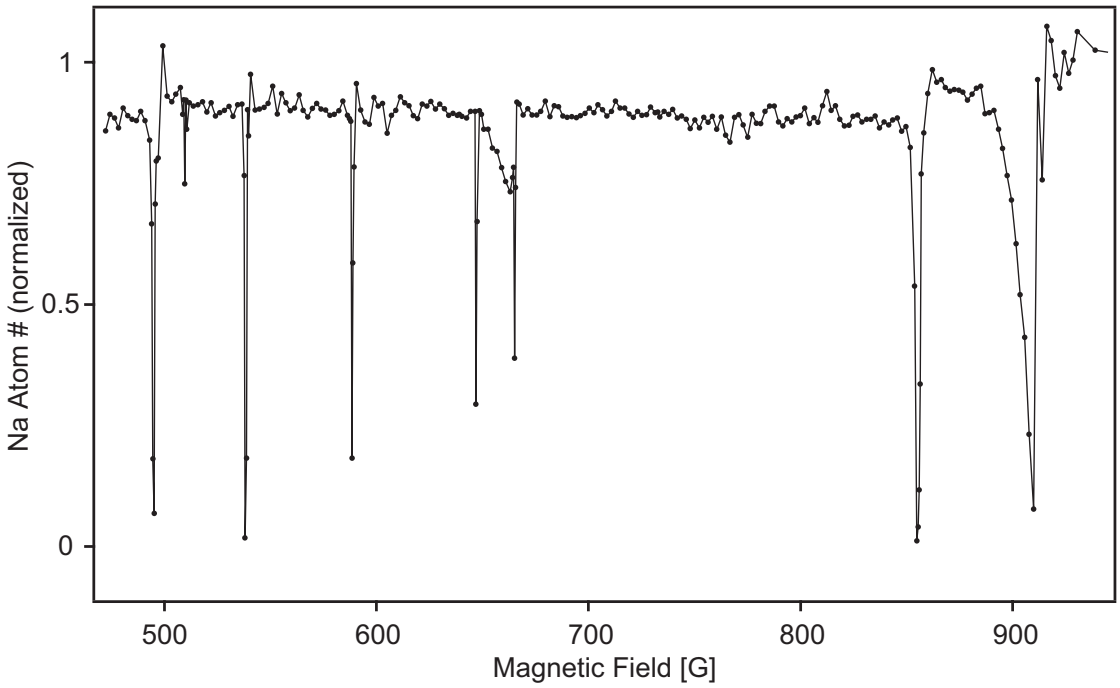

Figure 4-2: Magnetic field resonant losses in a |1,1> sodium sample. The lowest six loss features occur because of d-wave Feshbach resonances. The highest two are previously known s-wave resonances. For this data, the field was scanned across 2 G intervals, and the atom number was normalized to the atom number after a much faster scan across the same field range.

at 746.0, 759.6, and 795.6 G are interspecies lithium-sodium Feshbach resonances.

4.2 New Feshbach resonances in ^{6}Li and ^{23}Na

The observation of new Feshbach resonances in a pure sample of sodium was a surprise, because the same sample was scanned for losses in our lab years before, when the Feshbach resonances were observed for the first time, and only the two s-wave resonances at 855 and 910 G were observed. The result of a resonant loss scan performed in the same way as lithium-sodium scan, but across 2 G intervals, and normalized by dividing the atom number after slow (2 s) and fast (0.1 s) ramps, is shown in Figure 4-2.

The new resonances are narrower and exhibit lower losses than the previously known s-wave sodium resonances. This, combined with the more sensitive search

Table 4.1: New Feshbach resonances in ^{6}Li and ^{23}Na. The lithium and sodium states are labeled in the high-field basis.

Magnetic field [G]	Type	Li states	Na states	Theoretical prediction [G]
159.14±0.14	p-wave	|1>+|1>	—	159.15±0.04
185.09±0.08	p-wave	|1>+|2>	—	185.15±0.04
214.94±0.08	p-wave	|2>+|2>	—	214.90±0.04
494.9±0.2	d-wave	—	|1>+|1>	—
509.7±0.2	d-wave	—	|1>+|1>	—
538.4±0.2	d-wave	—	|1>+|1>	—
588.6±0.2	d-wave	—	|1>+|1>	—
647.2±0.2	d-wave	—	|1>+|1>	—
665.2±0.2	d-wave	—	|1>+|1>	—

procedure we used, and with the fact that the previous searches targeted a different field range, explains why they have not been observed before.

In addition to the sodium resonances, a p-wave resonance at 159 G was observed in a pure |1/2,1/2> lithium cloud. Additional searches revealed two related lithium p-wave resonances, and the position of these resonances was used to improve the value of the singlet scattering length in ^{6}Li [9]. The complete list of the new lithium-only and sodium-only resonances we observed is shown in Table 4.1.

4.3 Assignment of the molecular states involved in the ^{6}Li-^{23}Na resonances

If the ^{6}Li-^{23}Na interatomic potential was known, it would have been possible to predict the exact position of the interspecies resonances. However, it is possible to estimate with good accuracy the resonance positions if only the energy of the last triplet or singlet bound state of the ^{6}Li^{23}Na molecule, at zero magnetic field, is known.

Our search for resonances was performed without knowing any of these parameters, however the observation of resonances allowed us to estimate the energy of the last bound triplet state. Knowing this value, we were able to predict the full list of interspecies resonances due to this triplet molecular state.

Since Feshbach resonances occur when the energy of two incoming atoms matches the energy of a bound molecular state, the prediction of resonances involves calculating the the energy of the atoms, and of the molecule, as a function of magnetic field. For the incoming atoms, this is just the sum of their hyperfine and Zeeman energies, as the kinetic energy of ultracold atoms can be neglected.

The electronic and nuclear spin degrees of freedom generate a 48-fold multiplicity of a given electronic state of the ^{6}Li^{23}Na molecule. This degeneracy is lifted by hyperfine and Zeeman interactions and groups the molecular states into different manifolds. The strongest effect is given by the electronic spin coupling, which gives rise to separated singlet (12) and triplet (36) manifolds.

For the magnetic fields at which we observe the resonances, the molecular state is then specified in the $|S, m_S, m_{I,\,Li}, m_{I,\,Na}>$ basis, where S is the total electronic spin, m_S the electronic spin magnetic number, and $m_{I,\,Li}$, $m_{I,\,Na}$ the nuclear spin magnetic number of the lithium and sodium nuclei.

For s-wave collisions, the total magnetic number m_F is conserved. For the incoming atoms it is the sum of the atomic m_F's, and for the molecule by the sum of m_S, $m_{I,\,Li}$, and $m_{I,\,Na}$. Thus, a given pair of incoming atoms can couple only to a subset of molecular states defined by the total m_F.

The energy of the molecular hyperfine states within a m_F subset can be calculated relative to a constant equal to the molecular energy at zero field if the singlet-triplet separation is large. The Hamiltonian is:

$$H_{\rm int} = H_{\rm hf} + H_{\rm Zeeman}$$

with

$$H_{\rm hf} = \frac{h a_{\rm hf}^{\rm Li}}{2} \vec{S} \cdot \vec{i}_{\rm Li} + \frac{h a_{\rm hf}^{\rm Na}}{2} \vec{S} \cdot \vec{i}_{\rm Na}$$

and

$$H_{\rm Zeeman} = \mu_B \vec{B} \cdot (g_S \vec{S} + g_{\rm Li}\, \vec{i}_{\rm Li} + g_{\rm Na}\, \vec{i}_{\rm Na})$$

The energy levels for the m_F=1/2 and m_F=-1/2 subsets are plotted in Fig. 4-3,

Table 4.2: Predicted ^{6}Li-^{23}Na Feshbach resonances below 1100 G. Sodium and lithium states are given in the high-field basis. The triplet molecular state is characterized by the projection of the total electronic spin, and of the projections of the nuclear spins of ^{6}Li and ^{23}Na.

Magnetic field [G]	Na state	Li state	Molecular state $\|m_S, m_{i,Li}, m_{i,Na}\rangle$	Observed at [G]
717.4	|1>	|1>	|1, 1, -1/2>	746.0±0.4
763.1	|1>	|1>	|1, 0, 1/2>	759.6±0.2
790.7	|1>	|2>	|1, 1, -3/2>	—
821.1	|1>	|1>	|1, -1, 3/2>	795.6±0.2
836.4	|2>	|1>	|1, 1, -3/2>	—
848.2	|1>	|2>	|1, 0, -1/2>	—
876.7	|1>	|3>	|1, 0, -3/2>	—
895.9	|2>	|1>	|1, 0, -1/2>	—
921.1	|1>	|2>	|1, -1, 1/2>	—
924.1	|2>	|2>	|1, 0, -3/2>	—
949.2	|1>	|3>	|1, -1, -1/2>	—
970.2	|2>	|1>	|1, -1, 1/2>	—
992.2	|3>	|1>	|1, 0, -3/2>	—
998	|2>	|2>	|1, -1, -1/2>	—
1026.9	|2>	|3>	|1, -1, -3/2>	—
1066.7	|3>	|1>	|1, -1, -1/2>	—
1095.1	|3>	|2>	|1, -1, -3/2>	—

and the energy levels for the m_F=3/2 and m_F=-3/2 subsets can be found in Ref. [4]. If the (not hyperfine-split) molecular energy at zero magnetic field is not known, the absolute position of these curves is not fixed, but the shape of the curves remains the same. If Feshbach resonances are observed, the molecular energy can be estimated by plotting the energy of the incoming atoms, and by shifting the molecular curves up and down until the resonance positions match the crossings between atomic and molecular levels.

Such an analysis performed with the three resonances observed reveled that the triplet, and not singlet, molecular levels are the ones coupled to the atomic levels, and resulted in an estimate of the energy of the last bound triplet state of the ^{6}Li^{23}Na molecule of -5550 ± 140 MHz. The resulting predicted fields for the observed resonances, listed in Table 4.1, agree satisfactorily with the measured ones, given the relative simplicity of this approach.

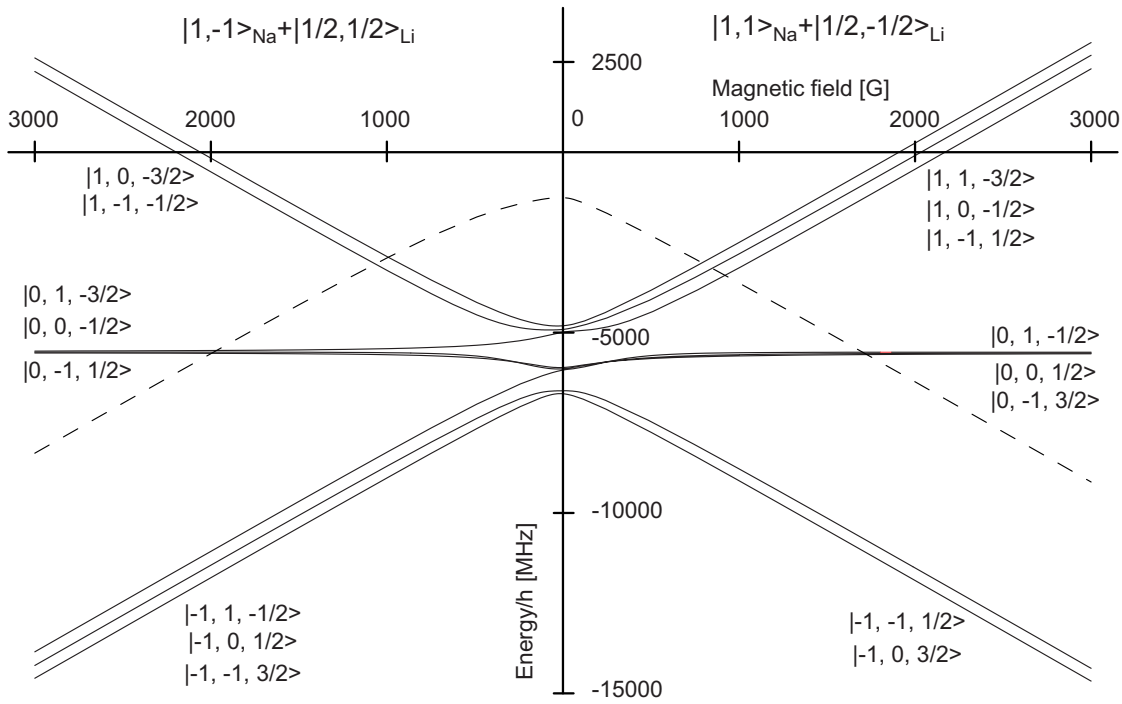

Figure 4-3: Plot of molecular energy levels. This plot contains two graphs, on the left side for total m_F=-1/2 and on the right side for total m_F=1/2. Solid lines show the magnetic field dependence of triplet molecular energy levels. The energy levels are given in the $|m_S, m_{i,Li}, m_{i,Na}>$ basis, where m_S is the total molecular electronic spin magnetic number ($S = 1$ for the triplet state), and $m_{i,Li}, m_{i,Na}$ the magnetic quantum numbers of the nuclear spins. This basis is appropriate for the magnetic fields at which the resonances occur. At low fields the $|F, m_F>$ molecular hyperfine basis is appropriate, and the states with the same F are degenerate at zero field. On each side, the dotted line represents the threshold energy of lithium and sodium atoms in a pair of hyperfine states which can couple in a s-wave collision to the respective molecular levels. Feshbach resonances occur where the atomic and molecular energies are equal, which corresponds in this figure to the crossing of solid and dashed lines.

Using the estimated molecular energy, the position of all resonances expected to occur due to this molecular state can be calculated. A full list, for all possible combinations of atomic hyperfine states, is given in Appendix G. Of practical interest are the ones occuring at experimentally accessible magnetic fields, and in atomic mixtures which are expected to have good collisional properties. They are listed in Table 4.2.

Two interspecies resonances between the same sodium state and different lithium states, and occuring at the same field, could be used to observe boson-induced interactions between fermions and possibly boson-induced Cooper paring [131, 54]. As it can be seen from the table, our simple model does not predict such coupled resonances, however the positions of the other resonances will have to be determined experimentally before this possibility is ruled out.

Chapter 5

Bose-Einstein condensation of ^{6}Li molecules

While the combination of laser cooling and evaporative cooling proved to be very successful for bringing both bosonic and fermionic atoms to quantum degeneracy, these techniques cannot not be used in the same fashion to cool molecules. Direct molecule cooling techniques as buffer-gas cooling [133] or electrostatic trapping [24] have not been successful yet in producing quantum degenerate molecules.

The first observation of Bose-Einstein condensation of molecules was achieved by creating ultracold molecules from ultracold fermionic atoms near a Feshbach resonance and is the subject of this chapter. Most of the experiments covered in this chapter have been reported in

M.W. Zwierlein, C. A. Stan, C. H. Schunck, S.M. F. Raupach, S. Gupta, Z. Hadzibabic, and W. Ketterle, 'Observation of Bose-Einstein Condensation of Molecules', Phys. Rev. Lett. 91, 250401 (2003)

(Included in Appendix E) Ref.[5]

5.1 Molecules and the Feshbach resonances

Although Feshbach resonances occur because of the coupling between a bound molecular state and two colliding atoms, the initial interest in their observation and use in ultracold atom experiments was geared towards tuning of the scattering length, which promised to bring an unprecedented level of control of the interaction strength. However, soon after the first observation of resonances in sodium [64] and rubidium [36] the initial enthusiasm was tempered by the observation of anomalously high decay rates near the resonances [123].

The high decay rates could be explained by taking into account the molecular state [127, 16]. The losses occur because near the resonance the atom-molecule coupling is strong enough to efficiently populate the molecular state, which is unstable on both sides of the resonance. In the region of negative scattering length the state has negative binding energy and experiences fast one-body decay. In the region of positive scattering length the molecule is bound, but since it is in a highly excited vibrational state it collisions will relax it to lower vibrational levels, with a large release of energy.

The accessibility of the molecular state as demonstrated by the decay rates suggested the possibility of using the Feshbach resonances for the production of ultracold molecules [127, 16, 89]. The first evidence for the formation of ultracold molecules came in an experiment which coherently coupled atoms and molecules in a rubidium BEC [42], and indicated a sub-millisecond lifetime of the molecular state.

Back in our lab at that time, we were puzzled by some features of our recent observation of Feshbach resonances in lithium, which we know now that were caused by molecule formation. One was the apparent shift of the resonance to lower fields, which occurs because molecules form and decay on the positive scattering length side.

More puzzling was the kinetics of the decay. Based on our previous experience with sodium resonances, we expected three-body decay, but two-body kinetics was observed instead. Our best guess at that time was that a long-lived quasi-bound state is formed and the decay occurs in two steps, similar to the resonance recombination in spin-polarized hydrogen. For hydrogen, the process *'proceeds in two stages: First a*

pair of H-atoms collide and are trapped into a long-lived quasi-bound state (resonance state); subsequently this quasi-molecule is stabilized in a collision with a third body in which it has a transition to a bound state' (from [119]).

This quote uses a chemistry language, and to translate it to atomic physics terminology 'quasi-bound' has to be understood as 'weakly bound', and 'bound state' as the 'ground state'. Taking this into account, what is described here is exactly what happens near a Feshbach resonance if we equate the quasi-bound state with a Feshbach-produced molecule. In hindsight, it seems remarkable to me that we came early so close to realizing that we are forming long-lived molecules. Unfortunately our assumption that the 'quasi-bound' state decays fast and an experimental accident (damage to the magnetic trap) prevented us from further studies at that point.

Using a Feshbach resonance, $^{40}K_2$ molecules have been first produced from a two-component Fermi gas a year later [110]. Within the next few months, this method was successfully applied to other two-component Fermi gases [125, 37] and to Bose gases [56, 135, 44]. All these experiments created molecules by using magnetic field sweeps, a production method which is covered next.

5.2 Adiabatic conversion of atoms into molecules near a Feshbach resonance

The first method by which molecules were produced, and which could be applied to both bosonic and fermionic atoms, was by using magnetic fields sweeps. The coupling between atomic and molecular levels results in an avoided crossing between these levels. As it can be seen in Figure 5-1, this allows us to cross between atomic and molecular levels.

If the rate of change of the magnetic field is slow enough, the crossing is traversed adiabatically. Starting from the side of the resonance in which the atoms have lower energy, a slow ramp will convert the atoms into molecules. If the ramp speed is fast, the system will evolve non-adiabatically as if no coupling exists, and will remain in

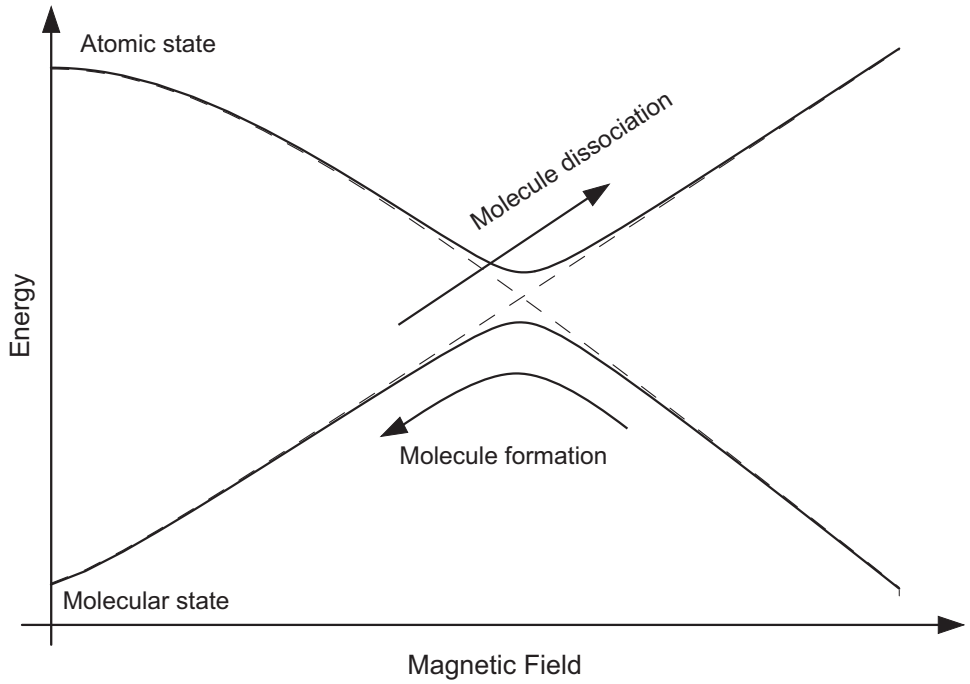

Figure 5-1: Crossing of atomic and molecular states near a Feshbach resonance. The coupling between states gives rise to an avoided crossing and connects the atomic and molecular levels, shown here in solid lines. The dashed lines indicate the energy dependence in the absence of coupling. To make molecules, a slow adiabatic ramp from high to low field is used. As molecules are unbound at fields above the resonance, they can be dissociated by a reverse field ramp.

its initial state, either atomic or molecular.

What is fast or slow is defined by the Landau-Zener probability that the system will make a non-adiabatic jump between the levels at the crossing [137, 116]:

$$P = e^{-2\pi(\frac{|H_{12}|^2}{\hbar(\partial E/\partial t)})}$$

where $|H_{12}|$ is the coupling matrix element, and
$(\partial E/\partial t) = (\partial(E_{atoms} - E_{molecule})/\partial B)(\partial B/\partial t)$ is the energy slew rate.

This simple Landau-Zener picture is complicated by the fact that the molecular state has negative binding energy on the side of the resonance on which it has a higher energy that the atomic state. Relative to the time scales used in our sweep experiments, a molecule with negative binding energy will decay very fast, which

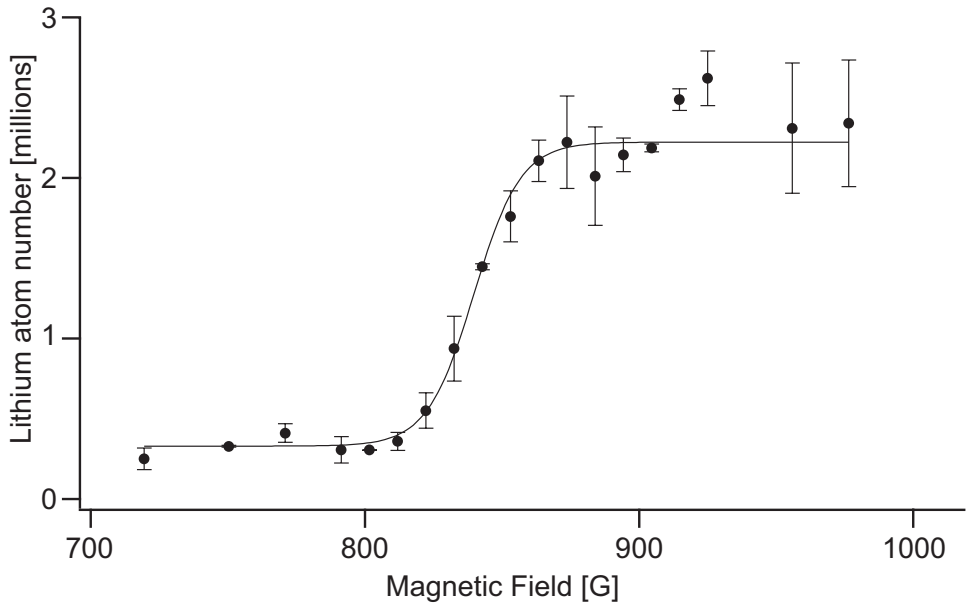

Figure 5-2: Production of lithium molecules at the 834 G Feshbach resonance. The |1>-|2> lithium mixture is cooled and held at 970 G, then the magnetic field is ramped to different end fields, after which the field is tuned off for imaging. At zero field, molecules do not absorb light resonant with atoms, and the molecule formation is seen as a loss in atom number. For this data, an atom-molecule conversion efficiency of 85% was observed.

means that starting with atoms, we cannot practically create quasi-bound molecules by using a reverse sweep. However, this allows us to efficiently dissociate molecules with a reverse ramp, which is needed to observe molecules.

Near the resonance, these molecules are very weakly bound and have a large size, which allows us to image their atomic components with light resonant with the atomic transitions. But as soon as the molecules are taken away from the resonance the molecular wavefunction is no longer the product of atomic wavefunctions, and the molecule is no longer resonant to the light at atomic resonance frequencies. Thus, molecule formation can be observed as a loss in atom numbers as the resonance is crossed, as seen in Figure 5-2.

The atom loss due to molecule formation is reversible if other losses do not occur, and the initial atom numbers can be observed if the molecules are dissociated by a reverse field ramp. The formed molecules are vibrationally excited, and will eventually

decay to the ground state. As the frequency of the radiative transition to the next lower vibrational state is in the gigahertz range, radiative decay will take far longer than the typical time duration of ultracold atom experiments. However, other single-body processes as inelastic spin relaxation can cause spontaneous decay of these molecules on much faster timescales [126]. Fortunately, this is not a limitation in experiments with ^{6}Li.

The two-body picture of molecular production near Feshbach resonances suggests that the production is a task easily achieved for most of the atomic species used in ultracold atom experiments. Nevertheless, in a real experiments the typical densities the atomic and molecular gas density is high enough that a high collision rate is established. Vibrational relaxation of the molecules occurs readily as a result of collisions, and the resulting kinetic energy release destroys the trapped molecular gas.

In the case of bosonic atoms, molecular loss due to collisions is severe for typical densities. Thus the atom-molecule conversion requires separation of molecules from the atom soon after production, and efficiencies of only a few percent could be initially achieved [56, 135, 44]. Still, in the low density limit the maximum conversion efficiency depends only on the phase-space density [59], and high conversion efficiencies have been observed in both bosonic and fermionic systems for unusually low densities ($\sim 10^{11}$ cm^{-3}). At low phase space density, the conversion efficiency is limited by the fact that in order to form a molecule, the constituent atoms need to be close in the phase space.

In the case of fermionic atoms, unexpectedly long molecular lifetimes have been observed [111, 125, 37]. In the case of ^{6}Li, molecules will not decay for many seconds, allowing almost lossless production of molecules by field ramps. The long lifetimes are a consequence of the suppression of vibrational relaxation near the resonance, because for spatially extended molecules made from fermions, inelastic collisions with other molecules or atoms are excluded by the Pauli principle [102, 103].

The molecules formed by field ramps have no additional kinetic energy. The small binding energy is converted into the interaction energy of the molecular magnetic

moment with the external field. This adiabatic formation can be regarded as a very exotic form of chemistry, since chemical reactions always generate or consume kinetic energy at the microscopic level.

5.3 Formation of ultracold molecules by three-body recombination

The adiabatic creation of weakly bound molecules implies that starting with a gas of atoms at zero temperature, a zero temperature molecular gas can be created. Since strongly interacting degenerate Fermi gases had been produced by evaporation in an optical trap [97], it seemed that a BEC of weakly bound ^{6}Li molecules could be produced by ramping the degenerate Fermi gas through the wide Feshbach resonance centered at 837 G. However, additional heating and incomplete atom-molecule conversion made a second stage of cooling on the repulsive side of the resonance necessary.

A more efficient method for production of degenerate molecular samples is possible in the case of ^{6}Li, because of the long molecular lifetime near the resonance. The discovery of efficient molecule production by three-body recombination at magnetic fields on the repulsive side of the resonance [65] led to a proposal for condensation of weakly bound ^{6}Li molecules [31], and we have used this approach ourselves to achieve a molecular BEC.

This proposal can be summarized as follows. In a mixture of two atomic species with diatomic molecules formed from these species, in which all components are in the ground motional state, the equilibrium phase-space densities are related by the equation:

$$\phi_M = \phi_N \phi_{N'} e^{E/kT}$$

where E is the molecular binding energy, and $\phi_M, \phi_N,$ and $\phi_{N'}$ are, respectively, the phase-space densities of the molecules, of the first atomic species, and of the second atomic species. The trap depth is assumed to be very large, so the atoms and

molecules cannot leave the trap.

This equation resembles the Saha ionization equation if the phase-space densities are replaced with normal densities, and it suggests that as the molecule is more deeply bound, the system will shift more towards molecule formation as the number of atoms is exponentially suppressed. However, if this equation is applied to the case of trapped ultracold atoms a different behavior is predicted. For deeply bound molecules, the energy released during formation heats the atomic sample significantly and reduces the phase-space density; counter-intuitively, if the binding energy is infinite, no cold molecules can form.

The equation also predicts that starting with an atomic gas the molecule production is inefficient right at the resonance. The equilibrium molecule conversion, as measured by the molecular phase-space density, initially increases, peaks and then drops as the field is swept away from the resonance towards the repulsive side. Close to resonance, the molecular phase space density increases approximately linearly with the binding energy.

Assuming that the atoms can be selectively removed from a thermally equilibrated mixture, an efficient evaporative cooling scheme can be devised. At finite temperature a pure molecular cloud is not in thermal equilibrium on the repulsive side of the resonance, and a fraction of unbound atoms will form. The dissociation of molecules is an endothermic process, so only molecules with sufficient kinetic energy can dissociate. The atoms resulted from the dissociation will have reduced kinetic energy, and if they thermalize with the molecular cloud the dissociation process will cool the sample.

In an optical trap, loosely bound molecules experience the same trapping frequencies as atoms and twice the trapping depth for atoms. The factor of two difference in trapping depth makes a big difference for evaporative cooling. At a molecular truncation parameter $U_m/k_BT = 10$, where U_m is the molecular trap depth, the molecule evaporation becomes negligible, but the atoms can be still removed from the trap as their truncation parameter is half of the molecular one.

This cooling method will work best at a value of the magnetic field dependent on the trap parameters. Too close to the resonance, molecule dissociation occurs without

a reduction in temperature (but the difference in trapping depths still favors atom evaporation), and too far from the resonance molecules will not have enough energy to dissociate (and the molecules are more likely to relax vibrationally). For the optimal value of the magnetic field, it was predicted that this cooling method works better than standard evaporative cooling and a five order of magnitude reduction in phase space density can be achieved in six seconds, shorter than the observed molecular lifetime.

5.4 Observation of molecular Bose-Einstein condensation

Given the favorable properties of ^{6}Li molecules, and the large number of ultracold lithium atoms we can achieve in our experiment, we were had good prospects for observing the molecular Bose-Einstein condensation. However, subtle technical failures prevented the normal operation of our apparatus through the summer and early fall of 2003, when most of the ultracold molecule creation experiments have been conducted. Fortunately, we have been able to fix these problems just in time to directly observe the Bose-Einstein condensation of ^{6}Li molecules.

We had tried before to cool an interacting mixture of lithium by evaporation in the optical trap, with mixed results. These experiments were performed on the repulsive side on the Feshbach resonance and aimed at the production of an ultracold interacting gas with properties similar to the one reported in [97]. Although we have been able to observe hydrodynamic expansion from the optical trap, which was a direct proof of the strongly interacting regime, the lifetime of our lithium spin mixture was short and we could not achieve good signal-to-noise ratios.

Cooling the mixture with the goal to condense molecules, we had a few unknowns. One was the proper choice of the magnetic field. 760-770 G , which is halfway between the peak loss observed in our experiment (680 G) and the then-predicted position of the resonance (850 G) was a reasonable starting point. Also, we did not know what

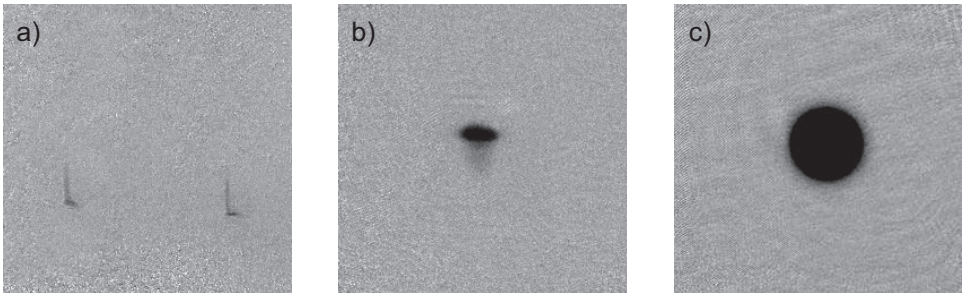

Figure 5-3: Images of ^{6}Li molecular Bose-Einstein condensates. These images have approximately the same field-of-view and normalization, showing the progress from the first signal to the current experiments. a) Top imaging image of one of the first molecular BECs produced. The two hyperfine states are imaged separately and simultaneously at high field. The condensate appears at the bottom of the molecular cloud and is spilled from the trap. Total molecule number is approximately 2×10^5. b) The optical trap asymmetry was compensated using a magnetic field gradient, and the two hyperfine states imaged together at zero field. A condensed molecule number of 7.3×10^5 is obtained from fitting. c) A recent molecular BEC with approximately 4 million molecules, in side imaging.

would be the exact signature of the condensation. Our lab has a tradition of producing evidence about new phenomena in the form of single absorption images which clearly reveal new features, and we hoped to observe such a image.

Initial expectations were that as molecules start to form, they could be seen as a distinct area in a absorption image taken after time-of-flight at high field, because they expand slower than the atoms at the same temperature because of their larger mass. Upon further cooling, a condensate would form, and an absorption picture would be 'trimodal' with three increasingly darker, visually distinct areas of the condensate, the molecular cloud, and the atomic cloud. The 'trimodal' distributions were never seen, and the reason for this is that at our usual evaporation field of 770 G, the binding energy of the molecules is a few times higher than the condensation temperature. By the time the condensation occurs, the thermally equilibrated cloud contains a negligible atom fraction.

Given our experimental parameters, the conversion of atoms into molecules occurs separately from the condensation of molecules, which was identified by a sharp increase in the optical density of the molecular cloud. The optical trap setup we were

using when this experiment was done had a rough and asymmetric axial profile. Also, at the ODT power levels at which condensation occurred, the trap depth could be controlled only in relatively large discrete steps. The result is that the sharp increase in the optical density of the cloud at condensation occurred simultaneously with the loss of condensed molecules from the trap, and the first molecular BEC images, shown in Figure 5-3, reveal the early spill of the condensate from the trap. Even taking into account the spilling, the condensation was unambiguous as a time-of-flight analysis revealed a very low kinetic energy of the trapped cloud.

A quick improvement of the optical trap was possible by using a magnetic field gradient to partially correct the axial asymmetry, and condensates with up to 900000 molecules have been obtained. This also increased the lifetime of the trapped condensate to values large enough for establishment of thermal equilibrium in all three dimensions. The short condensate lifetime, on the order of one hundred milliseconds, was caused by the imperfections of our optical trap, and triggered a major upgrade of our optical trap setup, described in Chapter 2. With the improved optical trap setup, condensates with 3-4 million molecules and lifetimes on the order of ten seconds are now routinely produced. These ^{6}Li molecular condensates provide us now with a standard starting point for the exploration of the strongly interacting regime in fermionic spin mixtures.

The production of Bose-Einstein condensates of weakly bound molecules was simultaneously reported by Debbie Jin's group at JILA [52] and Rudolf Grimm's group at Innsbruck [66]. In the JILA experiment, ^{40}K molecules were produced by a slow sweep across the resonance as the short lifetime of potassium molecules does not permit production of molecules by three-body recombination. The lifetime of the ^{40}K molecular BEC was too short to achieve three-dimensional thermalization. The first ^{6}Li molecular condensation experiment at Innsbruck used the same production method as the one we used. It offered only indirect evidence for the condensation, by studies of trap spilling and of collective excitation frequencies.

Our observation of molecular condensation was the latest of the three, and by direct observation of three-dimensional condensation completed the quest to condense

particles more complex than atoms.

Chapter 6

Fermion pairing and the condensation of fermion pairs in the strongly interacting regime

The production of the ^{6}Li molecular BEC provided to us an excellent starting point towards the investigation of the properties of the degenerate, strongly interacting fermion gases. Our first studies of the strongly interacting regime focused on the existence and nature of fermion pairing near the Feshbach resonance, at magnetic fields at which molecules are unbound in vacuum.

Using a detection technique developed at JILA and initially applied to study fermion pairing in a ^{40}K system [112], we have observed the condensation of ^{6}Li near a Feshbach resonance. The ^{6}Li pair condensation is the main subject of this chapter and was reported in

M.W. Zwierlein, C. A. Stan, C. H. Schunck, S.M. F. Raupach, A. J. Kerman, and W. Ketterle, 'Condensation of Pairs of Fermionic Atoms near a Feshbach Resonance', Phys. Rev. Lett. 92, 120403 (2004)

(Included in Appendix F) Ref.[6]

6.1 The conversion of fermions into composite bosons and the BEC-BCS crossover

One fundamental opportunity offered by the Feshbach resonances between fermionic atoms is the study of the creation of composite bosons. Unlike the usual 'instantaneous' composite particle generation by chemical or nuclear reactions, near a Feshbach resonance it is possible to explore in a continuous way the transformation of a fermionic ensemble into a bosonic one.

Fermions and bosons systems have very different mechanical-statistical properties at zero and low temperatures; one example is the energy of the system, which is higher for Fermi ensemble. If a given system can evolve between Fermi and Bose statistics, the question is how the two statistics are connected in the crossover region.

In the case of formation by collisions, the composite particle production is linked to a resonant enhancement of the effective interactions in the system and these interactions alter the characteristic properties of the Fermi and Bose systems in such a way that they connect in the crossover region.

In the case of ultracold molecules produced near a Feshbach resonance, we can take the total energy as an example of a variable which varies continuously across the crossover. The effective interaction is attractive on the atomic (fermionic) side of the resonance, repulsive on the molecular (bosonic) side of the resonance, and reaches very high values at the resonance. The interaction thus lowers the energy of the Fermi gas. Although the scattering length can have very high values, the energy change is unitarity limited at the resonance [55], effect which was observed experimentally in ^{6}Li [97, 48, 26]. On the molecular side the energy of the Bose gas is increased, but only up to the unitarity-limited value [58].

The molecular BEC described in the previous chapter is in the strongly interacting regime. At 770 G, as it can be seen in Figure 6-1 a), the BEC size is increased by interactions to the point where the characteristic thermal-condensate bimodal density profile is difficult to observe, although a condensate fraction can be still extracted by fitting. For an easy observation of the bimodal density profile, the interactions

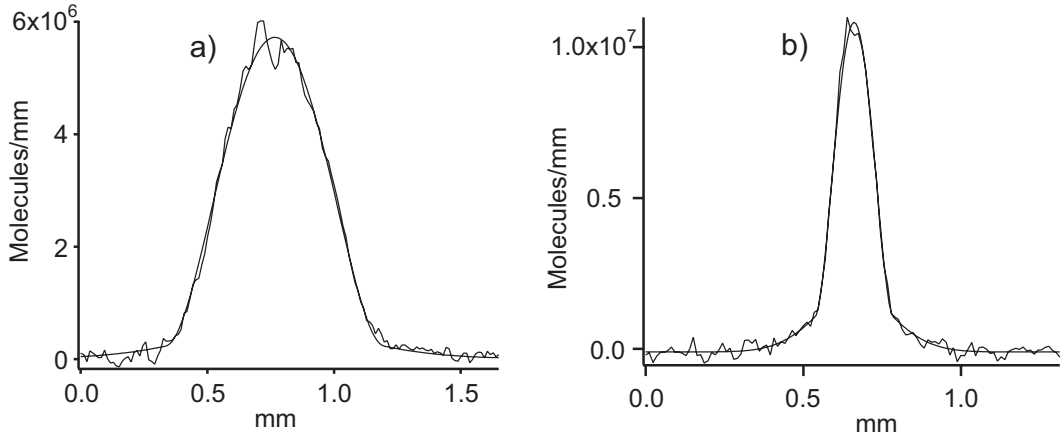

Figure 6-1: Molecular condensate size for different mean-field energies. Both graphs show integrated radial density profiles extracted from absorption images, for molecular BECs produced at 770G. Also shown is a two-component thermal and condensate fit to the data. a) The 10 ms time-of-flight is done at the production field, and the mean-field repulsion expands the condensate to a size similar to that of the thermal cloud. The condensate fraction is 85 %. b) The magnetic field is switched off at the beginning of the time-of-flight and the condensate expands less due to a reduced mean-field energy, resulting in clearly separated thermal and condensate profiles. The condensate fraction is 65 %.

have to be reduced shortly before the time-of-flight analysis (Figure 6-1 b)). Beside demonstrating visually the condensation, this probing technique leads to easier data analysis and provides reliable thermometry.

The first studies of the BEC-BCS crossover in ^{6}Li investigated the trapped size of the cloud at temperatures low enough to condense the molecules [22]. As the value of the magnetic field was varied from 740 G to 1440 G, the molecular BEC evolved reversibly into a strongly interacting Fermi gas. The size of the cloud, normalized to the size of a non-interacting Fermi gas with identical parameters, increased smoothly from the molecular to the atomic side of the resonance. A similar experiment mapped the release energy of the cloud relative to the Fermi energy using time-of-flight analysis [27], and reported also a smooth crossover from a Bose to a Fermi gas.

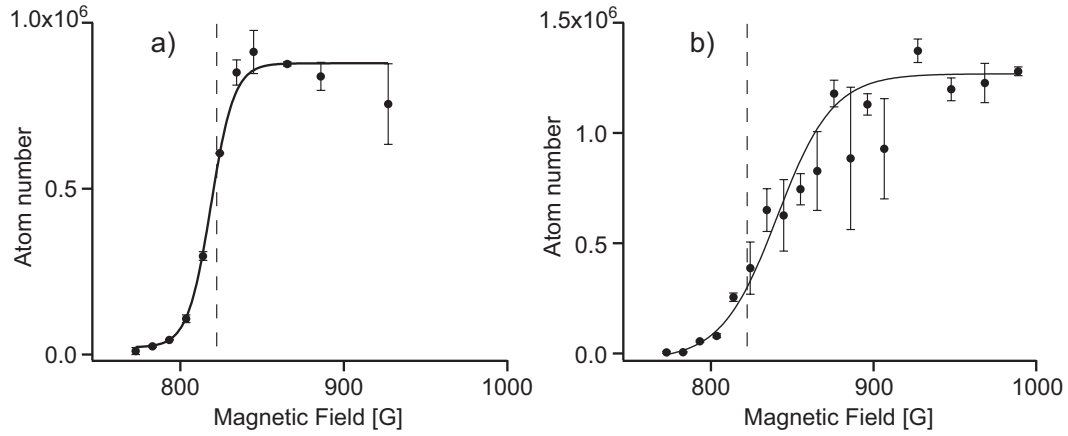

Figure 6-2: Fermion pairing on the atomic side of the Feshbach resonance. The number of unpaired atoms was measured as a function of the magnetic field for different densities. After producing a molecular BEC at 770 G, the field was slowly ramped to different values within the resonance region. The atom number was measured after switching off the magnetic field, which renders molecules invisible to our detection scheme. As the total number of atoms, paired and unpaired, is constant, the molecule number is given by half of the missing atom number. The dashed line indicates the resonance position as measured by the onset of molecule dissociation at very low densities. a) The field was switched off during time-of-flight to approach the low-density limit b) The field was switched off while the atoms were still trapped, indicating the existence of paired atoms on the atomic side of the resonance.

6.2 Fermion pairing above the Feshbach resonance

The continuous variation of physical variables as the magnetic field is tuned across the Feshbach resonance prevents the sudden appearance of qualitative features as the resonance is crossed from the molecular to the atomic side. However, fermion pairing on the atomic side of the resonance is a qualitatively new many-body effect, and one particularly suited to study in ultracold gases, where the simple two-body pairing (no bound molecules on the atomic side of the resonance) can be also explored.

Our first experimental observations suggesting fermion pairing above the Feshbach resonance came from the determination of Feshbach resonance shifts and broadening by molecule dissociation. As it can be seen in Figure 6-2, at high densities the persistence of a missing atomic fraction at fields above the resonance indicates the existence of fermion pairs which are converted into (invisible) molecules during the

imaging sequence.

The existence of stable atom pairs at a magnetic field at which molecules are unbound in vacuum can be understood in a simple zero temperature picture. Let's assume that an unbound molecule is formed from atoms in a two-component Fermi gas. In vacuum, this molecule would spontaneously decay with a lifetime which gets shorter as the (anti)binding energy increases [93]. After decay the constituent atoms will each carry half of the molecular (anti)binding energy. However, if the molecule is generated in a zero-temperature atomic mixture and if the (anti)binding energy is less then twice the Fermi energy, all the atomic states which would be populated after the dissociation are already occupied, so the molecular dissociation is Pauli suppressed. In an equilibrium state, we would have then a stabilized pair bosonic gas coexisting with two Fermi gases with Fermi energies equal to half of the (anti)binding energy. At finite temperatures, Pauli blocking will still increase the lifetime of the pair, which could be a significant effect in our experiments. For $T/T_F = 0.05$, the occupation number of the low energy states is $1 - 1 \times 10^{-8}$, resulting in a Pauli blocking factor for the dissociation of a very weakly unbound molecule of 10^{-16}.

While it would have been worthwhile to continue investigations of fermion pairing by resonance shifts, we have soon learned of a better method for investigation of fermion pairing developed at JILA [112]. The new experimental method involved a rapid magnetic field ramp technique which converts fermion pairs into stable molecules. Its advantage comes from the fact that since the rapid ramp operates on pairs of atoms, the molecules produced have the same kinetic energy as the original pair. Unlike pairs, molecules will not dissociate as the Fermi energy is lowered during time-of-flight so the momentum distribution of the molecules will be the same as the center-of-mass momentum distribution of the pairs. Also, because of the strong pair coupling near the Feshbach resonance the rapid ramp can be performed adiabatically in a timescale short compared to the other timescales in the system, so the momentum distribution will not be altered.

The rapid ramp method promised to offer a way to convert Cooper pairs in the BCS limit to individual particles which can be detected directly, and to which stan-

dard ultracold atom techniques can be applied. The results of the JILA experiment left open the possibility of detecting BCS-type pairing in strongly interacting Fermi gases by the projection method, and we have used this technique to investigate pairing in our ^{6}Li system.

6.3 Condensation of ^{6}Li fermionic atom pairs

In the ^{40}K JILA experiment not only fermion pairing, but also Bose condensation of these pairs was observed at magnetic fields at which two-body physics does not support a bound state. Since the collisional properties of ^{6}Li and ^{40}K are different [62] we have adapted the rapid ramp method to our system to observe and study this resonant condensation phenomenon.

The rapid ramp method is an accurate probe of the system properties only if it can be performed in a time which short comparative to the other equilibration time the system. If a measurement or an established theory predicting the equilibration time are not available, one can only state that this time is longer than the fastest timescale in the system, which in our case is the collision time. In the strongly interacting regime, unitarity limits the maximum collision rate to a value on the order of the inverse of the Fermi energy divided by $\hbar$.

Compared to the potassium experiment, the magnetic field range in Gauss which has to be swept during the rapid ramp is 200 times bigger. In addition, the Fermi energy of our lithium clouds is ten times bigger than the Fermi energy in the potassium experiments, leading to a desired rapid ramp sweep rate in our experiments a few thousands times faster than the one used in potassium, 20 G/ms. This is far beyond the analog control capabilities of our power supplies, so in the end we just switched off the current in our coils, which results in a non-linear decay of the field with an initial rate of 30 G/μs. It is possible to change this decay rate by tuning the impedance of the magnetic trap coils. However we have not done it since the electrical circuit is optimized to avoid generation of voltage spikes at switchoff. This rate is not fast enough to rule out collisions during the rapid ramp, but we have proven in subsequent

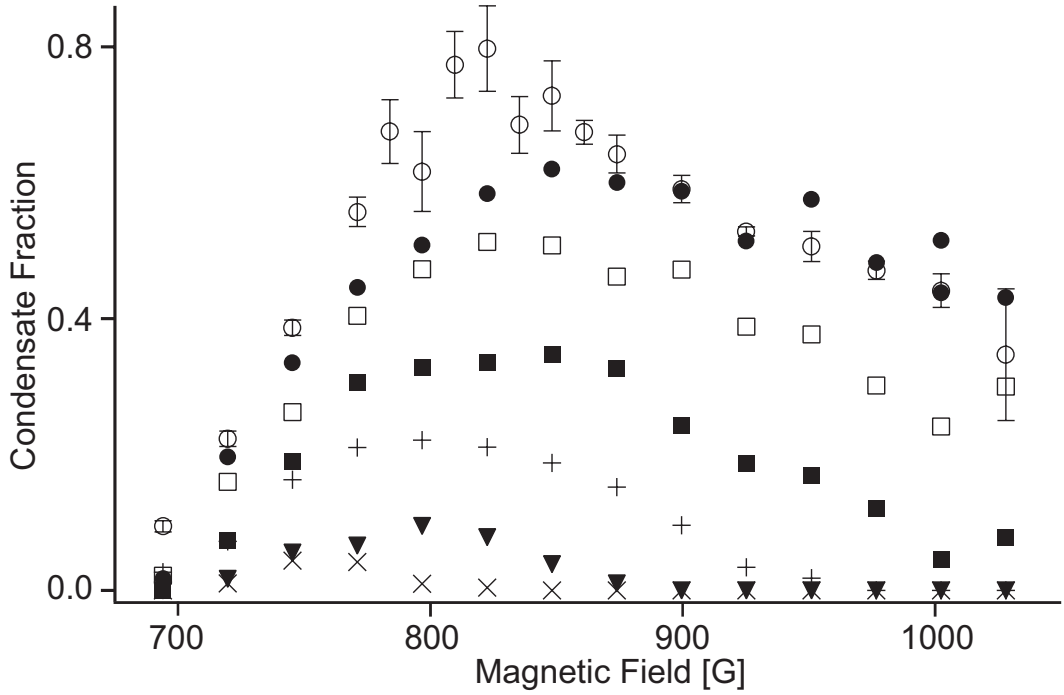

Figure 6-3: Fermion pair condensate fraction as a function of magnetic field and temperature. The different data sets are each characterized by the same temperature, which is parametrized by the molecular condensate fraction N_C/N_{tot} at 820 G (open circles: 0.8; filled circles: 0.58; open squares: 0.51; filled squares: 0.34; '+' : 0.21; triangles: 0.08; '×': <0.01).

experiments that equilibration takes place on a longer timescale [10].

The experimental procedure we used involved producing a molecular BEC at a field of 770 G, followed by an adiabatic ramp to different test fields. Then the optical trap was switched off and the rapid ramp was done after a variable wait time of up to 500 μs. After a few ms time-of-flight at zero field, the molecules were dissociated by ramping the field up and above the Feshbach resonance, and the resulting atoms were imaged at zero field. The delay between the trap release and the rapid ramp has the purpose of reducing the cloud density, thus slowing down the system dynamics. Of course, this delay must not be too big such that the pairs are dissociated; for up to 500 μs pair dissociation is not observable.

The molecular clouds produced after the rapid ramp showed a clear bimodal structure, reflecting the condensation of fermion pairs above the resonance. Condensate

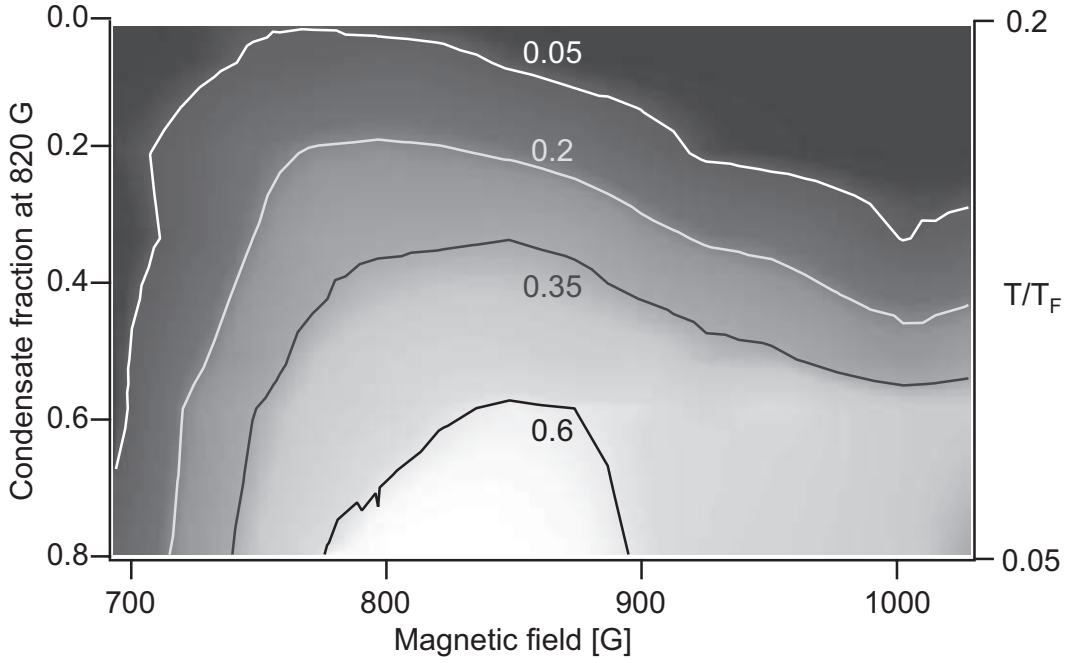

Figure 6-4: Contour plot of the pair condensate fraction. The plot was created by interpolating the data shown in Figure 6-3. The temperature is parametrized by the condensate fraction at 820 G, and by the degeneracy temperature T/T_F. The degeneracy temperature is difficult to measure accurately, and only the range is indicated in the figure. For maximum densities the region where $k_F|a| \geq 1$ extends from about 710 G onward.

fractions were calculated from absorption images for different fields and temperatures, as it can be seen in Figure 6-3. All the data points, including the ones below the resonance, were taken using the rapid ramp method. To change the temperature, the evaporation was stopped before obtaining a pure molecular BEC, and the cloud was heated parametrically for the highest temperature data sets. Because of the large background scattering length of ^{6}Li and of the high densities of our system, we were not able to probe deep in into the BCS side of the resonance and pair condensation was observed up to the highest fields we can generate.

A different way to present the data is a to generate a 'phase diagram' contour plot of the condensate fraction vs. magnetic field and temperature, as seen in Figure 6-4. Not included in this data is the observation that as the temperature is lowered, pair formation starts to occur before the pairs condense, which is different from the

weakly interacting BCS case in which Cooper pair formation and condensation occur simultaneously.

The exact position of the resonance was not known when our experiment was performed, and it was necessary to accurately measure the resonance position. This was done by starting with a molecular condensate at a field below the resonance, and then ramping up the field until molecule dissociation is observed. This was done at the lowest densities and slowest field ramps we could achieve in our experiment to avoid many-body effects, and we have obtained a value of 822 ± 3 G for the resonance position.

For a while, this was the best available position measurement of the 300 G wide resonance. However, the discrepancy with the 837 ± 5 G value obtained by rf spectroscopy of the ^{6}Li molecules [23] revealed that at finite densities and field ramp speeds molecules can be destroyed by two different mechanisms before their energy reaches the atomic dissociation threshold. The first mechanism is density dependent, as long-range molecules can be dissociated by few-body collisions when interparticle spacing matches molecular size [77]. Molecules can also be destroyed close to the resonance for field ramp rates at which the size of the molecule cannot follow adiabatically the field [37]. Extrapolation of these two effects to zero density and zero ramp rates leads to a corrected resonance position which agrrees with the spectroscopic measurements [9].

The error in the original resonance position measurement is does not influence the interpretation of the pair condensation experiments as the condensation occurs over a much larger field range. However, it reveals the 'fragility' of the molecules and pairs in a narrow field range near the resonance, which can explain the shift in the minimum damping rate of axial compression mode in [23] and the decreased vortex lattice lifetime in a narrow field range near the resonance [138].

One important question about the rapid ramp experiments was whether they probe the equilibrium state of the system or the pair condensates are formed during the rapid field ramp. Although the rapid ramp time is longer than the unitarity limited collision time, Pauli suppression was expected to enhance relaxation times by

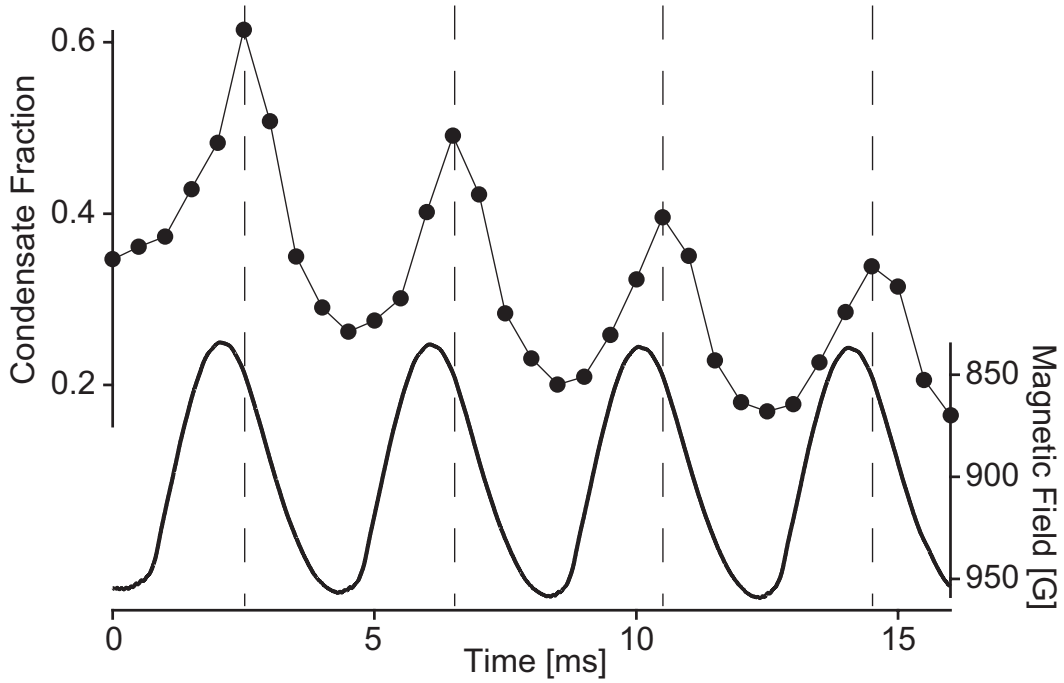

Figure 6-5: Formation dynamics of a fermion pair condensate. The condensate fraction of the fermion pair condensate was measured while the magnetic field was modulated at a high rate. The bottom line shows the variation of the magnetic field, and the filled circles show the measured condensate fraction. In this figure the magnetic field axis is inverted so that at equilibrium high values in the upper curve correspond to high values in the lower curve. The vertical dashed lines indicate the local maxima in the condensate fraction, which lags behind the maximum in the magnetic field curve by approximately 500 μs. The Fermi energy of the cloud is T_F=2μK.

a factor equal to $(T/T_F)^2$.

We have been able to measure the condensate formation time in a subsequent set of experiments [10]. The magnetic field was modulated at a high rate and the pair condensate fraction was measured at variable times after starting the modulation. As it can be seen in Figure 6-5 the relaxation time was measured to be τ_R=500$\pm$100 μs for a Fermi energy of 2μK. This is two orders of magnitude slower than the time needed for projection and proved that in our experiments the projection method probes the equilibrium state of the system. We have also found that molecule conversion during the rapid ramp is more efficient for condensed pairs than for thermal pairs which leads for an overestimate of low values of condensate fraction; fortunately this effect is negligible for the highest condensate fractions we observed.

The modulation of the magnetic field in these experiments required modulation of currents up to 500 A by 50 A at a rate up to 1 kHz [1]. At these high modulation rates, the lagging behind of the magnetic field due to eddy currents induced into the steel vacuum chamber was a concern. This delay was measured to be 85±5 μs by probing the atoms with a Zeeman-sensitive optical transition, and the amplitude was reduced to 95% of the dc value.

The maximum observed condensate fraction of 80% offers additional insight into the nature of the pairs. One of the questions still to be answered is whether these pairs are momentum-correlated Cooper-type pairs with a size much bigger than the interparticle spacing, or spatially localized pairs with a molecular character.

In the JILA experiment, it was assumed that delocalized pairs in the open channel would be converted into molecules by the rapid ramp. However, given the ramp speed and the poor spatial overlap between the delocalized pair and the molecular wavefunctions, it is unclear why a molecule would be formed from a long-range pair rather than from next-neighbor atoms. However, the maximum 15% condensate fraction observed in the potassium experiment leaves open the possibility that the rapid ramp has a limited conversion efficiency, producing pairs from both delocalized pairs and next-neighbor atoms.

The highest condensate fractions observed in our experiment approach unity. A random molecule creation from next-neighbor atoms cannot explain the large proportion of molecules with ground center-of-mass motion state, so most of the molecules have to be created from preformed pairs, which must then have a size comparable or smaller than the interparticle spacing.

The nature of pairs observed in the projection experiments was the subject of subsequent theoretical work. The model of molecules stabilized by the Fermi sea can be more rigorously explained in terms of a pair wavefunction which is composed of a closed channel (molecular) part and an open channel (Cooper pair) part [47]. In

[1] This once again challenged our abilities to control high currents. We have achieved this by using one of the high-current IGBT switches in an analog mode, a somewhat risky approach as the power dissipation in the transistor is very high. It was a nice surprise to see this working without initially damaging the equipment.

the field ranges in which pair condensation was observed, the pair wavefunction was predicted to be dominantly molecular [47].

Other theoretical papers explained the nature of the pairs as either Cooper pairs [41], an intermediate type of Cooper pairs which are spatially correlated and have a size comparable to the interparticle spacing [19], or ruled out molecular pairs for ^{6}Li but not for ^{40}K [84]. Given the recent observation of superfluidity in the crossover region for ^{6}Li [138], investigations of the nature of the pair might lead to a better understanding of the phenomenon of resonance superfluidity.

6.4 Resonant superfluidity of the strongly interacting ^{6}Li gas

The quest to observe superfluidity in a strongly interacting Fermi gas was one of the most important goals of ultracold fermion research, and was recently concluded by the observation of quantized vortex lattices in an interacting ^{6}Li gas [138]. Quantized vortices are an unambiguous signal of superfluid flow, but before this final proof a number of experiments incrementally strengthened the evidence for superfluidity, and are reviewed below.

The progress towards observing superfluidity was considerably accelerated by the production of molecular BECs [52, 66, 5, 22]. A molecular BEC is not absolutely necessary for the production of an ultracold fermionic gas in the superfluid regime; evaporative cooling in an optical trap in the repulsive regime can produce interacting fermionic gases for which measured temperatures are comparable or below the predicted transition temperature [97]. Nevertheless, the molecular BEC offers a convenient way for cooling and diagnosing the interacting gas. It also makes the application of standard BEC investigation techniques and the interpretation of the results more intuitive.

After the observation of molecular condensation, quite a few investigation paths have been taken by the groups studying ultracold fermions, most of them very suc-

cessful in providing scientifically relevant data about the physics of the BEC-BCS crossover.

A first generation of experiments investigated the variation of easily observable experimental parameters as the as the cloud size in trap [22] and the release energy of the cloud [26] and have reveled the smooth nature of the crossover.

The pair condensation experiments [112, 6] have been the first ones to investigate the microscopic behavior of the sample on the BCS side of the resonance and have been covered in the previous sections. Another microscopic approach was taken by the Innsbruck group which observed the pairing gap in ^{6}Li by spectroscopic methods [32]. At magnetic fields below the resonance, both atomic and molecular signals were observed similar to the spectrum previously observed in ^{40}K [110] with a separation equal to the molecular binding energy. As expected, the atomic signal was reduced as the temperature was lowered and the molecular fraction increased. Above the resonance, in addition to the atomic signal a second feature was observed at higher energies, indicating the existence of paired atoms. The shape and temperature dependence of the pair feature agreed well with a theoretical calculations for a superfluid Fermi gas in an inhomogenous system [73], thus offering evidence for superfluid behavior.

Another set of two experiments which offered evidence for superfluid behavior studied collective excitations. The first one measured the frequencies and damping rates of the radial breathing mode [71]. While the frequency of the breathing mode was in excellent agreement with the prediction for an hydrodynamic gas with unitarity-limited collisions, the damping rate decreased as the temperature was lowered. The hydrodynamic behavior can occur either because of superfluidity or because of collisions in a normal gas. However, in a normal gas Pauli suppression is expected to lower the collision rate, thus increasing the damping rate as the temperature is lowered, so the observed damping dependence on temperature is consistent with superfluid behavior.

The other experiment investigating collective oscillations [23] showed a strong dependence of the radial mode frequency on the coupling strength, including an abrupt

change in the mode frequency and anomalously strong damping at 910 G. While these features are not understood, it was suggested that they could be the signature of the transition from a superfluid to a normal phase.

Yet another type of experiment involved measurement of the heat capacity of an interacting ^{6}Li gas [72]. A jump in the heat capacity was observed as the gas temperature was lowered below $T = 0.27\ T_F$, which was interpreted as the signature of the transition to a superfluid state.

In the light of the recent observation of vortex lattices, although these intermediate experiments were not able to conclusively prove superfluidity, they generate opportunities for future investigations regarding the validity of the new theoretical models developed in conjunction with these experiments. Given the range of experimental approaches already available for studying the resonance superfluidity and the number of research groups which can produce ultracold interacting fermions, it is normal to expect fast progress towards understanding resonant fermionic superfluidity, and exciting research opportunities in the near future.

Chapter 7

Fermion pairing in atomic physics: future systems and geometries

For fermionic systems, the existence superfluid phase is connected to a pairing mechanism between fermions [21]. The pairing mechanism is linked the macroscopic properties of the superfluid phase, and the variety of pairing mechanisms encountered in the nature are responsible for the existence of a range of superfluid phenomena as metal superconductivity, high-T_c superconductivity, or the superfluidity of ^{3}He.

Ultracold atomic gases are a physical system which can be used to model condensed systems in the dilute limit, where system properties can be linked to first principles and microscopic behavior much more easily. Also, the degree of experimental control of system properties can in principle be used to create new strongly correlated systems, a promise which was partly fulfilled by the observation of resonance superfluidity in ^{6}Li.

This chapter presents a list of pairing mechanisms leading to superfluidity which given the current development of the ultracold atoms research could be observed and investigated in the next years.

7.1 Bare s-wave pairing

The classic example of s-wave pairing is the Cooper pairing, which is responsible for superconductivity in metals [21]. In the case of metals, it is a boson-induced interaction. Trapped ultracold fermionic gases are a even simpler system as pairing occurs due to a direct interaction between two different states. Bulk s-wave pairing is the simplest pairing mechanism, and in atomic physics experiments the strong interacting unitarity-limited regime is also accessible, making this type of pairing and the associated superfluidity most energetically favorable.

s-wave pairing and superfluidity was recently observed [112, 6, 32, 138] and was already covered in this thesis. This confirmed the promise of ultracold atom experiments as a tool to study fermionic superfluidity, and opens the path for new studies.

Higher partial wave pairing occurs in nature if the s-wave interaction is forbidden as in the case of p-wave pairing of superfluid ^{3}He [80], or in restricted geometries, as the planar d-wave pairing in high-T_c cuprate superconductors [130]. While these types of pairing might be more difficult to observe experimentally, they are extremely relevant as an approach to understanding the behavior and properties of condensed state superconductors and superfluids.

7.2 Spin-triplet pairing

The classic example of spin-triplet pairing is superfluid ^{3}He [80], and such pairing also occurs in exotic superconductors as Sr_2RuO_4 [83]. This type of superfluidity is described by a tensorial order parameter which leads the existence of anisotropic superfluid phases and, in the case of ^{3}He, to a rich phase diagram [134].

Spin-triplet pairing occurs if the spin-singlet pairing if forbidden, as it is the case in a system of polarized fermions. Due to the Pauli exclusion principle, only odd-wave components can contribute to the spatial part of the pair wavefunction, and the p-wave pairing is the most energetically favorable.

The critical temperature for p-wave pairing in a single-state ^{6}Li gas was estimated

based on the background value of the p-wave scattering length, $a_{\rm p}$, and predicted to be very low [61]:

$$T_{\rm c} \simeq \frac{E_{\rm F}}{k_{\rm B}} \exp\{-\frac{\pi}{2(k_{\rm F}|a_{\rm p}|)^3}\}$$

Analogous to the case of s-wave pairing in ^{6}Li spin mixtures, the recently observed p-wave Feshbach resonances in ^{6}Li can be used to increase the scattering length to values at which the product $\mathrm{k_F}|a_{\rm p}|$ is close to unity. Another proposal involves using dc electric fields to enhance $a_{\rm p}$ [136]. Thus, the transition temperature could be enhanced to experimentally reachable values.

An interesting point about spin-triplet pairing is that since it could be accessible only in a magnetic field (close to a Feshbach resonance), it could lead to the formation of a non-unitary superfluid phase [80]. Analog to the $\mathrm{A_1}$ phase in ^{3}He, pairing of the spin triplet component with the spins aligned to the external field might occur before the pairing of the anti-aligned triplet component.

7.3 Two-dimensional pairing

The interest in the pairing properties of 2D Fermi systems was triggered by experimental indications that the high-$\mathrm{T_c}$ superconductivity in cuprates originates in atomic layers within the material [130]. In 2D Fermi gases, bound states can be formed by s-wave attractive interactions even when they are infinitesimally small [117]. S-wave pairing in two dimensions has the peculiar property that the system has a Cooper instability if and only if a bound state exists, and in the BCS approximation the gap function and the chemical potential can be determined analytically [108]:

$$\Delta_0 = \sqrt{2E_F E_a}, \mu = E_F - \frac{E_a}{2},$$

where E_a is the free-space two-particle binding energy. The BCS limit corresponds to $E_a \ll E_F$, and the BEC limit to $E_a \gg E_F$. The crossover between the two regimes occurs as the chemical potential changes sign, $E_a = 2E_F$. In the crossover

regime, more accurate calculations predict better collisional properties than in the 3D case, and high superfluid transition temperatures, $T_C \simeq 0.1T_F$ [101]. The 2D p-wave pairing is predicted to have an exponential dependence on the interaction strength, as in the case of 3D pairing [109].

From the experimental point of view, the steps which have to be taken towards observation of 2D pairing are very similar to the ones already taken towards observation of bulk s-wave superfluidity. A first experimental goal would be the realization of a 2D Fermi gas, then the investigation of bound state properties as a function of interaction strength, and finally the observation of the 2D superfluid transition. In particular, the measurements of E_a and Δ_0 by RF spectroscopy should be straightforward.

Two-dimensional atom traps have been already used in our lab for the study of ^{23}Na Bose condensation in 1D and 2D geometries [49]. For a Fermi gas, the 2D requirement $\hbar\omega_t > E_F$, where ω_t is the trapping frequency in the tight direction, is more restrictive than for a BEC, in the sense that for the same trap geometry the number of fermions which can be trapped is smaller. The maximum fermion number is given by $N = (\frac{\omega_t}{\omega_{h1}})(\frac{\omega_t}{\omega_{h2}})$, with ω_{h2} and ω_{h2} the trapping frequencies in the weak horizontal directions. For the elliptical focus optical trap used in our 2D Bose experiments, the maximum fermion number would be approximately 2500, which is already enough to perform experiments. Given the 20-fold higher laser powers we can use now for optical trapping, it should be possible to increase N either by generating a more elliptical focus, by fast scanning of the trapping beam in a horizontal plane, by adding magnetic field gradients, or by a combination of these.

7.4 Boson-induced pairing

Interaction between fermions can be modified by their environment through higher-order processes. One classic example is the lattice-mediated electron-electron interaction in conventional superconductors. In the case of mixtures of two spin states of trapped fermions, it was predicted that induced interactions will weaken the bare attractive interactions, leading to a decrease in the transition temperature [54]. In ul-

tracold gas experiments, the goal is then to observe environment-induced interactions that enhance T_C. It is predicted that if the bare boson-boson interaction is repulsive the induced fermion-fermion interaction is attractive. The boson-induced attraction enhances the bare fermion attraction and in the case of s-wave pairing in the presence of bosons the critical temperature is given by [131]:

$$k_B T_C = \frac{\gamma}{\pi}(\frac{2}{e})^{7/3} E_F \exp(-\frac{\pi}{2\tan\delta_0^{tot}(k_F)})$$

with

$$\tan\delta_0^{tot}(k_F) \simeq -k_F a_{FF}(1 - \frac{a_{BF}^2}{a_{BB}a_{FF}}\frac{(m_B+m_F)^2}{m_B m_F})$$

where a_{BB}, a_{BF}, and a_{BF} are the boson-boson, boson-fermion, and fermion-fermion scattering lengths. This result assumes the same interaction between the boson and the two fermionic atoms, $a_{BF1} = a_{BF2} = a_{BF}$.

Since bosonic stability requires $a_{BB} > 0$, the main requirement for a strong induced interaction is a large boson-fermion scattering length. The recently observed ^{6}Li-^{23}Na Feshbach resonances could be used to tune the value of a_{BF} to enhance the induced interactions. The boson-induced effects could be initially studied in the strongly interacting s-wave case by simply adding sodium to a strongly interacting lithium mixture. While not dominant, boson-induced attraction might change the superfluid transition temperature.

To dominate the bare s-wave interaction, boson-induced s-wave pairing requires strong interaction of bosons with both fermionic states, and ideally requires the use of two coupled Feshbach resonances. Assuming particular values for the not accurately known singlet and triplet K-Rb scattering lengths, such resonances were predicted to occur in collisions between fermionic ^{40}K and bosonic ^{87}Rb [120].

For the case of ^{6}Li and ^{23}Na, the simple model presented in Chapter 4 predicts a few pairs of resonances separated by less than 1 G at rather impractical magnetic fields (Table G.1). However, since these predictions are unlikely to have an accuracy better than a few tens of Gauss, an experimental search for all interspecies resonances below 1100 G is the best approach for finding (or not!) useful coupled resonances in

the ^{6}Li - ^{23}Na system.

Enhancement of p-wave pairing does not require coupled Feshbach resonances. Estimates of highest possible transition temperatures in a 3D system seem too low to be observable [46], but in a 2D system the p-wave pairing gap can be of the order of the Fermi energy [94], similar to direct s-wave pairing in 2D.

Chapter 8

Conclusions

The ultracold fermion research at MIT started in the winter of 2000 with an idea for sympathethic cooling, one empty lab, and with mainly two graduate students, Zoran and myself. At that time, only one other lab had produced degenerate fermions (and they were not lithium atoms), and a few other ultracold fermions experiments were developed. In our case, it was not known if the collisional properties of sodium-lithium mixtures were favorable, and we have spent a first year and a half not knowing whether our work will lead to ultracold fermions.

One year into the project, the various parts of the experiments started to take shape, and the progress was boosted by the addition of three new members: Martin, Deep and Kai. With more than twice the numbers and being able to tap into their combined atom cooling knowledge, degenerate fermions have been produced within the next year.

Since we have been able to cool lithium, the results have not failed to appear, and the investigation of the new fermion physics continued at an ever-increasing rate, which is still a source of amazement to me. In the early days, even Wolfgang would say that work with fermions advances at half the pace of BEC research so we should not worry too much. But the cooling idea we were not sure it would work turned out to produce larger numbers of degenerate fermions than the number of degenerate bosons achieved in the same BEC1 machine.

The next period was marked by solid progress made by the original extended

team joined by Christian, first as a diploma student and then as a graduate student. The interacting regime in lithium was achieved and then investigated by studies of Feshbach resonance and then by rf spectroscopy, and these years were also defined by a continuous improvement of the machine, sometimes in radical ways as it was the case with the new magnetic trap, and sometimes more incremental.

The fall of 2003 came with the departure of more than half of the initial team. Only two veterans, Martin and me, were left to deal with a machine which performed poorly over the whole summer, at a time when fermion research started to speed up with the production of lithium molecules. But contrary to the expectations, the best time for our experiment had just started. With Christian, Sebastian and Jamie completing the lab, the next half year was the most productive ever, with molecular condensation, pair condensation and interspecies resonances observed one after the other.

During the last months of my stay at MIT, helping building the second fermion experiment was the best distraction from job hunting and thesis writing I could dream of. Jit-Kee, Dan, Widagdo and Yingmei are now approaching completion of this second project with fast steps, and many exciting projects are in sight.

Looking back, it was an amazing journey from almost nothing to seeing some of most important promises of ultracold fermion research becoming reality. For the near future, many of the most interesting experiments are already within reach: characterizing the fermionic superfluidity, putting fermions into optical lattices, making heteronuclear molecules, studying 2D fermion pairing, and other discoveries I cannot predict now. Given the great resources at hand in terms of equipment and knowledge, and the excellent people which are continuing the work, it might be just the beginning of a great time.

Appendix A

Multiple species atom source for laser-cooling experiments

C. A. Stan and W. Ketterle

"Multiple species atom source for laser-cooling experiments,"

Rev. Sci. Instrum. 76, 063113 (2005)

Multiple species atom source for laser-cooling experiments

C. A. Stan[a] and W. Ketterle
Department of Physics, MIT-Harvard Center for Ultracold Atoms, and Research Laboratory of Electronics, MIT, Cambridge, Massachusetts 02139

(Received 25 March 2005; accepted 26 April 2005; published online 1 June 2005)

We describe the design of a single beam, multiple species atom source in which the flux of any component can be separately adjusted. Using this design we have developed a ^{23}Na–^{6}Li atom source for ultracold atom experiments. The fluxes of lithium and sodium are independently tunable, allowing operation as a single ^{23}Na or ^{6}Li source as well as a double source with equal atomic fluxes in each component. © *2005 American Institute of Physics.* [DOI: 10.1063/1.1935433]

I. INTRODUCTION

In recent years a number of frontier atomic physics experiments have used more than one atomic species. The most precise measurement of the electrical dipole moment of the electron to date[1] used two atoms to suppress systematic errors. Ultracold mixtures of two atomic species are used for sympathethic cooling of fermions,[2–4] for the study of atomic Bose-Fermi mixtures,[5] and of interspecies Feshbach resonances.[6,7] Simultaneous laser cooling of the atomic components is used to study interspecies collisions,[8,9] and to produce ultracold heteronuclear molecules,[10] which might be used for quantum computation[11] or the observation of exotic many-body states.[12,13]

Vapor cells and atomic beams are the most common atom sources for cold atom experiments. In a vapor cell, an atomic trap is loaded from background gas. Higher background gas pressures result in faster loading rates, but above optimum pressure losses due to collisions with the background gas increase as fast as the loading rate. Multispecies vapor cells have been used to generate a slow beam of rubidium and cesium atoms.[8]

Loading an atomic trap from a collimated beam of atoms is compatible with ultrahigh vacuum and avoids background gas collisions. The flux of atoms slow enough to be captured by the trap can be considerably increased compared to a thermal beam by using a Zeeman slower.[14] The Zeeman slower system has higher loading rates than a vapor cell.

A multiple-species experiment can be designed with multiple independent beam sources, but this increases its complexity. We have developed a two-species atomic oven for ^{23}Na and ^{6}Li which works with a single Zeeman slower to load ^{23}Na and ^{6}Li magneto-optical traps (MOTs) simultaneously.

The article is organized as follows: In Sec. II we present the general design and operation criteria for a multiple species oven, and in Sec. III the construction of the sodium-lithium source. We describe the operation of this source and its performance in Sec. IV, and we discuss in Sec. V the applicability of the sodium-lithium design to other atomic species used in laser-cooling experiments.

[a]Electronic mail: thyx@mit.edu

II. GENERAL DESIGN CRITERIA FOR A MULTIPLE SPECIES SOURCE

Effusive ovens[15] are simple and efficient atom sources. They consist of an evacuated reservoir chamber in which the desired species is stored in solid or liquid form, and is in equilibrium with its vapor. The vapor effuses through a small opening toward the experiment. The flux is easily controlled by changing the oven temperature and thus the equilibrium vapor pressure in the reservoir.

The relation between the flux and the vapor pressure is linear as long as the vapor pressure is low enough that the flow through the oven nozzle is molecular. Equivalently, the mean free path at the vapor pressure is bigger than the nozzle size. Operation beyond the linear regime results in viscous or supersonic flows, characterized by higher total atom fluxes and by a depletion of the low velocity tail of the Maxwell distribution. Zeeman slowing usually captures the low-velocity tail and therefore requires operation of the oven in the linear regime.

If multiple atomic or molecular species must be present in the beam, loading a single reservoir with more than one pure substance is in general not appropriate. The vapor pressures at the same temperature are likely to be different. The ratio of fluxes is then fixed at approximately the ratio of the vapor pressures, which has a weak dependence on temperature. In the case of our experiment, sodium has a vapor pressure three orders of magnitude higher than lithium at the same temperature, meaning that at optimum sodium flux the lithium flux is too low, and at the optimum lithium flux the sodium consumption rate is impractical.

A solution to this problem is the use of multiple reservoirs, each holding a pure component, connected to a mixing chamber (Fig. 1). The design requirements for all reservoirs is that they should deliver their component to the mixing chamber at an adjustable rate. In steady state, the mixing chamber should not absorb the components. Then, the flux of one species through the oven nozzle equals the flux through the mixing nozzle, and can be tuned by changing the temperature of the reservoir.

For simplicity we will assume that the pressures in the reservoirs are much bigger than the pressure in the mixing chamber, which in its turn is much bigger than the pressure

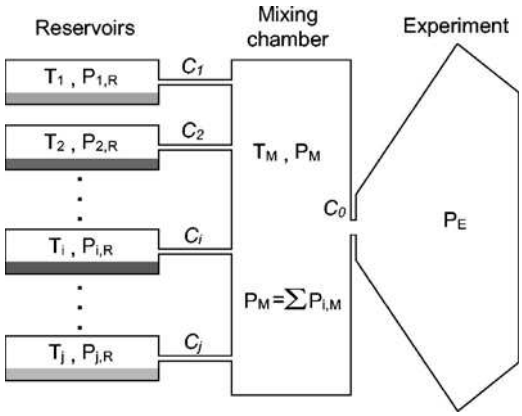

FIG. 1. Design of a multiple species oven. Reservoirs containing pure components are connected to a mixing chamber through mixing nozzles. The mixing chamber is connected to the experiment through the oven nozzle. $P_{i,R}$ are the saturated vapor pressures at the reservoir temperatures T_i. In the mixing chamber a gaseous mixture at temperature T_M is formed, with partial pressures $P_{i,M}$. P_E is the pressure in the experiment chamber. Nozzle vacuum conductances are shown in italics. For proper operation, $P_{i,R} \gg P_{i,M} \gg P_E$.

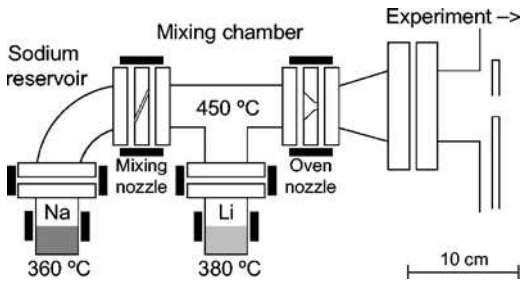

FIG. 2. Exploded cross-section view, to scale, of the ^{23}Na–^{6}Li source. The oven is built from 2.75 in. ConFlat fittings, made from 316 SS. Alkali receptacles are capped half nipples, and the nozzles are machined from double-sided blanks. The 2 mm diameter mixing nozzle is angled to achieve a length of 32 mm, and the thin oven nozzle has a diameter of 4 mm. A copper plate with a 7.5 mm hole, shown at the right edge of the figure, acts as a collimation aperture. Black rectangles represent the six resistive band heaters used for temperature adjustment. The shown temperatures of the alkali receptacles and of the mixing chamber are typical for double species operation.

outside the oven. Such pressure ratios are also the best choice for oven operation, as it will be seen below.

The throughput of the ith component, $Q_{i,R}$, from the ith reservoir to the mixing chamber is given by

$$Q_{i,R} = C_i(P_{i,R} - P_{i,M}) \simeq C_i P_{i,R},$$

where C_i is the conductance of the ith mixing nozzle, $P_{i,R}$ the vapor pressure in the ith reservoir, and $P_{i,M}$ the partial pressure in the mixing chamber. Assuming that the reservoirs are not contaminated with different species, and that $P_{i,M}$ is smaller than the saturated vapor pressure in the mixing chamber, the throughput of the component from the oven to the experiment is given by

$$Q_{i,T} = C_0 P_{i,M} = Q_{i,R} - P_{i,M} \sum_{j \neq i} C_j,$$

where C_0 is the vacuum conductance of the oven nozzle and $P_{i,M}$ is the partial pressure of component i in the mixing chamber. The second term in the sum denotes the loss of component i by backflow into other reservoirs. It can be made negligible if all the mixing nozzle conductances C_j are much smaller than C_0.

In steady state operation, assuming that all mixing nozzles have conductances much smaller than the oven nozzle,

$$Q_{i,T} = Q_{i,R} = C_i P_{i,R}$$

and the flux of component i from the oven can be tuned by heating the reservoir in the same way as for a simple effusive oven.

Backflow of other species from the mixing chamber into the reservoir is not desirable, for two reasons. First, these other species will be lost into the reservoir rather than making the effusive beam. Second, different species could react with or dissolve into the pure substance loaded in the reservoir, reducing its vapor pressure.[16]

Reducing the backflow to negligible levels and even complete suppression can be achieved by a proper design of the mixing nozzles. Backflow occurs through diffusion against the constant stream of atoms or molecules coming from the reservoir. If this stream is sufficiently fast it will blow away diffusing components before they could reach the reservoir.

We have estimated the parameters of the mixing nozzle by requiring that in the nozzle the diffusion speed of component j into component i is smaller than the macroscopic speed of the stream. For a nozzle made of a long cylindrical tube, the approximate condition for suppression is

$$\lambda_{j,P_{i,R}} < d,$$

where $\lambda_{j,P_{i,R}}$ is the mean free path of species j in the gas of i at reservoir i pressure $P_{i,R}$, and d is the nozzle diameter. An equivalent statement is that the flow in the mixing nozzle should be viscous or at least in the intermediate regime.

Chemical reactions and solution formation is also a concern for the mixing chamber, but negative effects can be diminished by raising the temperature of the chamber. As long as the partial pressures of different components are below their saturated vapor pressure, condensation will not occur, and the rate of chemical reactions will be significantly decreased. The guidelines for temperature settings are completed by the condition that the nozzles should have the highest temperatures in the oven to avoid clogging.

III. SODIUM-LITHIUM ATOM SOURCE

A schematic of our ^{23}Na–^{6}Li oven is given in Fig. 2. The oven follows the basic design principles described above, but its construction was simplified by putting the lithium in the mixing chamber rather than in its own reservoir. This modification was necessary to keep the maximum oven temperature at the specified operation limit of ConFlat knife-edge vacuum flanges, 450 °C. The vapor pressure required for proper operation of a lithium reservoir must be tens times bigger than the vapor pressure in the mixing chamber, and can be achieved only at higher temperatures. Building the oven from ConFlat parts makes it compatible with the rest of our vacuum chamber, and allows easy assembly and disassembly during alkali reloading.

Since the lithium is placed in the mixing chamber, chemical reaction and alloy formation are possible. The binary phase diagram of sodium and lithium[17] exhibits immiscibility regions. Above lithium's melting temperature of 180.6 °C, the mixture is liquid at all concentrations, but it can phase separate into sodium-rich and lithium-rich liquids. Above the critical temperature 303.2 °C, the sodium and the lithium are fully miscible.

A small amount of sodium always dissolves into the lithium during two species operation. Above the critical temperature there is only one liquid phase, a solution of sodium in lithium. The concentration of sodium can be estimated by assuming that the solution is ideal and thus obeys Raoult's law. Raoult's law states that the vapor pressure of the solute is smaller than the saturated vapor pressure by the atomic concentration of the solute in the solvent. The vapor pressure of sodium is three orders of magnitude higher than lithium's at the same temperature. In an alloy above which both elements have equal partial vapor pressures, the atomic concentration of sodium is then only 0.1%. The sodium-lithium mixture exhibits a tendency toward phase separation. Therefore a positive deviation from Raoult's law is expected,[18] and the real sodium concentration is smaller than our estimate. Since the sodium concentration is small, lithium vapor pressure is not decreased significantly by the presence of sodium.

The sodium-lithium oven is built from 2.75 in. ConFlat fittings. The presence of lithium, which reacts with metals more aggressively than other alkali, and the relatively high operating temperatures required the use of nonstandard materials for the fittings and the gaskets. Copper gaskets are the standard choice, but when heated to 400–450 °C they can bond to the knife edges, making disassembly difficult. Annealed nickel gaskets were chosen for their high temperature performance and for their good compatibility with molten alkali metals.

Nickel gaskets, even when fully annealed, are harder than copper gaskets, and their properties vary among manufacturers and different batches. As a result, reliable sealing and resealing was difficult when we used standard ConFlat fittings made from type 304 stainless steel. The knife edge dulls after only a few reseals, probably because of annealing of type 304 when it is cycled from room temperature to 400–450 °C.

We have overcome this problem by using slightly modified fittings made from type 316 stainless steel. A chromium-nickel steel, type 316's composition differs from type 304's by the addition of 2%–3% molybdenum. It is offered as a material option by vacuum manufacturers for its better high-temperature strength. We have found that type 316 fittings were indeed superior to standard type 304 fittings between 400 and 450 °C and could be resealed multiple times.

The fittings were modified by removing a 0.127 mm layer of material from the flange faces. By doing this the knife edge recession is reduced and the knife edge can cut deeper into the nickel gaskets, which we often found to be thinner than industry specifications. The modified fittings were manufactured by A&N Corporation (Williston, FL).[19]

The oven nozzle has a diameter of 4 mm, equal to the narrowest collimating aperture, a differential pumping tube. The mixing nozzle is a 2 mm diameter, 32 mm long tube angled with respect to the axis of the machine. Both nozzles were machined in double-sided ConFlat blanks.

For heating, band heaters are placed around flanges and around alkali receptacles. We have used custom Mi-Plus heaters manufactured by TEMPCO (Wood Dale, IL).[20] They can be operated at temperatures up to 760 °C, and have incorporated *K*-type thermocouples, ensuring reproducible temperature readout. The heater powers are 100 W for the alkali receptacles, 150 W for the receptacle flanges, and 300 W for the nozzle flanges.

The heaters are controlled by commercial temperature controllers. The oven is thermally insulated by wrapping first ceramic fiber tape to form a 1 cm thick layer of insulation. Two or three layers of household use aluminum foil are wrapped on top of this layer. Temperature stability is approximately 0.1 °C.

The oven is connected to a section of our apparatus in which the pressure is 1×10^{-8} Torr. In this section the beam is collimated to 5×10^{-5} sr divergence by a differential pumping tube with an inner diameter of 4 mm.

IV. OPERATION AND PERFORMANCE

The oven is loaded with 25 g of ^{23}Na and 10 g of isotopically enriched ^{6}Li (95% purity). Sodium is commercially available in sealed glass ampoules which we break just before loading. Enriched ^{6}Li is available as chunks under mineral oil, and has to be cleaned prior to loading. We had the ^{6}Li cleaned and repackaged into sealed glass ampoules by a materials preparation laboratory.[21]

The target alkali temperatures are achieved by setting the receptacle heaters to these temperatures, 360 °C for sodium and 380 °C for lithium. The heaters around the flanges of the receptacles are set to 20 °C above the alkali temperature for a smooth thermal gradient from the alkali receptacles to the nozzles. Nozzle heaters are both set to 450 °C. The nozzles are the hottest areas in the oven to prevent their clogging. When the experiment is not running, nozzle heaters are kept on while the other heaters are turned off. From this idle state, it takes less than 10 min to heat the oven to its operating temperatures.

The mixing nozzle operates in the viscous flow regime. Its conductance, 0.08 L/s, is difficult to calculate in this regime, and was measured from the sodium consumption rate. At 450 °C the calculated molecular flow conductance of the oven nozzle is 2.6 L/s for sodium and 5 L/s for lithium. This results in a ratio of sodium pressures in the reservoir and the mixing chamber of approximately 30. The partial pressures in the mixing chamber are 4×10^{-3} Torr for sodium and 4×10^{-5} Torr for lithium.

Alkali-alkali collision cross sections at room temperature are quite large, making the mean free paths in alkali vapor considerably shorter than those encountered in normal vacuum practice. We have estimated the cross sections using the Massey-Mohr formula[22]

$$\sigma = 5\times10^{11}(C_6/v)^{2/5},$$

where σ is the collision cross-section in cm^2, C_6 the van der Waals coefficient in erg cm^6, and v the speed in cm/s. For

sodium we have used the experimental value of C_6 given in Ref. 23 and for lithium the theoretical calculation given in Ref. 24.

The estimated mean free path of lithium in the sodium reservoir is 0.1 mm, satisfying the condition for backflow suppression given in the previous section. The estimated mean free paths for sodium and lithium in the mixing chamber are 1.7 and 2.8 mm, slightly lower than required for molecular flow through the 4 mm oven nozzle. In this regime the oven nozzle conductance, calculated using conductance tables given in Ref. 16, is not significantly changed from its molecular flow value.

Total sodium atom flux, measured from the sodium consumption rate, is 1.6×10^{17} s^{-1}. A lithium flux of 3×10^{15} s^{-1} was estimated from the vapor pressure. The fluxes in the collimated beam are approximately 10^4 times lower. The limits on flux tuning are given by different factors for sodium and lithium. For sodium, the minimum operating temperature is approximately 200 °C, the equilibrium temperature with only the nozzle heaters on. The upper limit 360 °C is given by the requirement that the flow through the oven nozzle is molecular. For lithium the upper limit 435 °C is given by the requirement that the nozzles are the hottest part of the oven. We have decided not to operate the lithium reservoir below the critical temperature 303.2 °C to avoid a possibly complicated dependence between reservoir temperature and atom flux. The atomic fluxes can be varied over three orders of magnitude, between 1.3×10^{14} and 1.6×10^{17} s^{-1} for sodium, and from 5×10^{13} to 3×10^{16} s^{-1} for lithium.

The Zeeman slower originally designed for sodium was modified for double operation by overlapping lithium laser slowing light with the sodium slowing light. With this double atom source we can load sodium, lithium, or overlapping double species MOTs. The lithium MOT traps 3×10^8 atoms and loads in approximately 4 s. The sodium MOT traps 10^{10} atoms and loads in approximately 2 s. The atom numbers given are accurate within a factor of 2. For the double species MOT, the number of lithium atoms is reduced to approximately half, as measured from the drop in MOT fluorescence intensity. The number of sodium atoms is not changed.

The double species MOT provides an excellent starting point for further cooling the mixture into quantum degeneracy. Bose-Einstein condensates of ^{23}Na with 2×10^7 atoms and degenerate ^{6}Li Fermi gases with 5×10^7 atoms are routinely produced.[25]

With a full 25 g sodium load, the oven operates continuously for 1200–1300 h. We have estimated that the 10 g lithium load should last for 10 000 hours at the maximum flux. Sodium changes are performed twice a year. We do not find any lithium deposits in the sodium reservoir, which proves that the mixing nozzle design suppresses lithium backflow. The low conductance mixing nozzle allows clean venting with high purity argon during the changes, and baking is not needed. The experiment can be run again within hours of sodium reloading.

Most of the effused sodium deposits on the collector plate and on the walls of the 4.5 in. ConFlat six-way cross to which the oven is attached. Sodium needs to be cleaned every 2–3 years. The deposition occurs in readily accessible areas and the cleaning procedure takes at most a few days.

V. DISCUSSION

Efficient loading of a multiple-species MOT using a multiple species oven requires the use of a Zeeman slowing scheme which operates for all species. While laser beams with different frequencies can be easily overlapped, the solenoid coil which generates the spatially varying magnetic field is the same for all species.

It is possible to design a solenoid which will operate for more than one alkali atom. The most important parameter for the design of a Zeeman slower is the maximum acceleration of an atom interacting with a resonant laser beam:

$$a_{\max}=\frac{\pi\hbar\Gamma}{m\lambda},$$

where Γ and λ are the linewidth and the wavelength of the resonant light, and m is the mass of the atom. In the case of alkali atoms, it is the atom mass which varies most from species to species. The maximum acceleration decreases from lithium to cesium.

The construction of the slowing coil defines the maximum speed of the atoms which can be slowed (the capture velocity), and the acceleration of the slowed atoms. This acceleration must be smaller than $a_{\max}$. Since $a_{\max}$ decreases with mass, a coil designed for a given alkali will work also for lighter species. However, at the same capture velocity and same temperature a smaller part of the Maxwell-Boltzmann distribution can be slowed for the lighter atom. In our experiment, the performance of sodium-designed coils at slowing lithium was satisfactory.

The use of a single beam, multiple atom source can significantly simplify the design of a multiple species laser-cooling experiment. The general design criteria given in Sec. II is applicable for any mixture of pure substances as long as chemical reactions do not occur between the components. The trichamber thallium-sodium oven described in Ref. 1, developed independently from ours, uses the same principle as our sodium-lithium source.

The ConFlat construction we adopted for our sodium-lithium oven does not require complicated machining and can be applied to many of the atomic isotopes used in laser-cooling experiments. The main limitation of the ConFlat design using 316 SS parts and nickel gaskets is its maximum operating temperature. Multiple reassembly can be easily achieved at temperatures up to 400 °C. We have been able to reassemble a flange heated to 500 °C and we have learned that the seals are reliable to at least 650 °C, although they might not be resealable.

Given the typical atomic fluxes needed in laser-cooling experiments, partial pressures in the mixing chamber should be around 1×10^{-3} Torr. Alkali isotopes of K, Rb, and Cs all have vapor pressures higher than sodium. Ca, Sr, and Yb isotopes which have been laser-cooled to high phase space densities[26–28] have vapor pressures comparable with lithium. The design described here should work for all these species.

ACKNOWLEDGMENTS

This work was supported by the NSF, ONR, USARO, and NASA. We thank Michele Saba and Zoran Hadzibabic for a critical reading of the manuscript.

[1] B. C. Regan, E. D. Commins, C. J. Schmidt, and D. DeMille, Phys. Rev. Lett. **88**, 071805 (2002).
[2] Z. Hadzibabic, C. A. Stan, K. Dieckmann, S. Gupta, M. W. Zwierlein, A. Görlitz, and W. Ketterle, Phys. Rev. Lett. **88**, 160401 (2002).
[3] A. G. Truscott, K. E. Strecker, W. I. McAlexander, G. B. Partridge, and R. G. Hulet, Science **291**, 2570 (2001).
[4] F. Schreck, L. Khaykovich, K. L. Corwin, G. Ferrari, T. Bourdel, J. Cubizolles, and C. Salomon, Phys. Rev. Lett. **87**, 080403 (2001).
[5] G. Modugno, G. Roati, F. Riboli, F. Ferlaino, R. J. Brecha, and M. Inguscio, Science **297**, 2240 (2002).
[6] C. A. Stan, M. W. Zwierlein, C. H. Schunck, S. M. F. Raupach, and W. Ketterle, Phys. Rev. Lett. **93**, 143001 (2004).
[7] S. Inouye, J. Goldwin, M. L. Olsen, C. Ticknor, J. L. Bohn, and D. S. Jin, Phys. Rev. Lett. **93**, 183201 (2004).
[8] N. Lundblad, D. C. Aveline, R. J. Thompson, J. M. Kohel, J. Ramirez-Serrano, W. K. Klipstein, D. G. Enzer, N. Yu, and N. Maleki, J. Opt. Soc. Am. B **21**, 3 (2004).
[9] M. S. Santos, P. Nussenzveig, L. G. Marcassa, K. Helmerson, J. Flemming, S. C. Zilio, and V. S. Bagnato, Phys. Rev. A **52**, R4340 (1996).
[10] J. P. Shaffer, W. Chalupczak, and N. P. Bigelow, Phys. Rev. Lett. **82**, 1124 (1999).
[11] D. DeMille, Phys. Rev. Lett. **88**, 067901 (2002).
[12] K. Góral, L. Santos, and M. Lewenstein, Phys. Rev. Lett. **88**, 170406 (2002).
[13] M. A. Baranov, M. S. Mar'enko, V. S. Rychkov, and G. V. Shlyapnikov, Phys. Rev. A **66**, 013606 (2002).
[14] W. D. Phillips and H. Metcalf, Phys. Rev. Lett. **48**, 596 (1982).
[15] K. J. Ross and B. Sonntag, Rev. Sci. Instrum. **66**, 4409 (1995).
[16] S. Dushman, *Scientific Foundations of Vacuum Technique* (Wiley, New York, 1962), pp. 104–111, 710–722.
[17] T. B. Massalski, H. Okamoto, P. R. Subramanian, and L. Kacprzak, *Binary Alloy Phase Diagrams* (ASM International, Materials Park, OH, 1990), pp. 2448–2450.
[18] H.-G. Lee, *Chemical Thermodynamics for Metals and Materials* (Imperial College Press, London, 1999), pp. 83–86.
[19] A&N Corporation, Williston, FL.
[20] TEMPCO Electric Heater Corporation, Wood Dale, IL.
[21] Materials Preparation Center, Ames Laboratory, Ames, IA.
[22] H. S. W. Massey and C. B. O. Mohr, Proc. R. Soc. London **A144**, 188 (1934).
[23] U. Buck and H. Pauly, Z. Phys. **185**, 155 (1965).
[24] P. R. Fontana, Phys. Rev. **123**, 1865 (1961).
[25] Z. Hadzibabic, S. Gupta, C. A. Stan, C. H. Schunck, M. W. Zwierlein, K. Dieckmann, and W. Ketterle, Phys. Rev. Lett. **91**, 160401 (2003).
[26] T. Binnewies, G. G. Wilpers, U. Sterr, F. Riehle, and J. Helmcke, Phys. Rev. Lett. **87**, 123002 (2001).
[27] H. Katori, T. Ido, Y. Isoya, and M. Kuwata-Gonokami, Phys. Rev. Lett. **82**, 1116 (1999).
[28] Y. Takasu, K. Maki, K. Komori, T. Takano, K. Honda, M. Kumakura, T. Yabuzaki, and Y. Takahashi, Phys. Rev. Lett. **91**, 040404 (2003).

Appendix B

Two-Species Mixture of Quantum Degenerate Bose and Fermi Gases

Z. Hadzibabic, C. A. Stan, K. Dieckmann, S. Gupta, M. W. Zwierlein, A. Görlitz, and W. Ketterle

"Two-Species Mixture of Quantum Degenerate Bose and Fermi Gases"
Phys. Rev. Lett. 88, 160401 (2002).

Two-Species Mixture of Quantum Degenerate Bose and Fermi Gases

Z. Hadzibabic, C. A. Stan, K. Dieckmann, S. Gupta, M. W. Zwierlein, A. Görlitz,* and W. Ketterle
Department of Physics, MIT-Harvard Center for Ultracold Atoms, and Research Laboratory of Electronics, MIT, Cambridge, Massachusetts 02139
(Received 26 December 2001; published 4 April 2002)

We have produced a macroscopic quantum system in which a ^{6}Li Fermi sea coexists with a large and stable ^{23}Na Bose-Einstein condensate. This was accomplished using interspecies sympathetic cooling of fermionic ^{6}Li in a thermal bath of bosonic ^{23}Na. The system features rapid thermalization and long lifetimes.

DOI: 10.1103/PhysRevLett.88.160401 PACS numbers: 05.30.Fk, 32.80.Pj, 39.10.+j, 67.60.–g

Experimental methods of laser and evaporative cooling, used in the production of atomic Bose-Einstein condensates (BEC) [1], have recently been extended to realize quantum degeneracy in trapped Fermi gases [2–5]. What makes gaseous fermionic systems particularly appealing to investigate is the relative ease with which their properties can be varied. This allows the exploration of a vast range of experimental regimes, from noninteracting to strongly correlated. In the first case, purely quantum statistical effects can be studied, such as the implications of Pauli exclusion on scattering properties of the system. In the other extreme, exciting new regimes of BCS-like fermionic superfluidity may be within reach [6–9]. An additional area of interest is the production of a dilute quantum degenerate mixture of Bose and Fermi gases, akin to the strongly interacting ^{4}He-^{3}He liquid. This would extend the list of possible experimental studies even further, to include effects such as interaction-driven phase separation [10] or BEC-induced interactions between fermions.

In this Letter, we report the production of a new macroscopic quantum system, in which a degenerate ^{6}Li Fermi gas coexists with a large and stable ^{23}Na BEC. We have achieved high numbers of both fermions ($>10^5$) and bosons ($>10^6$), and ^{6}Li quantum degeneracy characterized by a temperature of one-half the Fermi temperature (T_F). This provides us with the starting point for studies of the degenerate ^{6}Li Fermi gas, which is regarded as a particularly promising candidate for the BCS transition [6,7]. Further, favorable collisional properties make the ^{6}Li-^{23}Na system very promising for studies of the degenerate Bose-Fermi mixtures, including the limitations to the cooling process [11,12]. It is also worth noting that, in our experiment, a mixture of two different atomic species has been simultaneously brought into quantum degeneracy for the first time.

Our experimental approach is based on sympathetic cooling of fermions in a large bosonic "refrigerator." In contrast to the bosonic case, two-body elastic collisions are absent in a single-component Fermi gas at ultralow temperatures due to the Pauli exclusion principle. This lack of thermalization precludes direct implementation of forced evaporative cooling. Therefore, cooling of fermions into the quantum degenerate regime must rely on collisions between distinguishable atoms. In two experiments which produced degenerate Fermi gases, mixtures of two fermionic spin states were simultaneously evaporated and mutually cooled [2,5]. Two groups have also demonstrated sympathetic cooling of ^{6}Li by the ^{7}Li bosonic isotope, thus also producing the first quantum degenerate Bose-Fermi mixtures. However, this system has a limitation that, in the upper hyperfine state, the ^{7}Li condensate is unstable [3], while scattering properties in the lower hyperfine state make sympathetic cooling inefficient, and limit the size of both ^{6}Li and ^{7}Li samples [4]. We have overcome both of these limitations by using a large ^{23}Na cloud, instead of ^{7}Li, for sympathetic cooling of ^{6}Li. Our work provides the natural progression in the search for an ideal Bose-Fermi system, where a "good" Bose-Einstein condensate is chosen, and then combined with a favorable fermionic species. Similar two-species experiments are currently being pursued by three other groups [13–15]. Given the vast variety of collisional properties among alkali gases, and a limited choice of favorable Bose-Fermi combinations, the properties of the ^{6}Li-^{23}Na mixture are truly fortuitous. In our experiment, we have observed rapid interspecies thermalization, while low rates for both intra- and interspecies inelastic collisions result in a lifetime longer than 10 s. Both the presence of sufficient "good" (elastic) collisions needed for interspecies thermalization and the slow rate of "bad" (inelastic) collisions could not be taken for granted before our studies.

For this experiment, we have upgraded our ^{23}Na BEC apparatus [16] to allow for both lithium and sodium operation, while making minimal modifications to the original setup. The additional laser light needed for optical cooling of ^{6}Li was generated by a low power, diode laser system [17]. The lithium (671 nm) and sodium (589 nm) laser beams were overlapped using dichroic beam-splitters, and the spatial arrangement of the laser and atomic beams used to trap, cool, and detect lithium was identical to the original sodium setup. Specifically, a two-species magneto-optical trap (MOT) was loaded from a single two-species atomic beam, slowed in the same Zeeman slower previously used

in sodium-only experiments. The fact that the maximum spontaneous light force deceleration is twice as large for ^{6}Li as for ^{23}Na allowed us to slow lithium atoms without compromising the slowing efficiency for sodium.

To implement our experimental strategy, we have developed a two-species oven in which the vapors of ^{6}Li and ^{23}Na were mixed, and a single atomic beam containing both species was produced (Fig. 1). The main difficulty in designing such an oven is that, at the same temperature, the vapor pressure of lithium is 3 orders of magnitude lower than that of sodium. To achieve comparable atomic fluxes of both species, the alkali vapors must be produced in separate chambers, and then delivered to a mixing chamber, at controllable rates. In our design, the lithium chamber was also used for mixing. To operate the oven in either single- or two-species mode, we tuned the atomic fluxes independently by changing the temperatures of the alkali reservoirs. The maximum atom fluxes into the solid angle subtended by the MOT region were 3×10^{11} s^{-1} for ^{6}Li and 2×10^{12} s^{-1} for ^{23}Na.

Under typical operating conditions, 5 s of loading resulted in single-species MOTs with 2×10^7 lithium atoms or 6×10^9 sodium atoms. When both MOTs were operated simultaneously, interspecies light-assisted collisions reduced the number of lithium atoms by a factor of about 4, while the sodium atom number was not noticeably affected. The number of ^{6}Li atoms in the MOT was maximized when the trapping and the repumping light frequencies were tuned 25 MHz below the corresponding resonances. The resulting temperature of the lithium atoms was $\sim$700 μK.

Since the ^{23}Na BEC is produced in the $|F, m_F\rangle = |1, -1\rangle$ lower hyperfine ground state, to avoid inelastic spin-exchange collisions, it is preferred to magnetically trap ^{6}Li in the corresponding $|1/2, -1/2\rangle$ state. (Here, F is the total angular momentum, and m_F is its projection along the quantization axis.) However, the maximum magnetic trap depth in the $|1/2, -1/2\rangle$ state is only 330 μK (see Fig. 2), considerably lower than our MOT temperature. Further, due to the inefficiency of sub-Doppler cooling mechanisms, it is not possible to optically cool lithium to temperatures which would make magnetic trapping in this state efficient [17]. Therefore, to avoid drastic losses due to the limited trap depth, lithium atoms were optically pumped and then magnetically trapped in the $F = 3/2$ manifold. Before loading the magnetic trap, 4 ms were allowed for the sub-Doppler polarization gradient cooling of sodium, during which the lithium cloud was in free expansion. This reduced the transfer efficiency of lithium atoms into the trap by a factor of 2, limiting it to about 12%. We have thus magnetically trapped $\sim 6 \times 10^5$ ^{6}Li atoms in the upper hyperfine state and $\sim 2 \times 10^9$ ^{23}Na atoms in the lower one. At low energies, our cloverleaf magnetic trap is harmonic and axially symmetric. In the lower hyperfine states, the trapping frequencies for lithium (sodium) are $\omega_z = 2\pi \times 26$ (16) Hz axially and $\omega_r = 2\pi \times 354$ (221) Hz radially.

Once the atoms were loaded into the magnetic trap, we started the forced evaporative cooling of sodium [1]. A varying microwave field near 1.77 GHz was used to gradually lower the trap depth for ^{23}Na, selectively transferring the most energetic atoms into the untrapped $|2, -2\rangle$ state. This microwave field does not affect the ^{6}Li atoms, which were therefore not evaporated. Cooling of the lithium sample was instead achieved through thermal contact with sodium. We observed efficient sympathetic cooling of ^{6}Li in the *upper* hyperfine state by ^{23}Na in the *lower* one, and have successfully cooled this Bose-Fermi mixture into simultaneous quantum degeneracy. This observation indicates a surprisingly favorable ratio between

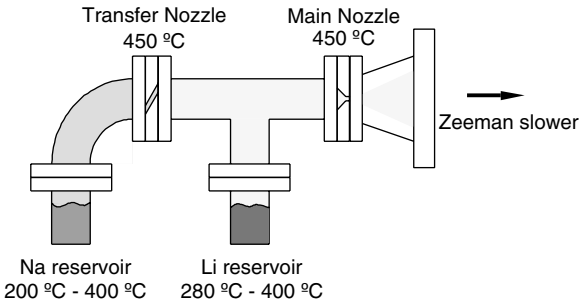

FIG. 1. Two-species oven. ^{6}Li and ^{23}Na vapors were produced in separate chambers to allow for independent control of the atom fluxes. The two species were mixed in the lithium chamber. The transfer nozzle has a conductance 40 times lower than the main nozzle, and limits the undesirable diffusion of lithium into the sodium chamber.

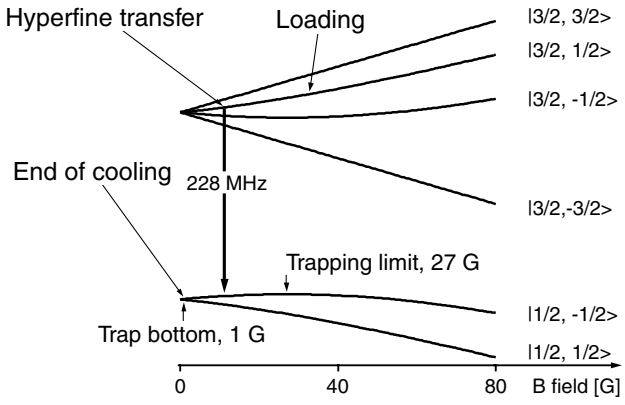

FIG. 2. ^{6}Li in the magnetic trap. Ground state energy levels: The six hyperfine states are labeled in the low magnetic field, $|F, m_F\rangle$ basis. The $|1/2, -1/2\rangle$ state becomes strong field seeking for fields above 27 G, limiting the trap depth to 330 μK. Cooling path: Atoms in the $|3/2, 1/2\rangle$ upper hyperfine state were loaded into the magnetic trap at a temperature of 700 μK. After the initial cooling stage to 50 μK, the atoms were transferred to the $|1/2, -1/2\rangle$ state, and further cooled to a final temperature of 330 nK.

the good and bad interspecies collisions in this mixture. The losses due to inelastic spin-exchange collisions took place only on a time scale of several seconds, comparable to the total evaporation time of 15 s.

In order to produce a collisionally stable Bose-Fermi mixture, it is necessary to transfer the lithium atoms to the lower hyperfine state. To minimize the initial losses due to spin-exchange collisions, this transfer should take place as early in the cooling process as possible. On the other hand, before lithium atoms can be efficiently trapped in the lower hyperfine state, they must be cooled significantly below 330 μK. Therefore, we implemented sympathetic cooling in two stages (see Fig. 2). We optimized the initial evaporation stage to reach a temperature of ~ 50 μK in 5 s, while losing less than half of the lithium atoms, and maintaining the conditions for efficient sodium evaporation. At this point, we found that a substantial fraction of lithium atoms was in the $|3/2, 1/2\rangle$ state. They could thus be transferred to the $|1/2, -1/2\rangle$ state on a single-photon rf transition at 228 MHz, which is, to first order, independent of the magnetic field. This simplification over a similar hyperfine transfer previously employed in [4] was not expected. After the rf pulse was applied, the remaining $F = 3/2$ atoms were optically pumped into untrapped hyperfine states, and expelled from the trap. If this "cleanup" light pulse was omitted, spin-exchange collisions between lithium atoms in different hyperfine states led to a rapid loss of atoms from the trap [18]. The overall efficiency of our hyperfine transfer was $\sim 50\%$. The evaporation was then resumed for another 10 s. We observed efficient sympathetic cooling of the $|1/2, -1/2\rangle$ atoms, and cooled both gases into quantum degeneracy without observable losses in the lithium atom number.

Figure 3(a) displays the effect of sympathetic cooling on the ^{6}Li cloud. Absorption images of the trapped ^{6}Li gas were taken after the ^{23}Na evaporation was terminated at different trap depths, and the sample was allowed to equilibrate for 1 s. Cooling (from top to bottom) is seen in the shrinking of the density distribution and an increase in the peak optical density. In contrast to standard evaporative cooling, and the mutual cooling between two Fermi species, the total number of atoms remains constant.

Quantitative analysis of the ^{6}Li clouds is depicted in Fig. 3(b). We performed two-dimensional fits to the recorded column densities using both a simple Gaussian model and a semiclassical (Thomas-Fermi) distribution for trapped noninteracting fermions. In the latter approach, the probability that an atom has position $\vec{r}$ and momentum $\vec{p}$ is obtained from the Fermi-Dirac distribution for the total (kinetic and potential) energy of the particle. The fitting function for the spatial distribution of atoms in the trap is then obtained by integrating over the momentum degrees of freedom. While the Gaussian model gives a valid description of the gas only in the classical, high temperature limit, the Thomas-Fermi approach is valid at all temperatures, as long as the number of particles in the system is large [19]. Indeed, at higher temperatures, the two fits performed equally well, and yielded the same temperature. However, at a temperature of about 400 nK, the classical fits started to fail. This was indicated by the relative growth of the reduced χ^2 values, by up to 20% above the corresponding values for the fermionic fits. For the coldest samples, Gaussian fits also overestimated the temperature by $\sim 15\%$. From the fitted number of atoms in the system ($N_{\mathrm{Li}} \sim 1.4 \times 10^5$, $T_F \approx 670$ nK), we found that the noticeable inadequacy of the classical fits occurred at $\sim 0.6\, T_F$, which is a clear signature of the Fermi degeneracy. Figure 3(b) shows projected line densities along the axial direction of the ^{6}Li cloud and the Thomas-Fermi fits to the data. The arrow indicates the size of the Fermi diameter, $D_F = 2\sqrt{2k_B T_F/(m\omega_z^2)}$, for the fitted atom number. The spatial extent of the coldest cloud ($T \approx 330$ nK $\approx 0.5\, T_F$) is already comparable to the minimum size the system would assume at zero temperature. Typical densities of the coldest lithium samples were $\sim 10^{12}$ cm^{-3}.

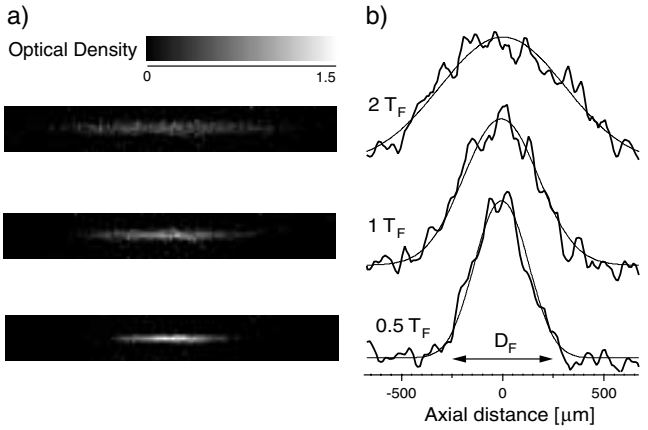

FIG. 3. Onset of Fermi degeneracy. Three pairs of images (top to bottom) correspond to $T/T_F = 2$, 1, and 0.5. (a) Column densities of the ^{6}Li cloud were recorded by absorption imaging. (b) Axial line density profiles and the Thomas-Fermi fits to the data are plotted. The arrow indicates the size of the Fermi diameter, D_F.

In Fig. 4, the temperature of the ^{6}Li cloud is plotted as a function of the final ^{23}Na trap depth. The coldest lithium samples were produced in coexistence with almost pure sodium condensates with $\sim 2 \times 10^6$ atoms. The lifetime of this degenerate mixture was limited to about 10 s by the three-body decay of the BEC, while the lithium cloud had a lifetime longer than 100 s. The lifetime of either species was not detectably affected by the presence of the other one. Even after sodium was lost from the trap, the energy of the lithium cloud did not increase noticeably (<5 nK/s) during its slow decay. We also compared the ^{6}Li temperatures with the temperatures of the ^{23}Na cloud, extracted from the thermal wings of the bosonic density distribution. In hotter samples, the two agreed to within 10%. However, for the coldest samples we observed a discrepancy between the two temperatures. The lowest measurable temperature

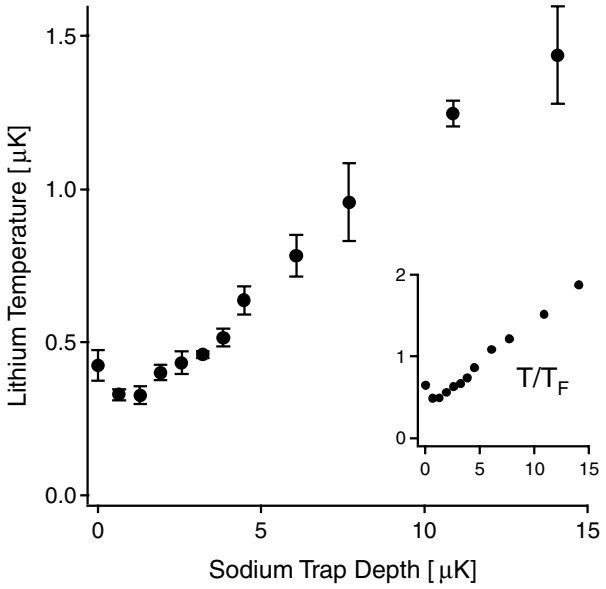

FIG. 4. Temperatures of the ^{6}Li cloud as a function of the ^{23}Na trap depth. Each data point is an average of three measurements. The error bars indicate the shot-to-shot fluctuations, while the uncertainties of the fits are comparable or smaller. In the case when sodium was completely evaporated from the trap (c.f. zero trap depth data point), the very last stage of sympathetic cooling became inefficient due to the vanishing heat capacity of the bosonic reservoir. The inset shows the same temperature data scaled to the Fermi temperature.

of sodium was $T \approx 170$ nK, about half the corresponding lithium value. We verified that, in these samples, extending the thermalization time at the end of evaporation up to 10 s did not lower the lithium temperature any farther. The reasons for the observed temperature discrepancy are worthy of further investigation. Simple spatial separation of the two clouds due to different gravitational sags can be readily ruled out. However, some form of phase separation of the two species [10], or constant heating of the fermionic cloud [12], could play a role.

In conclusion, we have produced a system in which a ^{6}Li Fermi sea coexists with a ^{23}Na BEC. This provides us with a starting point for studies of the degenerate Bose-Fermi mixtures. In particular, the observed temperature difference between the two spatially overlapped species might provide further insight into the limits of sympathetic cooling. Further, by loading the degenerate Fermi cloud into an optical trap, effects of magnetically tunable interactions between lithium atoms in different spin states can be studied [18]. A particularly appealing prospect is the observation of the BCS transition to a fermionic superfluid state, for which ^{6}Li is a very promising candidate.

We thank Florian Schreck for useful discussions and Christian Schunck for experimental assistance. This research was supported by NSF, ONR, ARO, NASA, and the David and Lucile Packard Foundation. M. W. Z. acknowledges the support of the Studienstiftung des deutschen Volkes and the Ecole Normale Supérieure, Paris.

*Current address: Universität Stuttgart, 5. Phys. Inst., Stuttgart, Germany.

[1] *Bose-Einstein Condensation in Atomic Gases,* Proceedings of the International School of Physics "Enrico Fermi," Course CXL, edited by M. Inguscio, S. Stringari, and C. Wieman (IOS Press, Amsterdam, 1999).
[2] B. DeMarco and D. S. Jin, Science **285**, 1703 (1999).
[3] A. G. Truscott, K. E. Strecker, W. I. McAlexander, G. B. Partridge, and R. G. Hulet, Science **291**, 2570 (2001).
[4] F. Schreck, L. Khaykovich, K. L. Corwin, G. Ferrari, T. Bourdel, J. Cubizolles, and C. Salomon, Phys. Rev. Lett. **87**, 080403 (2001).
[5] S. R. Granade, M. Gehm, K. M. O'Hara, and J. E. Thomas, Phys. Rev. Lett. **88**, 120405 (2002).
[6] H. T. C. Stoof, M. Houbiers, C. A. Sackett, and R. G. Hulet, Phys. Rev. Lett. **76**, 10 (1996).
[7] M. Houbiers, R. Ferwerda, H. T. C. Stoof, W. I. McAlexander, C. A. Sackett, and R. G. Hulet, Phys. Rev. A **56**, 4864 (1997).
[8] M. A. Baranov and D. S. Petrov, Phys. Rev. A **58**, R801 (1998).
[9] M. Holland, S. J. J. M. F. Kokkelmans, M. L. Chiofalo, and R. Walser, Phys. Rev. Lett. **87**, 120406 (2001).
[10] K. Mølmer, Phys. Rev. Lett. **80**, 1804 (1998).
[11] E. Timmermans and R. Côté, Phys. Rev. Lett. **80**, 3419 (1998).
[12] E. Timmermans, Phys. Rev. Lett. **87**, 240403 (2001).
[13] J. Goldwin, S. B. Papp, B. DeMarco, and D. S. Jin, Phys. Rev. A **65**, 021402(R) (2002).
[14] G. Modugno, G. Ferrari, G. Roati, R. J. Brecha, A. Simoni, and M. Inguscio, Science **294**, 1320 (2001).
[15] M. Mudrich, S. Kraft, K. Singer, R. Grimm, A. Mosk, and M. Weidemüller, physics/0111213.
[16] M. O. Mewes, M. R. Andrews, N. J. van Druten, D. M. Kurn, D. S. Durfee, and W. Ketterle, Phys. Rev. Lett. **77**, 416 (1996).
[17] U. Schünemann, H. Engler, M. Zielonkowski, M. Weidemüller, and R. Grimm, Opt. Commun. **158**, 263 (1998).
[18] M. Houbiers, H. T. C. Stoof, W. I. McAlexander, and R. G. Hulet, Phys. Rev. A **57**, R1497 (1998).
[19] D. A. Butts and D. S. Rokhsar, Phys. Rev. A **55**, 4346 (1997).

Appendix C

Fiftyfold Improvement in the Number of Quantum Degenerate Fermionic Atoms

Z. Hadzibabic, S. Gupta, C. A. Stan, C. H. Schunck, M. W. Zwierlein, K. Dieckmann, and W. Ketterle

"Fiftyfold Improvement in the Number of Quantum Degenerate Fermionic Atoms,"

Phys. Rev. Lett. 91, 160401 (2003)

Fiftyfold Improvement in the Number of Quantum Degenerate Fermionic Atoms

Z. Hadzibabic, S. Gupta, C. A. Stan, C. H. Schunck, M.W. Zwierlein, K. Dieckmann, and W. Ketterle
Department of Physics, MIT-Harvard Center for Ultracold Atoms, and Research Laboratory of Electronics, MIT, Cambridge, Massachusetts 02139, USA
(Received 2 June 2003; published 16 October 2003)

We have produced a quantum degenerate ^{6}Li Fermi gas with up to 7×10^7 atoms, an improvement by a factor of 50 over all previous experiments with degenerate Fermi gases. This was achieved by sympathetic cooling with bosonic ^{23}Na in the $F = 2$, upper hyperfine ground state. We have also achieved Bose-Einstein condensation of $F = 2$ sodium atoms by direct evaporation.

DOI: 10.1103/PhysRevLett.91.160401 PACS numbers: 05.30.Fk, 32.80.Pj, 39.25.+k, 67.60.–g

Over the last few years, there has been significant progress in the production of quantum degenerate atomic Fermi gases (^{40}K [1,2] and ^{6}Li [3–6]) and degenerate Bose-Fermi mixtures (^{7}Li-^{6}Li [3,4], ^{23}Na-^{6}Li [6], and ^{87}Rb-^{40}K [2]). These systems offer great promise for studies of new, interaction-driven quantum phenomena. The ultimate goal is the attainment of novel regimes of BCS-like superfluidity in a gaseous system [7–11]. The current efforts to induce and study strong interactions in a Fermi gas [12–21] are complemented with the ongoing efforts to improve fermion cooling methods, which would lead to lower temperatures and larger samples.

The main reason why studies of degenerate Fermi gases are still lagging behind the studies of atomic Bose-Einstein condensates (BECs) is the complexity of cooling methods. The Pauli exclusion principle prohibits elastic collisions between identical fermions at ultralow temperatures and makes evaporative cooling of spin-polarized fermionic samples impossible. For this reason, cooling of fermions must rely on some form of mutual or sympathetic cooling between two types of distinguishable particles, either two spin states of the same atom [1,5] or two different atoms [2–4,6]. A key element in fermion cooling is the design of better ''refrigerators'' for sympathetic cooling.

In this Letter, we report the first production of degenerate Fermi samples comparable in size with the largest alkali BECs [22]. We successfully cooled up to 7×10^7 magnetically trapped ^{6}Li atoms to below half the Fermi temperature (T_F). This is an improvement in atom number by a factor of 50 over the largest previously reported Fermi sea [21]. Further, in samples containing up to 3×10^7 atoms, we observed temperatures as low as $0.05\,T_F$, the lowest ever achieved. At these temperatures, the fractional occupation of the lowest energy state differs from unity by less than 10^{-8}.

As in our previous work [6], ^{6}Li atoms were magnetically trapped in the $F = 3/2$, upper hyperfine ground state, and sympathetically cooled by bosonic ^{23}Na. The crucial improvement was our achievement of forced evaporation of sodium in the $|F, m_F\rangle = |2, +2\rangle$, upper hyperfine ground state, producing large and stable BECs with up to 10^7 atoms. This allowed us to create a magnetically trapped ^{23}Na-^{6}Li, Bose-Fermi mixture which is stable against spin-exchange collisions at all densities, and dramatically boosted our fermion atom number.

The criteria for designing sympathetic cooling experiments include the heat capacity of the refrigerator, and the interspecies collisional properties, both elastic and inelastic [23]. Large and stable ^{23}Na condensates are an appealing choice for sympathetic cooling of fermions. Further, a favorable mass ratio allows for simultaneous Zeeman slowing of ^{23}Na and ^{6}Li [6], and for simultaneous magnetic trapping without large differences in the gravitational sag. The interspecies collisional properties are generally not predictable and have to be tested experimentally. In order to minimize all possible inelastic processes, the natural choice is to magnetically trap both species in their lower hyperfine ground states. However, at temperatures reachable by laser cooling ($\geq 300\ \mu$K), ^{6}Li can be efficiently magnetically trapped only in the upper hyperfine state, $F = 3/2$ [4,6] [Fig. 1(a)]. On the other hand, until now sodium had been successfully evaporated only in the lower, $F = 1$ hyperfine state. This was a limiting factor for sympathetic cooling of ^{6}Li, since the mixture of sodium in the lower, and lithium in the upper hyperfine state is not stable against spin-exchange collisions. The inelastic loss rate increases as the temperature is lowered and the density grows. In our previous work [6], we partially overcame this problem by transferring lithium atoms into the lower hyperfine state after an initial sympathetic cooling stage to $\sim 50\ \mu$K. By achieving forced evaporative cooling and Bose-Einstein condensation of sodium in the $F = 2$ state, we have now realized a more robust sympathetic cooling strategy and dramatically improved the size and temperature of a degenerate Fermi system.

We loaded $\sim 3 \times 10^9$ sodium and up to 10^8 lithium atoms in their upper hyperfine states from a two-species magneto-optical trap (MOT) into the magnetic trap. The adverse effect of light assisted collisions in a two-species MOT [6,24] was minimized by slightly displacing the two MOTs with respect to each other. This was achieved in a reproducible manner by aligning both MOTs to the

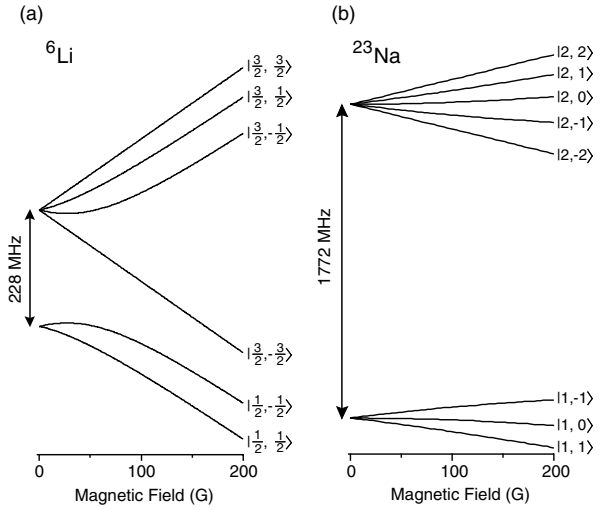

FIG. 1. Hyperfine structures of ^{6}Li and ^{23}Na. The states are labeled in the low field, $|F, m_F\rangle$ basis. (a) Because of finite trap depth of $\sim k_B \times 300\ \mu$K in the $|1/2, -1/2\rangle$ state, lithium can be efficiently loaded into the magnetic trap only in the upper, $F = 3/2$ hyperfine state. (b) Sodium is magnetically trappable in the $|1, -1\rangle$ and in the $|F = 2, m_F \geq 0\rangle$ states. Previously, sodium had been evaporatively cooled to BEC only in the $|1, -1\rangle$, lower hyperfine state.

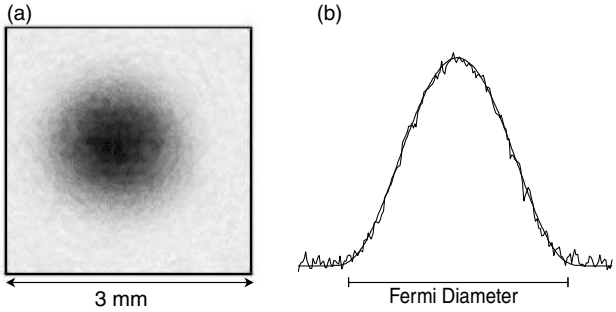

FIG. 2. Large and ultradegenerate Fermi sea. (a) Absorption image of 3×10^7 ^{6}Li atoms released from the trap and imaged after 12 ms of free expansion. (b) Axial (vertical) line density profile of the cloud in (a). A semiclassical fit (thin line) yields a temperature $T = 93$ nK $= 0.05 T_F$. At this temperature, the high energy wings of the cloud do not extend visibly beyond the Fermi energy, indicated in the figure by the momentum-space Fermi diameter.

zero of the magnetic field and then changing the balance of the ^{6}Li laser beams along one direction. The lithium MOT was thus displaced by 3–5 mm, comparable to the radius of the sodium cloud.

During the typical 30 s of sympathetic cooling, we observed no significant inelastic loss of lithium atoms (by three-body collisions or dipolar relaxation), the final number of degenerate atoms being at least half of the number initially loaded in the trap. On the other hand, we observed a favorable rate of elastic collisions between the two species, with the interspecies thermalization time being shorter than 1 s. Therefore, sodium atoms in the upper hyperfine state have ideal properties as a refrigerant for ^{6}Li.

Since our primary interest was cooling of fermions, we evaporated all sodium atoms in order to get lithium to the lowest possible temperatures. Even in our largest ^{6}Li samples, of $\sim 7 \times 10^7$ atoms, we achieved temperatures below $0.5 T_F$. Temperatures in the range 0.05–$0.2 T_F$ could be achieved by reducing the ^{6}Li atom numbers only slightly, to $\sim 3 \times 10^7$. Such big clouds had a high enough optical density for crisp absorption imaging even after ballistic expansion to a size larger than 1 mm [Fig. 2(a)].

Temperatures were extracted from the absorption images of expanding clouds released from the trap, using a semiclassical (Thomas-Fermi) fit to the Fermi-Dirac momentum distribution [6,25] [Fig. 2(b)]. In the ultradegenerate limit, the Fermi distribution is only weakly sensitive to the temperature. While the statistical uncertainty of our fits was generally very small, we have found that the fits along the axial and the radial direction of the cloud can yield slightly different temperatures. Using this discrepancy as the dominant source of uncertainty, we estimate the temperature of our coldest samples to be $0.05^{+0.03}_{-0.02} T_F$.

At present, it is not clear what are the fundamental limits of our sympathetic cooling strategy. One potential limitation could arise from the superfluid nature of the BEC, which prevents further cooling of fermions with velocities lower than the speed of sound in the condensate [23,26]. However, in our large ^{6}Li samples, the Fermi velocity, $\sqrt{2 k_B T_F / m}$, greatly exceeds the typical sound velocity in the largest ^{23}Na BECs. Further, when the sympathetic cooling was optimized to produce the largest and the coldest ^{6}Li samples, the ^{23}Na cloud remained thermal at all times. Therefore, we do not expect the superfluidity of bosons to be a limiting factor.

We have also produced stable degenerate Bose-Fermi mixtures, with more than 10^6 atoms in each species (Fig. 3). In typical samples, the peak density of ^{6}Li was $n_{\mathrm{Li}} \sim 3 \times 10^{12}$ cm^{-3}, while peak densities of the thermal and the condensed ^{23}Na components were $n_{\mathrm{Na}}^{\mathrm{th}} \sim 7 \times 10^{12}$ cm^{-3} and $n_{\mathrm{Na}}^{\mathrm{BEC}} \sim 5 \times 10^{13}$ cm^{-3}. At these densities, the mixture had a lifetime of several seconds. This observation could be used to estimate upper limits for the rate constants of various two- and three-body inelastic processes in the mixture.

In the rest of the Letter, we summarize the numerous steps which were introduced to prepare sodium in the $F = 2$ state as a refrigerant.

In contrast to ^{87}Rb, condensation of sodium by evaporative cooling was previously achieved only in the lower, $|1, -1\rangle$ hyperfine state. $F = 2$ sodium condensates could thus be studied only by transferring optically trapped $F = 1$ BECs into this state [27,28]. Condensation in the upper hyperfine state of sodium is more difficult than in the lower state for two reasons: (1) the requirement for efficient optical pumping in dense laser-cooled samples,

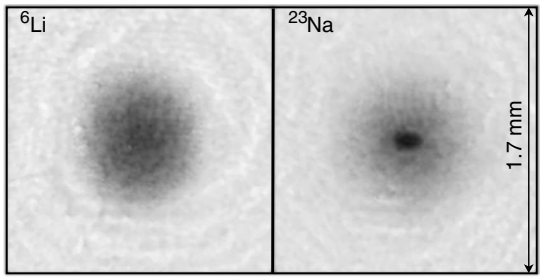

FIG. 3. Two-species mixture of degenerate Bose and Fermi gases. After release from the magnetic trap, both ^{6}Li and ^{23}Na clouds were imaged onto the same camera using separate light pulses. The times of free expansion of the two gases could be varied independently. This dual-imaging technique allowed for optimizing the cooling strategy for either single- or two-species experiments. For the displayed image, the expansion times were $t_{\mathrm{Li}} = 8$ ms and $t_{\mathrm{Na}} = 25$ ms, and the atom numbers were $N_{\mathrm{Li}} \sim 10^7$ and $N_{\mathrm{Na}} \sim 6 \times 10^6$. Sodium was cooled below the condensation temperature, corresponding to $\sim 0.2 T_F$ for the lithium cloud.

and (2) an order of magnitude higher three-body loss rate coefficient [27].

The basic setup of our experiment is described in [6]. In 10 s, we collected typically $\sim 10^{10}$ ^{23}Na atoms, and $\sim 10^8$ ^{6}Li atoms in a magneto-optical trap. Typical MOT temperatures were 0.7–1 mK. Sodium was collected in a dark spontaneous-force optical trap (SPOT) variant of the MOT [29], and therefore most of the atoms were in the $F = 1$ hyperfine state. Lithium was collected in a standard MOT, with about 2/3 of the atoms in the $F = 3/2$ state.

Before the transfer into the magnetic trap, the atoms were optically pumped into the stretched hyperfine ground states, $|2, +2\rangle$ for ^{23}Na, and $|3/2, +3/2\rangle$ for ^{6}Li. A magnetic guide field of 3 G was applied, and the atoms were optically pumped for 2 ms, using σ^+ polarized light tuned to the D_2 transitions. The intensities of the pumping laser beams were about 0.1 mW/cm^2. To achieve both F (hyperfine) and m_F (Zeeman) pumping, two light beams were used for each species.

In the case of lithium, the excited state hyperfine structure is not resolved, and the two laser beams were simply tuned in resonance with the $F = 1/2$ and the $F = 3/2$ ground state manifolds. In the case of sodium, we explored the efficiency of optical pumping using transitions to different excited hyperfine states F'. We observed the most efficient transfer into the magnetic trap if the $F = 1 \rightarrow F' = 1$ transition was used for hyperfine pumping, even though Clebsch-Gordan coefficients favor the $F = 1 \rightarrow F' = 2$ transition for more efficient pumping. Zeeman pumping of sodium was done on the $F = 2 \rightarrow F' = 2$ transition, in order to make $|2, +2\rangle$ a dark state and avoid unnecessary heating of the sample.

In this way, almost all the lithium atoms could be pumped into the $|3/2, +3/2\rangle$ state. On the other hand, the density of sodium atoms in the dark SPOT is $\geq 10^{11}$ cm^{-3}, and Zeeman pumping is notoriously difficult at such high densities. In our experiments, the fraction of atoms pumped into the $|2, +2\rangle$ state was limited to about 30%, with most of the remaining atoms distributed among the other m_F sublevels of the $F = 2$ manifold.

After the optical pumping stage, the atoms were loaded into a Ioffe-Pritchard magnetic trap with a radial gradient of 164 G/cm and axial curvature of 185 G/cm^2. Sodium atoms in all three $|F = 2, m_F \geq 0\rangle$ states are, at least weakly, magnetically trappable [Fig. 1(b)]. However, only pure $|2, +2\rangle$ samples are stable against inelastic spin-exchange collisions. A crucial step in preparing the samples for efficient forced evaporation was to actively remove $|F = 2, m_F = 0, +1\rangle$ atoms from the trap, before they engaged in inelastic collisions with the $|2, +2\rangle$ atoms. The atoms were loaded into a weak magnetic trap, with a high bias field of 80 G. This field splits the $F = 2$ Zeeman sublevels by $\sim k_B \times 2.8$ mK. Since this splitting was larger than the temperature of the cloud, the different states could be resolved in microwave or rf spectroscopy, and the $|F = 2, m_F = 0, +1\rangle$ atoms could be selectively transferred to the untrapped $|F = 1, m_F = 0, +1\rangle$ lower hyperfine states. This transfer was done with a microwave sweep near the ^{23}Na hyperfine splitting of 1.77 GHz. In this way, all the $|2, +2\rangle$ atoms initially loaded into trap could be preserved. We were also able to load some of the untrapped atoms produced during the sweep by optically pumping them out of the $F = 1$ ground states, thus giving them a second chance to fall into the $|2, +2\rangle$ state. The final setup consisted of two microwave sweeps, the first of 0.8 s duration with the optical pumping light on, and the second of 2.4 s duration without the light. In this way, the overall transfer efficiency from the MOT to the magnetic trap was improved to about 35%, comparable to our standard $F = 1$ BEC experiments [30].

After this purification of the $|2, +2\rangle$ sample, the magnetic trap was tightened by reducing the bias field to 3.8 G in 2.4 s. Resulting trapping frequencies were 204 Hz (400 Hz) radially and 34 Hz (67 Hz) axially for the sodium (lithium) stretched state. This provided good conditions for forced runaway evaporation of sodium. Evaporation was done on the $|2, +2\rangle \rightarrow |1, +1\rangle$ microwave transition near 1.77 GHz. In contrast to radio-frequency evaporation, this ensured that ^{6}Li was far off resonance. Further, microwave evaporation avoided any undesirable aspects of incomplete evaporation into the $|F = 2, m_F = 0, +1\rangle$ states, which could lead to inelastic losses [31].

After 15 s of evaporation, the sodium atoms reached a temperature of $T \sim 10$ μK. At this point, to avoid three-body losses in the $|2, +2\rangle$ state [27], the trap was weakened to frequencies of 49 Hz (96 Hz) radially, and 18 Hz (35 Hz) axially for sodium (lithium). The final evaporation to BEC took another 15 s. In this way, in the absence

of lithium atoms, we could produce almost pure $|2, +2\rangle$ BECs containing up to 10^7 atoms. The lifetime of the BEC in the weak trap was longer than 3 s. In contrast to our previous work [27,28], studies of $F = 2$ condensates are now possible without the added complexity of an optical trap.

In conclusion, by creating a superior refrigerant for sympathetic cooling of ^{6}Li, we have produced the coldest and the largest quantum degenerate Fermi gas so far. The atom numbers in our samples are comparable with the largest alkali BECs, and the temperatures are reaching the current practical detection limit. In analogy with Bose-Einstein condensates, we expect these large samples to ensure a sufficient signal-to-noise ratio for all the standard techniques of BEC research, such as velocimetry using long expansion times, rf spectroscopy with Stern-Gerlach separation during ballistic expansion, direct nondestructive imaging of the trapped clouds, and Bragg spectroscopy. The next challenge is to maintain a similar combination of number and temperature for an interacting two-component Fermi gas [20].

We thank A. E. Leanhardt for a critical reading of the manuscript. This work was supported by the NSF, ONR, ARO, and NASA.

Note added.—Very recently, a similar number of ^{6}Li atoms were cooled into quantum degeneracy using sympathetic cooling with ^{7}Li [32].

[1] B. DeMarco and D. S. Jin, Science **285**, 1703 (1999).
[2] G. Roati, F. Riboli, G. Modugno, and M. Inguscio, Phys. Rev. Lett. **89**, 150403 (2002).
[3] A. G. Truscott, K. E. Strecker, W. I. McAlexander, G. B. Partridge, and R. G. Hulet, Science **291**, 2570 (2001).
[4] F. Schreck, L. Khaykovich, K. L. Corwin, G. Ferrari, T. Bourdel, J. Cubizolles, and C. Salomon, Phys. Rev. Lett. **87**, 080403 (2001).
[5] S. R. Granade, M. E. Gehm, K. M. O'Hara, and J. E. Thomas, Phys. Rev. Lett. **88**, 120405 (2002).
[6] Z. Hadzibabic, C. A. Stan, K. Dieckmann, S. Gupta, M. W. Zwierlein, A. Görlitz, and W. Ketterle, Phys. Rev. Lett. **88**, 160401 (2002).
[7] M. Houbiers and H. T. C. Stoof, Phys. Rev. A **59**, 1556 (1999).
[8] M. Holland, S. J. J. M. F. Kokkelmans, M. L. Chiofalo, and R. Walser, Phys. Rev. Lett. **87**, 120406 (2001).
[9] E. Timmermans, K. Furuya, P. W. Milonni, and A. K. Kerman, Phys. Lett. A **285**, 228 (2001).
[10] Y. Ohashi and A. Griffin, Phys. Rev. Lett. **89**, 130402 (2002).
[11] W. Hofstetter, J. I. Cirac, P. Zoller, E. Demler, and M. D. Lukin, Phys. Rev. Lett. **89**, 220407 (2002).
[12] T. Loftus, C. A. Regal, C. Ticknor, J. L. Bohn, and D. S. Jin, Phys. Rev. Lett. **88**, 173201 (2002).
[13] K. Dieckmann, C. A. Stan, S. Gupta, Z. Hadzibabic, C. H. Schunck, and W. Ketterle, Phys. Rev. Lett. **89**, 203201 (2002).
[14] K. M. O'Hara, S. L. Hemmer, S. R. Granade, M. E. Gehm, J. E. Thomas, V. Venturi, E. Tiesinga, and C. J. Williams, Phys. Rev. A **66**, 041401 (2002).
[15] C. A. Regal, C. Ticknor, J. L. Bohn, and D. S. Jin, Phys. Rev. Lett. **90**, 053201 (2003).
[16] K. M. O'Hara, S. L. Hemmer, M. E. Gehm, S. R. Granade, and J. E. Thomas, Science **298**, 2179 (2002).
[17] M. E. Gehm, S. L. Hemmer, S. R. Granade, K. M. O'Hara, and J. E. Thomas, Phys. Rev. A **68**, 011401(R) (2003).
[18] C. A. Regal and D. S. Jin, Phys. Rev. Lett. **90**, 230404 (2003).
[19] T. Bourdel, J. Cubizolles, L. Khaykovich, K. M. F. Magalhães, S. J. J. M. F. Kokkelmans, G. V. Shlyapnikov, and C. Salomon, Phys. Rev. Lett. **91**, 020402 (2003).
[20] S. Gupta, Z. Hadzibabic, M. W. Zwierlein, C. A. Stan, K. Dieckmann, C. H. Schunck, E. G. M. van Kempen, B. J. Verhaar, and W. Ketterle, Science **300**, 1723 (2003).
[21] C. A. Regal, C. Ticknor, J. L. Bohn, and D. S. Jin, Nature (London) **424**, 47 (2003).
[22] J. R. Abo-Shaeer, C. Raman, J. M. Vogels, and W. Ketterle, Science **292**, 476 (2001).
[23] E. Timmermans and R. Côté, Phys. Rev. Lett. **80**, 3419 (1998).
[24] V. Wippel, C. Binder, and L. Windholz, Eur. Phys. J. D **21**, 101 (2002).
[25] D. A. Butts and D. S. Rokhsar, Phys. Rev. A **55**, 4346 (1997).
[26] A. P. Chikkatur, A. Görlitz, D. M. Stamper-Kurn, S. Inouye, S. Gupta, and W. Ketterle, Phys. Rev. Lett. **85**, 483 (2000).
[27] A. Görlitz, T. L. Gustavson, A. E. Leanhardt, R. Löw, A. P. Chikkatur, S. Gupta, S. Inouye, D. E. Pritchard, and W. Ketterle, Phys. Rev. Lett. **90**, 090401 (2003).
[28] A. E. Leanhardt, A. Görlitz, A. P. Chikkatur, D. Kielpinski, Y. Shin, D. E. Pritchard, and W. Ketterle, Phys. Rev. Lett. **89**, 190403 (2002).
[29] W. Ketterle, K. B. Davis, M. A. Joffe, A. Martin, and D. E. Pritchard, Phys. Rev. Lett. **70**, 2253 (1993).
[30] M.-O. Mewes, M. R. Andrews, N. J. van Druten, D. M. Kurn, D. S. Durfee, and W. Ketterle, Phys. Rev. Lett. **77**, 416 (1996).
[31] B. Desruelle, V. Boyer, S. G. Murdoch, G. Delannoy, P. Bouyer, A. Aspect, and M. Lécrivain, Phys. Rev. A **60**, R1759 (1999).
[32] K. E. Strecker, G. B. Partridge, and R. G. Hulet, Phys. Rev. Lett. **91**, 080406 (2003).

Appendix D

Observation of Feshbach Resonances between Two Different Atomic Species

C. A. Stan, M.W. Zwierlein, C. H. Schunck, S.M. F. Raupach, and W. Ketterle

"Observation of Feshbach Resonances between Two Different Atomic Species,"

Phys. Rev. Lett. 93, 143001 (2004)

Observation of Feshbach Resonances between Two Different Atomic Species

C. A. Stan, M.W. Zwierlein, C. H. Schunck, S. M. F. Raupach, and W. Ketterle
Department of Physics, MIT-Harvard Center for Ultracold Atoms, and Research Laboratory of Electronics, MIT, Cambridge, Massachusetts 02139, USA
(Received 4 June 2004; published 30 September 2004)

We have observed three Feshbach resonances in collisions between ^{6}Li and ^{23}Na atoms. The resonances were identified as narrow loss features when the magnetic field was varied. The molecular states causing these resonances have been identified, and additional ^{6}Li-^{23}Na resonances are predicted. These resonances will allow the study of degenerate Bose-Fermi mixtures with adjustable interactions and could be used to generate ultracold heteronuclear molecules.

DOI: 10.1103/PhysRevLett.93.143001 PACS numbers: 32.80.Pj, 34.50.–s, 67.60.–g

Feshbach resonances [1,2] have made it possible to control interactions in ultracold atomic gases. By tuning the magnetic field near a value where the energy of two free atoms coincides with a molecular bound state, the sign and strength of the atomic interactions can be varied. Such tunable interactions were used to Bose-Einstein condense atomic species with unfavorable collisional properties [3–5], for cooling fermionic mixtures to degeneracy [6], and to produce bright solitons [4,7]. Measurements of Feshbach resonances led to precise determinations of interatomic potentials [8]. An important recent application of Feshbach resonances was the production of ultracold molecules from ultracold atoms [9], and Bose-Einstein condensation of molecules [10].

So far, all experiments on Feshbach resonances studied collisions between two atoms of the same species. A few theoretical papers predicted Feshbach resonances between different atomic species [11], but these have not been observed. Interspecies Feshbach resonances should lead to a host of new scientific phenomena, including the study of ultracold Fermi-Bose mixtures with tunable interactions, for which boson-mediated Cooper pairing [12], phase separation [13], and supersolid order [14] have been predicted. These resonances may also be used to produce polar molecules, at phase-space densities higher than those obtained by heteronuclear photoassociation [15]. Eventually, such molecules could be used for quantum computation [16], for studies of correlated many-body systems [17,18], and for searches for an electronic dipole moment [19].

In this work, we studied collisions between fermionic ^{6}Li and bosonic ^{23}Na. In the absence of any theoretical prediction, it was not clear if there were any resonances in the accessible range of magnetic fields. Three s-wave Feshbach resonances were observed and assigned.

An ultracold mixture of ^{6}Li in the $|F, m_F\rangle = |3/2, 3/2\rangle$ and ^{23}Na in the $|F, m_F\rangle = |2, 2\rangle$ hyperfine states was produced by forced microwave evaporation of ^{23}Na in a magnetic trap as previously described in [20]. The evaporation was stopped before reaching quantum degeneracy, and the mixture was transferred into a single focus 1064 nm optical dipole trap with a waist of 25 μm and a maximum power of 9 W. The ^{6}Li and ^{23}Na atoms were then transferred to the $|1/2, 1/2\rangle$ and $|1, 1\rangle$ hyperfine states, respectively, by simultaneous RF Landau-Zener sweeps. The sweeps were done by ramping the magnetic field from nine to 10 G in 10 ms while keeping the RF frequencies constant at 249.8 MHz for ^{6}Li and 1790 MHz for ^{23}Na yielding a transfer efficiency close to 100%. This mixture of atoms in their lower hyperfine states was further cooled to quantum degeneracy by ramping down the laser power of the optical trap from 9 W to 220 mW in 1.4 s.

Atom numbers were determined from absorption images of the atom clouds. For imaging, a second Landau-Zener sweep was used to transfer lithium and sodium back into their upper hyperfine states, where both species could be probed using cycling transitions. Lithium and sodium were imaged at the end of the experiment by taking first a lithium and then a sodium absorption image in rapid succession. Typically, mixtures of 2×10^6 degenerate fermions at $T/T_F \approx 0.25$ with a condensed ^{23}Na cloud of 2×10^6 atoms were produced at a temperature of 900 nK. The peak densities were 1×10^{13} cm^{-3} for ^{6}Li and 2×10^{14} cm^{-3} for ^{23}Na. The lifetime of the mixture was longer than 10 s.

We searched for Feshbach resonances up to the maximum magnetic field available experimentally, 1025 G, by sweeping the magnetic field across 20 G intervals at a rate of 21 G/s and determining the number of atoms left. The intervals containing resonances were identified by a higher loss rate. Precise measurements of the resonance positions were done by starting at a field near the resonance, and varying the end point of a constant rate sweep towards or across the resonance. The resonances were located by a sudden drop in the atom number, as seen in Fig. 1 for the resonance at 746 G. The magnetic field was calibrated by driving, at the resonance fields, RF transitions between the $|1/2, -1/2\rangle$ and $|3/2, -3/2\rangle$, or between the $|1/2, -1/2\rangle$ and $|3/2, 1/2\rangle$ hyperfine states of ^{6}Li (written in the low-field basis).

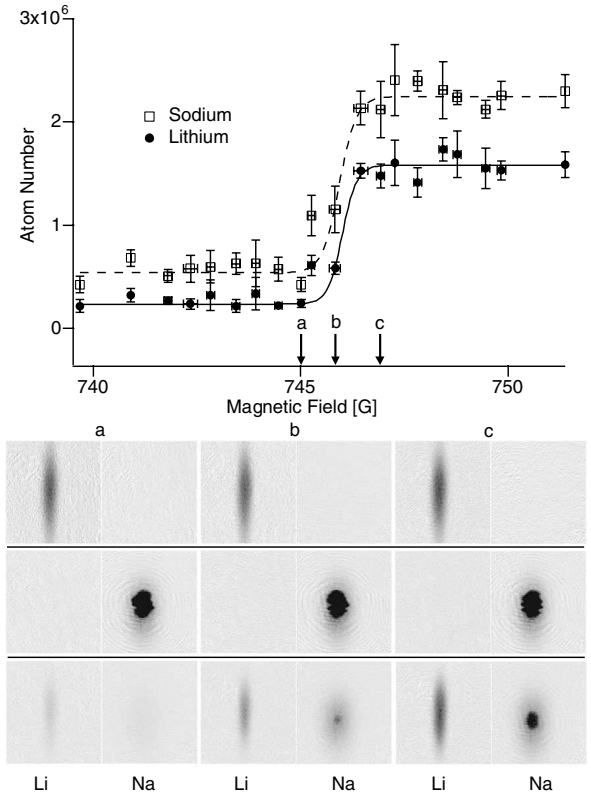

FIG. 1. Determination of the position of the Feshbach resonance at 746 G. The magnetic field was swept down at a rate of 5.7 G/s from a field above the resonance to a variable final field. As the resonance was crossed, a sharp loss in atom number was observed. Top: ^{6}Li (circles) and ^{23}Na (open squares) atom numbers vs the final field. The solid line (^{6}Li) and the dashed line (^{23}Na) are empirical tangent hyperbolic fits to the data. Both fits locate the resonance at 746.0 ± 0.4 G. Bottom: The absorption images show the lithium cloud on the left side and the sodium cloud on the right. They were taken at the three magnetic fields labeled *a*, *b*, and *c*. No losses were observed for lithium only (upper row) and sodium only (middle row), whereas the mixture (bottom row) showed the onset of losses of both species at the resonance. The sodium images clearly show the bimodal distribution characteristic for a Bose condensate. The field of view of each absorption image was 6 mm $\times$ 3 mm.

In the same magnetic field range, we have observed one ^{6}Li and six ^{23}Na single species Feshbach resonances which have not been observed before [21,22]. Interspecies ^{6}Li-^{23}Na resonances were identified after checking that for a pure sample of either lithium or sodium, no resonant losses occurred at the same field. Three ^{6}Li-^{23}Na resonances were observed, as listed in Table I.

The measured 10%–90% loss widths for the three resonances, between 0.8 and 0.4 G, are comparable to the short term magnetic noise, and are thus upper limits on the resonance widths. The sweep rate at which 50% of the atoms are lost is also a measure of the resonance strength [23] and is less sensitive to field noise. Its values are listed in Table I.

TABLE I. Location of ^{6}Li-^{23}Na Feshbach resonances and the assignment of the molecular states which cause the resonances. Here S, M_S, $m_{i,\mathrm{Li}}$, and $m_{i,\mathrm{Na}}$ denote the total electronic spin, the magnetic quantum number for total electronic spin, and the magnetic quantum number for the ^{6}Li and for the ^{23}Na nuclear spin. Also listed are the ramp speeds for which 50% of the atoms were lost.

Magnetic field (G)	Ramp speed (G/s)	Molecular state $\lvert S\ M_S\ m_{\mathrm{i,Li}}\ m_{\mathrm{i,Na}}\rangle$
746.0 ± 0.4	15	$\lvert 1\ 1\ -1\ 3/2\rangle$
759.6 ± 0.2	0.3	$\lvert 1\ 1\ 0\ 1/2\rangle$
795.6 ± 0.2	10	$\lvert 1\ 1\ 1\ -1/2\rangle$

The losses are either due to (inelastic) three-body recombination, or due to resonant molecule formation during the sweep. Other two-body loss mechanisms are not possible for ^{6}Li and ^{23}Na both in their lowest energy hyperfine state. It should be noted that in the mixture near single species sodium Feshbach resonances, enhanced losses were also observed for lithium, presumably in a three-body process involving a sodium dimer and a lithium atom. Also, sodium losses were observed near the single species lithium resonance.

We assign the molecular states causing these resonances by extending the approach presented in [24] to the case of two distinguishable atoms. Without the knowledge of the exact interatomic potentials the energies of the weakest bound molecular states cannot be predicted. However, one can still approximate the molecular hyperfine structure and Zeeman shifts and predict a pattern of Feshbach resonances with the molecular binding energy at zero magnetic field as the only adjustable parameter. We have checked that this procedure, applied to ^{23}Na, reproduces all Feshbach resonances measured experimentally or predicted by coupled channels calculations to within 5%.

The Coulomb interaction between two atoms naturally preserves their total electronic spin $\vec{S} = \vec{s}_1 + \vec{s}_2$. If we neglect the hyperfine interaction, S is thus a good quantum number and the bound states are either singlet ($S = 0$) or triplet ($S = 1$). The molecular hyperfine energy at zero field is approximated as the sum of the hyperfine interaction for the two atoms:

$$H_{\mathrm{hf}} = h a_{\mathrm{hf}}^{\mathrm{Li}} \vec{s}_1 \cdot \vec{i}_{\mathrm{Li}} + h a_{\mathrm{hf}}^{\mathrm{Na}} \vec{s}_2 \cdot \vec{i}_{\mathrm{Na}},$$

with $\vec{s}_{1,2}$ the spins of the two valence electrons, $\vec{i}_{\mathrm{Li(Na)}}$ the nuclear spin of the ^{6}Li (^{23}Na) nucleus ($i_{\mathrm{Li}} = 1$, $i_{\mathrm{Na}} = 3/2$), and the hyperfine constants $a_{\mathrm{hf}}^{\mathrm{Li}} = 152.1368(1)$ MHz, $a_{\mathrm{hf}}^{\mathrm{Na}} = 885.8131(1)$ MHz [25]. We rewrite H_{hf} in terms of $\vec{S}$:

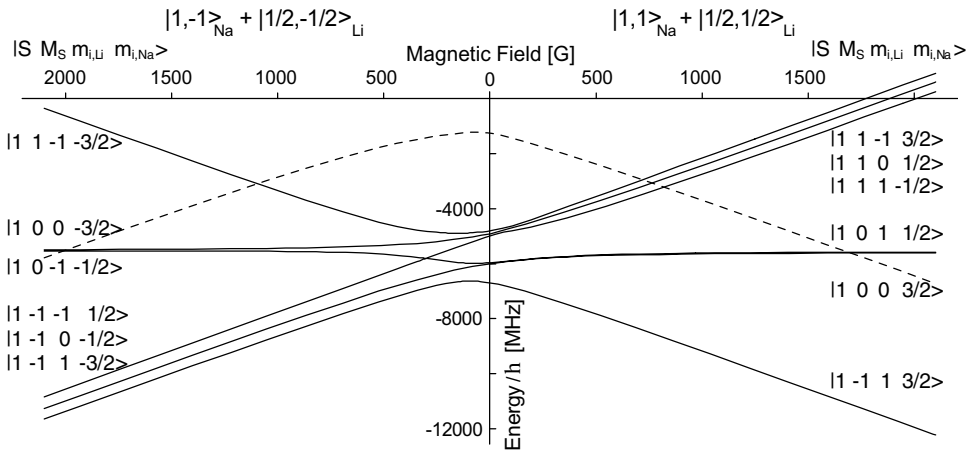

FIG. 2. Feshbach resonances in collisions between ^{6}Li in $|1/2, \pm 1/2\rangle$ and ^{23}Na in $|1, \pm 1\rangle$ hyperfine states. The solid lines show the energy dependence of triplet hyperfine molecular states for which coupling to the open channel is allowed by conservation of the total M_F. The dashed line shows the open channel energy threshold, equal to the sum of hyperfine energies of the incoming particle. The three observed Feshbach resonances occur in the $|1/2, 1/2\rangle_{\mathrm{Li}} + |1, 1\rangle_{\mathrm{Na}}$ collision channel, at the crossing of the threshold with three molecular states between 700 and 850 G. For this channel, two other resonances should occur near 1700 G. In the $|1/2, -1/2\rangle_{\mathrm{Li}} + |1, -1\rangle_{\mathrm{Na}}$ collision channel, one resonance can be predicted to occur near 1100 G and another two near 2000 G.

$$H_{\mathrm{hf}} = \frac{ha_{\mathrm{hf}}^{\mathrm{Li}}}{2}\vec{S}\cdot\vec{i}_{\mathrm{Li}} + \frac{ha_{\mathrm{hf}}^{\mathrm{Na}}}{2}\vec{S}\cdot\vec{i}_{\mathrm{Na}} + \frac{ha_{\mathrm{hf}}^{\mathrm{Li}}}{2}(\vec{s}_1 - \vec{s}_2)\cdot\vec{i}_{\mathrm{Li}} + \frac{ha_{\mathrm{hf}}^{\mathrm{Na}}}{2}(\vec{s}_2 - \vec{s}_1)\cdot\vec{i}_{\mathrm{Na}} = V_{\mathrm{hf}}^{+} + V_{\mathrm{hf}}^{-},$$

Here, V_{hf}^{+} contains the terms proportional to $\vec{S}$, and thus preserves the separation of the orbital from the spin problem. V_{hf}^{-}, however, mixes singlet and triplet states. Following [24], we will assume that the singlet-triplet spacing is large compared to $a_{\mathrm{hf}}^{\mathrm{Na}}$ and $a_{\mathrm{hf}}^{\mathrm{Li}}$, so that we can neglect V_{hf}^{-}. In this approach, the orbital (Coulomb) part of the interaction remains decoupled from the spin part, which alone is responsible for the magnetic field dependence of the states.

For nonzero magnetic field, the spin part of the molecular hyperfine states is described by the Hamiltonian

$$H_{\mathrm{int}}^{+} = V_{\mathrm{hf}}^{+} + V_{\mathrm{Zeeman}}$$

with

$$V_{\mathrm{Zeeman}} = \mu_B\vec{B}\cdot(g_S\vec{S} + g_{\mathrm{Li}}\vec{i}_{\mathrm{Li}} + g_{\mathrm{Na}}\vec{i}_{\mathrm{Na}}),$$

where g_S, g_{Li}, and g_{Na} are the g factors of the electron, of the ^{6}Li, and of the ^{23}Na nucleus. For collisions between $|1, 1\rangle_{\mathrm{Na}} + |1/2, 1/2\rangle_{\mathrm{Li}}$ the total $M_F = \frac{3}{2}$. In s-wave scattering, this incoming (open) channel can be coupled only to molecular states with the same M_F. In total, one can count two singlet and six triplet spin states with $M_F = \frac{3}{2}$.

Feshbach resonances occur at the magnetic fields at which a molecular hyperfine state has the same orbital plus hyperfine energy as the colliding atoms. The two almost degenerate singlet spin states cannot explain the existence of three well-separated resonances. Thus, the observed resonances can be assigned to three triplet spin states with $M_S = 1$, differing only in their nuclear magnetic quantum numbers, as shown in Fig. 2. Using the orbital energy E_B as a free parameter, we performed a least-squares fit of the level crossings of these states with the atomic threshold, to the three experimentally obtained resonance positions. This resulted in $E_B = -5550 \pm 140$ MHz, which represents an estimate of the energy of a weakly bound triplet state of the ^{6}Li-^{23}Na interatomic potential. The error was estimated by finding the values of E_B which fit either the lowest (746 G) or the highest (796 G) resonance. The resulting resonant magnetic fields are 717, 763. and 821 G. In view of the simplicity of the approach, the agreement with the observed resonance positions is satisfactory. Inverting the sign of the magnetic field, we obtain the level diagram for collisions of $|1, -1\rangle_{\mathrm{Na}} + |1/2, -1/2\rangle_{\mathrm{Li}}$ (Fig. 2) which predicts several additional resonances.

The observed Feshbach resonances may be used to produce ^{6}Li^{23}Na molecules by sweeping the magnetic field across the resonance. Atom pairs are converted into molecules by passing adiabatically through the Landau-Zener avoided crossing [9,23]. The efficiency of this conversion depends on the lifetime of the molecular cloud. In experiments with bosons, due to rapid vibrational relaxation, short molecular lifetimes on the order of a few ms have been observed. However, conversion efficiencies of a few % could still be obtained [26]. The lifetime could be substantially increased by removing the leftover unbound atoms with a short light pulse [27].

Fermionic atoms offer the advantage of long molecular lifetimes due to Pauli suppression [28–30]. In the case of ^{6}Li$_2$ and ^{40}K$_2$, highly vibrationally excited molecules were stable close to the resonance, where the molecules

have a dominant atomic character [31]. Further away from the resonance, as the molecules become more strongly bound, the fermionic statistics of the constituents is no longer dominant, and loss rates increase [28,29].

We expect the opposite behavior for fermionic molecules produced near interspecies Feshbach resonances between a bosonic and fermionic atom. Far away from the resonance, all collisions between the molecules should be Pauli suppressed. Near the resonance, the collisions of long-range molecules are better approximated as collisions of their fermionic and bosonic atoms, and no significant suppression of collisions is expected. Therefore, a long-lived cloud of heteronuclear fermionic molecules could be realized by sweeping the magnetic field across and beyond the Feshbach resonance, and removing unbound atoms of both species with resonant light pulses.

In conclusion, we have observed three ^{6}Li-^{23}Na Feshbach resonances and assigned them to weakly bound molecular states using a simple model. These resonances could be used for efficient production of ultracold heteronuclear molecules.

This work was supported by the NSF, ONR, ARO, and NASA. We thank Andrew Kerman for fruitful discussions and experimental assistance and Zoran Hadzibabic for a critical reading of the manuscript. S. Raupach is grateful to the Dr. Jürgen Ulderup Foundation for financial support.

Note added.—After this work was completed, the observation of Feshbach resonances in collisions between rubidium and potassium atoms was reported [32].

[1] S. Inouye, M. R. Andrews, J. Stenger, H.-J. Miesner, D. M. Stamper-Kurn, and W. Ketterle, Nature (London) **392**, 151 (1998); P. Courteille, R. S. Freeland, D. J. Heinzen, F. A. van Abeelen, and B. J. Verhaar, Phys. Rev. Lett. **81**, 69 (1998).

[2] W. C. Stwalley, Phys. Rev. Lett. **37**, 1628 (1976); E. Tiesinga, B. J. Verhaar, and H. T. C. Stoof, Phys. Rev. A **47**, 4114 (1993).

[3] S. L. Cornish, N. R. Claussen, J. L. Roberts, E. A. Cornell, and C. E. Wieman, Phys. Rev. Lett. **85**, 1795 (2000).

[4] L. Khaykovich, F. Schreck, G. Ferrari, T. Bourdel, J. Cubizolles, L. D. Carr, Y. Castin, and C. Salomon, Science **296**, 1290 (2002).

[5] T. Weber, J. Herbig, M. Mark, H.-C. Nägerl, and R. Grimm, Science **299**, 232 (2003).

[6] K. M. O'Hara, S. L. Hemmer, M. E. Gehm, S. R. Granade, and J. E. Thomas, Science **298**, 2179 (2002).

[7] K. E. Strecker, G. B. Partridge, A. G. Truscott, and R. G. Hulet, Nature (London) **417**, 150 (2002).

[8] P. J. Leo, C. J. Williams, and P. S. Julienne, Phys. Rev. Lett. **85**, 2721 (2000).

[9] C. A. Regal, C. Ticknor, J. L. Bohn, and D. S. Jin, Nature (London) **424**, 47 (2003).

[10] M. Greiner, C. A. Regal, and D. S. Jin, Nature (London) **426**, 537 (2003); S. Jochim, M. Bartenstein, A. Altmeyer, G. Hendl, S. Riedl, C. Chin, J. H. Denschlag, and R. Grimm, Science **302**, 2101 (2003); M. Bartenstein, A. Altmeyer, S. Riedl, S. Jochim, C. Chin, J. H. Denschlag, and R. Grimm, Phys. Rev. Lett. **92**, 120401 (2004); M. W. Zwierlein, C. A. Stan, C. H. Schunck, S. M. F. Raupach, S. Gupta, Z. Hadzibabic, and W. Ketterle, Phys. Rev. Lett. **91**, 250401 (2003).

[11] J. P. Burke, Jr., J. L. Bohn, B. D. Esry, and C. H. Greene, Phys. Rev. Lett. **80**, 2097 (1998); A. Simoni, F. Ferlaino, G. Roati, G. Modugno, and M. Inguscio, Phys. Rev. Lett. **90**, 163202 (2003).

[12] H. Heiselberg, C. J. Pethick, H. Smith, and L. Viverit, Phys. Rev. Lett. **85**, 2418 (2000); M. J. Bijlsma, B. A. Heringa, and H. T. C. Stoof, Phys. Rev. A **61**, 053601 (2000).

[13] K. Mølmer, Phys. Rev. Lett. **80**, 1804 (1998).

[14] H. P. Büchler and G. Blatter, Phys. Rev. Lett. **91**, 130404 (2003).

[15] J. P. Shaffer, W. Chalupczak, and N. P. Bigelow, Phys. Rev. Lett. **82**, 1124 (1999); U. Schlöder, C. Silber, and C. Zimmermann, Appl. Phys. B **73**, 801 (2001); M. W. Mancini, G. D. Telles, A. R. L. Caires, V. S. Bagnato, and L. G. Marcassa, Phys. Rev. Lett. **92**, 133203 (2004); A. J. Kerman, J. M. Sage, S. Sainis, T. Bergeman, and D. DeMille, Phys. Rev. Lett. **92**, 153001 (2004).

[16] D. DeMille, Phys. Rev. Lett. **88**, 067901 (2002).

[17] K. Goral, L. Santos, and M. Lewenstein, Phys. Rev. Lett. **88**, 170406 (2002).

[18] M. A. Baranov, M. S. Marenko, V. S. Rychkov, and G. V. Shlyapnikov, Phys. Rev. A **66**, 013606 (2002).

[19] M. G. Kozlov and L. N. Labzowsky, J. Phys. B **28**, 1933 (1995).

[20] Z. Hadzibabic, S. Gupta, C. A. Stan, C. H. Schunck, M. W. Zwierlein, K. Dieckmann, and W. Ketterle, Phys. Rev. Lett. **91**, 160401 (2003).

[21] C. H. Schunck, M. W. Zwierlein, C. A. Stan, S. M. F. Raupach, W. Ketterle, A. Simoni, E. Tiesinga, C. J. Williams, and P. S. Julienne, cond-mat/0407373.

[22] C. H. Schunck *et al.* (to be published).

[23] F. A. van Abeelen and B. J. Verhaar, Phys. Rev. Lett. **83**, 1550 (1999).

[24] A. J. Moerdijk, B. J. Verhaar, and A. Axelsson, Phys. Rev. A **51**, 4852 (1995).

[25] E. Arimondo, M. Inguscio, and P. Violino, Rev. Mod. Phys. **49**, 31 (1977).

[26] S. Dürr, T. Volz, and G. Rempe, cond-mat/0405606.

[27] K. Xu, T. Mukaiyama, J. R. Abo-Shaeer, J. K. Chin, D. E. Miller, and W. Ketterle, Phys. Rev. Lett. **91**, 210402 (2003).

[28] C. A. Regal, M. Greiner, and D. S. Jin, Phys. Rev. Lett. **92**, 083201 (2004).

[29] J. Cubizolles, T. Bourdel, S. J. J. M. F. Kokkelmans, G. V. Shlyapnikov, and C. Salomon, Phys. Rev. Lett. **91**, 240401 (2003).

[30] K. E. Strecker, G. B. Partridge, and R. G. Hulet, Phys. Rev. Lett. **91**, 080406 (2003).

[31] D. S. Petrov, C. Salomon, and G. V. Shlyapnikov, cond-mat/0309010.

[32] S. Inouye, J. Goldwin, M. L. Olsen, C. Ticknor, J. L. Bohn, and D. S. Jin, cond-mat/0406208.

Appendix E

Observation of Bose-Einstein Condensation of Molecules

M.W. Zwierlein, C. A. Stan, C. H. Schunck, S.M. F. Raupach, S. Gupta, Z. Hadzibabic, and W. Ketterle

"Observation of Bose-Einstein Condensation of Molecules,"

Phys. Rev. Lett. 91, 250401 (2003)

Observation of Bose-Einstein Condensation of Molecules

M. W. Zwierlein, C. A. Stan, C. H. Schunck, S. M. F. Raupach, S. Gupta, Z. Hadzibabic, and W. Ketterle
Department of Physics, MIT–Harvard Center for Ultracold Atoms, and Research Laboratory of Electronics, MIT, Cambridge, Massachusetts 02139, USA
(Received 27 November 2003; published 15 December 2003)

We have observed Bose-Einstein condensation of molecules. When a spin mixture of fermionic ^{6}Li atoms was evaporatively cooled in an optical dipole trap near a Feshbach resonance, the atomic gas was converted into $^6Li_2$ molecules. Below 600 nK, a Bose-Einstein condensate of up to 900 000 molecules was identified by the sudden onset of a bimodal density distribution. This condensate realizes the limit of tightly bound fermion pairs in the crossover between BCS superfluidity and Bose-Einstein condensation.

DOI: 10.1103/PhysRevLett.91.250401 PACS numbers: 03.75.Ss, 05.30.Jp

Over the past few years, many different approaches have been used to cool and trap molecules [1,2]. One major goal has been the creation of molecular Bose-Einstein condensates, which could lead to advances in molecular spectroscopy, studies of collisions, and precision tests of fundamental symmetries.

Recently, a new technique for creating ultracold molecules led to major advances towards molecular Bose-Einstein condensation (BEC). Molecules were produced from ultracold atoms [3–9] near a Feshbach resonance [10], where a molecular state is resonant with the atomic state and molecules can form without heat release. These molecules are highly vibrationally excited and would usually undergo fast decay. However, in the case of fermionic atoms the molecules showed very long lifetimes [7–9,11]. This has been attributed to Pauli suppression of the vibrational quenching process, which couples a very weakly bound molecular state to much more tightly bound lower lying vibrational states [12]. We have now been able to cool such molecules to Bose-Einstein condensation.

This Bose-Einstein condensate represents one extreme of the crossover from Bose-Einstein condensation of tightly bound pairs (molecules) to BCS superfluidity of Cooper pairs, where fermions form delocalized pairs in momentum space [13].

In most of the recent experiments, molecules were formed by sweeping an external magnetic field through the Feshbach resonance, adiabatically converting atoms to molecules [3–6,8]. This atom-molecule coupling is a coherent two-body process [14].

In the case of ^{6}Li, experimental work indicated [7,9] and theoretical work predicted [15,16] that cooling the atoms at constant magnetic field would create an atom-molecule mixture in thermal equilibrium. In this case, the atoms and molecules are coupled by three-body recombination [17]. For temperatures lower than the binding energy of the molecular state, an almost pure molecular gas should form, and at even lower temperatures, a molecular Bose-Einstein condensate. This work demonstrates that this surprisingly simple method to create molecular condensates works. The success of this approach depends on a very favorable ratio of collisional rates for formation and decay of molecules which may be unique to ^{6}Li.

The goal of molecular BEC was reached in several steps. Using Feshbach resonances, atomic condensates were put into an atom-molecule superposition state [2]. Pure molecular gases made of bosonic atoms were created close to [6] or clearly in [4] the quantum-degenerate regime, but the effective heating time (of about 2 ms in Ref. [4]) was too short to reach equilibrium. Earlier this month, while this work was in progress, two papers were submitted. Reference [18] observed a quantum-degenerate gas of potassium molecules with an effective lifetime of 5 to 10 ms, sufficiently long to reach equilibrium in two dimensions and to form a quasi- or nonequilibrium condensate [19]. Reference [20] provided indirect evidence for a long-lived condensate of lithium molecules [21]. Here we observe the formation of a condensate by evaporative cooling of a molecular gas close to equilibrium.

The basic scheme of the experiment is similar to our earlier work when we identified two Feshbach resonances in lithium by monitoring the loss of trapped atoms due to three-body recombination as a function of the external magnetic field [22]. This process leads to ultracold molecules in the highest vibrational state below the continuum. However, no attempt was made to detect these molecules because until very recently [7,9] they were believed to decay rapidly.

Our experimental setup was described in Refs. [22,23]. After laser cooling and sympathetic cooling with sodium atoms in a magnetic trap, 35×10^6 lithium atoms in the $|F, m_F\rangle = |3/2, 3/2\rangle$ state were transferred into an optical trap formed by a single far detuned laser beam with up to 7 W of power at 1064 nm. The beam had a 20 μm waist and was aligned horizontally along the symmetry axis of the magnetic trap. This generated a 650 μK deep trapping potential with 15 kHz radial and 175 Hz axial trapping frequencies. They were determined with an accuracy of 10% by exciting dipolar oscillations with an atomic

sodium condensate and scaling them to lithium atoms using the ratios of polarizabilities and masses.

The ^{6}Li atoms were then transferred to the lowest energy state $|1\rangle$, using an adiabatic frequency sweep around the lithium hyperfine splitting of 228 MHz. dc magnetic fields of up to 1025 G could be applied, a range encompassing the $|1\rangle - |2\rangle$ Feshbach resonance [22,24,25], where $|2\rangle$ denotes the second lowest hyperfine state of ^{6}Li.

Most of our experiments were performed at a magnetic field of 770 G. This was below but still within the width of the broad Feshbach resonance. Here the atomic scattering length is positive corresponding to a stable weakly bound molecular state. Using rf-induced transitions near 80 MHz, an equal mixture of states $|1\rangle$ and $|2\rangle$ was prepared with a ratio of temperature T to Fermi temperature T_F around 0.3. The sample was cooled in 350 ms by ramping down the laser power of the optical trap to typically 10^{-3} of the maximum power resulting in a calculated trap depth for unbound atoms of 650 nK. The weakly bound molecules have twice the atomic polarizability. They experience the same trap frequencies and twice the trap depth as the lithium atoms. Therefore, we expect mainly atoms to be evaporated.

Atoms and molecules were detected by absorption imaging after ballistic expansion times of 1 to 30 ms. During the time of flight, the magnetic field was suddenly switched off, and atoms in both states were imaged simultaneously since the two optical transition frequencies are equal at zero field. Molecules were detected by first dissociating them by sweeping the magnetic field across the Feshbach resonance up to 925 G and then by imaging the resulting atoms at zero field. With the Feshbach sweep, molecules and residual atoms were imaged together. Without it, only the unbound atoms were detected after switching off the magnetic field. We have found that during the initial phase of the evaporative cooling the atomic population dominated. A significant molecule fraction formed around $T \sim 2\ \mu$K, and in the final phase of the cooling, no atoms could be discerned. The absorption images and profiles shown in Figs. 1 and 2 therefore represent purely molecular column densities.

When the laser power of the optical dipole trap was ramped down, the shrinking size of the cloud in absorption imaging signaled lower temperatures. Very abruptly, the smooth distribution changed to a bimodal distribution—the well-known "smoking gun" of Bose-Einstein condensation [26,27] (Figs. 1 and 2). Because of a slight asymmetry of our trapping potential, the centers of the condensate and of the thermal cloud were shifted.

The phase transition could be identified by plotting the effective area of the cloud vs laser power P [Fig. 3(a)]. At the phase transition, there was an abrupt change in slope, whereas the temperature changed smoothly. For a classical gas, the area depends only on temperature and trap frequencies, which vary smoothly with P.

Quantitative information on temperature, total atom number, and condensate fraction was obtained by fitting

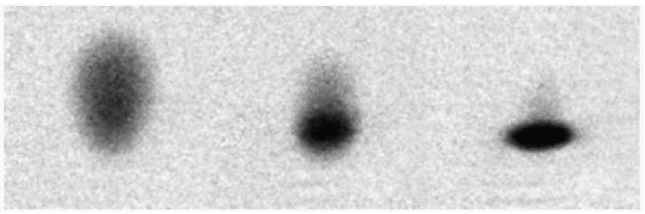

FIG. 1. Observation of Bose-Einstein condensation in a molecular gas. Shown are three single-shot absorption images after 6 ms of ballistic expansion for progressively lower temperatures (left to right). The appearance of a dark spot marks the onset of BEC. The field of view for each image is 1.4×1.4 mm^2. The long axis of the optical dipole trap was vertical in the image.

axial profiles (such as in Fig. 2) using a bimodal distribution: a Bose-Einstein distribution for the broad normal component and a Thomas-Fermi distribution for the narrow (condensate) component. Condensates containing up to 900 000 molecules and condensate fractions of up to 75% were obtained. The onset of BEC was observed at a temperature of 600 nK with 1.4×10^6 molecules. For an ideal gas with this number of molecules, the predicted BEC transition temperature $T_C = 0.94\,\hbar\bar{\omega}\,N^{1/3}/k_B$ is 650 nK, where $\bar{\omega}$ denotes the geometric mean of the three trapping frequencies. This agreement is fortuitous, given the uncertainty in the trap frequencies at low power [28].

The cooldown is characterized in Fig. 3. Axial temperatures were obtained from the spatial extent of the thermal cloud (the size stayed almost constant during the time of flight). The axial temperatures are in arbitrary

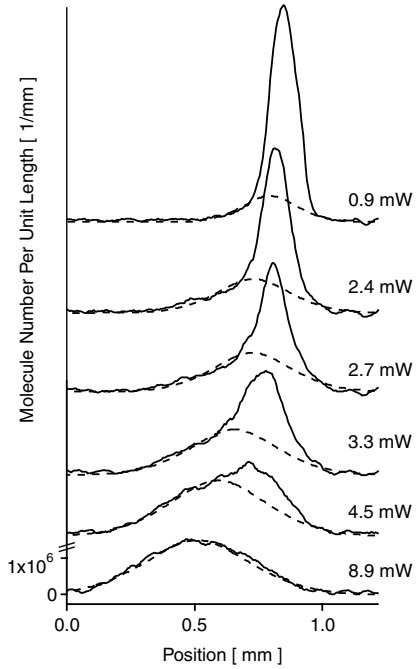

FIG. 2. Bimodality in the density distribution of a molecular gas. Shown are radially averaged profiles through absorption images such as those in Fig. 1, as a function of final laser power. The dashed lines are fits to the thermal clouds.

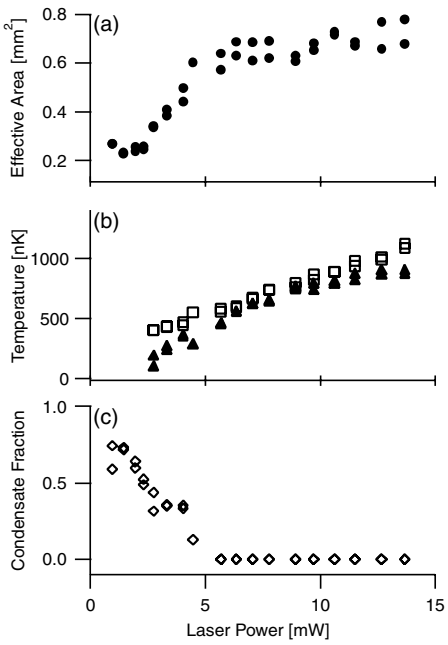

FIG. 3. Characterization of the phase transition. (a) The effective area is the integrated optical density divided by the peak optical density of the absorption images. The "sudden shrinking" of the area coincides with the appearance of a bimodal density distribution and indicates the BEC phase transition. (b) The radial (squares) and axial (triangles) temperatures varied smoothly during the evaporation. The axial temperatures are in arbitrary units. (c) Condensate fraction. Below the critical temperature, the condensate fraction increased from zero to up to 75%.

units [28]. Absolute radial temperatures were obtained from the ballistic expansion. All of our temperature measurements are consistent with equilibration in three dimensions.

From the expansion of the largest condensates, we determined the mean-field energy μ to be 300 ± 100 nK. The peak density n of the condensate was obtained from the fit to be 7×10^{13} cm^{-3}. The relation $\mu = 4\pi\hbar^2 an/m$, where m is the molecular mass, implies a molecular scattering length of $a = 8$ nm with an uncertainty of $\pm 60\%$. These uncertainties were estimated from the discrepancy of fits done at different times of flight which were not fully consistent. This might reflect asymmetries and anharmonicities of the trapping potential which were not characterized.

It was predicted that the molecular scattering length a is 0.6 times the atomic scattering length a_a [12]. At our magnetic field of 770 G, the predicted value of a_a lies between 140 and 340 nm depending on the uncertain position of the Feshbach resonance between 810 and 850 G [25]. The discrepancy between the predicted and observed values of a needs further study.

The molecular gas decayed faster than extrapolated from Refs. [7,9]. Just above T_c, the thermal cloud had a peak density of 1×10^{13} cm^{-3} and an initial decay time of about 1 s. Condensate numbers decayed to one third after a hold time of 30 ms. Those short lifetimes may reflect leakage or heating in our optical dipole trap at low laser power. In the present experiments, the laser power was not stabilized. The lifetime of the thermal gas is much longer than estimated values of the axial trap period of 100 ms and of the collision time of 2 ms, which should lead to full equilibrium. Depending on how the condensate grew during the evaporative cooling, its lifetime may have been too short to develop phase coherence in the axial direction [19].

Using the experimentally determined scattering length, we find that the molecular cloud at T_c has a ratio of mean-free path to radius close to 10 and should show only negligible anisotropy during ballistic expansion [19]. Therefore, the onset of strongly anisotropic expansion is a distinguishing feature of the molecular condensate (Fig. 1).

The $^6Li_2$ molecules are extremely weakly bound. The molecular binding energy depends on the atomic scattering length a_a as $\hbar^2/ma_a^2$ [29]. For an assumed $a_a = 200$ nm the binding energy is 2 μK. The molecular state which causes the Feshbach resonance is the $X\,^1\Sigma_g^+$, $v = 38$ state. This state is tightly bound, but near the Feshbach resonance it is strongly mixed with the state of the colliding atoms, and the molecular wave function is spread out over an extension of order $a_a/2$ [29].

Direct evidence for the large size of the molecules was obtained by resonant imaging during ballistic expansion at high magnetic fields. At 770 G, molecules could be directly imaged using light in resonance with the atoms at the same field. The absorption was comparable to the zero-field absorption signal obtained after dissociating the molecules. This shows that the molecular bond is so weak that the absorption line is shifted from the atomic line by less than a linewidth Γ. The molecules are expected to absorb most strongly near the outer turning point R. The excited state potential is split by the resonant van der Waals interaction $\zeta\hbar\Gamma(\lambda\!\!\!^{-}/R)^3$, where $\lambda\!\!\!^{-}$ is the resonant wavelength divided by 2π and ζ is $\pm 3/4, \pm 3/2$ for different excited molecular states. The observed absorption signal implies a molecular size $R \geq 100$ nm. It is this huge size compared with the much smaller size of the molecule in lower vibrational states which, together with Fermi statistics, inhibits vibrational relaxation and leads to the long lifetimes [12].

Condensates were observed after evaporative cooling at various magnetic fields between 720 and 820 G. At the lower magnetic fields, the condensate expanded more slowly, consistent with the predictions of a smaller repulsive mean-field energy.

In future work, we plan to use the molecular BEC as the starting point for studying the BEC-BCS crossover [13]. By ramping up the magnetic field across the Feshbach resonance, the molecules are dissociated into fermionic atoms and the interaction between the atoms changes from repulsive to attractive, allowing for the formation of Cooper pairs. Starting with an almost pure

condensate and conserving entropy, a Fermi sea should form with temperatures well within the range where BCS type superfluidity has been predicted [30,31].

In conclusion, we have realized Bose-Einstein condensates of up to 900 000 molecules by evaporative cooling of a spin mixture of fermionic lithium atoms.

This work was supported by the NSF, ONR, ARO, and NASA. We thank A. Leanhardt for helpful comments. S. Raupach is grateful to the Dr. Jürgen Ulderup foundation for financial support.

Note added.—In an optical trap with a slightly enlarged beam waist, we were recently able to hold molecular condensates for up to 400 ms (or three axial trapping periods) which should result in 3D equilibration. The $1/e$ decay time was about 200 ms.

[1] J. D. Weinstein, R. DeCarvalho, T. Guillet, B. Friedrich, and J. M. Doyle, Nature (London) **395**, 148 (1998); T. Takekoshi, B. M. Patterson, and R. J. Knize, Phys. Rev. Lett. **81**, 5105 (1998); R. Wynar, R. S. Freeland, D. J. Han, C. Ryu, and D. J. Heinzen, Science **287**, 1016 (2000); H. L. Bethlem, G. Berden, F. M. H. Crompvoets, R. T. Jongma, A. J. A. van Roij, and G. Meijer, Nature (London) **406**, 491 (2000); C. Chin, A. J. Kerman, V. Vuletic, and S. Chu, Phys. Rev. Lett. **90**, 033201 (2003).

[2] E. A. Donley, N. R. Claussen, S. T. Thompson, and C. E. Wieman, Nature (London) **417**, 529 (2002).

[3] C. A. Regal, C. Ticknor, J. L. Bohn, and D. S. Jin, Nature (London) **424**, 47 (2003).

[4] K. Xu, T. Mukaiyama, J. R. Abo-Shaeer, J. K. Chin, D. E. Miller, and W. Ketterle, Phys. Rev. Lett. **91**, 210402 (2003).

[5] S. Dürr, T. Volz, A. Marte, and G. Rempe, e-print cond-mat/0307440.

[6] J. Herbig, T. Kraemer, M. Mark, T. Weber, C. Chin, H.-C. Nägerl, and R. Grimm, Science **301**, 1510 (2003).

[7] J. Cubizolles, T. Bourdel, S. J. J. M. F. Kokkelmans, G. V. Shlyapnikov, and C. Salomon, Phys. Rev. Lett. **91**, 240401 (2003).

[8] K. E. Strecker, G. B. Partridge, and R. G. Hulet, Phys. Rev. Lett. **91**, 080406 (2003).

[9] S. Jochim, M. Bartenstein, A. Altmeyer, G. Hendl, C. Chin, J. H. Denschlag, and R. Grimm, Phys. Rev. Lett. **91**, 240402 (2003).

[10] W. C. Stwalley, Phys. Rev. Lett. **37**, 1628 (1976); E. Tiesinga, B. J. Verhaar, and H. T. C. Stoof, Phys. Rev. A **47**, 4114 (1993); S. Inouye, M. R. Andrews, J. Stenger, H.-J. Miesner, D. M. Stamper-Kurn, and W. Ketterle, Nature (London) **392**, 151 (1998); P. Courteille, R. S. Freeland, D. J. Heinzen, F. A. van Abeelen, and B. J. Verhaar, Phys. Rev. Lett. **81**, 69 (1998).

[11] C. A. Regal, M. Greiner, and D. S. Jin, e-print cond-mat/0308606.

[12] D. S. Petrov, C. Salomon, and G. V. Shlyapnikov, e-print cond-mat/0309010.

[13] M. Randeria, in *Bose-Einstein Condensation*, edited by A. Griffin, D. Snoke, and S. Stringari (Cambridge University, Cambridge, 1995), pp. 355–392; H. T. C. Stoof, M. Houbiers, C. A. Sackett, and R. G. Hulet, Phys. Rev. Lett. **76**, 10 (1996); E. Timmermans, K. Furuya, P. W. Milonni, and A. K. Kerman, Phys. Lett. A **285**, 228 (2001); M. Holland, S. J. J. M. F. Kokkelmans, M. L. Chiofalo, and R. Walser, Phys. Rev. Lett. **87**, 120406 (2001); Y. Ohashi and A. Griffin, Phys. Rev. Lett. **89**, 130402 (2003).

[14] P. D. Drummond, K. V. Kheruntsyan, and H. He, Phys. Rev. Lett. **81**, 3055 (1998); P. Tommasini, E. Timmermans, M. Hussein, and A. Kerman, e-print cond-mat/9804015; F. A. van Abeelen and B. J. Verhaar, Phys. Rev. Lett. **83**, 1550 (1999); F. H. Mies, E. Tiesinga, and P. S. Julienne, Phys. Rev. A **61**, 022721 (2000).

[15] S. J. J. M. F. Kokkelmans, G. V. Shlyapnikov, and C. Salomon, e-print cond-mat/0308384.

[16] C. Chin and R. Grimm, e-print cond-mat/0309078.

[17] P. O. Fedichev, M. W. Reynolds, and G. V. Shlyapnikov, Phys. Rev. Lett. **77**, 2921 (1996); B. D. Esry, C. H. Greene, and H. Suno, Phys. Rev. A **65**, 010705 (2001); D. S. Petrov, Phys. Rev. A **67**, 010703 (2003).

[18] M. Greiner, C. A. Regal, and D. S. Jin, Nature (London) **426**, 537 (2003).

[19] I. Shvarchuck, C. Buggle, D. S. Petrov, K. Dieckmann, M. Zielonkowski, M. Kemmann, T. G. Tiecke, W. v. Klitzing, G. V. Shlyapnikov, and J. T. M. Walraven, Phys. Rev. Lett. **89**, 270404 (2002).

[20] S. Jochim, M. Bartenstein, A. Altmeyer, G. Hendl, S. Riedl, C. Chin, J. H. Denschlag, and R. Grimm, Science (to be published).

[21] This work inferred the presence of a condensate from the number of particles in a shallow trap and the magnetic field dependence of the loss rate consistent with mean-field effects. No observation of a phase transition or measurements of equilibration, temperature, or condensate fraction were reported.

[22] K. Dieckmann, C. A. Stan, S. Gupta, Z. Hadzibabic, C. H. Schunck, and W. Ketterle, Phys. Rev. Lett. **89**, 203201 (2002).

[23] Z. Hadzibabic, S. Gupta, C. A. Stan, C. H. Schunck, M. W. Zwierlein, K. Dieckmann, and W. Ketterle, Phys. Rev. Lett. **91**, 160401 (2003).

[24] T. Bourdel, J. Cubizolles, L. Khaykovich, K. M. F. Magalhães, S. J. J. M. F. Kokkelmans, G. V. Shlyapnikov, and C. Salomon, Phys. Rev. Lett. **91**, 020402 (2003).

[25] S. Gupta, Z. Hadzibabic, M. W. Zwierlein, C. A. Stan, K. Dieckmann, C. H. Schunck, E. G. M. v. Kempen, B. J. Verhaar, and W. Ketterle, Science **300**, 1723 (2003).

[26] M. H. Anderson, J. R. Ensher, M. R. Matthews, C. E. Wieman, and E. A. Cornell, Science **269**, 198 (1995).

[27] K. B. Davis, M.-O. Mewes, M. R. Andrews, N. J. van Druten, D. S. Durfee, D. M. Kurn, and W. Ketterle, Phys. Rev. Lett. **75**, 3969 (1995).

[28] The trap frequencies were scaled from measurements done at full power. The axial frequency was affected by small magnetic field curvatures which were negligible at high laser power.

[29] T. Köhler, T. Gasenzer, P. S. Julienne, and K. Burnett, Phys. Rev. Lett. **91**, 230401 (2003).

[30] L. D. Carr, G. V. Shlyapnikov, and Y. Castin, e-print cond-mat/0308306.

[31] J. N. Milstein, S. J. J. M. F. Kokkelmans, and M. J. Holland, Phys. Rev. A **66**, 043604 (2002).

Appendix F

Condensation of Pairs of Fermionic Atoms near a Feshbach Resonance

M.W. Zwierlein, C. A. Stan, C. H. Schunck, S.M. F. Raupach, A. J. Kerman, and W. Ketterle

"Condensation of Pairs of Fermionic Atoms near a Feshbach Resonance,"

Phys. Rev. Lett. 92, 120403 (2004)

Condensation of Pairs of Fermionic Atoms near a Feshbach Resonance

M. W. Zwierlein, C. A. Stan, C. H. Schunck, S. M. F. Raupach, A. J. Kerman, and W. Ketterle
Department of Physics, MIT-Harvard Center for Ultracold Atoms, and Research Laboratory of Electronics, MIT, Cambridge, Massachusetts 02139, USA
(Received 1 March 2004; published 25 March 2004)

We have observed Bose-Einstein condensation of pairs of fermionic atoms in an ultracold ^{6}Li gas at magnetic fields above a Feshbach resonance, where no stable $^6Li_2$ molecules would exist in vacuum. We accurately determined the position of the resonance to be 822 ± 3 G. Molecular Bose-Einstein condensates were detected after a fast magnetic field ramp, which transferred pairs of atoms at close distances into bound molecules. Condensate fractions as high as 80% were obtained. The large condensate fractions are interpreted in terms of preexisting molecules which are quasistable even above the two-body Feshbach resonance due to the presence of the degenerate Fermi gas.

DOI: 10.1103/PhysRevLett.92.120403 PACS numbers: 03.75.Ss, 05.30.Fk

Ultracold atomic gases have become a medium to realize novel phenomena in condensed matter physics and test many-body theories in new regimes. The particle densities are 10^8 times lower than in solids, but at temperatures in the nanokelvin range, which are now routinely achieved, interactions and correlations become important. Of particular interest are pairing phenomena in fermionic gases, which have direct analogies to superconductivity [1].

The interactions which drive the pairing in these gases can be controlled using a Feshbach resonance [2], in which a molecular level is Zeeman tuned through zero binding energy using an external magnetic field. This provides an opportunity to experimentally probe what is known as the BCS-BEC crossover; as the strength of the effective attractive interaction between particles is increased a continuous transition from condensation of delocalized Cooper pairs to condensation of tightly bound bosonic molecules is predicted [3–6]. Whereas in the BCS limit the pairing is a strictly many-body effect [7], in the BEC limit a pair of fermions is bound even as an isolated molecule. A novel form of high-temperature superfluidity has been predicted to emerge in the crossover region [3–6]. Until recently, the observation of condensation phenomena in fermionic atomic gases was restricted to the extreme BEC limit, where several groups have observed Bose-Einstein condensation of diatomic molecules [8–11].

An important step was recently reported, in which condensation of atomic ^{40}K fermion pairs was observed on the BCS side of a Feshbach resonance [12]. It was argued that those pairs were not bound into molecules, but merely moved together in a correlated fashion, similar to Cooper pairs of electrons in a superconductor [13]. However, the exact nature of these pairs remained unclear. In this Letter, we apply similar techniques to ^{6}Li atoms, which have very different collisional properties [14], and observe the pair condensation phenomenon above a Feshbach resonance. In contrast to the previous work, where at most 15% of the atom pairs were condensed [12], condensate fractions of up to 80% were observed. We argue that such a high condensate fraction is unlikely for pairs which are long range, but rather it indicates a condensate of short-range atom pairs which are essentially molecular in character even on the BCS side of the resonance.

A simple argument supports this possibility. In the basic picture of a Feshbach resonance, a molecular state above the dissociation threshold has a finite lifetime, which becomes shorter as the energy of the state increases, as recently observed [15]. In the presence of the Fermi sea, its lifetime will be increased due to Pauli blocking. The molecular level will be populated until its energy becomes larger than twice the Fermi energy corresponding to the total number of atoms. The BCS-BEC crossover is expected to occur at this point, and not at the location of the two-body Feshbach resonance [5,6].

The basic setup of our experiment was described in [10]. By sympathetic cooling of ^{6}Li atoms with ^{23}Na in a magnetic trap, a degenerate gas of about 3×10^7 ^{6}Li fermions at $\sim 0.3 T/T_F$ was created. After transfer into an optical dipole trap (maximum power 9 W focused to an e^{-2} radius of 25 μm), an equal mixture of atoms in the lowest two hyperfine states $|1\rangle$ and $|2\rangle$ was prepared. The sample was evaporatively cooled at a magnetic field of 770 G using an exponential ramp-down (time scale $\sim$ 400 ms) of the optical trap to a final laser power of 15 mW. This created essentially pure Bose-Einstein condensates of up to 3×10^6 $^6Li_2$ molecules. The observed trap vibrational frequencies could be described by the following expression: $\nu_{\mathrm{rad}} \approx 115$ Hz $\sqrt{P}$, $\nu_{\mathrm{ax}} \approx 1.1$ Hz $\sqrt{P + 120B}$, where P is the optical power in mW, and B is the magnetic field in kG. The latter dependence arises from the residual axial curvature of the magnetic field. Considerable improvements over our previous setup [10] led to an improved e^{-1} condensate lifetime of 10 s at 770 G. Moreover, within the experimental uncertainty in the total number of molecules ($\sim$50%), mean-field

measurements were consistent with a molecule-molecule scattering length of $0.6a$, where a is the atomic scattering length [16,17].

Previously, the location of the ^{6}Li Feshbach resonance was determined either by observing a peak in the inelastic loss [18] or the interaction energy of a $|1\rangle - |2\rangle$ mixture [19]. A more accurate determination can be made by mapping out the onset of dissociation of the molecular state [12,15]. After releasing an almost pure molecular sample from the trap at 770 G, the magnetic field was linearly ramped up in 10 ms to a variable value. During that time, the particle density dropped by a factor of 1000. If the field crossed the resonance, molecules dissociated into atoms. These atoms were then imaged at zero field, where the remaining molecules were not detected [10]. The Feshbach resonance appeared as a sharp onset in the number of detected atoms (Fig. 1). The speed of the downward ramp to zero field had to be chosen carefully. Fast ramps could dissociate very weakly bound molecules [20], such that the Feshbach resonance appeared systematically shifted to lower fields. For too slow a ramp-down, on the other hand, we found that even for clouds as dilute as $\sim 3 \times 10^{10}$ cm^{-3} molecules were recreated, lowering the measured atomic fraction. However, when we varied the ramp rate over more than 3 orders of magnitude, we found a range of rates which gave identical thresholds at 822 ± 3 G (Fig. 1).

To produce samples in the crossover region, we started with an essentially pure Bose-Einstein condensate of molecules formed at 770 G. The laser power of the optical trap was increased in 500 ms from 15 to 25 mW in order to accommodate larger Fermi clouds above the resonance. In some experiments, we used a deeper trap with up to 150 mW of power; the additional compression was carried out after ramping in 500 ms to 900 G to avoid enhanced losses on the BEC side of the resonance. Once the final trap depth was reached, the magnetic field was ramped in 500 ms to values between 650 and 1025 G. The adiabaticity of this ramp was checked by ramping back to 770 G and observing an identical density profile and condensate fraction, similar to studies in Ref. [8]. At 1025 G, the total peak density of the spin mixture in the deepest trap was 3×10^{13} cm^{-3}, corresponding to a Fermi energy of 3.6 μK and inverse Fermi wave vector $k_F^{-1} \simeq 2000 a_0$, where a_0 denotes the Bohr radius.

To probe the gas, we released it from the trap, and after a variable delay τ_d of usually 40 μs, applied a rapid transfer technique [12]: the magnetic field was switched off exponentially to zero with an initial slew rate of 30 G/μs, which adiabatically converted pairs of atoms into deeply bound molecules at zero field [21]. As long as no collisions or other dynamics occur during this ramp, the velocity distribution of the resulting molecules then constitutes a probe of the atom pairs' center-of-mass motion before the measurement. After 3–6 ms time of flight at zero field, we dissociated the molecules with a 3 ms field pulse to 900 G and imaged the resulting atoms after 2 ms at zero field [10,22]. We could also selectively detect any remaining atoms by omitting the dissociation pulse, and we observed that for $\tau_d \leq 500$ μs, less than 10% of the sample consisted of atoms, independent of the initial magnetic field. At longer delay times, the atom-molecule conversion became less efficient due to the decreased density.

Typical absorption pictures of molecular clouds after the rapid transfer ramp are shown in Fig. 2 for different temperatures, clearly exhibiting a bimodal distribution. This is evidence for condensation of pairs of ^{6}Li atoms on the BCS side of the Feshbach resonance. The condensate fractions were extracted from images like these, using a Gaussian fit function for the "thermal" part and a

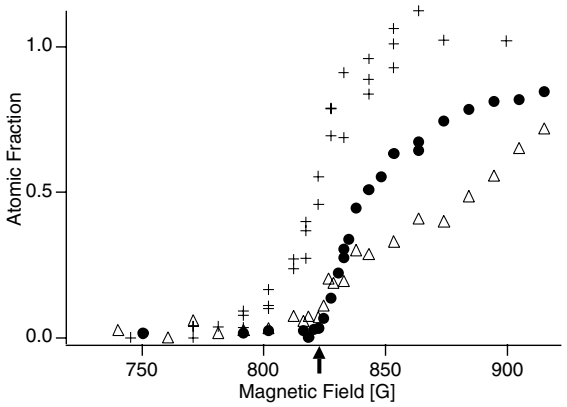

FIG. 1. Determination of the Feshbach resonance position. Shown is the onset of molecule dissociation when the magnetic field was slowly raised and then ramped down to zero field with a variable rate: Using a switch-off of the power supply at an initial rate of 30 G/μs (crosses), a linear ramp to zero field of 100 G/ms (circles), a linear ramp for 16 ms at 12.5 G/ms, followed by switch off (triangles). The identical threshold for the two lowest ramp rates determines the resonance position to be 822 ± 3 G, marked by an arrow.

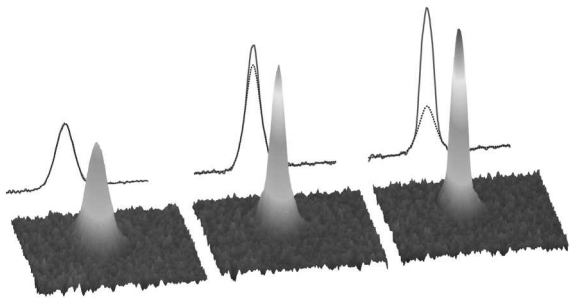

FIG. 2 (color online). Emergence of a Bose-Einstein condensate of atom pairs as the temperature was lowered. Shown are column densities (after 6 ms of time of flight) of the fermion mixture after a rapid transfer ramp from 900 G for three different initial temperatures $T/T_F \approx 0.2$, 0.1 and 0.05, together with their axially integrated radial density profiles. The dashed line is a Gaussian fit to the thermal component. Condensate fractions are 0.0, 0.1, and 0.6. Each cloud consists of about 2×10^6 molecules. The field of view is 3×3 mm.

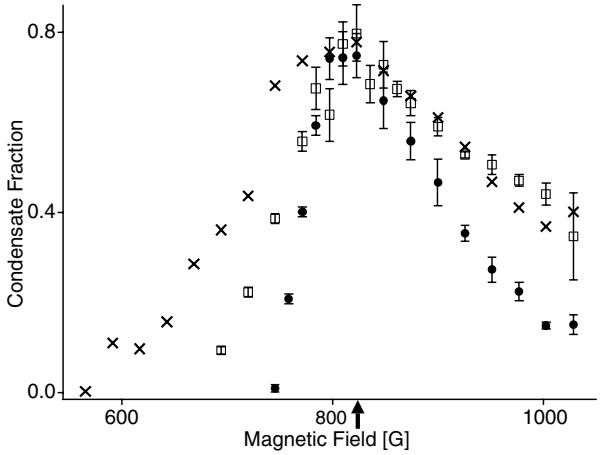

FIG. 3. Condensate fraction after the rapid transfer vs initial magnetic field, for different hold times at that field in the shallow trap ($P = 25$ mW). Crosses: 2 ms hold time, after 500 ms ramp to 1000 G and 4 ms ramp to the desired field; squares and circles: 100 ms and 10 s hold time, after 500 ms ramp from 770 G. The reduction of the condensate fraction for long hold times far on the left side of the resonance is probably due to the rapidly increasing inelastic losses for the more tightly bound molecules [20,23]. The lower condensate fraction at high field for long hold times is probably an effect of lower density since the number of atoms had decayed by a factor of 4 without change in temperature.

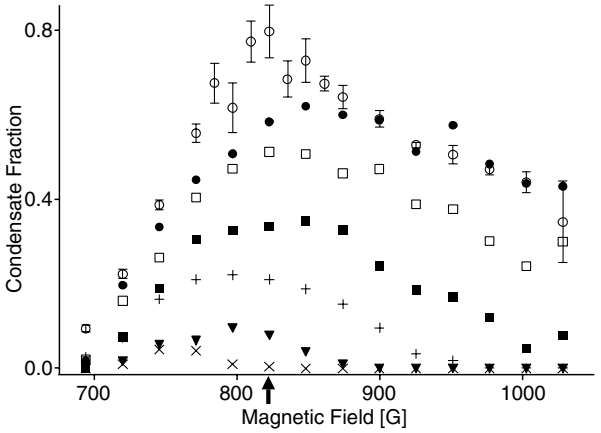

FIG. 4. Condensate fraction for different temperatures as a function of magnetic field. The temperature of the molecular cloud was varied by stopping the evaporative cooling earlier and applying parametric heating before ramping to the final magnetic field. Temperatures are parametrized by the molecular condensate fraction N_0/N at 820 G (open circles: 0.8; filled circles: 0.58; open squares: 0.51; filled squares: 0.34; "+": 0.21; triangles: 0.08; "×": <0.01). The lowest temperature was realized in the shallow trap ($P = 25$ mW); the higher temperatures required a deeper trap ($P = 150$ mW).

Thomas-Fermi profile for the "condensate." Figures 3–5 show the observed condensate fraction as a function of both magnetic field and temperature. The striking features of these data are the high condensate fraction of 80% near resonance, and the persistence of large condensate fractions on the BCS side of the resonance all the way to our maximum field of 1025 G. After 10 s hold time, this value was still as high as 20%. These observations were independent of whether the final magnetic field was approached starting with a Fermi sea or a molecular condensate. Note that for our peak densities, the strongly interacting region of $k_F|a| > 1$ extends from 710 G onward.

There is experimental evidence that the observed pair condensates existed before the sweep and were not produced during the sweep by collisions. First, the observed condensate fraction depended on the initial magnetic field. Second, the condensate fraction did not change when we varied the delay time τ_d (between release of the atoms from the trap and the magnetic field ramp) from 0 to 200 μs, although the density of the cloud changed by a factor of ~4 [25]. However, we cannot rule out with certainty that the momentum distribution of the pairs is modified by collisions during the ramp [26]. At our highest densities, it takes about 4 μs to take the molecules created during the ramp out of the strongly interacting region ($k_F|a| \geq 1$). A classical gas at the Fermi temperature would have a unitarity limited collision time comparable to the inverse of the Fermi energy divided by $\hbar$, which is about 2 μs. However, this may be affected by Pauli blocking for the atoms and bosonic stimulation for the molecules.

Assuming that collisions during the ramp can be neglected, it is still crucial to ask what exactly happens during the rapid transfer ramp, and what kind of pairs would likely be detected. A reasonable assumption is that atoms form molecules preferentially with their nearest neighbor, independent of the center-of-mass velocity of the pair. If, as our data show, a large fraction of the

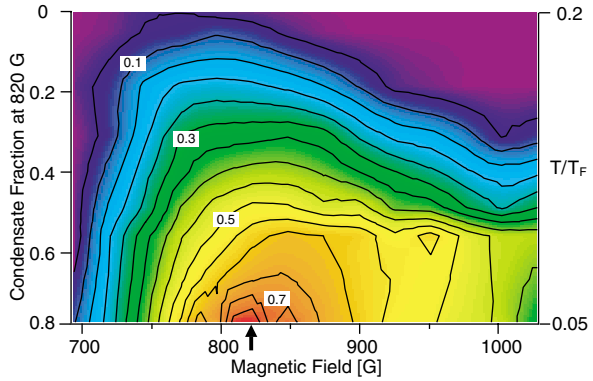

FIG. 5 (color online). Temperature and magnetic field ranges over which pair condensation was observed (using the same data as in Fig. 4). The right axis shows the range in T/T_F (measured at 1025 G) which was covered. For high degeneracies, fitting T/T_F was less reliable and we regard the condensate fraction as a superior "thermometer." Note that for an isentropic crossover from a BEC to a Fermi sea, T/T_F is approximately linearly related to the condensate fraction on the BEC side [24]. For our maximum densities the region where $k_F|a| \geq 1$ extends from about 710 G onward.

detected molecules are in a zero-momentum state after the fast transfer, this means that nearest neighbors had opposite momenta. If the distance between the fermions with opposite momenta making up each pair were comparable to or larger than the interatomic distance (as in long-range Cooper pairs) one would not expect to find high condensate fractions; on the contrary, the transfer into a tightly bound molecular state would randomly pick one of the nearest neighbors, resulting in a thermal molecule. We regard our observed high condensate fractions as evidence for the existence of condensed atomic pairs above the Feshbach resonance, which are smaller in size than the interatomic distance and, therefore, molecular in character. Their stability may be affected by Pauli blocking and mean-field effects, but their binding should be a two-body effect and not a many-body effect as in the case of Cooper pairs.

In conclusion, we have observed $^6Li_2$ molecular Bose-Einstein condensates after a fast downward magnetic field ramp starting with equilibrium samples at fields on either side of the broad ^{6}Li Feshbach resonance. Since there are no truly bound molecular states above the resonance, we tentatively interpret our results as a Bose-Einstein condensate of pairs of atoms which are molecular in character and stabilized by the existence of the Fermi sea. This condensate would drain particles from the Fermi sea and lead to a reduced atomic Fermi energy roughly equal to half the energy of the molecular level [5,6]. Indeed, both in Ref. [8] and in the present work, a reduction in the size of the cloud was observed as the Feshbach resonance was approached from above, which may be due to this effect. In agreement with theoretical predictions [6] we have observed pair condensation in the regime where $T/T_F < 0.2$ and $k_F|a| > 1$ (Fig. 5). The exact nature of the atom pairs remains to be elucidated; they could be related to virtual states or scattering resonances in the continuum; they may turn out to be the tight-binding limit of Cooper pairs. It is also possible that the pair condensate is a superposition state of molecules and Cooper pairs [4–6]. We regard the characterizing feature of the BCS-BEC crossover a qualitative change of the pairing phenomenon which has not yet been observed.

This work was supported by NSF, ONR, ARO, and NASA. We thank Walter Hofstetter, Michele Saba, and Zoran Hadzibabic for stimulating discussions. S. R. is grateful to the Dr. Jürgen Ulderup foundation for financial support.

[1] H. T. C. Stoof and M. Houbiers, in *Bose-Einstein Condensation in Atomic Gases, Proceedings of the International School of Physics Enrico Fermi, Course CXL*, edited by M. Inguscio, S. Stringari, and C. Wieman (IOS Press, Amsterdam, 1999), pp. 537–553.

[2] E. Tiesinga, B. J. Verhaar, and H. T. C. Stoof, Phys. Rev. A **47**, 4114 (1993); W. C. Stwalley, Phys. Rev. Lett. **37**, 1628 (1976); S. Inouye *et al.*, Nature (London) **392**, 151 (1998); P. Courteille *et al.*, Phys. Rev. Lett. **81**, 69 (1998).

[3] D. M. Eagles, Phys. Rev. **186**, 456 (1969); A. J. Leggett, in *Modern Trends in the Theory of Condensed Matter. Proceedings of the XVIth Karpacz Winter School of Theoretical Physics, Karpacz, Poland, 1980* (Springer-Verlag, Berlin, Karpacz, Poland, 1980), pp. 13–27; P. Nozières and S. Schmitt-Rink, J. Low Temp. Phys. **59**, 195 (1985).

[4] E. Timmermans *et al.*, Phys. Lett. A **285**, 228 (2001); M. Holland *et al.*, Phys. Rev. Lett. **87**, 120406 (2001); J. Stajic *et al.*, e-print cond-mat/0309329; A. Perali *et al.*, e-print cond-mat/0311309; R. Combescot, e-print cond-mat/0310583; J. Kinnunen, M. Rodriguez, and P. Törmä, e-print cond-mat/0401543.

[5] Y. Ohashi and A. Griffin, Phys. Rev. Lett. **89**, 130402 (2002).

[6] G. M. Falco and H. T. C. Stoof, e-print cond-mat/0402579.

[7] M. Houbiers *et al.*, Phys. Rev. A **56**, 4864 (1997).

[8] S. Jochim *et al.*, Science **302**, 2101 (2003); M. Bartenstein *et al.*, Phys. Rev. Lett. **92**, 120401 (2004).

[9] M. Greiner, C. A. Regal, and D. S. Jin, Nature (London) **426**, 537 (2003).

[10] M. W. Zwierlein *et al.*, Phys. Rev. Lett. **91**, 250401 (2003).

[11] T. Bourdel *et al.*, e-print cond-mat/0403091.

[12] C. A. Regal, M. Greiner, and D. S. Jin, Phys. Rev. Lett. **92**, 040403 (2004).

[13] NIST and University of Colorado at Boulder press release, January 28, 2004; http://www.nist.gov/public_affairs/releases/fermi_condensate.htm.

[14] M. Houbiers *et al.*, Phys. Rev. A **57**, R1497 (1998).

[15] T. Mukaiyama *et al.*, e-print cond-mat/0311558 [Phys. Rev. Lett.(to be published)].

[16] D. S. Petrov, C. Salomon, and G. V. Shlyapnikov, e-print cond-mat/0309010.

[17] The smaller value reported in our previous work [10] was based on an incorrect extrapolation of trap frequencies to 100 times lower power. The radial trap frequency was strongly influenced by multiple intensity maxima in the optical focus.

[18] K. Dieckmann *et al.*, Phys. Rev. Lett. **89**, 203201 (2002).

[19] T. Bourdel *et al.*, Phys. Rev. Lett. **91**, 020402 (2003).

[20] J. Cubizolles *et al.*, Phys. Rev. Lett. **91**, 240401 (2003).

[21] According to Fig. 1, this fast ramp can dissociate weakly bound molecules at low density, but at high density we observed an atom-molecule conversion $\geq 90\%$.

[22] At this point the cloud was sufficiently dilute that the final switch off of the field did not reconvert atoms into molecules.

[23] S. Jochim *et al.*, Phys. Rev. Lett. **91**, 240402 (2003).

[24] L. D. Carr, G. V. Shlyapnikov, and Y. Castin, e-print cond-mat/0308306 [Phys. Rev. Lett. (to be published)].

[25] The condensate peak broadened for longer τ_d and could not be reliably discerned after 200 μs.

[26] In the ^{40}K experiment, the ratio of the effective sweep rate through resonance and Fermi energy was similar [12].

Appendix G

List of Predicted s-wave ^{6}Li-^{23}Na Feshbach Resonances

This appendix lists the prediction for all the ^{6}Li-^{23}Na Feshbach resonances, obtained as described in Chapter 4. The last column lists the collisional properties of the lithium-sodium mixtures, covered in more detail in Chapter 3. The ones labeled 'Yes' are stable against spin-exchange collisions and have lifetimes in excess of a few seconds at typical ultracold atom experiments. For the ones labeled 'Maybe', based on experimental observations, the mixture lifetime is expected or was observed to be long enough to perform typical experiments. The mixtures labeled with 'No' are expected to have strong losses.

Table G.1: Predicted ^{6}Li-^{23}Na Feshbach resonances. Sodium and lithium states are given in the high-field basis. The triplet molecular state is characterized by the projection of the total electronic spin, and of the projections of the nuclear spins of ^{6}Li and ^{23}Na.

Magnetic Field [G]	Na state	Li state	Molecular state $\|m_S, m_{i,Li}, m_{i,Na}\rangle$	Good mixture?
717.4	|1>	|1>	|1, 1, -1/2>	Yes
763.1	|1>	|1>	|1, 0, 1/2>	Yes
790.7	|1>	|2>	|1, 1, -3/2>	Maybe
821.1	|1>	|1>	|1, -1, 3/2>	Yes
836.4	|2>	|1>	|1, 1, -3/2>	Maybe
848.2	|1>	|2>	|1, 0, -1/2>	Maybe
876.7	|1>	|3>	|1, 0, -3/2>	Maybe
895.9	|2>	|1>	|1, 0, -1/2>	Maybe
921.1	|1>	|2>	|1, -1, 1/2>	Maybe
924.1	|2>	|2>	|1, 0, -3/2>	Maybe
949.2	|1>	|3>	|1, -1, -1/2>	Maybe
970.2	|2>	|1>	|1, -1, 1/2>	Maybe
992.2	|3>	|1>	|1, 0, -3/2>	Maybe
998	|2>	|2>	|1, -1, -1/2>	Maybe
1026.9	|2>	|3>	|1, -1, -3/2>	Maybe
1066.7	|3>	|1>	|1, -1, -1/2>	Maybe
1095.1	|3>	|2>	|1, -1, -3/2>	Yes
1206.5	|4>	|1>	|1, -1, -3/2>	No
1493	|1>	|5>	|1, 1, -1/2>	Maybe
1493.9	|1>	|6>	|1, 1, 1/2>	Yes
1603.5	|1>	|4>	|1, 1, -3/2>	Maybe
1603.9	|1>	|5>	|1, 0, 1/2>	Maybe
1605.7	|1>	|6>	|1, 0, 3/2>	Yes
1659.5	|2>	|6>	|1, 1, -1/2>	Maybe
1689.4	|1>	|1>	|0, 1, 1/2>	Yes
1699.3	|1>	|1>	|0, 0, 3/2>	Yes
1703	|1>	|2>	|0, 1, -1/2>	Maybe
1711.1	|1>	|3>	|0, 1, -3/2>	Maybe
1716.6	|1>	|2>	|0, 0, 1/2>	Maybe
1726.5	|1>	|2>	|0, -1, 3/2>	Maybe
1728.4	|1>	|4>	|1, 0, -1/2>	Maybe
1729.4	|1>	|5>	|1, -1, 3/2>	Maybe
1731.1	|1>	|3>	|0, 0, -1/2>	Maybe
1744.6	|1>	|3>	|0, -1, 1/2>	Maybe
1774.1	|2>	|6>	|1, 0, 1/2>	Maybe
1774.5	|2>	|5>	|1, 1, -3/2>	Maybe
1817.1	|2>	|1>	|0, 1, -1/2>	Maybe

continued on next page

Table G.1: *continued*

Magnetic Field [G]	Na state	Li state	Molecular state $\|m_S, m_{i,Li}, m_{i,Na}\rangle$	Good mixture?
1825.9	|2>	|2>	|0, 1, -3/2>	Maybe
1830.1	|2>	|1>	|0, 0, 1/2>	Maybe
1839.8	|2>	|1>	|0, -1, 3/2>	Maybe
1840.1	|5>	|1>	|1, 0, -3/2>	No
1844.6	|2>	|2>	|0, 0, -1/2>	Maybe
1854	|6>	|1>	|1, 1, -3/2>	No
1854.2	|2>	|3>	|0, 0, -3/2>	Maybe
1855	|7>	|1>	|1, 1, -1/2>	No
1857.6	|2>	|2>	|0, -1, 1/2>	Maybe
1869.4	|1>	|4>	|1, -1, 1/2>	Maybe
1872.9	|2>	|3>	|0, -1, -1/2>	Maybe
1901.2	|2>	|4>	|1, 0, -3/2>	Maybe
1901.7	|2>	|5>	|1, 0, -1/2>	Maybe
1901.8	|2>	|6>	|1, -1, 3/2>	Maybe
1951.7	|8>	|1>	|1, 1, 1/2>	Yes
1965.9	|7>	|1>	|1, 0, 1/2>	No
1967.6	|3>	|1>	|0, 1, -3/2>	Maybe
1971.7	|3>	|6>	|1, 1, -3/2>	Maybe
1974.3	|5>	|1>	|1, -1, -1/2>	No
1974.9	|6>	|1>	|1, 0, -1/2>	No
1984.6	|3>	|1>	|0, 0, -1/2>	Maybe
1995	|3>	|2>	|0, 0, -3/2>	Yes
1996.9	|3>	|1>	|0, -1, 1/2>	Maybe
2006	|8>	|2>	|1, 1, -1/2>	No
2012.1	|3>	|2>	|0, -1, -1/2>	Yes
2019.6	|7>	|2>	|1, 1, -3/2>	No
2023.2	|3>	|3>	|0, -1, -3/2>	Yes
2027.5	|5>	|2>	|1, -1, -3/2>	No
2028.3	|6>	|2>	|1, 0, -3/2>	No
2042	|2>	|4>	|1, -1, -1/2>	Maybe
2042.8	|2>	|5>	|1, -1, 1/2>	Maybe
2065.6	|8>	|1>	|1, 0, 3/2>	Yes
2089.1	|7>	|1>	|1, -1, 3/2>	No
2099.2	|3>	|6>	|1, 0, -1/2>	Maybe
2099.5	|3>	|5>	|1, 0, -3/2>	Maybe
2109.4	|6>	|1>	|1, -1, 1/2>	No
2119.6	|8>	|2>	|1, 0, 1/2>	No
2142.6	|7>	|2>	|1, 0, -1/2>	No
2162.4	|6>	|2>	|1, -1, -1/2>	No
2171.4	|4>	|1>	|0, 0, -3/2>	No
2174.8	|8>	|3>	|1, 1, -3/2>	No

continued on next page

Table G.1: *continued*

Magnetic Field [G]	Na state	Li state	Molecular state $\|m_S, m_{i,Li}, m_{i,Na}\rangle$	Good mixture?
2186.4	|4>	|1>	|0, -1, -1/2>	No
2197.2	|7>	|3>	|1, 0, -3/2>	No
2198.4	|4>	|2>	|0, -1, -3/2>	Yes
2216.5	|6>	|3>	|1, -1, -3/2>	No
2238.8	|3>	|4>	|1, -1, -3/2>	Maybe
2239	|3>	|6>	|1, -1, 1/2>	Maybe
2239.1	|3>	|5>	|1, -1, -1/2>	Maybe
2244.8	|8>	|2>	|1, -1, 3/2>	No
2277.9	|7>	|2>	|1, -1, 1/2>	No
2299.6	|8>	|3>	|1, 0, -1/2>	No
2328	|4>	|6>	|1, 0, -3/2>	No
2332.1	|7>	|3>	|1, -1, -1/2>	No
2435.9	|8>	|3>	|1, -1, 1/2>	No
2464	|4>	|6>	|1, -1, -1/2>	No
2464.4	|4>	|5>	|1, -1, -3/2>	No

Appendix H

Manufacturers and suppliers

This appendix lists most of the manufacturers and suppliers I have used for building, upgrading and maintaining the experiment. It is by no means a complete list of the suppliers needed to build ultracold atom experiments. However, it contains both the most frequently used suppliers and those manufacturers which supplied special items and I could only find after spending a lot of time searching. I hope it will be an useful reference for new lab members.

H.1 General supplies and materials

MIT ECAT

Address On-campus

Web http://web.mit.edu/ecat/

Notes MIT's purchase site from partner suppliers: Airgas, Apple Computer, Dell Computer, DHL, GovConnection, Grainger, Minuteman Press of Cambridge, Nextel, Office Depot, Verizon Wireless, VWR International. Heavily discounted, sometimes as low as 25% for chemical supplies.

McMaster-Carr

Address New Brunswick, NJ

Web http://www.mcmaster.com/

Notes One of the biggest industrial supplies distributors. This is our main source for raw materials, tools and basic electrical supplies. Convenient and fast web search interface, short lead times, low prices.

Grainger

Address Boston, MA

Web http://www.grainger.com/

Notes Another industrial supplier. A place to search if McMaster doesn't have it. Slow search interface, but it sells directly to MIT via ECAT.

Graybar

Address St. Louis, MO

Web http://www.graybar.com/

Notes Tools, wire & cable, infrastructure supplies.

Cole-Parmer

Address Vernon Hills, IL

Web http://www.coleparmer.com/

Notes Big general chemistry and biology lab supplier. A good place to search for very basic lab equipment.

VWR International

Address Boston, MA

Web http://www.vwrsp.com/

Notes Very similar to Cole-Parmer. Has a stockroom on campus (Room 56-070), and good discounts.

Fisher Scientific

Address Pittsburgh, PA

Web https://www1.fishersci.com/index.jsp

Notes Large lab supplier, an alternative to Cole-Parmer and VWR.

H.2 Chemical supplies

Sigma-Aldrich

Address St. Louis, MO

Web http://www.sigmaaldrich.com/

Notes Chemical supplier conglomerate, contains by now the Sigma, Aldrich, Fluka, Riedel-deHaën, Supelco, and SAEN brands. Sells enriched Lithium-6.

Alfa Aesar

Address Ward Hill, MA

Web http://www.alfa.com/alf/index.htm

Notes Laboratory chemical supplier. It has a comprehensive pure metals offering.

ESPI (Electronic Space Products International)

Address Ashland, OR

Web http://www.espi-metals.com/index.htm

Notes Pure metals supplier, one good choice for getting ampoule-sealed sodium.

Strem Chemicals

Address Newburyport, MA

Web http://www.strem.com/code/index.ghc

Notes A smaller chemicals supplier, oriented more towards the research market. The other good source for ampoule-sealed sodium, they tend to have lower prices than ESPI.

Icon Isotopes

Address Summit, NJ

Web http://www.iconisotopes.com/

Notes A source for enriched Lithium-6; they normally process the metallic lithium into reagents, but we have been able to get the raw metal.

Materials Preparation Center

Address Ames, IA

Web http://www.mpc.ameslab.gov/services/metal_alloys.html

Notes This small government lab specializes in preparation and processing of unusual and rare materials. They accept orders only from the government or universities, and only when an alternate service provider does not exist. They have cleaned and repackaged our enriched Lithium-6.

H.3 Electronics

Newark InOne (formerly Newark electronics)

Address Lowell, MA

Web http://www.newark.com/

Notes The supplier of electronic components we use most. The web interface allows stock checks. Good delivery time.

Dig-Key Corporation

Address Thief River Falls, MN

Web http://www.digikey.com/

Notes If Newark doesn't have it in stock, check Digi-Key. The alternative to Newark, with very similar product range and prices. Good web interface also.

MPJA (Marlin P. Jones & Assoc., Inc.)

Address Lake Park, FL

Web http://www.mpja.com/contact.asp

Notes The very cheap components source, sometimes as low as one-tenth of the standard prices. This also means a small product range and lower reliability.

JDR Microdevices

Address San Jose, CA

Web http://www.jdr.com/interact/default.asp

Notes This small computer components supplier sells the 'grey' electronics boxes, which are the best 19" rackmount enclosures I could find.

Belden CDT Electronics Division

Address Richmond, IN

Web http://www.belden.com/

Notes One of the biggest wire and cable manufacturers, including industry-standard and higher quality coaxial cables.

Bergquist Company

Address Chanhassen, MN

Web http://www.bergquistcompany.com/

Notes Manufacturer of thermally conductive films and sheets used for heatsinking, the alternative solution to heat conductive grease.

C&H Technology, Inc.

Address Minnetonka, MN

Web http://www.chtechnology.com/

Notes Manufacturer of power electronics, including high-current diodes, air and liquid heatsinks.

R-Theta Inc.

Address Mississauga, ON, Canada

Web http://www.r-theta.com/indexf.html

Notes Manufacturer of heatsinks and water-cooled plates for electronic components. This is the manufacturer of the heatsink bars we are using. In bulk (500$ minimum order), their extruded heatsinks are a factor of ten cheaper than the heatsinks available from distributors.

Aavid Thermalloy

Address Concord, NH

Web http://www.aavidthermalloy.com/

Notes Another heatsink and water-cooled plate manufacturer, with a similar product range as R-Theta. We have not bought extrusions from them due to their higher minimum order limit.

MELCOR Corporation

Address Trenton, NJ

Web http://www.melcor.com/

Notes Thermoelectric cooling elements and electronics cooling equipment.

H.4 Heating and Temperature

Omega Engineering Inc.

Address Stamford, CT

Web http://www.omega.com/

Notes This is the default place to start looking for heating and temperature measurement hardware. In addition to a comprehensive list of temperature products, Omega also offers a wide variety of force/pressure/flow transducers and process control equipment.

TEMPCO Electric Heater Corporation

Address Wood Dale, IL

Web http://www.tempco.com/

Notes Manufacturer of electrical heaters, temperature sensors and controllers. The products are similar to the one offered by Omega, but often cheaper or with more features. They are the manufacturers of the custom band heaters for the sodium-lithium ovens.

Ogden Manufacturing Co.

Address Arlington Heights, IL

Web http://www.ogdenmfg.com/

Notes Electrical heater manufacturer.

Plastic Process Equipment, Inc.

Address Macedonia, OH

Web http://www.ppe.com/default.htm

Notes Another electrical heater manufacturer from which we have ordered in the past.

Cotronics Corp.

Address Brooklyn, NY

Web http://cotronics.com/vo/cotr/

Notes Manufacturer of high-temperature epoxy resins and ceramic adhesives. The magnetic trap in BEC1 was mold into a solid single piece using a Cotronics epoxy resin. Their non-magnetic resins are an excellent choice for bonding high-current coils.

H.5 Instruments

H.5.1 Handheld frequency counters

Optoelectronics, Inc.

Address Ft. Lauderdale, FL

Web http://www.optoelectronics.com/

Notes Manufacturer of handheld frequency counters with LCD display.

STARTEK International, Inc.

Address Ft. Lauderdale, FL

Web http://www.startekvideo.com/

Notes Manufacturer of handheld frequency counters with LED display. The company no longer produces these very practical counters, but still services them and sometimes will have a few to sell.

H.5.2 General instruments

Aeroflex Incorporated

Address Plainview , NY

Web http://www.aeroflex.com/

Notes Manufacturer of RF signal sources and test equipment.

Agilent Technologies (formerly Hewlett-Packard)

Address Englewood, CO

Web http://www.home.agilent.com/USeng/home.html

Notes High-end manufacturer of a wide range of test and measurement equipment. High quality, good technical support, high prices. Most of the frequency synthesizers we bought recently are from Agilent. We are also bought one of their 6-1/2 digit multimeters for precise magnetic field calibration; we have chosen it over a Keithley unit because of its better trigger timing jitter.

Keithley Instruments

Address Cleveland, OH

Web http://www.keithley.com/

Notes Test and measurement equipment manufacturer. Their product range overlaps partially with Agilent's, where they produce similar products, only slightly better or worse than Agilent's. Their multimeter-based data acquisition units are in particular a good deal and we use them for temperature interlock. Keithley also produces a range of PC data acquisition cards which sometimes have better specs than the ones made by National Instruments.

Stanford Research Systems

Address Sunnyvale,CA

Web http://www.thinksrs.com/

Notes Manufacturer of quality scientific instruments. Some of their products are unique in their capabilities, as the high-frequency lock-in amplifiers. We are using their lock-in amplifiers, a low-noise current preamplifier, and a few of their 30 MHz DDS synthesizers.

Rohde & Schwarz USA

Address Columbia, MD

Web http://www.rohde-schwarz.com/

Notes Synthesizers, handheld spectrum analyzers, power meters.

F.W. Bell (part of Sypris Test&Measurement)

Address Orlando, FL

Web http://www.fwbell.com/

Notes Manufacturers of high precision magnetometers. They also produce the fast, high-accuracy closed loop current sensors used in our magnetic trap setup.

H.5.3 Power supplies

Lambda Americas Inc. (formerly Lambda EMI, formerly Electronic Measurements Inc.)

Address Neptune, NJ

Web http://www.lambda-emi.com/

Notes Manufacturer of most of the high-current dc power supplies we use today. The 650 μs response time of the ESS series is not yet matched by other manufacturers. Currently the maximum output of the ESS series is 15 kW; we could use higher outputs to produce higher magnetic fields.

Elgar Electronics Corporation

Address San Diego, CA

Web http://www.elgar.com/

Notes Elgar owns the Sorensen and PowerTen brands. Both have in their product lines efficient, up to 30 kW dc power supplies.

Kepco, Inc.

Address Flushing, NY

Web http://www.kepcopower.com/

Notes Programmable dc power supplies.

Xantrex Technology

Address Vancouver, BC, Canada

Web http://www.xantrex.com/index.asp

Notes Programmable dc power supplies, comparable to Lambda and Sorensen products.

H.5.4 rf power meters

Aeroflex, Wichita Division (formerly IFR, formerly Marconi Instruments)

Address Wichita, KS

Web http://www.aeroflex.com/

Notes Manufacturer of the white handheld RF power meter we use.

LP Technologies, Inc.

Address Wichita, KS

Web http://www.lptech.com/

Notes Manufacturer of the black handheld RF power meter we use. This power meter is much cheaper, but has questionable accuracy and very few features.

Giga-tronics Incorporated

Address San Ramon, CA

Web http://www.gigatronics.com/

Boonton Electronics

Address Parsippany, NJ

Web http://www.boonton.com/

H.6 Optics

Thorlabs, Inc.

Address Newton, NJ

Web http://www.thorlabs.com/

Notes The best price/quality ratio for optic mounts and components. Their product range increased significantly during the last few years. Our group can also take advantage of a special 8% discount. Most of the mounts we use are made by ThorLabs. We also use their hardware to drive laser diodes.

Melles Griot

Address Carlsbad, CA; Rochester, NY

Web http://www.mellesgriot.com/

Notes Comprehensive laser and optics manufacturer and distributor. Except for optical tables, we do not buy a lot from them.

Newport Corporation

Address Irvine, CA

Web http://www.newport.com/

Notes Optics and laser manufacturer and distributor. My favorite source for higher quality optomechanics. They have recently bought Spectra-Physics.

CVI Laser, LLC

Address Putnam, CT

Web http://www.cvilaser.com/

Notes High-quality and high-power coated optics. They also manufactured the dichroic mirrors we use.

Meadowlark Optics

Address Frederick, CO

Web http://www.meadowlark.com/

Notes Polarization optics.

Edmund Optics Inc. (Edmund Industrial Optics)

Address Barrington, NJ

Web http://www.edmundoptics.com/US/

Notes Budget optics and optical components.

Fiber Instrument Sales, Inc.

Address Oriskany, NY

Web http://www.fiberinstrumentsales.com/

Notes Fiber optics supplier, including connectors and assembly equipment.

Kinetic Systems, Inc.

Address Boston, MA

Web http://www.kineticsystems.com/

Notes Optical tables and vibration isolation products.

TMC Technical Manufacturing Corporation

Address Peabody, MA

Web http://www.techmfg.com/

Notes Optical tables and vibration isolation products.

Lenox Laser

Address Glen Arm, MD

Web http://www.lenoxlaser.com/index.html

Notes High-energy pinholes.

Reynard Corporation

Address San Clemente, CA

Web http://www.reynardcorp.com/

Notes Optical components, including filters, polarizers, and high-energy pinholes.

OPTHOS Instruments, Inc.

Address Rockville, MD

Web http://www.e-opthos.com/index.htm

Notes Na, K, Rb, and Cs absorption cells.

H.6.1 Acousto-optical modulators

IntraAction Corp.

Address Bellwood, IL

Web http://www.intraaction.com/

Notes IntraAction's AOMs have excellent prices and good performance. Unfortunately, they almost never deliver as promised, especially for high-frequency models. It happened more than once that an AOM promised in two weeks was delivered after 4 or 6 months.

Isomet Corporation

Address Springfield, VA

Web http://www.isomet.com/

Notes Low-frequency (<400 MHz) modulators.

Crystal Technology, Inc.

Address Palo Alto, CA

Web http://www.crystaltechnology.com/

Notes Modulators up to 350 MHz center frequency. Most of the 350 MHz TeO_2 modulators we have used mysteriously lowered their efficiency after one or two months of operation.

Brimrose Corporation of America

Address Baltimore, MD

Web http://www.brimrose.com/

Notes AOMs up to 3500 MHz, with very good quoted efficiency. Much more expensive than other manufacturers.

H.7 rf and microwave

Mini-Circuits

Address Brooklyn, NY

Web http://www.minicircuits.com/

Notes Mini-Circuits is our main source of microwave components. It packages discrete components into shielded, connectorized units. They have most of the components we need, and they are typically in stock. Their low point is the reliability and price of rf amplifiers, but they compensate for it by usually having them in stock.

Aeroflex/Inmet, Inc. (formerly Inmet Microwave)

Address Ann Arbor, MI

Web http://www.inmetcorp.com/

Notes High-power passive components.

Midwest Microwave

Address Saline, MI

Web http://ebiz.midwest-microwave.com/cgi-bin/mmb2c/main.html

Notes High-power passive components, including custom low-loss cable assemblies.

Pasternack Enterprises, Inc.

Address Irvine, CA

Web http://www.pasternack.com/

Notes Coaxial cables and connectors.

Semflex

Address Mesa, AZ

Web http://www.semflex.com/homepage.htm

Notes Low-loss and high-power cable assemblies. Expensive.

Narda Microwave

Address Folsom, CA; Hauppauge, NY

Web http://www.nardamicrowave.com/

Notes Active and passive components.

RF Associates Inc.

Address Topsfield, MA

Web http://www.rfassociates-ne.com/

Notes Local RF and microwave distributor.

H.7.1 Amplifiers

Delta RF Technology

Address Sparks, NV

Web http://www.drft.com/

Notes One of the best amplifier suppliers. Their units are rugged, reliable, and relatively cheap. Availability is occasionally a problem.

Ophir RF

Address Los Angeles, CA

Web http://www.ophirrf.com/

Notes Ophir specializes in high-power (>1W) amplifiers. We have used some of their 10W amplifier modules with very good results. Somewhat expensive though.

Empower RF Systems, Inc.

Address Inglewood, CA

Web http://www.empowerrf.com/

Notes Large number of quality models, sometimes low priced; we have used them. They are almost never stocking them, so the lead time is typically 4-6 weeks.

NEXTEC Microwave & RF

Address Santa Clara, CA

Web http://www.nextec-rf.com/

Notes Amplifer modules with design and specifications comparable to Mini-Circuits models.

HD Communications Corp.

Address Ronkonkoma, NY

Web http://www.rfamplifiers.com/

Notes Wide amplifier module range.

KMIC Technology, Inc.

Address San Jose, CA

Web http://www.kmictech.com/

MITEQ

Address Hauppauge, NY

Web http://www.miteq.com/index.html

H.7.2 VCOs and compact synthesizers

Bonn Hungary Electronics

Address Budapest, Hungary

Web http://www.bonn-hungary.hu/

Notes Frequency synthesizers can be built in sizes comparable to a cigarette pack, sacrificing somewhat the frequency accuracy setting resolution. However, they cost one quarter the price of a standard benchtop synthesizer. Most of the compact synthesizers require external digital or analog frequency control, but Bonn offers a model with display and front panel setting which covers 0.3 to 3 GHz in 50 kHz steps in a very compact size.

APA Wireless Technologies

Address Fort Lauderdale, FL

Web http://www.apawireless.com/

CERNEX, Inc.

Address Sunnyvale, CA

Web http://www.cernex.com/

Elcom Technologies

Address Rockleigh, NJ

Web http://www.elcom-tech.com/

General Electronic Devices

Address San Marcos, CA

Web http://www.gedlm.com/

Herley Industries, Inc.

Address Lancaster, PA

Web http://www.herley.com/

Meret Optical Communications, Inc.

Address San Diego, CA

Web http://www.meretoptical.com/

Sirenza Microdevices, Inc.

Address Broomfield, CO

Web http://www.sirenza.com/corporate_home.asp

Synergy Microwave Corporation

Address Paterson, NJ

Web http://www.synergymwave.com/

TRAK Microwave Corporation

Address Tampa, FL

Web http://www.trak.com/

H.8 Safety

Trinity Technologies

Address Minneapolis, MN

Web http://www.lasersafety.com/

Notes Laser safety products: eyewear, windows, sheets, barriers.

Safety Label Solutions, Inc.

Address Milford, PA

Web http://safetylabelsolutions.com/

Notes Safety labels.

H.9 Transducers, control and infrastructure

Humphrey Products Company

Address Kalamazoo, MI

Web http://www.controlandpower.com/catalog/html/humphrey.htm

Notes Humphrey solenoid valves are used in most pneumatically controlled vacuum devices, for example in the gate valves and motion feedthroughs.

Legris Connectic

Address Mesa, AZ

Web http://www.legris.com/Legris/en_US/home2.nsf/vuid/HomePage

Notes Manufacturer of push-on pneumatic connectors. Legris connectors are used in MDC gate valves and are much easier to install than compression fittings.

Swagelok Company

Address Solon, OH

Web http://www.swagelok.com/

Notes In addition to its own brand of compression fittings, Swagelok offers a comprehensive assortment of quality fluid connectors, tubing and valves.

Parker Instrumentation

Address Huntsville, AL

Web http://www.parker.com/instrumentation/

Notes Parker Instrumentation offers a wider range of fluid fittings, valves, tubing and manifolds than Swagelok.

80/20 Inc.

Address Columbia City, IN

Web http://www.8020.net/

Notes The leading US supplier of aluminum T-slotted profiles for framing and support structures.

ElastoMetall Kentucky LLC

Address Frankfort, KY

Web http://www.elastometall.com/

Notes Passive vibration isolation products. We have used steel-rubber-steel joints from ElastoMetall to mount mechanical shutters and to reduce vibrations generated by our water distribution panel.

Flowmeter Directory

Web http://www.flowmeterdirectory.com/

Notes Comprehensive online resource for fluid flowmeters.

McMillan Company

Address Georgetown, TX

Web http://www.mcmflow.com/

Notes Cheap turbine fluid flowmeters. Most of the flowmeters used in our experiments are made by them. We had reliability problems using them in the BEC1, and we had later switched to thermal flowmeters. They work well if the water is not algae-contaminated though.

weber Sensors Inc.

Address Woodstock, GA

Web http://www.captor.com/wsi.htm

Notes Manufacturer of fluid flowmeters. Their 'flow-captor' inline thermal flow meters have no internal moving parts and are used in the BEC1 watercooling circuit.

Purolator Air Filtration

Address Henderson, NC

Web http://www.purolatorair.com/

Notes Air filters for the laminar flow boxes.

Parker Process Filtration

Address Indianapolis, IN

Web http://www.parker.com/filtration/

Notes Quality filter cartridges for the water cooling system.

MSC Filtration Technologies

Address Enfield, CT

Web http://www.mscliquidfiltration.com/

Notes Liquid and air filtration equipment.

Leslie's Swimming Pool Supplies

Address Phoenix, AZ

Web http://www.lesliespool.com/

Notes Algicides and cleaning substances the water cooling system.

Weber Industries, Inc. (Webtrol Pumps)

Address St. Louis, MO

Web http://www.webtrol.com/

Notes Manufacturer of Webtrol line of heavy duty, high-pressure booster pumps. The booster pump in BEC1 is a Webtrol.

Process Equipment & Supply Inc.

Address Cleveland, OH

Web http://www.proequip.com/

Notes Manufacturer of the Branson brand of ultrasonic cleaners and ultrasonic cleaning solutions.

EH Hinds

Address Watertown, MA

Notes Heavy equipment hauling and machinery moving. We have used their services for the delivery and installation of optical tables. They can also deal with other heavy equipment.

H.10 Vacuum

A&N Corporation

Address Williston, FL

Web http://www.ancorp.com/

Notes A&N is the only company which we found so far capable of producing quality custom fitting for the two-species oven. They have also a well-stocked, comprehensive line of ConFlat fittings.

BOC Edwards

Address Wilmington, MA

Web http://www.bocedwards.com/

Notes BOC Edwards offers a large variety of vacuum components. We have bought roughing pumps from them.

Duniway Stockroom Corp.

Address Mountain View, CA

Web http://www.duniway.com/

Notes Competitively priced and second-hand components. The source for extra-long vacuum bolts and studs.

Huntington Mechanical Laboratories, Inc.

Address Mountain View, CA

Web http://huntvac.com/

Notes Huntington offers a comprehensive list of motion feedthroughs, and produces custom chambers and bellows.

James Glass Company

Address Hanover, MA

Notes Glassblowers for scientific equipment, including UHV glass cells.

Kurt J. Lesker Company

Address Clairton, PA

Web http://www.lesker.com/newweb/index.cfm

Notes Kurt J. Lesker manufactures and distributes a full range of vacuum hardware. We also had a good experience with their custom built hardware.

MDC Vacuum Products Corporation

Address Hayward, CA

Web http://www.mdc-vacuum.com/

Notes MDC manufactures a full line of ConFlat fittings, valves and feedthroughs. The only UHV gate valve supplier we have used in the past six years. Recently, their competitive pricing and availability made MDC our principal source for fittings.

Nor-Cal Products, Inc.

Address Yreka, CA

Web http://www.n-c.com/

Notes Another comprehensive vacuum supplier. We have not bought from them in quite a while now.

Pfeiffer Vacuum

Address Nashua, NH

Web http://www.pfeiffer-vacuum.com/

Notes Major vacuum supplier. We have bought from them a helium leak checker recently, and we use a few older Pfeiffer-Balzers turbopumps and roughing pumps.

Systems Design & Fabrication, Inc.

Address Fall River, MA

Web http://www.systemsfab.com/

Notes Systems Design & Fabrication took over Varian's custom manufacturing. They have manufactured the first set of hardware for BEC2's two species oven. We had major problems getting leak-tight seals with their fittings.

Thermionics Vacuum Products

Address Port Townsend, WA

Web http://www.thermionics.com/

Notes Thermionics Vacuum provides a complete line of high and ultra high vacuum components, including motion feedthroughs. In particular, they are one of the few ion pump manufacturers.

Vacs SEV Co.,Ltd.

Address Tokyo, Japan

Web http://sev-vacuum.com/

Notes Special vacuum gaskets, including the (possibly) best ConFlat nickel gaskets available. We have recently bought gaskets from them.

Varian, Inc. Vacuum Technologies

Address Lexington, MA

Web http://www.varianinc.com/cgi-bin/nav?/products/vacuum/

Notes Varian manufactures a complete line of UHV components. They are the only manufacturer supplying all types of pumps and vacuum gauges. All of our ion pumps and titanium sublimation pumps are made by Varian, as well as most of our turbopumps. We also use almost exclusively Varian hardware for vacuum measurement. They have recently terminated their custom chamber building business.

Veeco Instruments

Address Woodbury, NY

Web http://www.veeco.com/

Notes Veeco manufactures vacuum equipment for the semiconductor industry, relevant to us being their fast linear beam shutters and heated viewports.

Bibliography

[1] C. A. Stan and W. Ketterle. Multiple species atom source for laser-cooling experiments. *Rev. Sci. Instrum.*, 76:063113, 2005.

[2] Z. Hadzibabic, C. A. Stan, K. Dieckmann, S. Gupta, M. W. Zwierlein, A. Görlitz and W. Ketterle. Two species mixture of quantum degenerate Bose and Fermi gases. *Phys. Rev. Lett.*, 88:160401, 2002.

[3] Z. Hadzibabic, S. Gupta, C. A. Stan, C. H. Schunck, M. W. Zwierlein, K. Dieckmann and W. Ketterle. Fifty-fold improvement in the number of quantum degenerate fermionic atoms. *Phys. Rev. Lett.*, 91:160401, 2003.

[4] C. A. Stan, M. W. Zwierlein, C. H. Schunck, S. M. F. Raupach and W. Ketterle. Observation of Feshbach resonances between two different atomic species. *Phys. Rev. Lett.*, 93:143001, 2004.

[5] M. W. Zwierlein, C. A. Stan, C. H. Schunck, S. M. F. Raupach, S. Gupta, Z. Hadzibabic and W. Ketterle. Observation of Bose-Einstein Condensation of Molecules. *Phys. Rev. Lett.*, 91:250401, 2003.

[6] M. W. Zwierlein, C. A. Stan, C. H. Schunck, S. M. F. Raupach, A. J. Kerman and W. Ketterle. Condensation of Pairs of Fermionic Atoms near a Feshbach Resonance. *Phys. Rev. Lett.*, 92:120403, 2004.

[7] K. Dieckmann, C. A. Stan, S. Gupta, Z. Hadzibabic, C. Schunck and W. Ketterle. Decay of ultracold Fermionic lithium gas near a Feshbach resonance. *Phys. Rev. Lett.*, 89:203201, 2002.

[8] S. Gupta, Z. Hadzibabic, M. W. Zwierlein, C. A. Stan, K. Dieckmann, C. H. Schunck, E. G. M. v. Kempen, B. J. Verhaar and W. Ketterle. RF Spectroscopy of Ultracold Fermions. *Science*, 300:1723-1726, 2003.

[9] C. H. Schunck, M. W. Zwierlein, C. A. Stan, S. M. F. Raupach and W. Ketterle. Feshbach resonances in fermionic lithium-6. *Phys. Rev. A*, 71:045601, 2005.

[10] M. W. Zwierlein, C. H. Schunck, C. A. Stan, S. M. F. Raupach and W. Ketterle. Formation Dynamics of a Fermion Pair Condensate. *Phys. Rev. Lett.*, 94:180401, 2005.

[11] Z. Hadzibabic. *Studies of a Quantum Degenerate Fermionic Lithium Gas*. Ph.D. Thesis, Massachusetts Institute of Technology, 2003.

[12] S. Gupta. *Experiments with Degenerate Bose and Fermi Gases*. Ph.D. Thesis, Massachusetts Institute of Technology, 2003.

[13] M. Zwierlein. *Cooling and Trapping a Bose-Fermi Mixture of Dilute Atomic Gases*. Stage de Recherche, MIP, 2^e Année Thesis, École Normale Supérieure Paris, France, 2001.

[14] C. Schunck. *Study of an ultracold cloud of fermionic lithum-6 atoms near a Feshbach resonance*. Diploma Thesis, University of Heidelberg, Germany, 2002.

[15] S. M. F. Raupach. *Experimental Investigations of Novel Quantum States in Condensed Matter: Scattering Resonances and the Fermion-Boson Crossover in Ultracold Alkali-Vapours*. Diploma Thesis, University of Leipzig, Germany, 2004.

[16] F. A. van Abeelen and B. J. Verhaar. Time-Dependent Feshbach Resonance Scattering and Anomalous Decay of a Na Bose-Einstein Condensate. *Phys. Rev. Lett.*, 83:1550-1553, 1999.

[17] E. R. I. Abraham, W. I. McAlexander, J. M. Gerton, R. G. Hulet, R. Côté and A. Dalgarno. Triplet s-wave resonance in 6 Li collisions and scattering lengths of ^{6}Li and ^{7}Li. *Phys. Rev. A*, 55:R3299, 1997.

[18] M. H. Anderson, J. R. Ensher, M. R. Matthews, C. E. Wieman and E. A. Cornell. Observation of Bose-Einstein Condensation in a Dilute Atomic Vapor. *Science*, 269:198-201, 1995.

[19] A. V. Avdeenkov and J. L. Bohn. Pair wave functions in atomic Fermi condensates. *Phys. Rev. A*, 71:023609, 2005.

[20] M. A. Baranov, M. S. Mar'enko, V. S. Rychkov and G. V. Shlyapnikov. Superfluid pairing in a polarized dipolar Fermi gas. *Phys. Rev. A*, 66:013606, 2002.

[21] J. Bardeen, L. N. Cooper and J. R. Schrieffer. Theory of Superconductivity. *Phys. Rev.*, 108:1175, 1957.

[22] M. Bartenstein, A. Altmeyer, S. Riedl, S. Jochim, C. Chin, J. H. Denschlag and R. Grimm. Crossover from a molecular Bose-Einstein condensate to a degenerate Fermi gas. *Phys. Rev. Lett.*, 92:120401, 2004.

[23] M. Bartenstein, A. Altmeyer, S. Riedl, S. Jochim, C. Chin, J. H. Denschlag and R. Grimm. Collective Excitations of a Degenerate Gas at the BEC-BCS Crossover. *Phys. Rev. Lett.*, 92:203201, 2004.

[24] H. L. Bethlem, G. Berden, F. M. H. Crompvoets, R. T. Jongma, A. J. A. van Roij and G. Meijer. Electrostatic trapping of ammonia molecules. *Nature*, 406:491, 2000.

[25] M. J. Bijlsma, B. A. Heringa and H. T. C. Stoof. Phonon exchange in dilute Fermi-Bose mixtures: Tailoring the Fermi-Fermi interaction. *Phys. Rev. A*, 61:053601, 2000.

[26] T. Bourdel, J. Cubizolles, L. Khaykovich, K. M. F. Magalhães, S. J. J. M. F. Kokkelmans, G. V. Shlyapnikov and C. Salomon. Measurement of the Interaction Energy near a Feshbach Resonance in a ^{6}Li Fermi Gas. *Phys. Rev. Lett.*, 91:020402, 2003.

[27] T. Bourdel, L. Khaykovich, J. Cubizolles, J. Zhang, F. Chevy, M. Teichmann, L. Tarruell, S. J. J. M. F. Kokkelmans and C. Salomon. Experimental Study of the BEC-BCS Crossover Region in Lithium 6. *Phys. Rev. Lett.*, 93:050401, 2004.

[28] U. Buck and H. Pauly. Measurement of the van der Waals potential between alkali atoms. *Z. Phys.*, 185:155-168, 1965.

[29] H. P. Büchler and G. Blatter. Supersolid versus Phase Separation in Atomic Bose-Fermi Mixtures. *Phys. Rev. Lett.*, 91:130404-130404, 2003.

[30] A. P. Chikkatur. *Colliding and Moving Bose-Einstein Condensates: Studies of superfluidity and optical tweezers for condensate transport.* Ph.D. Thesis, Massachusetts Institute of Technology, 2002.

[31] C. Chin and R. Grimm. Thermal equilibrium and efficient evaporation of an ultracold atom-molecule mixture. *Phys. Rev. A*, 69:033612, 2004.

[32] C. Chin, M. Bartenstein, A. Altmeyer, S. Riedl, S. Jochim, J. H. Denschlag and R. Grimm. Observation of the Pairing Gap in a Strongly Interacting Fermi Gas. *Science*, 305:1128-1130, 2004.

[33] S. Chu. The manipulation of neutral particles. *Rev. Mod. Phys.*, 70:685, 1998.

[34] C. N. Cohen-Tannoudji. Manipulating atoms with photons. *Rev. Mod. Phys.*, 70:707, 1998.

[35] E. A. Cornell and C. E. Wieman. Bose-Einstein condensation in a dilute gas, the first 70 years and some recent experiments. *Rev. Mod. Phys.*, 74:875, 2002.

[36] P. Courteille, R. S. Freeland, D. J. Heinzen, F. A. van Abeelen and B. J. Verhaar. Observation of a Feshbach resonance in cold atom scattering. *Phys. Rev. Lett.*, 81:69-72, 1998.

[37] J. Cubizolles, T. Bourdel, S. J. J. M. F. Kokkelmans, G. V. Shlyapnikov and C. Salomon. Production of Long-Lived Ultracold Li_2 Molecules from a Fermi gas. *Phys. Rev. Lett.*, 91:240401, 2003.

[38] J. Dalibard. Collisional dynamics of ultra-cold atomic gases, in *Bose-Einstein Condensation in Atomic Gases*, M. Inguscio and S. Stringari and C.E. Wieman eds., pp. 321-350. IOS Press, 1999.

[39] K. B. Davis, M.-O. Mewes, M. R. Andrews, N. J. van Druten, D. S. Durfee, D. M. Kurn and W. Ketterle. Bose-Einstein Condensation in a Gas of Sodium Atoms. *Phys. Rev. Lett.*, 75:3969-3973, 1995.

[40] D. DeMille. Quantum Computation with Trapped Polar Molecules. *Phys. Rev. Lett.*, 88:067901-067904, 2002.

[41] R. B. Diener and T.-L. Ho. *Projecting Fermion Pair Condensates into Molecular Condensates.* preprint cond-mat/0404517, 2004.

[42] E. A. Donley, N. R. Claussen, S. T. Thompson and C. E. Wieman. Atom-molecule coherence in a BoseEinstein condensate. *Nature*, 417:529, 2002.

[43] D. Durfee. *Dynamic Properties of Dilute Bose-Einstein Condensates.* Ph.D. Thesis, Massachusetts Institute of Technology, 1999.

[44] S. Dürr, T. Volz, A. Marte and G. Rempe. Observation of Molecules Produced from a Bose-Einstein Condensate. *Phys. Rev. Lett.*, 92:020406-020404, 2004.

[45] D. M. Eagles. Possible Pairing without Superconductivity at Low Carrier Concentrations in Bulk and Thin-Film Superconducting Semiconductors. *Phys. Rev.*, 186:456463, 1969.

[46] D. V. Efremov and L. Viverit. p-wave Cooper pairing of fermions in mixtures of dilute Fermi and Bose gases. *Phys. Rev. B*, 65:134519, 2002.

[47] G. M. Falco and H. T. C. Stoof. Crossover Temperature of Bose-Einstein Condensation in an Atomic Fermi Gas. *Phys. Rev. Lett.*, 92:130401, 2004.

[48] M. E. Gehm, S. L. Hemmer, S. R. Granade, K. M. O'Hara and J. E. Thomas. Mechanical stability of a strongly interacting Fermi gas of atoms. *Phys. Rev. A*, 68:011401, 2003.

[49] A. Görlitz, J. M. Vogels, A. E. Leanhardt, C. Raman, T. L. Gustavson, J. R. Abo-Shaeer, A. P. Chikkatur, S. Gupta, S. Inouye, T. Rosenband and W. Ketterle. Realization of Bose-Einstein condensates in lower dimensions. *Phys. Rev. Lett.*, 87:130402-130404, 2001.

[50] A. Görlitz, T. L. Gustavson, A. E. Leanhardt, R. Lw, A. P. Chikkatur, S. Gupta, S. Inouye, D. E. Pritchard and W. Ketterle. Sodium Bose-Einstein Condensates in the F=2 State in a Large-volume Optical Trap. *Phys. Rev. Lett.*, 90:090401, 2003.

[51] K. Góral, L. Santos and M. Lewenstein. Quantum Phases of Dipolar Bosons in Optical Lattices. *Phys. Rev. Lett.*, 88:170406-170404, 2002.

[52] M. Greiner, C. A. Regal and D. S. Jin. Emergence of a molecular BoseEinstein condensate from a Fermi gas. *Nature*, 426:537, 2003.

[53] T. W. Hänsch and A. L. Schawlow. Cooling of gases by laser radiation. *Opt. Commun.*, 13:68, 1975.

[54] H. Heiselberg, C. J. Pethick, H. Smith and L. Viverit. Influence of Induced Interactions on the Superfluid Transition in Dilute Fermi Gases. *Phys. Rev. Lett.*, 85:2418, 2000.

[55] H. Heiselberg. Fermi systems with long scattering lengths. *Phys. Rev. A*, 63:043606, 2001.

[56] J. Herbig, T. Kraemer, M. Mark, T. Weber, C. Chin, H.-C. Nägerl and R. Grimm. Preparation of a Pure Molecular Quantum Gas. *Science*, 301:1510, 2003.

[57] H. F. Hess. Evaporative cooling of magnetically trapped and compressed spin-polarized hydrogen. *Phys. Rev. B*, 34:3476, 1986.

[58] T.-L. Ho. Universal Thermodynamics of Degenerate Quantum Gases in the Unitarity Limit. *Phys. Rev. Lett.*, 92:090402, 2004.

[59] E. Hodby, S. T. Thompson, C. A. Regal, M. Greiner, A. C. Wilson, D. S. Jin, E. A. Cornell and C. E. Wieman. Production Efficiency of Ultracold Feshbach Molecules in Bosonic and Fermionic Systems. *Phys. Rev. Lett.*, 94:120402, 2005.

[60] M. Holland, S. J. J. M. F. Kokkelmans, M. L. Chiofalo and R. Walser. Resonance Superfluidity in a Quantum Degenerate Fermi Gas. *Phys. Rev. Lett.*, 87:120406, 2001.

[61] M. Houbiers, R. Ferwerda and H. T. C. Stoof. Superfluid state of atomic ^{6}Li in a magnetic trap. *Phys. Rev. A*, 56:4864, 1997.

[62] M. Houbiers, H. T. C. Stoof, W. I. McAlexander and R. G. Hulet. Elastic and inelastic collisions of ^{6}Li atoms in magnetic and optical traps. *Phys. Rev. A*, 57:R1497, 1998.

[63] M. Inguscio, S. Stringari and C. E. Wieman. *Bose-Einstein condensation in atomic gases*. IOS Press, Amsterdam, 1999.

[64] S. Inouye, M. R. Andrews, J. Stenger, H.-J. Miesner, D. M. Stamper-Kurn and W. Ketterle. Observation of Feshbach resonances in a Bose-Einstein condensate. *Nature*, 392:151-154, 1998.

[65] S. Jochim, M. Bartenstein, A. Altmeyer, G. Hendl, C. Chin, J. H. Denschlag and R. Grimm. Pure Gas of Optically Trapped Molecules Created from Fermionic Atoms. *Phys. Rev. Lett.*, 91:240402, 2003.

[66] S. Jochim, M. Bartenstein, A. Altmeyer, G. Hendl, S. Riedl, C. Chin, J. Hecker Denschlag and R. Grimm. Bose-Einstein Condensation of Molecules. *Science*, 302:2101, 2003.

[67] M. A. Joffe. *Trapping and cooling atoms at high densities*. Ph.D. Thesis, Massachusetts Institute of Technology, 1993.

[68] W. Ketterle and N. J. van Druten. Evaporative cooling of trapped atoms, in *Advances in Atomic, Molecular, and Optical Physics*, B. Bederson and H. Walther eds., pp. 181-236. Academic Press, San Diego, 1996.

[69] W. Ketterle, D. S. Durfee and D. M. Stamper-Kurn. Making, probing and understanding Bose-Einstein condensates, in *Bose-Einstein condensation in atomic gases*, M. Inguscio, S. Stringari and C.E. Wieman eds., pp. 67-176. IOS Press, Amsterdam, 1999.

[70] W. Ketterle. When atoms behave as waves: Bose-Einstein condensation and the atom laser, in *Les Prix Nobel 2001*, pp. 118-154. The Nobel Foundation, Stockholm, 2002.

[71] J. Kinast, S. L. Hemmer, M. E. Gehm, A. Turlapov and J. E. Thomas. Evidence for Superfluidity in a Resonantly Interacting Fermi Gas. *Phys. Rev. Lett.*, 92:150402, 2004.

[72] J. Kinast, A. Turlapov, J. E. Thomas, Q. Chen, J. Stajic and K. Levin. Heat Capacity of a Strongly-Interacting Fermi Gas. *Science*, 307:1296, 2005.

[73] J. Kinnunen, M. Rodriguez and P. Torma. Pairing Gap and In-Gap Excitations in Trapped Fermionic Superfluids. *Science*, 305:1131, 2004.

[74] C. Kittel and H. Kroemer. *Thermal Physics*. W. H. Freeman, New York, 1980.

[75] S. J. J. M. F. Kokkelmans, J. N. Milstein, M. L. Chiofalo, R. Walser and M. J. Holland. Resonance superfluidity: Renormalization of resonance scattering theory. *Phys. Rev. A*, 65:053617, 2002.

[76] M. G. Kozlov and L. N. Labzowsky. Parity Violation Effects in Diatomics. *J. Phys. B: At. Mol. Opt. Phys.*, 28:1933-1961, 1995.

[77] T. Köhler, T. Gasenzer, P. S. Julienne and K. Burnett. Long-range nature of Feshbach molecules in Bose-Einstein condensates. *Phys. Rev. Lett.*, 91:230401, 2003.

[78] C. E. Kuklewicz. *Surface excitations and critical velocity of a Bose-Einstein condensate*. S.M. Thesis, Massachusetts Institute of Technology, 2000.

[79] A. E. Leanhardt, A. Görlitz, A. P. Chikkatur, D. Kielpinski, Y. Shin, D. E. Pritchard and W. Ketterle. Imprinting vortices in a Bose-Einstein condensate using topological phases. *Phys. Rev. Lett.*, 89:190403, 2002.

[80] A. J. Leggett. A theoretical description of the new phases of liquid ^{3}He. *Rev. Mod. Phys.*, 47:331, 1975.

[81] A. J. Leggett. Diatomic molecules and Cooper pairs, in *Proceedings of the XVIth Karpacz Winter School of Theoretical Physics*, Karpacz, Poland, 1980, pp. 13-27, Springer-Verlag, Berlin.

[82] K. G. Libbrecht, R. A. Boyd, P. A. Willems, T. L. Gustavson and D. K. Kim. Teaching physics with 670 nm diode lasersconstruction of stabilized lasers and lithium cells. *Am. J. Phys.*, 63:729, 1995.

[83] A. P. Mackenzie and Y. Maeno. The superconductivity of Sr_2RuO_4 and the physics of spin-triplet pairing. *Rev. Mod. Phys.*, 75:657-656, 2003.

[84] M. Mackie and J. Piilo. Feshbach-Resonant Interactions in ^{40}K and ^{6}Li Degenerate Fermi Gases. *Phys. Rev. Lett.*, 94:060403, 2005.

[85] A. G. Martin, K. Helmerson, V. S. Bagnato, G. P. Lafyatis and D. E. Pritchard. rf Spectroscopy of Trapped Neutral Atoms. *Phys. Rev. Lett.*, 61:2431, 1988.

[86] N. Masuhara, J. M. Doyle, J. C. Sandberg, D. Kleppner, T. J. Greytak, H. F. Hess and G. P. Kochanski. Evaporative Cooling of Spin-Polarized Atomic Hydrogen. *Phys. Rev. Lett.*, 61:935-938, 1988.

[87] H. J. Metcalf and P. v. d. Straten. *Laser Cooling and Trapping*. Springer, 2001.

[88] M. O. Mewes, M. R. Andrews, N. J. van Druten, D. M. Kurn, D. S. Durfee and W. Ketterle. Bose-Einstein condensation in a tightly confining DC magnetic trap. *Phys. Rev. Lett.*, 77:416-419, 1996.

[89] F. H. Mies, E. Tiesinga and P. S. Julienne. Manipulation of Feshbach Resonances in Ultracold Atomic Collisions using Time-dependent Magnetic Fields. *Phys. Rev. A*, 61:022721, 2000.

[90] A. L. Migdall, J. V. Prodan, W. D. Phillips, T. H. Bergeman and H. J. Metcalf. First Observation of Magnetically Trapped Neutral Atoms. *Phys. Rev. Lett.*, 54:2596, 1985.

[91] J. N. Milstein, S. J. J. M. F. Kokkelmans and M. J. Holland. Resonance theory of the crossover from Bardeen-Cooper-Schrieffer superfluidity to Bose-Einstein condensation in a dilute Fermi gas. *Phys. Rev. A*, 66:043604, 2002.

[92] K. Mølmer. Bose Condensates and Fermi Gases at Zero Temperature. *Phys. Rev. Lett.*, 80:1804, 1998.

[93] T. Mukaiyama, J. R. Abo-Shaeer, K. Xu, J. K. Chin and W. Ketterle. Dissociation and Decay of Ultracold Sodium Molecules. *Phys. Rev. Lett.*, 92:180402, 2004.

[94] J. Mur-Petit, A. Polls, M. Baldo and H.-J. Schulze. Pairing in two-dimensional boson-fermion mixtures. *Phys. Rev. A*, 69:023606, 2004.

[95] P. Nozières and S. Schmitt-Rink. Bose condensation in an attractive fermion gas: from weak to strong coupling superconductivity. *J. Low Temp. Phys.*, 59:195-211, 1985.

[96] K. M. O'Hara. *Optical Trapping and Evaporative Coolinf of Fermionic Atoms.* Ph.D. Thesis, Duke University, 2000.

[97] K. M. O'Hara, S. L. Hemmer, M. E. Gehm, S. R. Granade and J. E. Thomas. Observation of a Strongly Interacting Degenerate Fermi Gas of Atoms. *Science*, 298:2179, 2002.

[98] K. M. O'Hara, S. L. Hemmer, S. R. Granade, M. E. Gehm, J. E. Thomas, V.Venturi, E. Tiesinga and C. J. Williams. Measurement of the Zero Crossing in a Feshbach Resonance of Fermionic ^{6}Li. *Phys. Rev. A*, 66:041401(R), 2002.

[99] Y. Ohashi and A. Griffin. BCS-BEC Crossover in a Gas of Fermi Atoms with a Feshbach Resonance. *Phys. Rev. Lett.*, 89:130402, 2002.

[100] C. J. Pethick and H. Smith. *Bose-Einstein Condensation in Dilute Gases.* Cambridge University Press, 2001.

[101] D. S. Petrov, M. A. Baranov and G. V. Shlyapnikov. Superfluid transition in quasi-two-dimensional Fermi gases. *Phys. Rev. A*, 67:031601, 2003.

[102] D. S. Petrov, C. Salomon and G. V. Shlyapnikov. Weakly Bound Dimers of Fermionic Atoms. *Phys. Rev. Lett.*, 93:090404-090404, 2004.

[103] D. S. Petrov, C. Salomon and G. V. Shlyapnikov. Scattering properties of weakly bound dimers of fermionic atoms. *Phys. Rev. A*, 71:012708, 2005.

[104] W. D. Phillips and H. Metcalf. Laser deceleration of an atomic beam. *Phys. Rev. Lett.*, 48:596, 1982.

[105] W. D. Phillips. Laser cooling and trapping of neutral atoms. *Rev. Mod. Phys.*, 70:721, 1998.

[106] E. L. Raab, M. Prentiss, A. Cable, S. Chu and D. E. Pritchard. Trapping of Neutral Sodium with Radiation Pressure. *Phys. Rev. Lett.*, 59:2631 - 2634, 1987.

[107] N. F. Ramsey. *Molecular beams.* Clarendon Press, Oxford, 1963.

[108] M. Randeria, J.-M. Duan and L.-Y. Shieh. Bound states, Cooper pairing, and Bose condensation in two dimensions. *Phys. Rev. Lett.*, 62:981, 1989.

[109] M. Randeria, J. M. Duan and L. Y. Shieh. Superconductivity in a two-dimensional Fermi gas: Evolution from Cooper pairing to Bose condensation. *Phys. Rev. B*, 41:327343, 1990.

[110] C. A. Regal, C. Ticknor, J. L. Bohn and D. S. Jin. Creation of ultracold molecules from a Fermi gas of atoms. *Nature*, 424:47, 2003.

[111] C. A. Regal, M. Greiner and D. S. Jin. Lifetime of molecule-atom mixtures near a Feshbach resonance in 40K. *Phys. Rev. Lett.*, 92:083201, 2004.

[112] C. A. Regal, M. Greiner and D. S. Jin. Observation of Resonance Condensation of Fermionic Atom Pairs. *Phys. Rev. Lett.*, 92:040403, 2004.

[113] B. C. Regan, E. D. Commins, C. J. Schmidt and D. DeMille. New Limit on the Electron Electric Dipole Moment. *Phys. Rev. Lett.*, 88:071805, 2002.

[114] S. Rosin and I. I. Rabi. Effective Collision Cross Sections of the Alkali Atoms in Various Gases. *Phys. Rev.*, 48:373, 1935.

[115] K. J. Ross and B. Sonntag. High temperature metal atom beam sources. *Rev. Sci. Instrum.*, 66:4409-4433, 1995.

[116] J. R. Rubbmark, M. M. Kash, M. G. Littman and D. Kleppner. Dynamical effects at avoided level crossings: A study of the Landau-Zener effect using Rydberg atoms. *Phys. Rev. A*, 23:3107, 1981.

[117] S. Schmitt-Rink and C. M. Varma. Pairing in two dimensions. *Phys. Rev. Lett.*, 63:445, 1989.

[118] F. Schreck, L. Khaykovich, K. L. Corwin, G. Ferrari, T. Bourdel, J. Cubizolles and C. Salomon. Quasipure Bose-Einstein Condensate Immersed in a Fermi Sea. *Phys. Rev. Lett.*, 87:080403-080404, 2001.

[119] I. F. Silvera and J. T. M. Walraven. Spin-Polarized Atomic Hydrogen, in *Progress in Low Temperature Physics*, D.F. Brewer ed., p. 139. Elsevier, Amsterdam, 1986.

[120] A. Simoni, F. Ferlaino, G. Roati, G. Modugno and M. Inguscio. Magnetic Control of the Interaction in Ultracold K-Rb Mixtures. *Phys. Rev. Lett.*, 90:163202-163204, 2003.

[121] D. M. Stamper-Kurn, M. R. Andrews, A. P. Chikkatur, S. Inouye, H.-J. Miesner, J. Stenger and W. Ketterle. Optical confinement of a Bose-Einstein condensate. *Phys. Rev. Lett.*, 80:2027-2030, 1998.

[122] D. M. Stamper-Kurn. *Peeking and poking at a new quantum fluid: Studies of gaseous Bose-Einstein condensates in magnetic and optical traps.* Ph.D. Thesis, Massachusetts Institute of Technology, 1999.

[123] J. Stenger, S. Inouye, M. R. Andrews, H.-J. Miesner, D. M. Stamper-Kurn and W. Ketterle. Strongly enhanced inelastic collisions in a Bose-Einstein condensate near Feshbach resonances. *Phys. Rev. Lett.*, 82:2422-2425, 1999.

[124] H. T. C. Stoof, M. Houbiers, C. A. Sackett and R. G. Hulet. Superfluidity of spin polarized ^{6}Li. *Phys. Rev. Lett.*, 76:10, 1996.

[125] K. E. Strecker, G. B. Partridge and R. G. Hulet. Conversion of an Atomic Fermi Gas to a Long-Lived Molecular Bose Gas. *Phys. Rev. Lett.*, 91:080406, 2003.

[126] S. T. Thompson, E. Hodby and C. E. Wieman. Spontaneous Dissociation of ^{85}Rb Feshbach Molecules. *Phys. Rev. Lett.*, 94:020401, 2005.

[127] E. Timmermans, P. Tommasini, R. Côté, M. Hussein and A. Kerman. Rarified Liquid Properties of Hybrid Atomic-Molecular Bose-Einstein Condensates. *Phys. Rev. Lett.*, 83:2691, 1999.

[128] E. Timmermans, K. Furuya, P. W. Milonni and A. K. Kerman. Prospect of creating a composite Fermi Bose superfluid. *Phys. Lett. A*, 285:228, 2001.

[129] A. G. Truscott, K. E. Strecker, W. I. McAlexander, G. B. Partridge and R. G. Hulet. Observation of Fermi Pressure in a Gas of Trapped Atoms. *Science*, 291:2570-2572, 2001.

[130] C. C. Tsuei and J. R. Kirtley. Pairing symmetry in cuprate superconductors. *Rev. Mod. Phys.*, 72:969, 2000.

[131] L. Viverit. Boson-induced s-wave pairing in dilute boson-fermion mixtures. *Phys. Rev. A*, 66:023605, 2002.

[132] J. M. Vogels. *Feshbach Resonances in Bose-Einstein condensates*. Ph.D. Thesis, Eindhoven University of Technology, 1999.

[133] J. D. Weinstein, R. DeCarvalho, T. Guillet, B. Friedrich and J. M. Doyle. Magnetic trapping of calcium monohydride molecules at millikelvin temperatures. *Nature*, 395:148-150, 1998.

[134] J. C. Wheatley. Experimental properties of superfluid ^{3}He. *Rev. Mod. Phys.*, 47:415, 1975.

[135] K. Xu, T. Mukaiyama, J. R. Abo-Shaeer, J. K. Chin, D. E. Miller and W. Ketterle. Formation of Quantum-Degenerate Sodium Molecules. *Phys. Rev. Lett.*, 91:210402, 2003.

[136] L. You and M. Marinescu. Prospects for p-wave paired Bardeen-Cooper-Schrieffer states of fermionic atoms. *Phys. Rev. A*, 60:2324, 1999.

[137] C. Zener. Non-Adiabatic Crossing of Energy Levels. *Proc. R. Soc. London, Ser. A*, 137:696, 1932.

[138] M. W. Zwierlein, J. R. Abo-Shaeer, A. Schirotzek, C. H. Schunck and W. Ketterle. *Vortices and Superfluidity in a Strongly Interacting Fermi Gas.* , 2005.